Paper originally prepared for 3rd Congress to be held in Sao Paulo Brazil in June 1978 which was cancelled. JT 10/31/78

September, 1978.

Dear Sir,

Attached you will find information on the III International Congress on Water Resources that will be held in Mexico City from the 23rd to the 27th April, 1979.

We shall be looking forward to your visit!

Kind regards,

El Comité Organizador.

CALIFORNIA UNDERSEA AQUEDUCT

HYDRODYNAMIC LOADING AND SCOUR & APPENDIX III

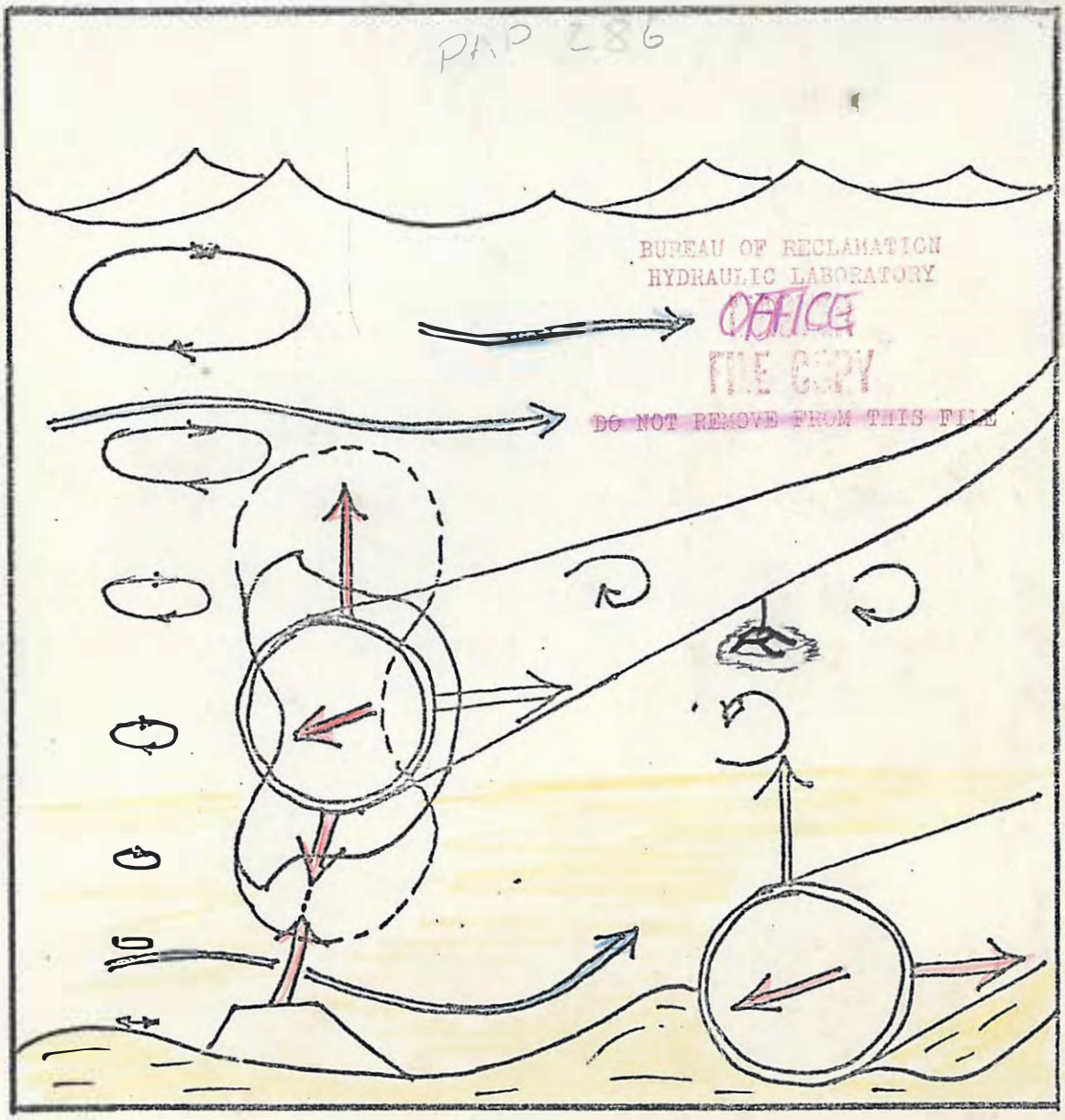

DESIGN DATA REFERENCE BOOK

DECEMBER 1, 1972

SEE PAP 309 For Condensed Version

CALIFORNIA UNDERSEA AQUEDUCT

Appraisal Study

HYDRODYNAMIC LOADING & SCOUR

Design Data Reference Book

December 1, 1972

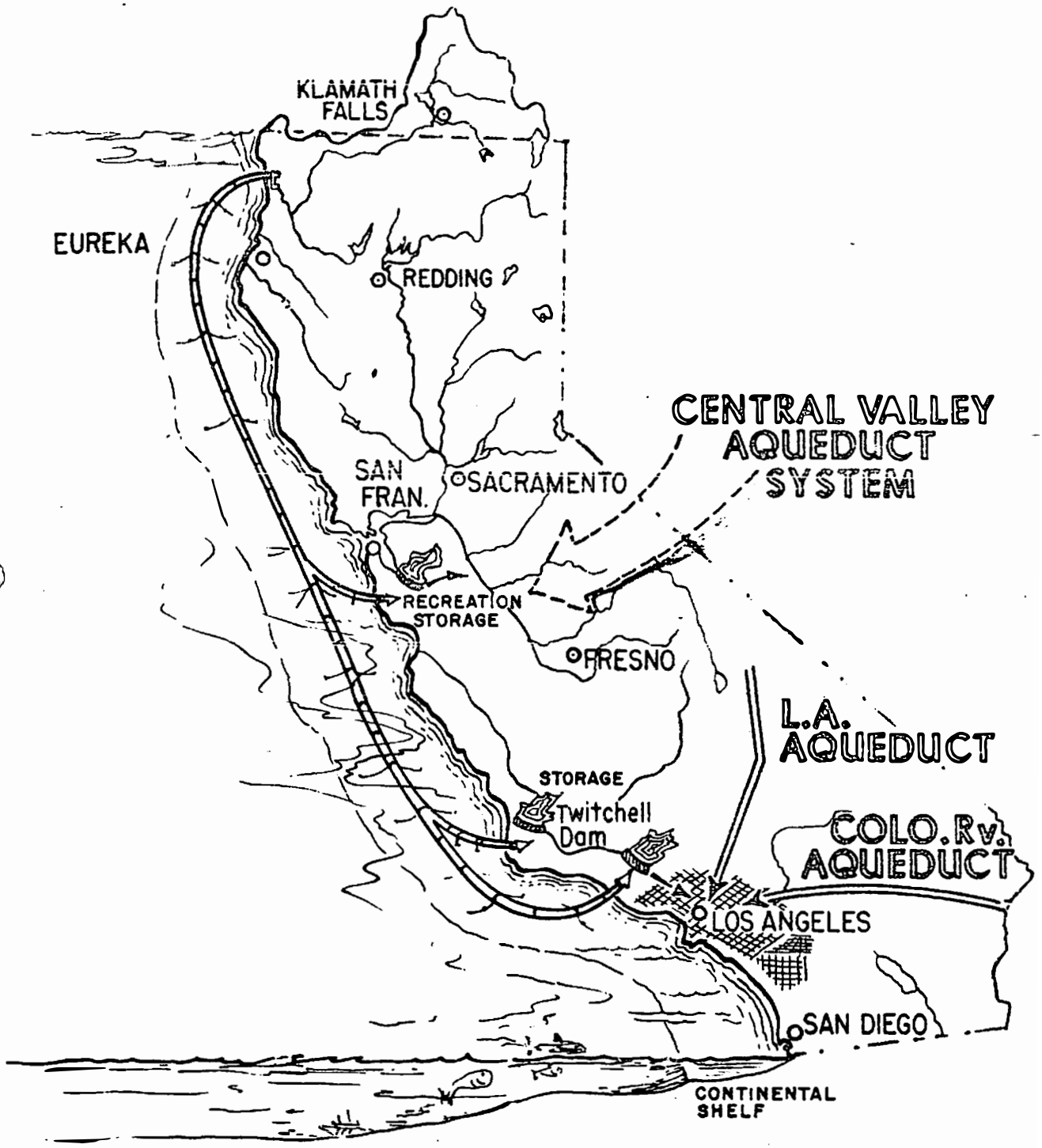

UNDERSEA AQUEDUCT
CALIFORNIA

CONTENTS

CONTENTS - Continued

CONTENTS - Continued

CONTENTS - Continued

CONTENTS - Continued

CONTENTS - Continued

INTRODUCTION

An undersea aqueduct has been proposed to transport water from the Eel-Klamath River areas of northwestern California to central and southern California. In 1971 the Bureau of Reclamation started a reconnaissance investigation for the aqueduct, and a "Study Work Plan For California Undersea Aqueduct Reconnaissance Investigation" was issued in September 1971. The report will serve as a guide for conducting the investigation. A systems approach was used and the reconnaissance investigation was divided into many phases. One phase was the preparation of a design data reference book "Hydrodynamics Loading and Scour," which would provide design data to predict forces on undersea pipelines. The responsibility of preparing the design data reference book was assigned to the Hydraulics Branch which formed a task force consisting of J. C. Schuster, R. A. Dodge, and E. R. Zeigler to complete the assignment.

Several planning assumptions were developed in the Study Work Plan. The following design assumptions relate to the "Hydrodynamic Loading and Scour" reference book.

1. The aqueduct would deliver 1 to 4 x 10^6 acre-feet of water per year.

2. The aqueduct would include one or more pipes 20 to 32 feet in diameter.

3. The aqueduct must be located on the Continental Shelf at a depth not exceeding 65 fathoms or about 400 feet.

4. Design emphasis chould be given to concepts of a buried pipeline, pipeline partially buried or resting on the bottom, and a flexible buoyant pipeline, Figure 1.

Figure 1. Concepts of pipeline configurations.

5 The aqueduct should be designed for a min life of 100 years and under consideration of a 200 year seismic and hydrological [illegible]

PURPOSE

The purpose and scope of the "~~Hydrodynamics Loading and Scour~~" design data reference book are outlined in the following excerpt from the Study Work Plan.

"Work Item - Hydrodynamic Loading and Scour

"Scope of Work

"The study will summarize design data to predict hydrodynamic loadings on various aqueduct configurations. In addition, probable scour patterns for each configuration will be estimated for the range of sea floor materials expected. The work will culminate in a design data reference book. The work should be coordinated with the other ← work items in the oceanographic studies.

"Work Statement

"A literature search is required to define areas in which design data are inadequate. The following data are essential for design and will be supplied for all pipeline configurations:

1. Drag and lift loadings with both steady-state and oscillatory flows
2. Effects of salinity and temperature on fluid density
3. Scour tendencies for pipelines
4. Dynamic behavior of submerged masses suspended by cables from oscillating supports
5. Pressure distribution around pipelines
6. Pipe friction factors

"Additional data needs arising from the conceptual alternative screening studies will also be obtained.

"If the data are not available from the literature, analytic and hydraulic model studies will be conducted to supplement the known data."

ORGANIZATION OF THE DESIGN DATA REFERENCE BOOK AND COMMENTS ON THE ASSIGNMENT

Numerous references were catalogued during the literature search and review for hydrodynamic and scour information. Many of these references were examined, but relatively few contained data that could be applied directly in solving the critical problems. Pertinent references are footnoted or listed where the subject is discussed. References of the literature search are listed in the bibliography.

Many facets of hydraulics are involved in the Hydrodynamic Loading and Scour Task Force assignment. In organizing the design data reference book the team treated parts of the assignment as distinctive subjects in separate sections. A discussion, presentation of formulas, and in some cases example problems illustrating use of the formulas, were included in the sections. The intent is that this detailed information would serve as "building blocks" for other sections of the reference book.

For example, Section 1, "Hydrodynamics Affecting The Conduit" gives a general description of water motion and hydrodynamic forces acting on the conduit for the three concepts. For a more thorough understanding of the forces and formulas for computing the forces, the reader is referred to the "building block" sections.

The task force was unable to provide formulas that would accurately predict dynamic behavior of the buoyant conduit, as prescribed in

Work Item 4, "Dynamic behavior of submerged masses suspended by cable from oscillating supports." Fluctuating pressures and velocities occurring in fluid flow past a circular cylinder most likely are of a statistical nature. Present ~~hydraulic~~ theory is not developed to accurately compute the statistical hydrodynamic loads, or how the conduit would react to these loads. Another factor influencing dynamic behavior of the conduit is the movement of the conduit in response to the hydrodynamic loads. The amount of conduit movement is dependent upon structural properties such as size, thickness, strength, flexibility, and the applied forces. Yet the hydrodynamic loads vary because conduit movement changes velocity and acceleration of the flow relative to the conduit. The task force considered conduit movement and the effect of the hydrodynamic loading in only a general sense.

No formulas about Tsunami waves are given in this design data reference book. One reference (1 / page 121) states that solitary wave theory approximates the Tsunami waveform (very long waves). Equations are given for water velocity beneath the waves. These equations are dependent upon the stillwater depth and wave height above the still-water level. No information was found about the Tsunami wave heights which may occur over the Continental Shelf, for use in the solitary wave equations. Formulas for computing water movement are given in

1/ Ippen, A.T. Ed., Estuary and Coastline Hydrodynamics, Engineering Society Monographs, Mc Graw-Hill Book Company, Inc 1966

the section "Water Movement Caused By Waves and Effect Upon The Conduit." However, wave parameters of wave length (L), wave height (H), and wave period (T) are needed for use in these formulas. Probably these wave parameters will have various values for different locations off the California Coast. This wave parameter information is not included in this design reference book but will be available from reports specified in the "Study Work Plan For The California Undersea Aqueduct Reconnaissance Investigation," see pages 50-53.

The task force found areas where the available data appeared insufficient for accurately defining hydrodynamic loads or conditions acting on the conduit. Areas which require more or better information are noted in the section "Study Needs." There was insufficient time to perform hydraulic model studies for supplementing the data.

SECTION 1

HYDRODYNAMICS AFFECTING THE CONDUIT

Buried Concept

Buoyant forces acting upon the buried conduit are probably insignificant under normal conditions, but in the event of soil liquifaction the buoyant force increases. The buoyant force equation can be used to predict the upward thrust acting on the conduit, Section 3, "Buoyant Force - Considerations for the Buried Concept."

A buried conduit is normally protected from hydrodynamic forces produced by movement of the ocean water. Hydrodynamic forces acting upon the buried conduit would be due to flow of water within the conduit. Friction force of water flowing in the conduit for straight reaches would probably be negligible with respect to longitudinal movement; but forces occurring at bends should be considered, Section 5 "Internal Headloss and Fluid Forces of Conduit Bends" explains forces that the conduit must resist.

Partially Buried or Resting on the Bottom Concept

Hydrodynamic forces acting on the conduit are shown in Figure 1.1.

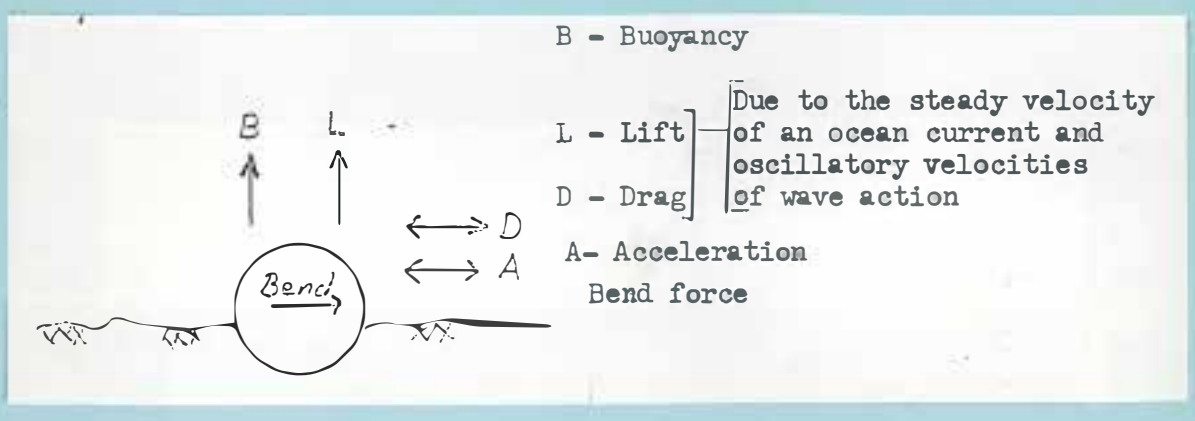

Figure 1.1 - Forces on conduit for partially buried or resting on the bottom concept

The buoyant force is a static type force and is present in still or moving water. Section 3 "Buoyant Force" describes how to compute the force and the possible variation in force that might occur from changes in water turbidity or liquifaction of the soil.

The bend force, composed of two forces, one static and one dynamic, acts from within the conduit. The static force results from the internal water pressure and the dynamic force is caused by the internal water velocity. An explanation and method of computing bend forces is given in Section 5 " Internal Headloss and Fluid Forces at Conduit Bends." The lift and drag forces occur when the ocean water has a normal component of movement relative to the conduit. For the condition of an ocean current flowing past the conduit, a steady type velocity acts on the conduit. The resulting drag force acts in the same direction as the current. Unsteady drag forces can occur because of a periodic vortex formation on the down current side of the pipeline, Section 7.

Wave action produces an oscillating motion to water velocities below the wave. Near the ocean bed the water oscillates in a general horizontal direction and experiences an accelerated motion. The velocity periodically increases and decreases and reverses direction to add an acceleration component of unsteadiness to the lift and drag forces. Explanations, formulas, and coefficients for cumputing lift, drag, and acceleration forces are given in Section 6, (Lift and Drag). The designer should use Section 6 to obtain the appropriate value for the required lift, drag, and inertial (acceleration) coefficients. Values

of these coefficients vary depending on the location of the conduit with respect to the ocean bottom. Formulas are given for computing water velocity and accelerations in Section 7 "Water Movement Caused by Waves and Effect Upon the Conduit." These are the water velocities and accelerations to use in the lift, drag, and acceleration force equations.

The conduit can be subject to both a steady velocity of an ocean current and unsteady velocities caused by wave action. In this case the velocity to be used in the lift and drag force equations is the fector addition of the ocean current velocity and the oscillatory velocity. For the acceleration force equation the only source of water acceleration is believed to be that of the wave action.

Buoyant Concept

Normal and parallel hydrodynamic forces act upon the buoyant conduit, Figure 12. Possibly the normal forces are predominate, but an effort should be made to define the parallel forces in relation to the total load on the support.

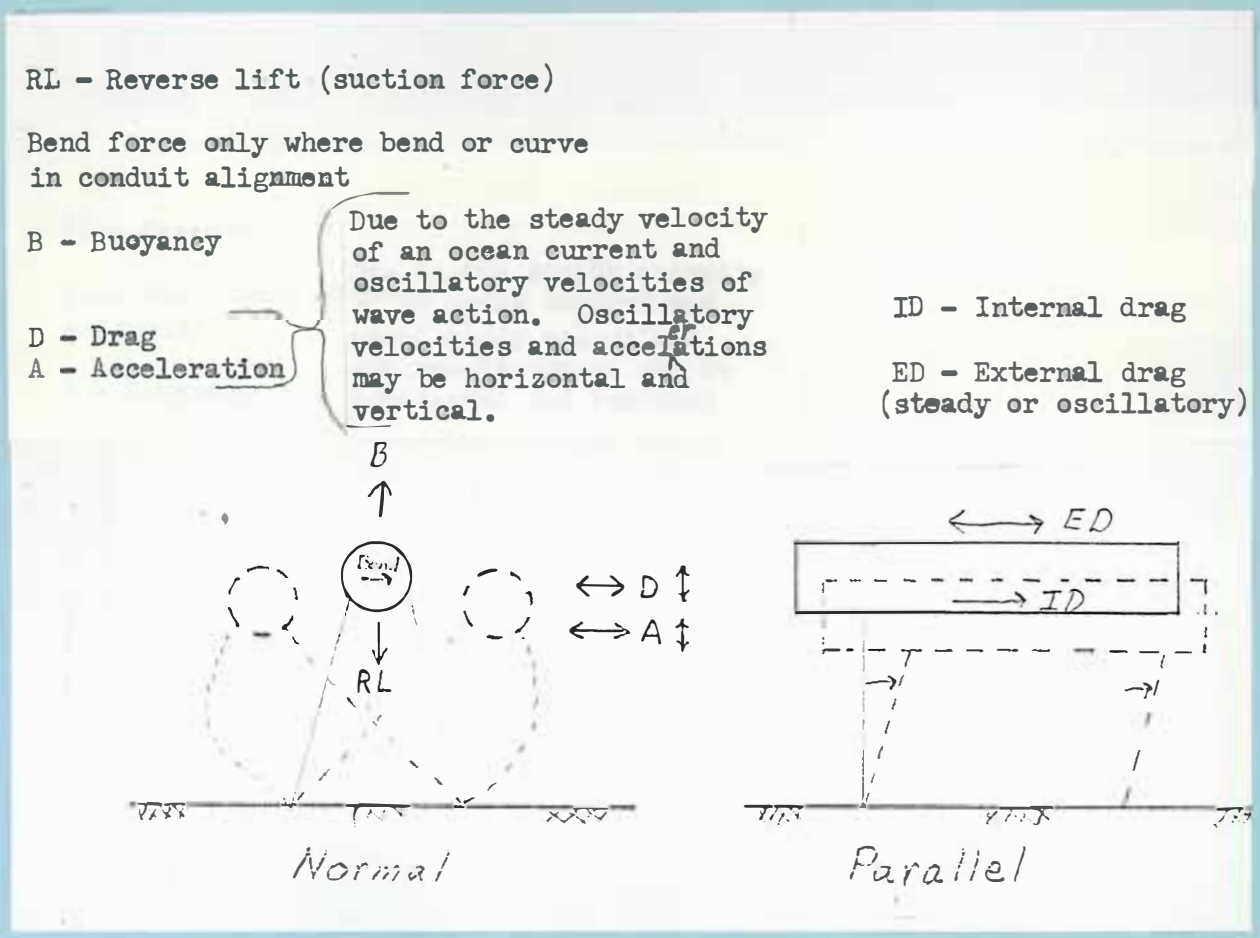

Figure 1.2 - Forces on conduit for the buoyant concept

Establishing the buoyant force is critical for this concept. Buoyancy of the conduit is very sensitive to the specific weight of fluid surrounding the conduit, (specific weight is a measure of density). Specific weights for fresh water, salt water with various salinities, and different temperatures are given in Section 2 "Water Properties," and should be used with Section 3 to compute the force. Water density can change in the ocean environment to produce changing loads on the pipe supports; for greater loads, use Section 3, Consideration of Dense Turbid Water, and for lesser loads, use Section 3, Consideration of Fouling.

A steady ocean current acting at an angle to the conduit produces two components of drag, one normal (D) and one parallel (ED) to the

conduit. A suction force can be generated by locating the conduit to close to the bottom. Water velocity under the pipe is increased and an unstable low pressure area is created beneath the pipe resulting in a reverse lift (RL). Explanations and methods of computing reverse lift, normal and parallel drag forces are given in Section 6.

The flow of water in the pipe produces forces that may move the conduit. These are bend and internal drag (ID) forces of the flowing water on the conduit walls. These bend and friction forces are explained in Sections 4 and 5.

The buoyant conduit is more susceptible to oscillatory water motion than the previous concepts. Above the ocean bed oscillatory motion of the water is not neecessarily linear. There are horizontal and vertical accelerations and velocities of the water acting upon the conduit which periodically reverse direction. Wave crests acting at an angle produce drag forces both normal (D) and parallel (ED) on the conduit. A reverse lift (RL) force occurs if the conduit is too close to the ocean bottom. This force would vary with respect to the magnitude of the normal velocity component. Acceleration forces act only in a direction normal to the conduit. Explanations and methods of computing reverse lift, normal and parallel drag forces, and acceleration forces are given in Section 6 and for computing water velocity and acceleration in Section 8. When the conduit moves, then relative accelerations and velocities between pipe and water should be used in the force equation, See Section 8, "Buoyant Concept."

For a conduit subject to both ocean current and wave action, the velocity to use in the lift and drag force equations is the vector addition of the ocean current velocity and the oscillatory velocity.

Each Concept

Friction and bend head losses are common to each of the pipeline concepts. These head losses are explained in Sections 4 and 5 on friction and bend losses.

The "California Undersea Aqueduct Report on Alternative Concepts" contains Figures B1 and B2 (Appendix B) showing head loss for various pipe diameters and given discharges. Although the head losses are limited to rugosity values of ε = 0.008 feet and ε = 0.000064 feet, the data may prove useful to the designers.

Water Hammer

The transmission and reflection of water hammer pressure surges in the aqueduct straight sections, bends and junctions were not included in the design data book. Analysis should be made for each concept to find the effects of pipeline orientation, concentrations of head-loss and momentum, and the motion of the piping system at junctions. The forces of water hammer pressures on the bouyant concept may materially affect the transmission and reflection characteristics of pressure waves at junctions and bends.

The effect on the bouyant concept of water released from a complete separation of the aqueduct or large hole broken in the wall was not analyzed in detail. Momentum relationships in Section 5 would be of use in analyzing the possible "firehose" movement of the aqueduct.

SECTION 2

FLUID PROPERTIES

Background

In hydrodynamics the equation of continuity of flow is derived by accounting for the rate of mass (M) entering and leaving a stationary element of fluid. The equation of motion for the same element can be developed by accounting for the rate of momentum entering, momentum leaving, and the forces acting on the system. Momentum is the product of velocity (V) and mass (M). Force ($\bar{F}$) is the vector defined in terms of the mass (M) as

$$\bar{F} = M\bar{a} \quad \ldots\ldots\ldots\ldots\ldots\ldots \quad (1)$$

where ($\bar{a}$) is an acceleration vector. Mass is the measure of the inertia or resistance of a fluid flow to changes of direction and/or velocity. When we consider gravity (g) as the only acceleration acting on the mass, then the force acting ~~in~~ the direction of the gravitational field is called weight (W) expressed as

$$W = Mg \quad \ldots\ldots\ldots\ldots\ldots\ldots \quad (2)$$

Using equations (1) and (2) to solve for (M), equating and then solving for ($\bar{F}$) results in

$$\bar{F} = \frac{W}{g}\bar{a}$$

where (W/g) is ~~a way to express~~ mass expressed in engineering units called slugs.

Differences of density can be the driving force of ocean currents. For sedimentation and scour, the difference in mass or weight between the seawater and sediment is a driving or a resisting force depending on whether a partical is setting or resting on the bed.

Fluid flow may have a change in mass or weight at different points in the flow system. Thus it is useful to define weight and mass in terms of a unit volume.

$$\gamma = \frac{W}{1\ ft^3}$$

$$\rho = \frac{M}{1\ ft^3} \quad \text{where}$$

W = weight, lbs

M = mass, slugs, $\frac{lb\ sec^2}{ft}$

γ = specific weight, lb/ft^3

ρ = density, slugs/ft^3, $\frac{lb\ sec^2}{ft^4}$

Using these definitions and substitution into equation (2.2)

$$\gamma = \rho g \quad . \quad . \quad . \quad . \quad . \quad . \quad . \quad . \quad . \quad (2.3)$$

Stagnation pressures, drag forces and lift forces are proportional to

$$(\rho V^2),\ \frac{(\gamma V^2)}{g},\ \text{or}\ (MV^2)$$

Therefore mass expressed in the form of density or specific weight is a fundamental property in fluid statics and dynamics.

A substance that continues to deform under a shear stress, no matter how small, by definition is a fluid. In real flow, internal shear forces cause heat or frictional losses. If the velocity is great enough, disturbances at boundaries can amplify into general turbulence throughout the entire flow. The property by which a fluid resists shear is called viscosity. Viscosity can be thought of as the inverse of fluidity.

Viscosity (μ) is defined as the ratio of shearing stress (τ) to the rate of strain. The rate of strain is the velocity gradient (dv/dy). Thus dynamic viscosity is defined as

$$\mu = \frac{\tau}{\frac{dv}{dy}} \quad \ldots\ldots\ldots\ldots \quad (4)$$

μ = dynamic viscosity, $\frac{lb/sec}{ft^2}$

τ = shearing stress, lb/ft^2

$\frac{dv}{dy}$ = velocity gradient, $\frac{1}{sec}$

Equation (4) is generally used for steady state flow conditions. However, the kinematic viscosity is used for unsteady flow conditions. Kinematic viscosity (ν) is defined as:

$$\nu = \frac{\mu}{\rho} \quad \ldots\ldots\ldots\ldots \quad (5)$$

When hydrodynamic equations of motion are transformed into dimensionless variable form, both Froude numbers (N_F) and Reynolds numbers (N_R) are formed and expressed as

$$N_F = \frac{V^2}{Lg} \quad \ldots\ldots\ldots\ldots\ldots\ldots \quad (6)$$

and

$$N_R = \frac{VL\rho}{\mu} \text{ or } \frac{VL}{\nu} \quad \ldots\ldots\ldots\ldots \quad (7)$$

where (V) is a characteristic velocity and (L) is a characteristic length. These numbers are often used for relating results of hydraulic model tests to prototype conditions. The Froude number (N_F) is the important parameter when gravity and free surface wave action dominates. The Reynolds number is the important parameter when frictional and form losses dominate. Also the Reynolds number is used to indicate whether fluid flow is laminar or turbulent.

Effects of Temperature, Pressure, and Salinity on Density and Viscosity

Both density and viscosity vary with temperature, pressure, and salinity. Thus the range of variations and the effect of these factors on fluid properties must be considered.

For the area of the California Undersea Aqueduct, temperature of the water varies from about 44° F to 60° F. Pressure in terms of ocean depth will vary from 0 to about 600 feet. Salinity varies from about 33 to 35 ppt (parts per thousand by weight). Increases of pressure will

increase the density (ρ) of the fluid because water is slightly compressible. For water the bulk modulus is high and the relationship

$$P = \gamma h = \rho g h \quad . \quad . \quad . \quad . \quad . \quad . \quad . \quad . \quad . \quad . \quad . \quad (8)$$

is usually assumed rather than integrating the variation of density (ρ).

For example, sea water at 1 atmosphere ~~64°~~ 56° F and ~~35~~ 34 ppt has a specific weight of 64.00 pounds per cubic foot. At the same temperature and at a depth of 300 feet the specific weight increases by about 0.03 pounds per cubic foot. Thus pressure effect on both (ρ) and (γ) can be considered negligible, ~~in regard to the California Undersea Aqueduct.~~ The effect of pressure on viscosity is even less significant. Therefore the fluid property curves in Figures 2.1 and 2.2 show only the effects of temperature and salinity.

In Figure 2.1 and 2.2 Density (ρ) and specific weight (γ) are shown as a function of temperature and salinity. The solid lined curves are plotted from data for fresh water and for sea water of 35 ppt.

The curves for intermediate values of salinity (the dashed lines) are based on the assumption that density and specific weight of sea water at different salinities will vary similarly to aqueous solutions of (NaCl). The most probable ranges of density ~~Figure~~ and specific weight ~~Figure~~ for water surrounding the aqueduct are shown by the shaded areas between 33 and 35 ppt and 44° to 60° F.

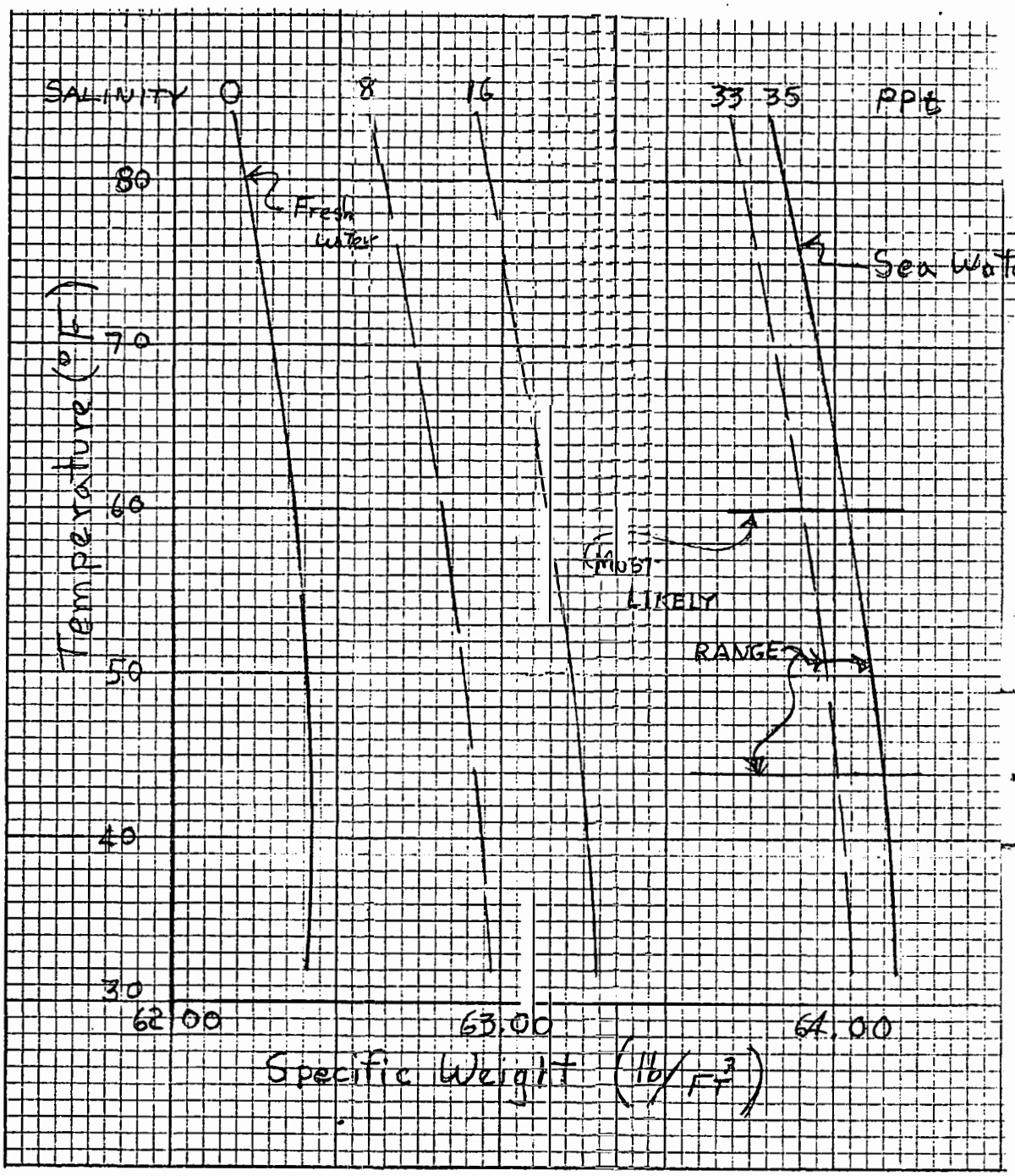

FIGURE 2.2 SPECIFIC WEIGHT CHANGE WITH TEMPERATURE

Kinematic viscosity is plotted in Figure 2.3 for both fresh water and sea water of ~~335~~ 33 to 35 ppt. The most likely ranges indicate that salinity has virtually no effect on viscosity and only temperature need be considered.

Effects of Concentrated Suspended Sediment on Density

A fluid, containing sufficient quantities of clay sediment that can sustain a small shear (T_B) before yielding, ~~can~~ no longer ~~be called~~ a true fluid. These plastic suspensions have a viscosity (η_d) that applies to the flow after yielding takes place. Bingham[2,1/] expressed this as follows:

if $\tau_\alpha > \tau_\beta$

then $$\tau_\alpha - \tau_\beta = \eta_d \frac{du}{dz} \quad \ldots\ldots\ldots \quad (9)$$

where

τ_α = applied shear

τ_β = yield shear

η_d = differential viscosity

du/dz = shear strain or velocity gradient with respect to distance

---

2-1/ Bingham, E. C., Fluidity and Plasticity, McGraw-Hill, 1922

This is the same notation used by M. M. Dass from Einstein et al 2.2/. Table 2.1 from their tests of a deep marine sediment that passed through No. 140 sieve is included here. The value of relative density (third column) and viscosity ratio (last column) in the table may have application to sediment density flow and floatation problems.

J. D. Skoda from Einstein et al 2.2/ cites literature on turbidity currents presumably containing larger size sediment than in Dass and infers densities up to 10 percent greater than the surrounding fluid and postulates densities up to 100 percent greater.

A high value of fluid density also has been cited for a pipeline where floatation occured due to fluidized sediment in a trench 2.3/. The water and suspended sediment were acting like a fluid with a specific gravity of 2.0.

2.2/ H. A. Einstein, "A Literature Review on Erosion and Deposition of Sediment Near Structures in the Ocean," 1970.

2.3/ Anonymous, ASCE Preliminary Research on Pipeline Floatation, Report of the Pipeline Floatation Research Council and R. A. Rait, Journal of Pipeline Division, Vol. 92, PLI, March 1966, pp 27-71.

TABLE 2.1 2.2

Table II

RELATIVE DIFFERENTIAL VISCOSITY AND BINGHAM SHEAR STRENGTH (TESTS 1 & 2)

Suspension concentration gm/litre	Salinity gm/litre	$\frac{\rho_s}{\rho_L}$	Intercept at $\frac{1}{t} = 0$ cm	$h_o \frac{\rho_s}{\rho_L}$ cm	$\frac{d}{3} h_\beta = h - \frac{\rho_s}{\rho_L}\frac{v^2}{2g} + \frac{\rho_s}{\rho_L} h_o$ cm	h_β cm	$\tau_\beta = \frac{h_\beta \rho_L g r}{2L}$ dynes/cm^2	Distilled water calibration slope cm/sec	Slope $\left(h - \frac{\rho_s}{\rho_L}\frac{v^2}{2g}\right)$ / $\frac{1}{t}$ susp.	$\frac{\eta_d}{\eta_1}$
TEST 1										
0	0	1.0	-11.9	+11.9	0	0	0	1016.6	1016.6	1.00
46.4	1.04	1.03	-9.25	+12.25	3.0	2.25	3.96	"	1093	1.08
92.4	2.12	1.05	-8.0	+12.50	4.50	3.375	5.94	"	1260	1.24
115.0	2.54	1.07	-7.25	+12.71	5.46	4.09	7.20	"	1480	1.46
168.0	3.70	1.10	-6.25	+13.10	6.85	5.14	9.05	"	2060	2.01
TEST 2										
0	0	1.00	-11.9	+11.9	0	0	0	1016.6	1016.6	1.00
12	30.93	1.04	-10.75	+12.38	1.63	1.22	2.14	"	1114	1.1
42	"	1.05	-9.75	+12.50	2.75	2.06	3.62	"	1175	1.16
55	"	1.06	-9.25	+12.61	3.38	2.52	4.43	"	1195	1.18
72	"	1.07	-8.25	+12.71	4.46	3.34	5.86	"	1275	1.255
82.5	"	1.08	-7.75	+12.85	5.10	3.82	6.71	"	1315	1.295

DRAFT Schuster:rf-s
November 28, 1972

SECTION 3

BUOYANT FORCE

Formula for Computing Buoyant Force

A buoyant force results when an object is immersed in a fluid. This force acts vertically upward through the object's center of gravity and is equal to the weight of fluid displaced by the object. The object will float or sink if it is lighter or heavier than the weight of the displaced fluid. For a pipe filled with fresh water and submerged in the ocean, the resultant buoyant force (Frb) in pounds per linear foot of pipe is given by equation (3.1) Figure 3.1.

$$Frb = F_b - W_f - W_p = \frac{\pi}{4} D_o^2 \gamma_s - \frac{\pi}{4} D_i^2 \gamma_f - \frac{\pi}{4} (D_o^2 - D_i^2) \gamma_p \quad (3.1)$$

D_o = outside pipe diameter, ft

D_i = inside pipe diameter, ft

γ_s = specific wgt ocean water, lb/ft^3

γ_f = specific wgt fresh water, lb/ft^3

γ_p = specific wgt pipe material, lb/ft^3

F_b = buoyant force due to the wgt of the displaced fluid, lbs/ft

Frb = resultant buoyant force of the conduit, lb/ft

W_f = wgt fresh water in pipe, lb/ft

W_p = wgt pipe, lbs/ft

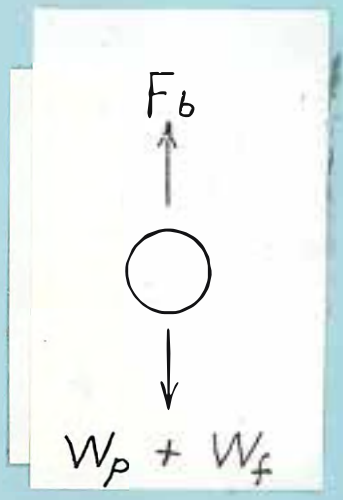

W_p and W_f act through pipe centerline

Figure 3.1 Symbol notation and development of equation (3.1)

The resultant buoyant force on a glass reinforced plastic pipe filled with fresh water would be about 900 lbs/ft

Example Problem

Assume 1 inch pipe wall and inside pipe diameter 30 feet,

γ_p = 112 lb/ft^3, and water temperature 50° F

From Section 2 γ_f = 62.41 lbs/ft^3 and γ_s = 64.22 lbs/ft^3 */

$$Frb = \frac{\pi}{4} D_o \gamma_s - \frac{\pi}{4} D_i^2 \gamma_f - \frac{\pi}{4} (D_o^2 - D_i^2) \gamma_p \qquad D_o = 30' + 2''$$

$$D_o = 30.167'$$

$$Frb = \frac{\pi}{4} (30.167)^2 (64.22) - \frac{\pi}{4} (30)^2 (62.41) - \frac{\pi}{4} [(30.167)^2 - (30)^2](112)$$

$$Frb = 45{,}901 - 44{,}115 - 884 = 902 \text{ lbs/ft}$$

Figure 3.2 ~~next sheet~~ is a graph of the resultant buoyant forces for various pipe diameters and wall thicknesses. The buoyant force obtained from the graph for the pipe dimensions of the example is 760 lbs/ft. This value is considerably less than 902 lbs/ft and shows the importance ~~dependency of the resulting~~ buoyant force of selecting the correct values of γ_s and γ_f.

*/ The γ_s = 64.22 lbs/ft^3 value was used in numerous example problems. The value is believed to be excessive for probable conditions of the undersea aqueduct, Figure 2.2. A difference of about 0.1 lb/ft^3 was not detected until refinements were made on the data in the Fluid Property Section. The decision was made not to change the example problems throughout the text.

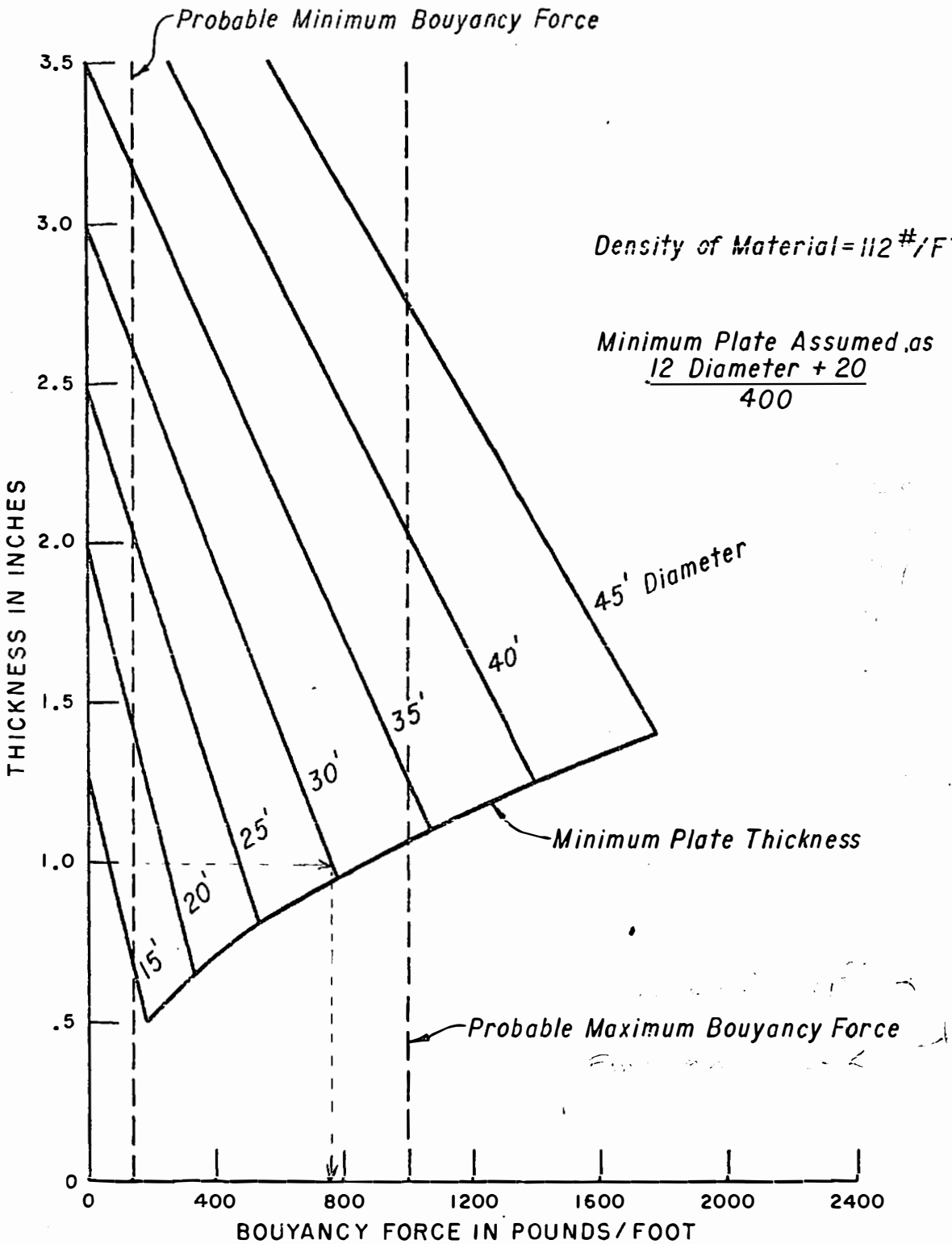

FIG. B3 THICKNESS Vs. BOUYANCY FORCE FOR SEVERAL DIAMETERS GLASS REINFORCED PLASTIC PIPE

Figure 3.2 – Bouyant Force – Taken from "Report on Alternate Concepts" "USBR"

Consideration of Dense Turbid Water

A turbidity current acting on the continental shelf is described differently than the density current in a reservoir. An excerpt is taken from Reference 3.1/ for ocean literature terminology.

> "A distinction should be made between a turbidity flowage and a turbidity current. A turbidity flowage, also called a suspension or density current, is defined as a low-density (1.0 - 1.10 gm/cc), low-velocity (flow rate less than 6 knots) suspension of eroded sediment and water. A turbidity current is defined as a high-density (1.10 gm/cc or denser), high-velocity (flow rate greater than 6 knots) suspension of sediment and water which originated as a sediment slide and dispersed into a dense sediment and water suspension. Both phenomena are gravity-driven. Turbidity flowages have been observed from surface ships and submersibles in the vicinity of rivers with high sediment discharge. Turbidity currents, on the other hand, have never been observed, and their cause and effect are inferential and speculative. Because of the nature of turbidity

---

3.1/ K. R. Demars and D. G. Anderson, Environmental Factors Affecting the Emplacement of Seafloor Installation, Naval Facilities Engineering Command, October 1970, 84 pages.

current phoenomena, their occurence is highly controversial and not widely accepted."

The reference also discusses turbidity currents under "Evidence of Occurence" and "Probable Mechanism."

According to the literature, severe turbidity currents apparently will not occur at the pipeline location on the continental shelf, Figure 3.3.

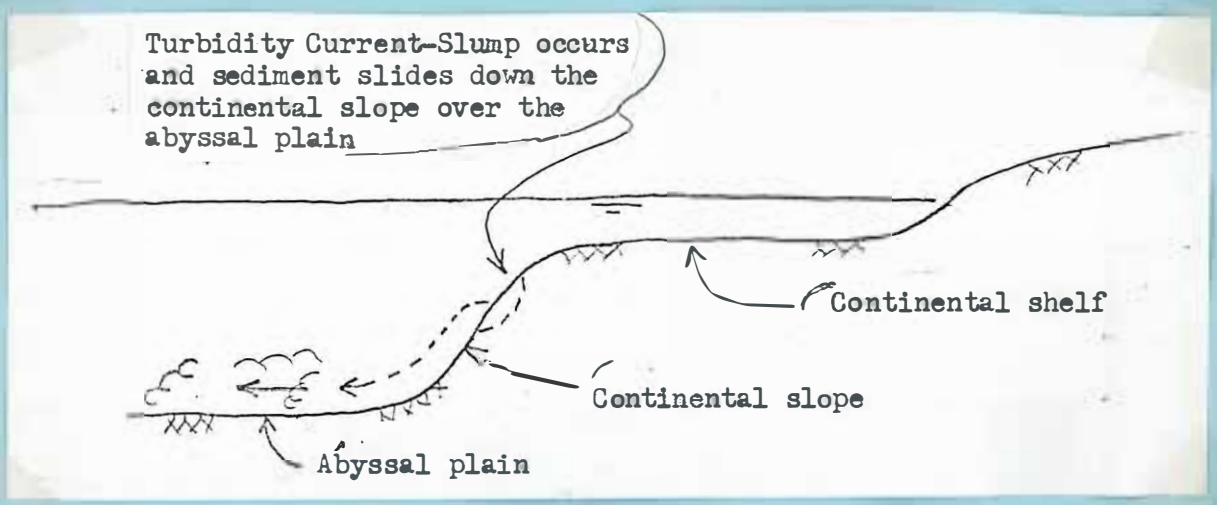

Figure 3.3 - Location of density currents with respect to the continental shelf

Turbidity currents are believed to be located mainly along the continental slope and dissipate outward on the abyssal plain. Possibly the slumps occur more readily near or at mouths of submarine canyons which may terminate on the continental slope. Steepness of the continental slope is in the range of 45°, thus encouraging sliding action.

Suspended sediment increases the fluid density. Turbid water could occur in the vicinity of rivers having high sediment discharge or be caused by extreme wave action stirring the ocean bottom. Discussion of turbidity currents and turbidity flows were found in the literature but the information was meager on the density of the sediment laden water. The density of turbidity currents which have occurred in Lake Mead were 1 to 10 percent greater than the surrounding fluid; but no useful information was found for density of turbid ocean water, Reference 3.2/.

3.2/ H. A. Einstein and R. L. Wiegel, "A Literature Review on Erosion and Deposition of Sediment Near Structures in the Ocean," U.S. Naval Civil Engineering Laboratory, Port Hueneme, California, February 1970, 183 pages.

Example Problem

A resultant buoyant force acting upon the conduit is computed for the condition of turbid water with 1 percent and 10 percent greater density than the surrounding ocean water. Assume conduit properties of the previous example,

Compute specific weight γ_t of turbid water

$\gamma_t = 1.01\ \gamma_s = (1.01)(64.22) = 64.86$ 1 percent

$\gamma_t = 1.10\ \gamma_s = (1.1)(64.22) = 70.64$ 10 percent

Using equation (1)

$$Frb = \frac{\pi}{4} D_o^2\ \gamma_t - \frac{\pi}{4} D_i^2\ \gamma_f - \frac{\pi}{4} (D_o^2 - D_i^2)\ \gamma_p$$

$$Frb = \frac{\pi}{4} (30.167)^2(64.86) - 44{,}115 - 884 = (714.8)(64.86) - 44{,}999$$

$Frb = 46{,}362 - 44{,}999 \approx 1360$ lbs/ft 1 percent

$Frb = (714.8)(70.64) - 44{,}999 \approx 5490$ lb/ft 10 percent

A 1 percent increase in specific weight of the fluid surrounding the pipe increases the resultant buoyant force by about 50 percent, and 500 percent for a 10 percent increase. For the buoyant concept density changes of this amount would substantially increase the load on the conduit support structures.

Consideration for the Buried Concept

Even though the conduit is buried, a buoyant force still acts upon the conduit. For example, assume the condition of the conduit buried in sand, Figure 3.4. The conduit is immersed in a fluid and a hydrostatic pressure acts upon the conduit. This hydrostatic pressure is caused by the water depth and equation (3.1) can be used to compute the resultant buoyant force due to water.

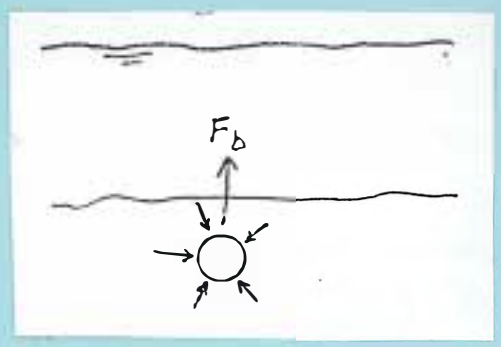

Figure 3.4 - Hydrostatic fluid pressure acts externally on the conduit producing a buoyant force. F_b.

Probably for the buried concept the pipe would be heavier than the buoyant concept pipe. The pipe weight (W_p) term of equation (3.1) is assumed larger than in the previous example problems ~~for the buoyant concept~~. Therefore the resultant force, Frb, would be negative or acting in a downward direction ~~(note the W_p term and sign convention of Figure 3.1)~~.

Liquefaction of the soil medium surrounding the conduit is a troublesome issue concerning buoyant force for the buried concept. ~~Liquefaction was defined in reference (C)~~. "The term 'liquefaction' has been applied to the process by which a saturated mass of soil is caused by external forces to suddenly lose its shearing strength and to behave as a fluid," reference 3.3. Thus when

---

3.3 (C) F. E. Richart, Jr., J. R. Hall, Jr., and R. D. Woods, "Vibration of Soils and Foundations, Prentice-Hall, Englewood Cliffs, New Jersey, 1970, Page 6-36.

liquefaction occurs, the specific weight for the medium surrounding the conduit is greater than that of ocean water. The fluid surrounding the pipe ~~now~~ has the weight of the soil particles adding to the specific weight of water.

The California Undersea Aqueduct is located in an area prone to earthquakes. Vibratory forces of earthquakes are known to cause liquefaction of submarine soils. Also there is a possibility that turbulence of water flowing in the conduit could vibrate the conduit, especially near conduit bends. Vibration of the conduit could liquefy the soil as shown in Figure 3.5 ~~4~~.

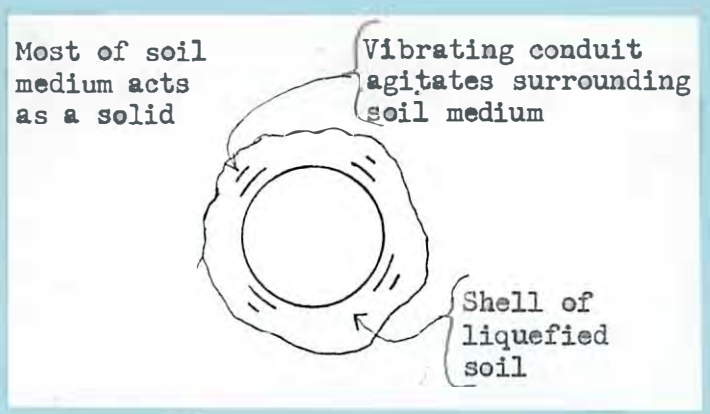

Figure 3.5 ~~4~~. - Envisioned liquefaction to a relatively small portion of soil medium surrounding the conduit.

In the pipeline industry the problem of pipelines in liquefied soils is termed "Pipeline Flotation". Reference 3.4 (~~D~~) notes - "Pipeline flotation is rapidly becoming a general term to cover all undesired motion of pipelines in saturated soils and sediments during and after laying." The report

---

3.4 (~~D~~) (Anonymous), ASCE Preliminary Research on Pipeline Flotation, Report of the Pipeline Flotation Research Council and R. A. Rait, Journal of the Pipeline Division, Vol 92, PL1, March 1966, pp 27-71.

concluded, "that violent agitation will form a liquid-like substance of soil and that objects such as pipelines will float or sink in the 'dense Liquid' depending on the object." Pipeline flotation tables of a "completely preliminary and tentative nature" ~~were~~ are given in ~~the~~ reference ~~(D)~~. Thus from these tables for 2-inch to 60-inch diameter pipes in various density soils, a range of ~~the~~ pipe weight could be determined where the pipeline was expected to neither rise nor sink.

One example of pipeline flotation was given in reference ~~(E)~~. The pipeline was situated in a trench excavated along the ocean bottom. Backfilling was left to the natural sedimentation processes. Later a storm of hurricane magnitude passed over the area. It was believed that under severe storm action sand was transported into the trench. The resulting pressure surges and oscillating velocity of the waves kept the sand in a liquefied state. The medium surrounding the pipe had an approximate specific gravity of 2.0. Roughly, a 3 mile length of the pipeline was floated ~~up~~ from the trench bottom to ~~an~~ the elevation ~~similar to~~ of the surrounding ocean bottom.

~~(E)~~ R. J. Brown, Soil Mechanics Important in Marine Pipeline Construction, The Oil and Gas Journal, pp 151-155, Sept. 16, 1957.

Example Problem

An example of ~~what~~ the resultant buoyant force that may act on a buried conduit is given for assumed conditions of liquefaction.

Steel pipe 2" thick with 2" thick covering of concrete, internal diameter of pipe is 30'. Compute Frb for buried conduit in liquefied sand with specific gravity = 2.0.

Given - γ steel, = 490 lb/ft^3, γ concrete = 150 lb/ft^3, γ liquefied sand = (2)(62.4) $\approx$ 125 lb/ft^3, diameters 30', 30' + 2" = 30.167', and 30' + 4" = 30.333'.

~~Use symbol notation of Figure 3.1~~

Weight steel pipe = $\frac{\pi}{4}$ $(30.167^2 - 30.0^2)(490) \approx$ 3870 lbs/ft

Weight concrete coating = $\frac{\pi}{4}$ $(30.333^2 - 30.167^2)(150) \approx$ 1180 lb/ft

W_p = 3870 + 1180 = 5050 lb/ft

Weight fresh water in pipe W_f = 44,115 lb/ft $\approx$ 44,120 lb/ft
(from first buoyant force example problem)

$F_b = \frac{\pi}{4}(30.333)^2(125)$ = 90,330 lbs/ft

Frb = $F_b - W_f - W_p$ = 90,330 - 44,120 - 5050 = 41,160 lb/ft (UPWARD)

Consideration for the Partially Buried Concept

If soil liquefaction occurs for the partially buried conduit then the buoyant force F_b, as noted in Figure , is composed of two parts. The two parts of the buoyant force F_b are shown in Figure .

$$F_b = F_{b1} + F_{b2} \qquad A_1 + A_2 = \frac{\pi}{4} D_o^2$$

$$F_{b1} = \gamma_1 A_1 \qquad F_{b2} = \gamma_2 A_2$$

F_b = buoyant force due to the weight of the two displaced fluids, lb/ft

F_{b1} = part of the buoyant force due to the conduit immersed in liquefied soil, lb/ft

F_{b2} = part of the buoyant force due to the conduit immersed in salt water, lb/ft

A_1 = area of conduit immersed in the liquefied soil, ft^2

A_2 = area of conduit immersed in salt water, ft^2

D_o = outside pipe diameter, ft

γ_1 = specific weight of liquefied soil, lb/ft^3

γ_2 = specific weight of salty ocean water, lb/ft^3

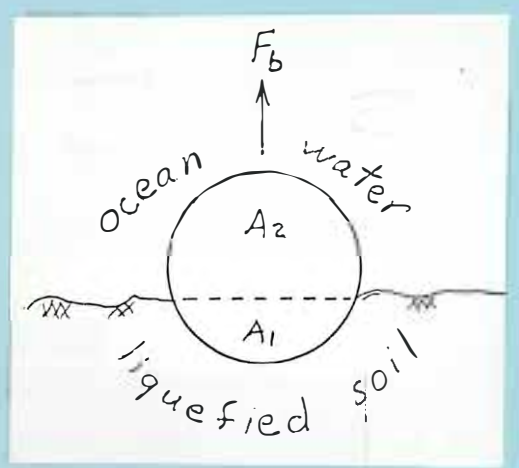

Figure - Explanation of buoyant force in a two liquid medium.

Depending on the combination of pipe weights and buoyant forces, the conduit will rise or sink in the liquefied soil. Using the notation of Figure 3.1,

if $F_b > W_f + W_p$ the conduit will rise,

if $F_b < W_f + W_p$ the conduit will sink,

and if $F_b = W_f + W_p$ the conduit is at equilibrium and ~~is considered~~ WOULD floating in the liquefied soil.

Consideration of Fouling - Buoyant Concept

A definition of marine fouling ~~was~~ IS given in reference 3.6. "Fouling is a term applied to assemblages of animals and plants when they grow on artificial structures instead of naturally occurring rocks, stones, and other objects." Consequences due to fouling were noted, "The accumulation of colonies of barnacles and mussels (specific gravities 1.2 to 1.4) on buoys can eventually sink a floating device unless sufficient extra positive buoyancy is allowed." Thus fouling is a hazard of unknown extent for the buoyant concept.

~~There was not conclusive~~ Reliable data about weights and thickness of marine fouling, or depths at which it ~~that~~ occurs, are incorrect. ~~in marine fouling.~~ Figure 3.6 ~~showed~~ shows that the greatest weight (lb/ft^2) ~~was~~

3.6 Kreppert, E. G. and Clark, F. N., The Possible Effects of a Proposed Undersea Aqueduct on Marine Ecology and of the Marine Environment on the Aqueduct, Marine Advisors, Inc., La Jolla, California, February 1969, p 57.

occurs ^ in the upper 30 feet of water, and that fouling ~~occurred~~ has been experienced 450 feet below the water surface. Other examples of fouling weights ~~were~~ are given:

1. "Under conditions more favorable to fouling than the aqueduct design conditions, as much as 5 or 6 pounds of barnacles may collect on a square foot of surface in less than a year."

2. The maximum rate of mussel accumulation is 11 pounds/square foot/year; and the maximum weight recorded is nearly 26 pounds per square foot during a 35 month period.

3. "Thickness of mussel fouling on navigation buoys is occasionally great as one foot."

4. "At a depth of 130 feet at its lower end, a 32-foot-long, 20-inch-diameter cyclinder with 700 pounds of positive buoyancy was moored one mile offshore from Point Mugu, California, in a water depth of 500 feet. Three years and two months after installation, the growth accumulated during submergence was identified." Names of the various growths, ~~were given,~~ and in some cases growth dimensions, ~~These dimensions~~ were given — barnacle (up to 2 inches in diameter at base), sponge (up to 3 inches in height), jingle shells (up to 4 inches in diameter), sea anemones (some up to 5 inches in diameter at the base), and scallops (some up to 5 inches in diameter).

At the initial installation of the proposed aqueduct the outside pipe surface will be smooth. Soon the outside surface will become rough due to fouling. Therefore, the outside pipe surface must be considered as a "rough surface" when making drag force computations. From the above item 4, it is expected that roughness projections will be in the order of 6 inches.

The fouling weight that will occur in a given time period for the buoyant concept is a matter of conjecture. The best information appears to be from the above item 4. In this case the surface area is 168 square feet and the fouling weight is 700 lbs/168 ft^2, for a 3 year time period. If the conduit is located at deeper depths (200 to 400 feet), the expected growth weight would be less.

An example illustrating loss of buoyancy for a 30-foot diameter pipe with a 5 lb/ft^2 fouling weight is given.

$(\pi 30)(5) = 470$ lb/ft

This value would be subtracted from Frb of equation (3.1).

SECTION 4

FRICTION HEADLOSS AND FORCE ON THE CONDUIT

Introduction

A boundary such as the inside and outside walls of the conduit, resists the flow of water. The boundary causes a shearing stress on the water and a tangential friction force results on the boundary.

Formulas are given - (1) for computing headloss through the pipe (2) for computing power needed to maintain flow inside the pipe, and (3) for computing the friction force, both inside and outside of the pipe, caused by water flowing parallel with the pipe.

Formula for Computing the Headloss

The headloss is defined by the Darcy-Weisbach equation (1),

$$h_f = \frac{fLV^2}{D2g} \qquad (1),$$

where h_f = headloss for conduit length L, feet of water

f = dimensionless friction factor, obtained from Engineering Monograph No. 7 (Figure 1) 1/

L = length of the conduit, ft

D = inside diameter of the conduit, ft

V = average velocity of water flowing in the conduit, ~~(Q/A, pipe discharge Q divided by internal pipe area A)~~, ft/sec

g = acceleration of gravity (32.3), ft/sec^2

1/ USBR, Friction Factors for Large Conduits Flowing Full, Engineering Monograph 7, 1965, 67 pages.

$\frac{V^2}{2g} = H_v$, the velocity head in the pipe, ft

Determining the Friction Factor "f"

Difficulty is encountered in selecting an appropriate value for the friction factor f for equation (1). Diagrams giving the value of the friction factor are available. Generally these diagrams were prepared from laboratory tests on operating pipe lines. The majority of these test data are for small diameter pipes as compared to the proposed 30-foot diameter Aqueduct. Engineering Monograph No. 7 gives data for large conduits, but there is a scarcity of information in the range of 30-foot diameter conduits. Figure 4.1

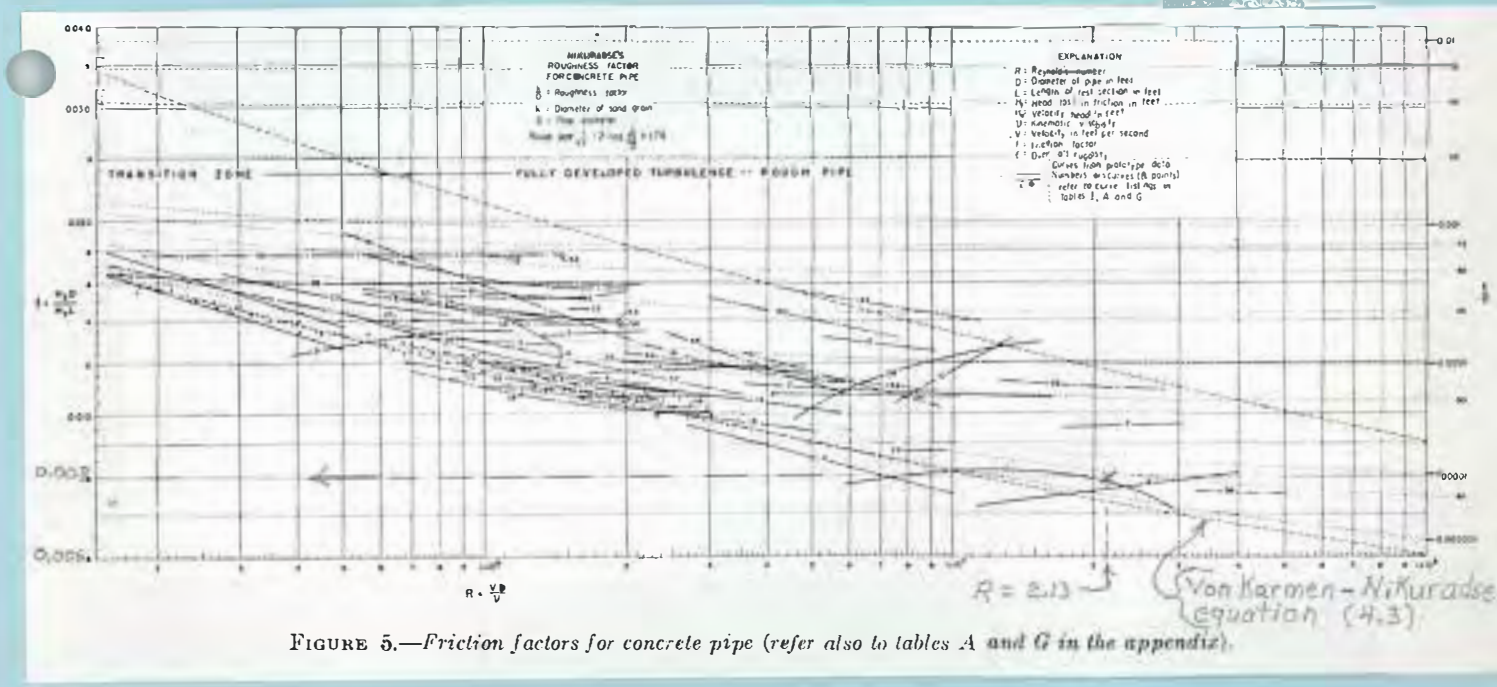

FIGURE 5.—*Friction factors for concrete pipe (refer also to tables A and G in the appendix).*

Figure 4.1 - Friction Factor Diagram 4.1/

4.1

Values of the friction factor f are listed at the left side of the diagram, the Reynolds Number R at the bottom, and the ε/D ratio at the right side. The Reynolds Number R and the ε/D ratio must be calculated to use the diagram to find f,

$$R = \frac{VD}{\nu} \text{ and } \varepsilon/D$$ (~~this ratio is~~ also defined as "relative roughness"),

where R = Reynolds Number, dimensionless

V = average velocity of water flowing in the conduit, ft/sec

ν = kinematic viscosity of fresh water in the conduit, ft^2/sec (see Section 2/

ε = rugosity, ft

D = inside diameter of the conduit, ft

Values for most of the above symbols are determined by specified conditions of the problem. Selecting a rugosity value requires the use of "engineering judgement." Roughness, such as small projections from the internal pipe wall and spacing of these projections, influence the rugosity value. Roughness increases with age of the pipe as incrustations form on the pipe walls after years of operation. Should this occur on the California Undersea Aqueduct cleaning the pipe walls to preserve the capacity may prove economically feasible.

A smooth-walled pipe is desired to minimize friction loss. ~~Rugosity values for smooth pipe are given on pages 28 and 29 of Engineering~~

~~4.17 op cit~~

~~Monograph No. 7.~~ a ~~The~~ range of rugosity values ~~(0.00003 ft ≤ ε ≤ 0.0002 ft)~~ for steel and concrete listed at the ~~bottom portion~~ of the ~~pages 28 and 29 represent smooth~~ pipe, are given in Engineering Monograph No. 7.

Use of the Friction Factor Diagram and Headloss Computation

Assumed conditions for the example are as follows:

$D = 30$ ft

$V = 10$ ft/sec

$\varepsilon = 0.000120$ ft

T = temperature of the water, 50° F

$L = 1000$ ft

from Section 2, $\nu = (1.41)10^{-5}$ ft^2/sec

$$R = \frac{VD}{\nu} = \frac{(10)(30)}{(1.41)10^{-5}} = (2.13)10^7$$

$$\frac{\varepsilon}{D} = \frac{0.000120}{30} = 0.000004$$

Entering the diagram of Figure 4.1 with $R = (2.13)\ 10^7$ and $\varepsilon/D = 0.000004$ the value of $f = 0.008$ is obtained. Using equation (4.1)

$$h_f = \frac{fLV^2}{D2g} = \frac{(0.008)(1000)(10)^2}{(30)(2)(32.2)} = 0.414 \text{ ft.}$$

In this example problem there would be 0.414-foot friction headloss along a 1000-foot length of the conduit

Establishing a Minimum Value for the Friction Factor

Pipes constructed of plastic materials or having coatings of plastic materials have a very smooth internal wall surface. Surface roughness is small and relative to the diameter of large pipes may be assumed negligible. The Von Karmen-Nikuradse equation (3), for smooth-walled pipes and Reynolds numbers greater than about 3000,

$$\frac{1}{\sqrt{f}} = 2 \log_{10} R\sqrt{f} - 0.8 \quad (4.3),$$

may be used for computing the friction factor. This friction factor should be considered a minimum.

For conditions of the example problem where $R = (2.13)\ 10^7$ and assuming a smooth-wall pipe, equation (2) gives $f = 0.0073$. A "trial and error" method was used in solving for f in equation (3).

Power Needed to Maintain Flow Inside the Conduit

Power is required to force the water through the pipe and maintain a given velocity. This power must equal the headloss and represents the tangential force on the pipe. The power, in units of horsepower, can be computed from equation (2),

$$P_{hp} = \frac{Q\gamma h_f}{550} \quad (2),$$

where P_{hp} = horsepower needed for pipe length L (the L of equation (1))

Q = pipe discharge, ft^3/sec

γ = specific weight of water, lb/ft^3 (see section 2)

h_f = headloss from equation (1), ft

500 = conversion factor, $\frac{ft\text{-}lb/sec}{hp}$

The horsepower used in transporting the water through a 1,000-foot conduit length is computed using equation 4.3. Use h_f = 0.414 foot, from problem "Example Use of the Friction Factor Diagram and Headloss Computation."

$$Q = VA = V\frac{\pi D^2}{4} = (10)\frac{(\pi 30^2)}{4} = 7070 \text{ ft}^3/\text{sec}$$

γ = 62.4 lb/ft^3, from section 2

$$P_{hp} = \frac{Q\gamma_{hf}}{550} = \frac{(7070)(62.4)(0.414)}{550} = 332 \text{ hp}$$

Formula for Computing the Internal Friction Force

The friction force that the pipe exerts on the flowing water is in the opposite direction of the flowing water. Equations for computing the friction force F_i are derived in Figure 4.2:

$$F_i = \frac{\pi\rho f L D V^2}{8} \qquad (4.4a) \qquad F_i = A\gamma h_f \qquad (4.4b)$$

The direction of F_i shown in Figure 4.2 is for the reaction of the pipe and will be transferred to the support structure, Figure 4.3a.

For the buoyant concept where the pipe can move, the friction force should be considered as acting in the direction of the flowing water, as illustrated in Figure 4.3b.

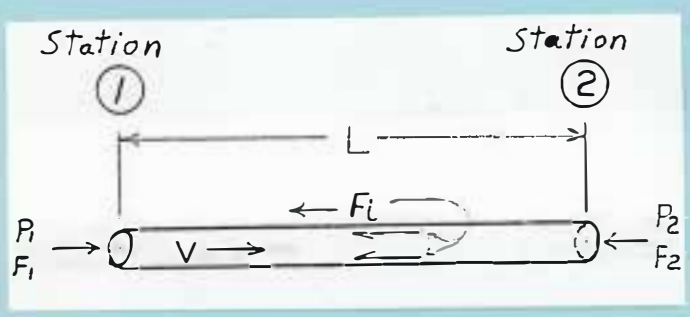

Free-body diagram for pipe of length L

Subscripts refer to ends of pipe in the free-body diagram

$F_1 = P_1A \quad F_2 = P_2A$

Pressure drop from Station 1 to 2

$\gamma h_f = \Delta p = P_1 - P_2$

$\Delta p = \gamma h_f = (\gamma)\frac{fLV^2}{D^2g}, \quad \rho = \frac{\gamma}{g}$

D2g

$\Delta p = \rho f \frac{LV^2}{2D}$

Fi

$F_1 = Fi + F_2$

$Fi = F_1 - F_2 = P_1A - P_2A = A(P_1 - P_2) = A(\Delta P) = \frac{\pi D^2}{2}\left(\frac{\rho f L V^2}{2D}\right)$

Fi

$Fi = \pi\rho \frac{fLDV^2}{8}$ (4.4a) or $\overline{Fi} = A(\Delta p) = A\gamma h_f$ (4.4b)

Symbol Notation

γ = specific weight water, lb/~~sec~~ ft^3 ~~(See sec)~~

ρ = density fresh water, $\frac{\text{lb-sec}^2}{\text{ft4}}$ ~~(See sec)~~ pound ft^4

g = acceleration of gravity, ft/sec^2

L = length of pipe, ft

D = diameter of pipe, ft

A = pipe area, ft^2

P = pressure, lb/ft^2

Fi = friction force the pipe exerts on water flowing through pipe, lb

F_1, F_2 = force acting on ~~each~~ ends of free body diagram, lbs.

h_f = headloss, ft (equation 4.1)

f = friction factor, dimensionless, (Figure 4.1)

V = average velocity, ft/sec

Figure 4.2 - Derivation of equation 4.4

Using equation (4) and conditions from the example problem:

D = 30 ft f = 0.008 (dimensionless)

V = 10 ft/sec ρ = 1.94 lb-sec^2/ft^4

L = 1000 ft

The force tending to move the pipe would be

$$F_i = \frac{\pi \rho f V^2 L D}{8} = \frac{\pi (1.94)(0.008)(10^2)(1000)(30)}{8} = 18{,}280 \text{ lbs.}$$

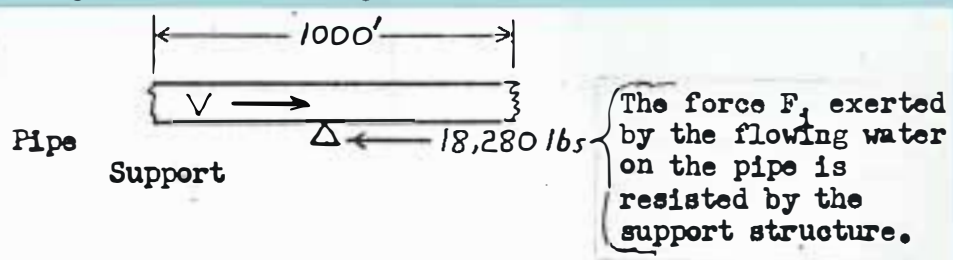

Figure 4.3a - **Reaction of the support structure**

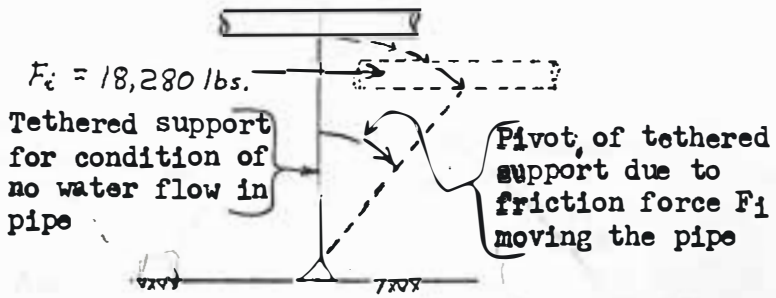

Figure 4.3b - **Consideration of the friction force F_i for the Buoyant Concept**

Figure 4.3 - Effect of the friction force

Formula For Computing the External Friction Force

A friction force, parallel with the pipe, occurs on the outside surface when ocean currents have a velocity component along the pipe. For a given ocean current this friction force is probably the greatest when the direction of the ocean current is parallel with the pipe. Formulas

for computing this friction force are not readily available; especially if the velocity is at an angle with the conduit.

Various assumptions were made and an equation was developed which gives some measure of the friction force. For a given length L of pipe the external friction force is given by equation (4.5).

$$F_o = (0.13)\, V^2 D^{2/3} L \qquad (4.5)$$

where F_o = friction force pipe exerts on ocean water flowing parallel to pipe, lbs

V = velocity of ocean water flowing parallel to pipe, ft/sec

D = outside pipe diameter, ft

L = length of pipe, ft

Friction force on the outside surface, Figure 4.4, was assumed similar to that on the inside surface, Figure 4.2.

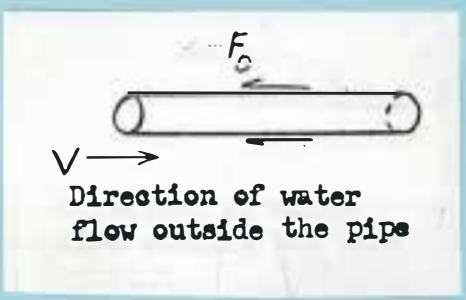

Figure 4.3 - Flow conditions outside the pipe

Equation (4.4a) is assumed to give a measure of this force. The friction factor value can be estimated from the following relationship; but there is considerable question of how to define the hydraulic radus (R) for the outside of the pipe.

$$f = \frac{8g\,n^2}{(1.49)^2\, R^{1/3}} \qquad (4.6)$$

where g = acceleration of gravity, ft/sec^2

n = Manning's n

R = hydraulic radius, ft.

The outside pipe surface will be rough because of marine fouling. Roughness heights of approximately 6 inches can be expected. Since the roughness (6 inch projections) has a similarity to the cobblestone channel, assume Mannings n = 0.030. Substituting n = 0.030 and equation 4.6 into equation 4.4a, equation 4.5 was obtained.

$$F_o = \frac{\pi \rho f L D V^2}{8} = \frac{\pi \rho L D V^2}{8} \quad \frac{8gn^2}{(1.49)^2 R^{1/3}}$$

$$F_o = (0.13)\, V^2 D^{2/3}\, L \qquad (4.5)$$

$$\rho = \frac{\gamma}{g} \text{ and } \gamma = 64.4$$

for pipe the hydraulic radius R is D/4.

For example:

Let V = 2 fps

D = 30 + 2(.5) = 31 ft.

L = 1000 ft

$F_o = (0.13)(2)^2(31)^{2/3}(1000)$

$F_o = 0.52 \times 9.9 \times 1000 \approx 5150$ lbs.

per thousand feet of pipe.

Section 5

INTERNAL HEADLOSS AND FLUID FORCES OF CONDUIT BENDS

Introduction

Bends in the conduit produce an eddy-type headloss in addition to the wall function. Pipe bends also resist forces produced by the turning of fluid. In this section formulas are given to compute headloss for bends and the fluid force exerted upon the bend.

Bend Headloss Formula

There are two types of headloss occurring within a conduit bend. One is a friction-type headloss (h_f) and the second is a form headloss (h_b) caused by the shape of the bend. The form headloss (h_b) is computed from equation (1)

$$h_b = \frac{CV^2}{2g} \qquad (5.1),$$

where h_b = headloss in feet of water, ft

C = dimensionless loss coefficient

V = average velocity of water flowing in conduit, ft/sec

g = acceleration of gravity, 32.2 ft/sec^2

The total headloss h_t occurring in the bend is

$$h_t = h_f + h_b \qquad (5.2),$$

where h_f is the friction headloss computed using the pipe length along the centerline of the bend, and the form headloss.

$$h_t = \frac{fLV^2}{Dzg} + C\frac{V^2}{2g} \qquad (5.3)$$

42

Value for the Loss Coefficient C

Values for the loss coefficient C have been determined from experimental tests. This C value can vary depending upon geometry of the bend. The value of C for form loss only for 90° bends is given in Figure 5.1. It is recommended that the "Smooth Pipe" curve of Figure 1 be used, because the conduit diameter is large and the anticipated ε/D ratio approaches that of a smooth pipe.

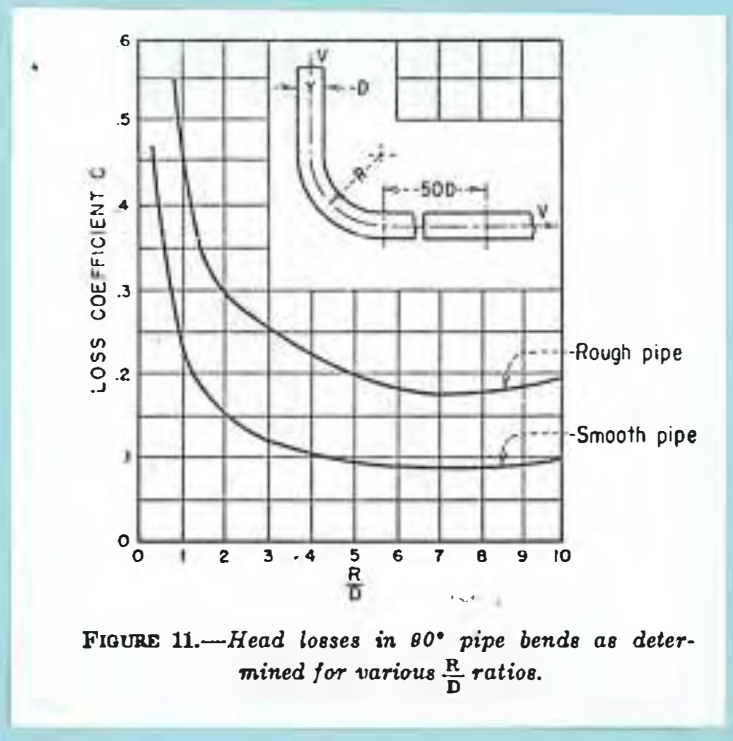

FIGURE 11.—*Head losses in 90° pipe bends as determined for various* $\frac{R}{D}$ *ratios.*

Figure 5.1. Taken from Water Resources Technical Publication Engineering Monograph No. 3, Welded Steel Penstocks. U.S. Department of Interior, Bureau of Reclamation, 1967, page 11.

If the bend angle is less than 90° Figure 5.2 should be used to obtain the headloss coefficient C.

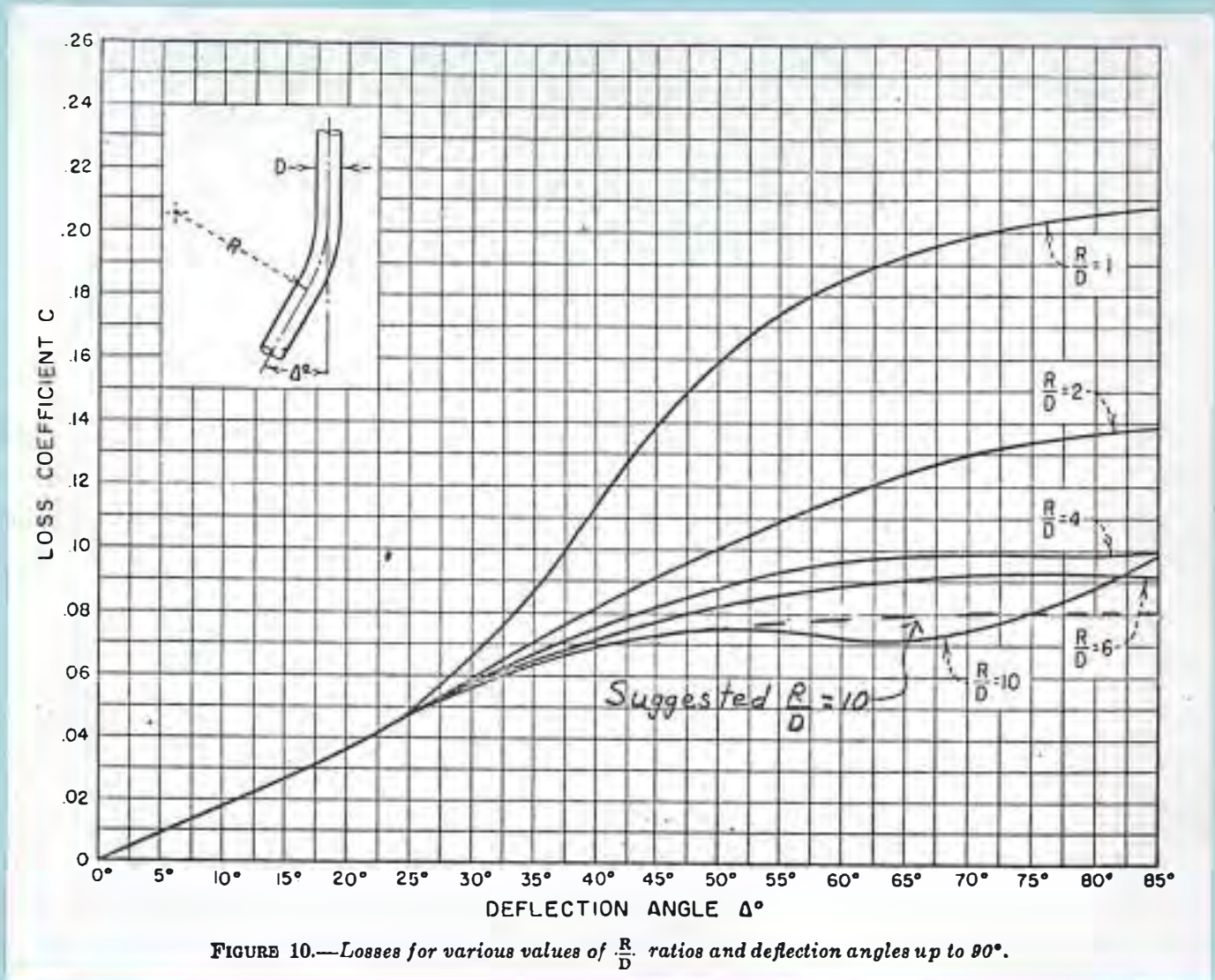

FIGURE 10.—*Losses for various values of $\frac{R}{D}$ ratios and deflection angles up to 90°.*

Figure 5.2 Taken from Water Resources Technical Publication Engineering Monograph No. 3, Welded Steel Penstocks, U.S. Department of Interior, Bureau of Reclamation, 1967, page 10. The R/D = 10.curve of the original figure was altered by authors of this report (Hydrodynamic Loading, California Undersea Aqueduct.)

Available information does not show the R/D ratio at which the form headloss (h_b) is significant when compared with the friction headloss (h_f). In reference (A) the loss coefficient C for R/D > 10 approximated the lower portion of the curve shown in Figure 5.1. Therefore, for the range of $10 \leq R/D \leq 20$, C = 0.08 is recommended for use in equation (1). For values of R/D > 20 it is suggested that the form headloss (h_b) should be neglected and only the friction headloss (h_f) should be used for the bend.

Value of C for Miter Bends

Miter bends could be used for curving the conduit alignment. One proposal (B) suggested slightly angled flanges on the pipes. The pipes 400 feet long would have the flange at a small offset angle from the perpendicular of the pipe centerline. Thus a miter is formed at each pipe connection. The angle of the miter bend would be α and the angle of the flange $\alpha/2$ (see definition sketch). The angle range of the suggested miter (α) is and 1° 40' to 3°.

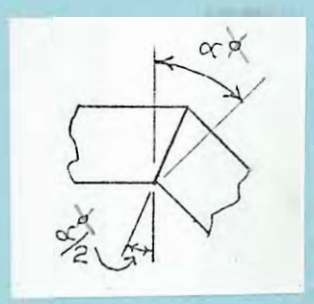

Miter bend definition sketch

(A) Mecher, W. A., Discussion of "Factors Influencing Flow in Large Conduits", ASCE Journal of Hyd. Div., Vol. 92, No. HY4, July 1966, page 207.

(B) Litton Systems AMTD, Ocean Environment and Design Considerations in a Prereconnaissance Study of a California Aqueduct, June 1969, page 3-110.

Values of the loss coefficient were not found for miter bends of such small angle. However, in reference (5.3 C) values for loss coefficient of miter bends from 5° to 90° were listed for smooth and rough pipes. This data is given below and plotted on Figure 5.3. Smooth pipe data is believed

Loss Coefficient for Miter Bends

α	5°	10°	15°	22.5°	30°	45°	60°	90°
Smooth	0.016	0.034	0.042	0.066	0.130	0.236	0.471	1.129
Rough	0.024	0.044	0.062	0.154	0.165	0.320	0.684	1.265

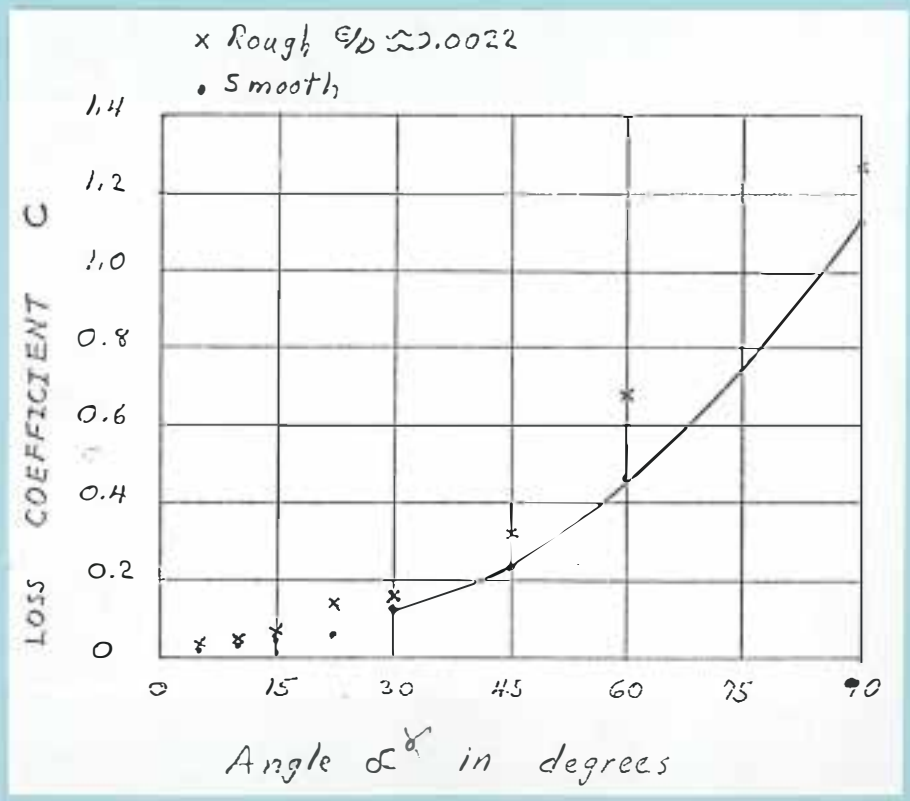

Figure 5.3 - Plot of Loss Coeficients from Table

to represent aqueduct conditions better than the rough pipe data. The

e/ Hydraulic Institute, Pipe Friction Manual, Third Edition, 1961, page 32.

curve drawn through data points for large angles shows the loss coefficient apparently varying by a power of the angle α. To obtain a loss coefficient for small miter bends the data of the five smallest angles, Figure 5.3, were plotted and a curve fitted through the data points, Figure 5.4.

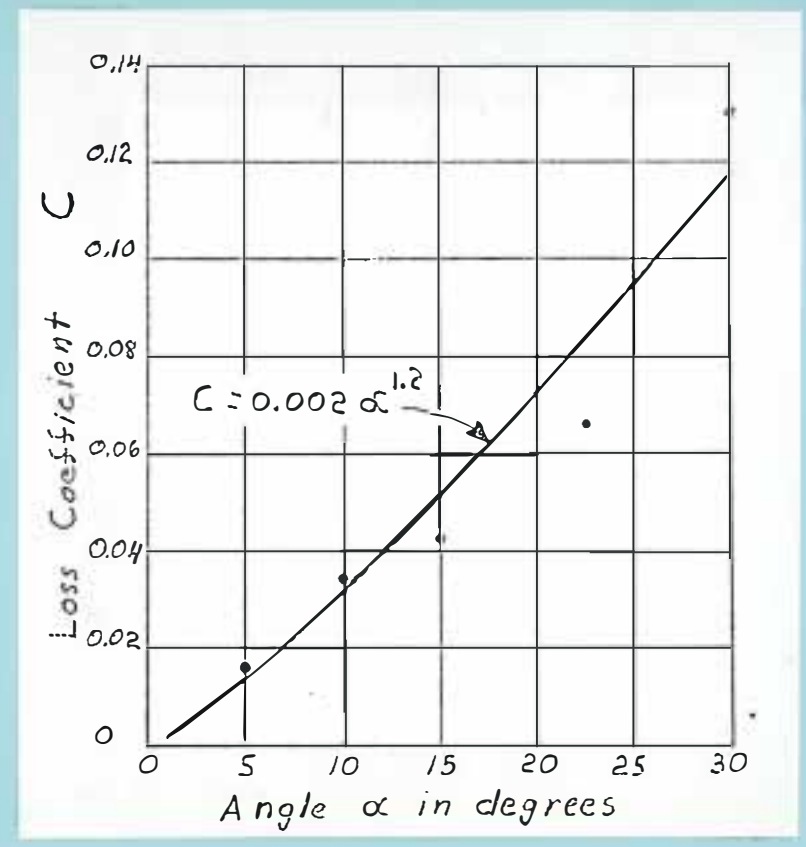

Figure 5.4 - Curve fit through loss coefficient data points of smaller angle miter bends.

Equation (3) may be used to compute the form headloss for miter bends,

$$C = 0.002\ \alpha^{1.2} \qquad (5.3),$$

where α is the angle shown in the definition sketch.

~~Headloss~~ Example Problems

Assume D = 30 feet, V = 10 ft/sec, f = 0.008, and compute the total headloss (h_t) for:

(1) R/D = 1 and $\Delta = 90°$.

(2) R/D = 7 and $\Delta = 65°$.

(3) Use 400-foot length pipes with a 1-1/2° flange angle to make a 90° bend ($\Delta = 90°$); ~~from definition sketch details of the miter bend~~ $\alpha/2 = 1\text{-}1/2°$ and $\alpha = 3°$.

(4) Use 400-foot length pipes, 5° angle flange to make $\Delta = 90°$.

(5) Compare headloss of bends for (3) and (4).

(1) The total headloss from point A to B on the conduit, equation (2)

$$h_t = h_f + h_b$$

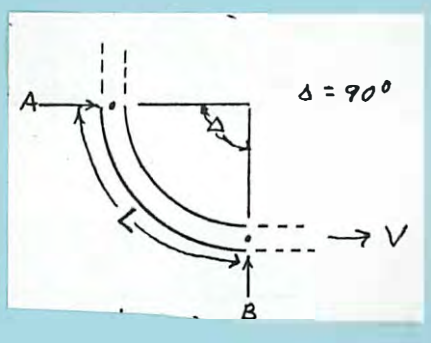

From Figure 1, C = 0.23, and equation (1)

$$h_b = \frac{CV^2}{2g} = \frac{(0.23)(10^2)}{(2)(32.2)} = 0.36 \text{ ft.}$$

Since R/D = 1, R = D and $L = \frac{90}{360}(2\pi R) = \frac{180}{360}\pi D = \frac{\pi D}{2}$, and by equation (1), Section 4,

$$h_f = f\frac{L}{D}\frac{V^2}{2g} = (0.008)\left(\frac{\frac{\pi D}{2}}{D}\right)\frac{(10^2)}{64.4} = 0.02 \text{ ft}$$

$$h_t = h_f + h_b = 0.02 + 0.36 = 0.38 \text{ ft.}$$

(2) From Figure 2, C = 0.088

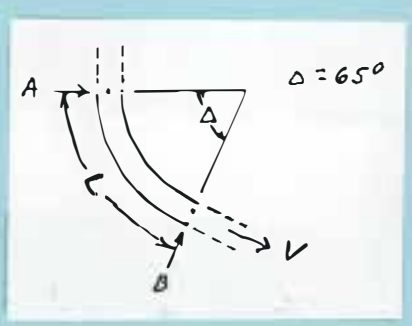

$$h_b = C \frac{V^2}{2g} = (0.088) \frac{(10^2)}{64.4} = 0.14 \text{ ft}$$

R/D = 7 and R = 7D, $L = \frac{65}{360} (2\pi R)$

$$L = \frac{65}{360} \; 2\pi 7D = 7.94 \; D \neq \text{~~7.94 D~~}$$

$$h_f = f \frac{L}{D} \frac{V^2}{2g} = (0.008) \frac{(7.94 \; D) \; (10^2)}{D \qquad 64.4} = 0.10 \text{ ft}$$

$$h_t = h_f + h_b = 0.10 + 0.14 = 0.24 \text{ ft}$$

(3) For 1-1/2° flanges and 3° miter ~~bends~~ ~~it~~ would ~~take~~ 30 lengths of pipe to make the 90° bend. Of the pipe joints 29 would be 3° miter ~~bends~~ and 2 (first and last) would ~~be~~ 1-1/2° miter ~~bends~~.

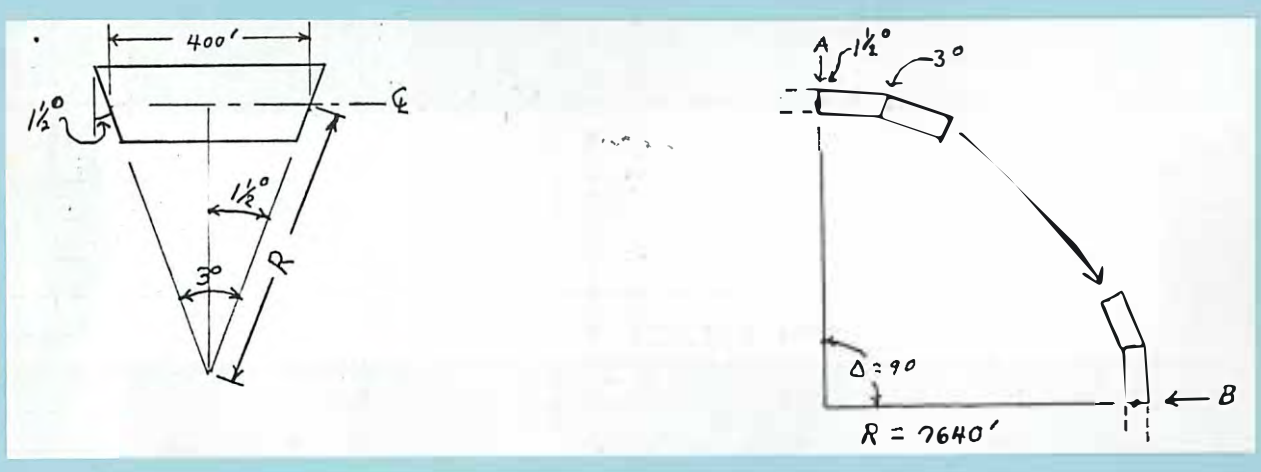

$$R = \frac{\frac{400}{2}}{\sin 1\text{-}1/2^\circ} = \frac{200}{0.02618} \approx 7640 \text{ ft}$$

Using equation (3) $C = 0.0002 \; \alpha^{1.2}$

$C = (0.002)(3)^{1.2} = 0.0075$ for 3° miter bend

$C = (0.002)(1.5)^{1.2} = 0.0024$ for 1-1/2° miter bend

(3) Continued

Accumulative C for 29 3° miter sections and 2 1-1/2° miter sections

$$29 \times 0.0075 = 0.218$$

$$2 \times 0.0024 = \underline{0.005}$$

$$C = 0.223$$

$$h_b = C \frac{V^2}{2g} = (0.223) \frac{(10^2)}{64.4} = 0.35 \text{ ft}$$

$$L = 400 \times 30 = 12{,}000 \text{ feet}$$

$$h_f = f \frac{L}{D} \frac{V^2}{2g} = (0.008) \frac{(12{,}000)}{30} \frac{(10^2)}{64.4} = 4.97 \text{ ft}$$

$$h_t = h_f + h_b = 4.97 + 0.35 = 5.32 \text{ ft}$$

(4) For 5° flanges and 10° miter sections there be 9 lengths of pipe to make the 90° bend. Of the pipe joints 8 would be 10° miter sections and 2 5° miter sections.

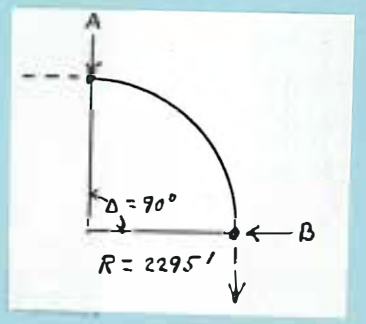

$$R = \frac{\frac{400}{2}}{\sin 5^\circ} = \frac{200}{0.08716} \approx 2295 \text{ feet}$$

$$C = 0.002\ (10)^{1.2} = 0.0317$$

$$C = 0.002\ (5)^{1.2} = 0.0138$$

Accumulative C for 8 10° miter bends and 2 50° miter bends

$$8 \times 0.0317 = 0.254$$

$$2 \times \underline{0.0138 = 0.028}$$

$$C = 0.282$$

$$h_b = C\frac{V^2}{2g} = (0.282)\frac{(10^2)}{64.4} = 0.44 \text{ ft} \qquad L = 400 \times 9 = 3600 \text{ ft}$$

$$h_f = f\frac{L}{D}\frac{V^2}{2g} = (0.008)\frac{(3600)}{30}\frac{(10^2)}{64.4} \qquad h_f = 1.49 \text{ ft}$$

$$h_t = h_f + h_b = 1.49 + 0.44 = 1.93 \text{ ft}$$

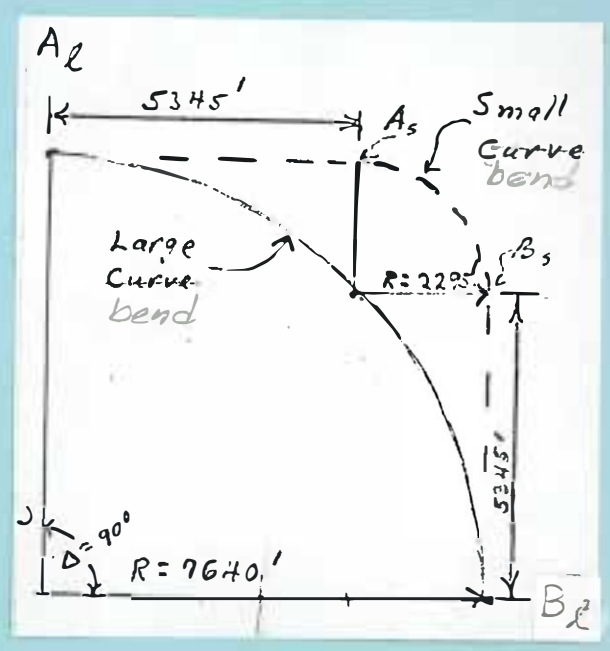

(5) The curve with 10° miter sections has the smallest headloss. However, the small radius curve does not traverse the same distance as points Aℓ and Bℓ of the large radius curve. To make a comparison between large and small bends the headloss for two 5345-foot lengths must be accounted for.

$$L = 2 \times 5345 = 10{,}690 \text{ feet}$$

$$h_f = f\frac{L}{D}\frac{V^2}{2g} = (0.008)\left(\frac{10{,}690}{30}\right)\left(\frac{10^2}{64.4}\right) = 4.43 \text{ ft}$$

This friction loss of 4.43 feet must be added to the small bend loss for comparison with the large bend.

$$1.93 + 4.43 = 6.36 \text{ ft (small bend)}$$

$$-5.32 \text{ ft (large bend)}$$

$$1.04 \text{ ft}$$

Thus, for the distance between points A and B the small bend has a 1.04-foot greater headloss than the large bend.

Fluid Forces Acting on the Bend

There are three fluid forces (pressure, momentum, and friction) acting on a bend, Figure 5.5. Fluid pressure forces, F_{p1} and F_{p2}, act on the end of a bend. The flowing water has momentum in the direction of flow and exerts a force F_m upon the bend when the flow direction is changed. There is also a friction force F_c which in many cases is negligible. However, for the buoyant condition, forces can move the conduit and the friction force F_c should be computed to determine the possibility of movement.

These fluid bend forces are of two different types, one static and one dynamic. The pressure force F_p is a static force and occurs whether water is still or moving within the conduit. The dynamic forces of momentum F_m and friction F_c occur only when water is flowing within the conduit. When considering the buoyant concept, the effect of the static and dynamic forces must be separated. This separation will be discussed after introducing the bend force formula.

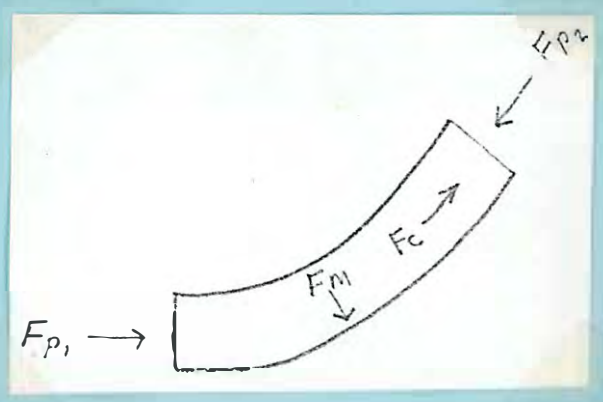

Figure 5.5 - Fluid forces acting on a bend.

Formulas for Bend Forces

In reference (D) a development of equations for the bend force is given; however the friction force F_c is excluded. Symbols that appear in the equations are shown in Figure 5.6. The subscript 1 refers to conditions at the entrance of the bend and subscript 2 at the exit of the bend,

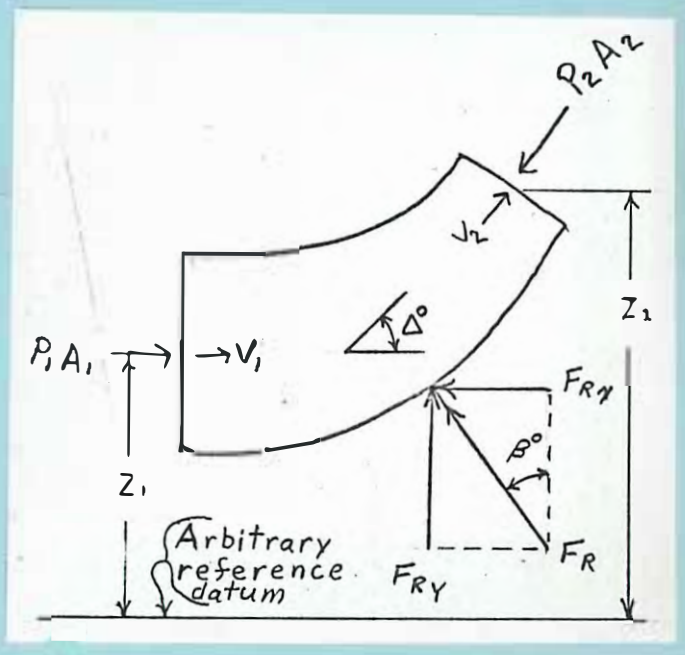

Figure 5.6 - Relation of symbols used in bend force equations

(D)/ R. C. Binder, Fluid Mechanics, Second Edition, Prentice-Hall, 1949, pg 154-155.

where Q = discharge, ft^3/sec

ρ = density, $lb\ sec^2/ft^4$

P_1, P_2 = pressure, lb/ft^2

A_1, A_2 = flow area, ft^2

V_1, V_2 = average velocity, ft/sec

F_R = resultant force of the bend on the fluid, with components F_{Rx} and F_{Ry}, lbs. (F_{Rx} and F_{Ry} is a total force and includes the static and dynamic force.)

Equations for forces F_{Rx}, F_{Ry}, and F_R are given below. The correspondence of terms in the equations to forces of Figure 5.5 are $F_{P1} = P_1A_1$, $F_{P2} = P_2A_2$, and $F_M = Q\rho(V_2\cos\Delta - V_1)$.

$$F_{Rx} = P_1A_1 - P_2A_2\cos\Delta - Q\rho(V_2\cos\Delta - V_1) \qquad (5.4)$$

$$F_{Ry} = P_2A_2\sin\Delta + Q\rho V_2\sin\Delta \qquad (5.5)$$

$$F_R = \sqrt{F_{Rx}^2 + F_{Ry}^2}\ , \qquad (5.6)$$

and the angle β can be found from

$$\tan\beta = \frac{F_{Rx}}{F_{Ry}} \qquad (5.7)$$

For conditions of a reducing bend where $P_1 \neq P_2$, $A_1 \neq A_2$, and $V_1 \neq V_2$ equations 8 and 9 can be used for determining values which may be unknown at the entrance and exit of the bend.

$$Q = V_1A_1 = V_2A_2 \qquad (5.8)$$

$$\frac{P_1}{\gamma} + \frac{V_1^2}{2g} + Z_1 = \frac{P_2}{\gamma} + \frac{V_2^2}{2g} + Z_2 \qquad (5.9)$$

ρ = specific weight water, lb/ft^3 (See Section 2)

g = acceleration of gravity (32.2), ft/sec^2

Z_1, Z_2 = entrance and exit centerline elevation above an arbitrary datum, ft, if bend is horizontal $Z_1 = Z_2 = 0$.

If the conduit bend is of the same pipe diameter, and friction force F_c is neglected, then $P_1 = P_2 = P, A_1 = A_2 = A$, $V_1 = V_2 = V$, also $Q = VA$, and the force equations can be simplified.

$$F_{Rx} = P_1A_1 - P_2A_2\cos\Delta - Q\rho(V_2\cos - V_1)$$

$$F_{Rx} = PA - PA\cos\Delta - VA\rho(V\cos\Delta - V)$$

$$F_{Rx} = PA(1-\cos\Delta) + VA\rho V(1-\cos\Delta)$$

$$F_{Rx} = (P + \rho V^2)\, A\, (1 - \cos\ ) \qquad (5.4a)$$

$$F_{Ry} = P_2A_2\sin\Delta + Q\rho V_2\sin\Delta$$

$$F_{Ry} = PA\sin\Delta + VA\rho\sin\Delta$$

$$F_{Ry} = (P + \rho V^2)\, A\, \sin\Delta \qquad (5.5a)$$

$$F_R = \sqrt{F_{Rx}^2 + F_{Ry}^2}$$

$$F_R = [(P + \rho V^2)^2\, A^2(1 - \cos\ )^2 + (P + \rho V^2)^2\, A^2\sin^2\Delta]^{1/2}$$

$$F_R = (P + \rho V^2)\, A\, (1 - 2\cos\Delta + \cos^2\Delta)^{1/2}, \qquad \sin\Delta + \cos^2\Delta = 1$$

$$F_R = (P + \rho V^2)\, A\, (2 - 2\cos\Delta)^{1/2} \qquad \sqrt{2 - 2\cos\Delta} = 2\sin\Delta/2$$

$$F_R = (P + \rho V^2)\, A\, 2\sin\Delta/2 \qquad (5.6a)$$

By symmetry $\beta = \Delta/2$ (5.7a)

(also by substitution of $\beta = \Delta/2$, F_{Rx}(5.4a), F_{Ry}(5.5a) into (5.7).

~~$F_R = (P + V^2) A \sin \Delta/2$~~

In Figure 5.6, F_R is resisting the fluid forces occurring within the bend. The first inclination is to view F_R as the total force applied to keep the conduit from moving. But F_R in the free body diagram was established to keep the bend system in a static or equilibrium condition. Therefore, F_R is composed of both a static and dynamic fluid force, shown by the P and V^2 terms within the brackets of equation (5.6a). Thus, the dynamic force tending to move the conduit is ρV^2 A $2\sin \Delta/2$ and acts in the reverse direction of F_R. (See example problem)

For the buoyant concept the friction force F_c should be calculated, Figure 5.5. If the friction force is significant then an adjustment should be made to the pressure P_2 at the exit of the bend for friction force (F_c in Figure 5.5). Because of the friction and bend headloss there is less pressure at the exit than at the entrance

of the bend. Test results from a hydraulic laboratory study 5.5/ showed agreement with equation

$$P_2 = P_1 - \gamma h_t, \qquad (5.10)$$

where symbols have previously been defined and h_t is from equation (5.2.). Also h_t is used in equation (5.11) to compute F_c.

$$F_c = \gamma A h_t.$$

The friction force F_c is assumed to be evenly distributed along the bend. Thus, the force is considered to act tangential to the conduit centerline, and at the mid-angle ($\Delta/2$) of the bend.

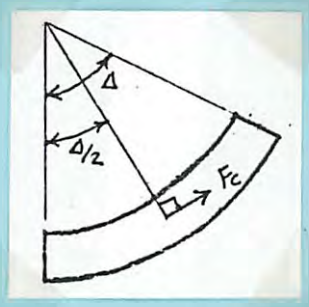

Bend Force Example Problems

Assume the conduit centerline is located at a 240-foot ocean depth, D = 30 feet, γ_s salt water 64.22 lb/ft^3, γ_f fresh water in pipe 62.41 lb/ft^3, and internal pressure within the conduit is produced by a reservoir water surface 125 feet above sea level.

5.5/ Hydraulic model investigation of headloss in penstocks of the Grand Coulee Third Powerplant, Hydraulics Branch Laboratory Report to be published.

(1) Compute fluid force for a $\Delta = 90°$ bend, R/D = 1, and neglect the friction force F_c

(a) V = 10 ft/sec, and at a point downstream (down the pipe along the direction of water flow) where 10 feet of headloss has occurred,

(b) at a point downstream where 110 feet of headloss has occurred,

(c) when V = 0 and full reservoir head is acting on the bend.

(2) Compute fluid force on bend for problem 3 of "Headloss Example Problems" and for conditions (a) and (b) of the above problem, but consider the friction force F_c.

(1a) Use conditions at pipe centerline to compute effective internal pressure within pipe.

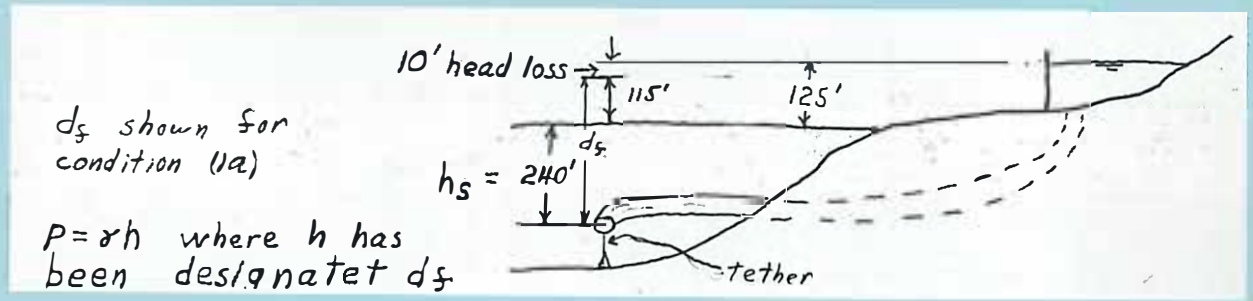

pressure within pipe $\gamma_f d_f$ = (62.41)(240+125-10) = 22,156 lb/ft^2

pressure outside pipe $-\gamma_s h_s$ = (64.22)(240) = -15,413

effective internal pressure within the pipe = 6,743 lb/ft^2

Use equation (5.6a) $F_R = (P + \rho V^2)(A)2\sin\Delta/2$

$F_R = \left(6{,}743 + (1.94)(10)^2\right)\left(\frac{\pi 30^2}{4}\right)2 \sin 90°/2 = 6937\ (707)\ 2\ (0.707)$

F_R = 6,937,000 lbs

equation (5.7a) $\beta = \Delta/2 = 90°/2 = 45°$

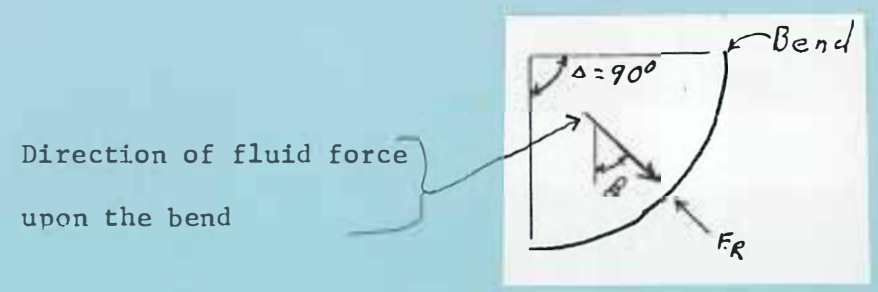

(1b) pressure within pipe = $\gamma_f d_f$ = (62.41)(240 + 125 - 110) = 15,915 lb/ft^2

- pressure outside pipe = -15,413

effective pressure within pipe 502 lb/ft^2

$F_R = \left(P + \rho V^2\right) A\ 2 \sin \Delta/2 = [502 + (1.94)(10^2)]$ ~~(0.707)~~ (.707) (2)(0.707)

F_R = 696,000 lbs. $\beta = 45°$

(1c) pressure within pipe = $\gamma_f d_f$ = (62.41)(240 + 125) = 22,780 lb/ft^2

pressure outside pipe - 15,413

effective pressure within pipe 7,367 lb/ft^2

$F_R = \left(P + \rho V^2\right) A2 \sin \Delta/2 = [7367 + (1.94)(0^2)]$ (707)(2)(0.707)

F_R = 7,367,000 lbs. $\beta = 45°$

(2a) Need to consider headloss for the bend. From Problem 3 of "Headloss Example Problems" h_t = 5.32 ft. From preceding problem (1a) P_1 = 6743 lb/ft^2.

Equation (5.10) $P_2 = P_1 - \gamma h_t = 6743 - (62.41)(5.32) = 6743 - 332 =$

6411 lb/ft^2

Equation (5.4) $FRx = P_1A_1 - P_2A_2 \cos\Delta - Q\rho(V_2\cos\Delta - V_1)$

$Q = VA$

$Q = (10)(707)$

$Q = 7070$ ft^3/sec

$FRx = (6743)(707) - (6411 - 707)(0) - (7070)(1.94)\ /(10)(0) - 10/$

$FRx = 4,904,459$ lbs

Equation (5.5) $FRy = P_2A_2 \sin\Delta + Q\rho V_2 \sin\Delta = (6411)(707)(1) +$

$(7070)(1.94)(10)(1)$

$FRy = 4,669,735$ lbs

Equation (5.11) $Fc = \gamma A h_t = (62.41)(707)(5.32) = 234,739$ lbs

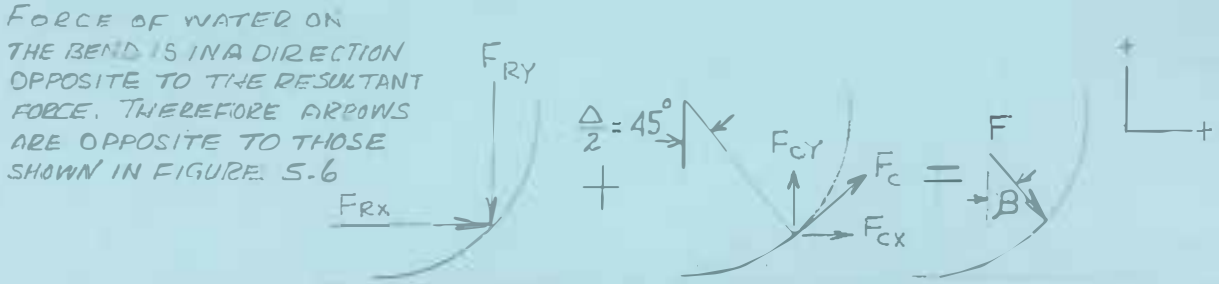

Definition sketch showing component forces of F

$Fcx = Fc \cos\Delta/2 = 234,739\ (\cos 45°) = 165,960$ lbs

$Fcy = Fc \sin \Delta/2 = 234,739 (\sin 45°) = 165,960$ lbs

$Fx = FRx + Fcx = 4,904,459 + 165,960 = 5,070,419$ lbs

$Fy = FRy + Fcy = -4,669,735 + 165,960 = -4,503,775$ lbs

$F = \sqrt{Fx^2 + Fy^2} = [(5,070,419)^2 + (-4,503,775)^2]^{1/2} \approx 6,782,000$ lbs

$$\text{Tan } \beta = \frac{Fx}{Fy} = \frac{5,070,419}{4,503,775} = 1.1258$$

$\beta = 48° 23'$

(2b) From (1b) $P_1 = 502$ lb/ft^2

$P_2 = P_1 - \gamma h_t = 502 - (62.41)(5.32) = 170$ lb/ft^2

$FRx = P_1A_1 - P_2A_2 \cos\Delta - Q\rho(V_2\cos\Delta - V_1)$

$FRx = (502)(707) - (170)(707)(0) - (7070)(1.94)[(10)(0) - 10] = 492,072$ lbs

$FRy = P_2A_2 \sin\Delta + Q\rho V_2 \sin\Delta = (170)(707) + (7070)(1.94)(10)(1)$

$FRy = 257,348$ lbs

Fc, Fcx, and Fcy same as (2a)

$Fx = FRx + Fcx = 492,072 + 165,960 = 658,032$ lbs

$Fy = FRy + Fcy = -257,348 + 165,960 = -91,388$ lbs

$F = \sqrt{Fx^2 + Fy^2} = [(658,032)^2 + (-91,388)^2]^{1/2} \approx 664,400$ lbs

$$\text{Tan } \beta = \frac{Fx}{Fy} = \frac{658,032}{91,388} = 7.20$$

$\beta = 82° \ 6'$

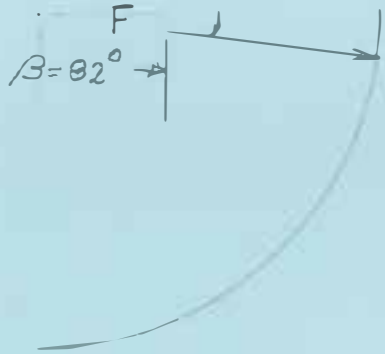

SECTION 6

HYDRODYNAMIC FORCES ON CONDUIT

Pressure Variation Around Bodies of Revolution

At low velocities the variation in pressure in the potential flow around an immersed body is nearly hydrostatic. At high velocities unbalanced normal stresses are large and require detailed knowledge of pressure distribution for structural stability, Figure 6.1.

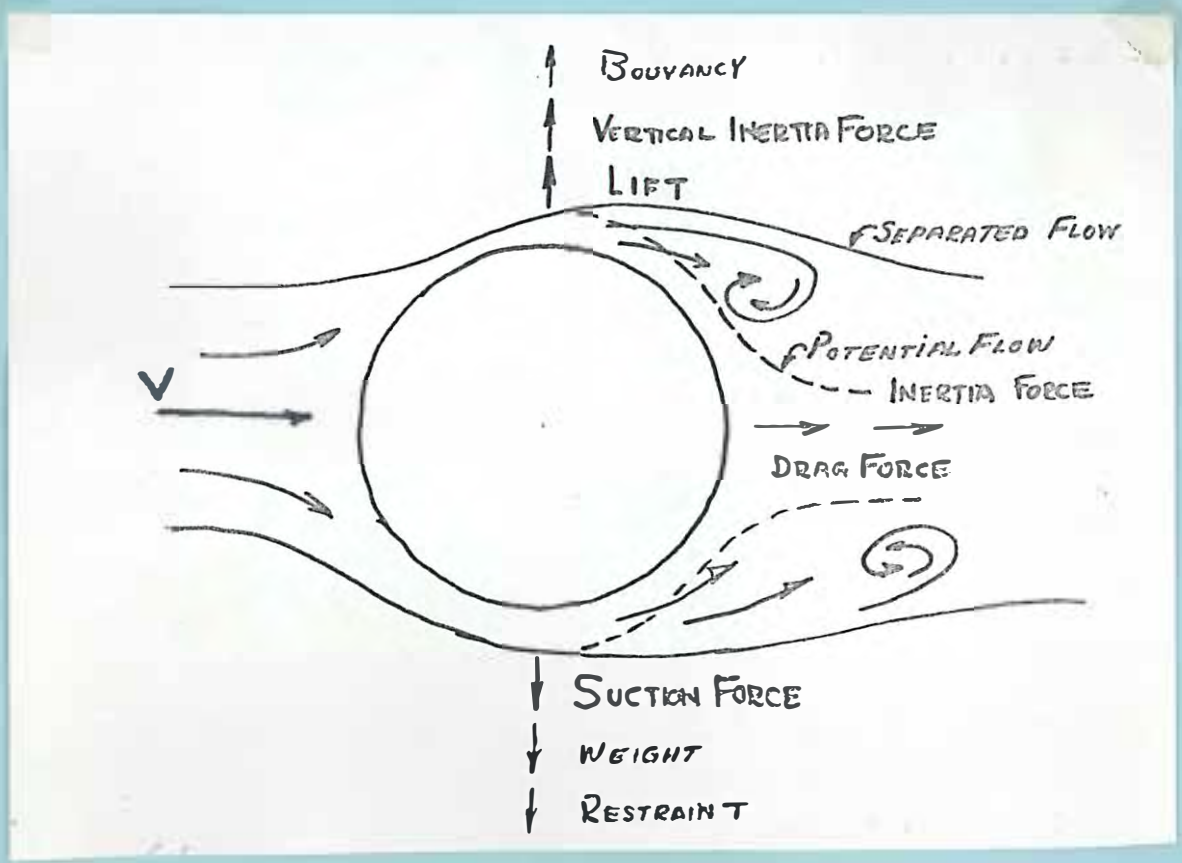

Figure 6.1 Forces on bouyant cylinder

A very costly example of the need for accurate information on the pressure variation was the 1940 failure of the Tacoma Bridge caused by not considering the oscillation effect of a high speed wind.

Velocity increases produce a changing zone of separation with an accompanying shift in the force acting on the body, Figures 6.1 and 6.2.

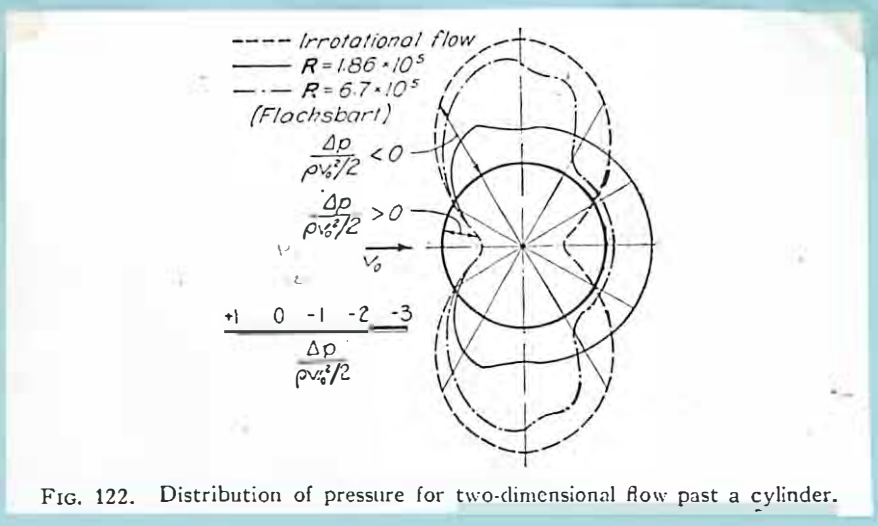

FIG. 122. Distribution of pressure for two-dimensional flow past a cylinder.

Figure 6.2 - Cylinder Pressure Distribution 6.1/

The separation zones further exhibit a periodic change as the zone of low pressure shifts from side to side. A variable thrust in the form of a stable trail of vortices is coupled with a drag force in the direction of flow, Figure 6.3.

6.1/ Rouse, Hunter, Elementary Mechanics of Fluids, John Wiley and Sons, Inc., 1946.

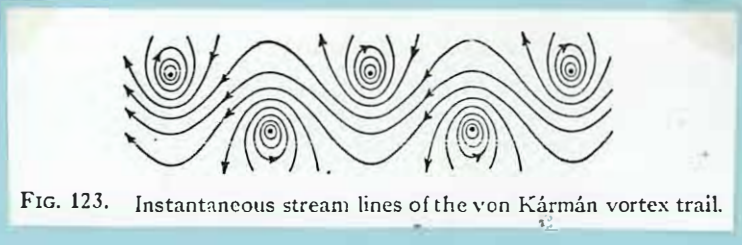

FIG. 123. Instantaneous stream lines of the von Kármán vortex trail.

Figure 6.3 - Separation Periodicity 6.1/

The total longitudinal force exerted by the moving fluid on the body is a summation of the components of normal and tangential stresses on the boundary surface. These forces are fluctuating for the velocities expected to affect the aqueduct.

6.1/ Op cit

Modeling Hydrodynamic Forces

A dynamic similarity of the forces acting on a cylinder has been derived by dimensional analysis. These forces have been related through a dimensionless parameter of the Reynolds number (R). This number relates the inertia force to the friction force.

$$R = \frac{\rho VD}{\mu} \quad \text{where}$$

V = average approach velocity

D = diameter of cylinder

μ = dynamic viscosity of fluid

ρ = density

Lift and drag force equations have been derived in a similar manner. The force acting on the body is the surface integral of all normal and shearing stresses. Dimensional analysis leads to the conclusion that for geometrically similar systems a lift and drag coefficient may be related to a dimensionless group formed of V, D, ρ, and μ in the form of the Reynolds number. The component of the resultant force in pounds in the direction of the undisturbed initial velocity is the drag F_D, and the component perpendicular to the velocity is the lift F_L. Figure 6.1.

The dimensionless coefficients of drag and lift are defined for a unit length of cylinder

$$C_D = \frac{F_D}{\rho\, DV^2/2} \qquad C_L = \frac{F_L}{\rho\, DV^2/2}$$

Design of the undersea aqueduct requires a dynamic similarity between models used in obtaining experimental drag and lift coefficients and the aqueduct pipe. According to model laws for predominant viscous forces

$$\frac{L_r\, V_r}{(\mu/\rho)r} = 1 \text{ where}$$

L_r, V_r, and $(\mu/\rho)_r$ are the ratios of the geometric and dynamic similarities of the model and prototype. Thus for dynamic similarity between the cylinders used for experiment and the pipeline

$$\frac{L_m\, V_m}{(\mu/\rho)m} = \frac{L_p\, V_p}{(\mu/\rho)p}$$

Model cylinders in available data have ranged from fractions of an inch to 24 inches in diameter. One set of data has information on coefficients measured from cylinders having diameters ranging from 3 to 24 inches. 6.2/

6.2/ Beckman, Herbert, Thibodeaux, M. H., "Wave Force Measurements for Offshore Pipelines," Journal of Waterways and Harbors, ASCE, WW2, May 1962, page 125, and Discussion WW1, February 1963, page 61.

Assuming a range of about 0.3 to 2 feet in cylinder diameter for experimental data and 30 feet for the prototype pipe then

$$\frac{L_m}{L_p} = \frac{0.3}{30} = \frac{1}{100} \text{ and } \frac{2}{30} = \frac{1}{15}$$

Therefore the range of model to prototype scaling is 15 to 100.

Because most of the data is on smaller size cylinders, an example will be based on the 0.3 foot diameter cylinder.

Experimental data have been obtained from the use of water and air as the flowing fluid. Assuming water in the model and seawater in the prototype, the kinematic viscosities at 50° F would be

$$\mu/\rho = \nu_{50°} = \begin{matrix} 1.5X10^{-5} \text{ fresh} \\ 1.9X10^{-5} \text{ sea} \end{matrix}$$

Thus

$$\frac{0.3xV_m}{1.5x10^{-5}} = \frac{30xV_p}{1.7x10^{-5}}$$

and

$$\frac{Vm}{Vp} = \frac{1.5}{1.7} \times \frac{30}{0.3} = 88$$

If the expected velocity in the vicinity of the undersea pipe [redacted] about 5 to 8 feet per second, then

$$V_m = V_p \times 88 = 5 \times 88 = 440 \text{ fps}$$

A Reynolds number computed from this velocity would be in the order of

$$R = \frac{440 \times 0.3}{1.5 \times 10^{-5}} = 8.8 \times 10^6$$

There is not a significant amount of experimental data available in this Reynolds number range, Figure 6.4,

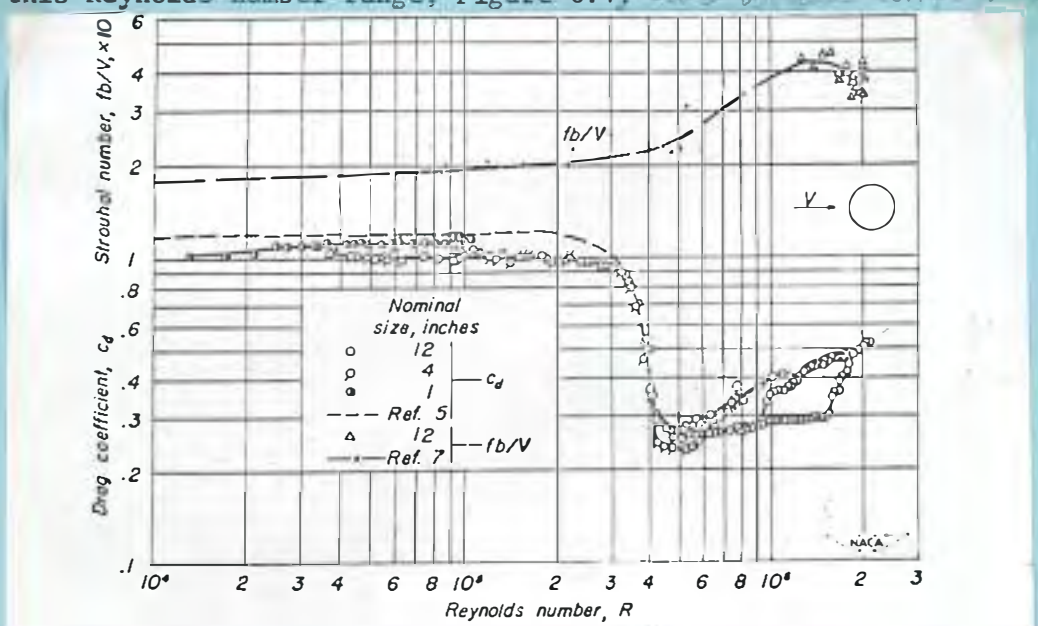

Figure 5.-Variation of drag coefficient and Strouhal number with Reynolds number for the circular cylinders.

Figure 6.4 6.3/

[redacted]

6.3/ Delaney, N. K., Sorenson, N. E., "Low Speed Drag of Cylinders of Various Shapes," NACA Technical Note 3038, November 1953.

The velocity of the expected currents flowing past the underseas aqueduct is very low compared to that used in experimental studies. For example, a Reynolds number for a 0.3-foot cylinder at a velocity of 5 fps would be

$$R = \frac{0.3 \times 5}{1.5 \times 10^{-5}} = 1 \times 10^{5}$$

This value of 1×10^{5} is an order of magnitude less than indicated as needed by similarity relationships. However, the 5 fps velocity occurs in both the model and the prototype and the large difference in Reynolds number is caused by the difference in cylinder diameters (0.3 and 30) and fluid viscosity.

The drag and lift forces are dependent on the separation pattern of the flow around the cylinder. These patterns in turn are controlled by the flow velocity and turbulence level in the flow surrounding the cylinder, Figure 6.1. The low Reynolds numbers are usually associated with potential flows and high Reynolds numbers with separated flows. The relationships are not well defined especially in oscillating flows because of the change in pressure distribution with the pattern of separation.

The possibility of the lack of correspondence between the experimental drag and the drag occurring on the aqueduct may be indicated by comparing the coefficients in Figure 6.5. 6.3/

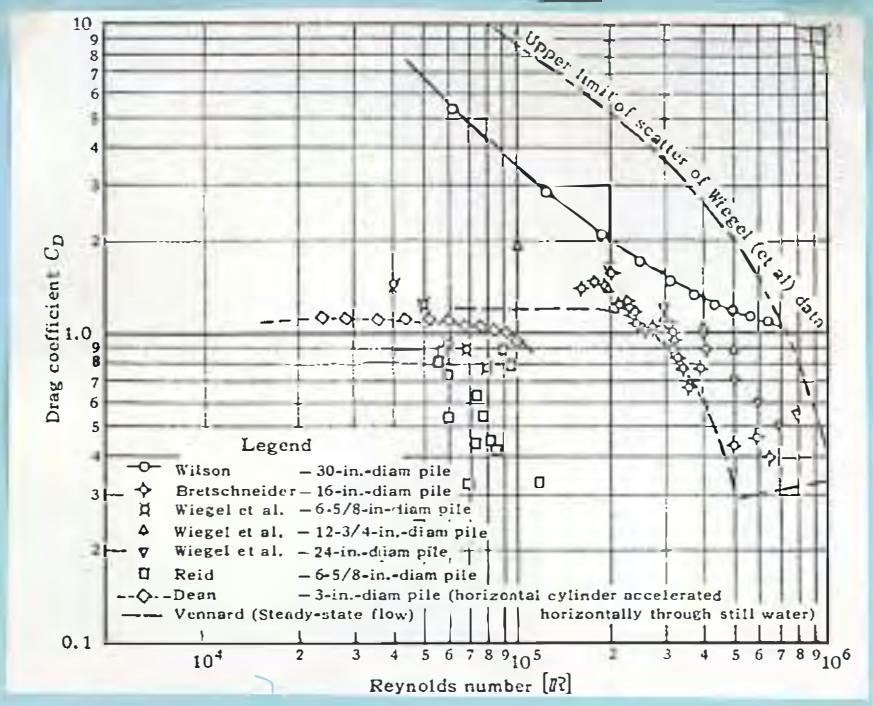

Figure 6.5 - Drag coefficients for smooth cylinders. 6.4/

A 3-inch cylinder ~~was~~ is assumed to be a model for a 24-inch cylinder. A C_D value of about 0.95 occurs at a Reynolds number of 1×10^5. At the 3-inch model velocity, the Reynolds number for the 24-inch cylinder would be

$$\frac{24}{3} \times 1 \times 10^5 = 8 \times 10^5$$

6.3/ Op cit

6.4/ Wilson B. W., and Reid, R. O., "A Discussion of Wave Force Coefficients for OffshorePipelines." J. Proc. ASCE, WW1, pp 61-63, February 1963.

The coefficient of drag value 0.95 is nearly twice the 0.5 value measured for the 24-inch cylinder at a Reynolds number of 8×10^5. A similar example compared the 6-5/8-inch cylinder with the 24-inch.

$$C_D \approx 0.6 \qquad \text{Reynolds Number } 7.5 \times 10^4$$

$$\frac{24}{6\text{-}5/8} \times 7.5 \times 10^4 = 2.7 \times 10^5.$$

The 24-inch experimental curve passes through a C_D value of 0.6 but at an approximate Reynolds number value of 6×10^5 instead of 2.7×10^5. Thus, extrapolation of data may not be reliable on the coefficients from "small models" to conduits the size of the aqueduct

Reasoning of a similar nature applies to the frequency of vortex shedding and oscillation of the pipeline. Experimental data available on the vortex shedding frequency may be limited by the size of cylinder used in the study.

The frequency of the vortex shedding is dependent on the flow velocity and separation of flow from the cylinder. For large pipes and low current velocities, the frequency of shedding obtained from small cylinders may not scale in an accurate manner.

The dimensionless parameter commonly used for relating the vortex frequency to Reynolds number is the Strouhal number

$$S = \frac{f\ D}{V}$$

where

f = measured vortex frequency

D = diameter of cylinder

V = average approach velocity

Parts of this relationship are not well defined because of flow turbulence level and the change in pressure distribution as the flow clings or separates from the cylinder. Experimental values do not extend to the Reynolds numbers indicated by similitude relationships of the model cylinders and the aqueduct, Figure 6.4.

Flow separation patterns and therefore pressure distributions are different on smooth and rough cylinders. A part of the variations of drag, lift, and oscillation forces noted in experimental data has been related to changes in boundary turbulence caused by roughness. Higher drag coefficients have been shown to occur at lower Reynolds numbers on cylinders with sand-roughened surfaces, Figure 6.6.

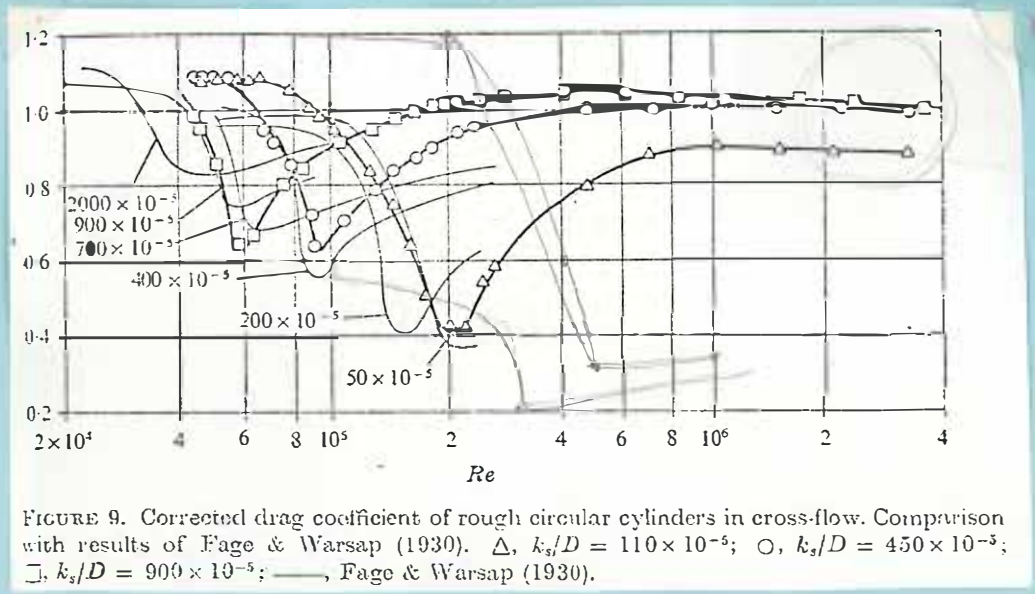

FIGURE 9. Corrected drag coefficient of rough circular cylinders in cross-flow. Comparison with results of Fage & Warsap (1930). △, $k_s/D = 110 \times 10^{-5}$; ○, $k_s/D = 450 \times 10^{-5}$; □, $k_s/D = 900 \times 10^{-5}$; ——, Fage & Warsap (1930).

Figure 6.6 - Drag coefficient for rough cylinders. 6.5/

6.5/ Achenback, E., "Influence of Surface Roughness on the Crossflow Around a Circular Cylinder," Journal Fluid Mech., Vol. 46, part 2, pp 321-335.

The large difference between the diameter of the model cylinders, for which data is available, and the diameter of the aqueduct is a basis for reasonable doubt on the validity of extrapolating the drag, lift, and "mass" or "inertia" coefficients from a model to a prototype force. However, because data from large cylinders was not available, the "small model" data discussed in this section is used in recommending values of the coefficients. Table 6.1.

Table 6.1

SUMMARY OF RECOMMENDED

Drag C_D, Lift C_L, and Inertia C_M Coefficients

and Strouhal Numbers

Coefficient	Recommended	Probable range
	Bouyant concept	
Drag		
Single cylinder		
Normal flow	1.2	0.25 to 1.3 Figure 6.4
45°	(3 max)	Figure 6.14
Paired cylinders		
Separation 4D		
Upstream	1	Figure 6.7
Downstream	0.5	
Lift		
Single cylinder	0.5	h/d = 0, 0.6 h/d = 0.3, 0.1 Figure 6.8
Paired cylinders		
Separation		
4D h/d = 0.02		
Upstream	0.7	Figure 6.9
Downstream	0.4	
Inertia		
Single cylinder	2	0.7 to 5 Table 6.2 and text
Strouhal number		0.2 to 0.45 Figure 6.10
	Compare to pipe natural bending frequency	

Table 6.1 (continued)

Contact or Partly Embedded Concept

Coefficient	Recommended	Probable range
Drag		
Single cylinder	0.9	0.85 to 0.93
Lift		
Single	1.5	1.48 to 1.11
Inertia	NOT KNOWN	
Strouhal number		
Single Paired	Compare to pipe natural bending frequency	Variation in ratio of natural frequency to vortex frequency f/fs = 2 to 5 Figure 6.13
Variation with current angle	90° 0.2 60° 0.1	Figure 6.14

Drag Force - Buoyant Concept

The major force on a pipe in a steady current is the drag force. The drag force has two additive components, a form or pressure drag and a skin friction distribution around the cylinder

$$C_D = C_p + C_f$$

Artificial roughness of round sand grains were applied to the surface of a 150 mm cylinder by E. Achenback.[6.5] The sand grains were applied to the outside surface of the cylinder in a manner used by Nikuradse on pipe interiors. The relative roughness ranged from a

$$K_s/D = 110 \times 10^{-5} \text{ to } K_s/D = 900 \times 10^{-5}, \quad \text{Figure 6.5}$$

The studies indicated a frictional drag of the order of 2 to 3 percent maximum of the total drag. Pressure distribution or form drag appeared to be the predominant part of the total drag.

A relative roughness can be calculated by estimating the height of protective coating, sand grain roughness, or plastic surface on the aqueduct pipe. For example, estimating a $K_S = 0.001$ foot the relative roughness for a 30-foot pipe would be

$$K_s/D = \frac{0.001}{30} = 3.3 \times 10^{-5}$$

and indicate a very smooth cylinder.

6.5 op. cit. Achenback

Marine growths on the pipe roughen the surface but the character of the roughness and the effect on the total drag have not had thorough study. An estimate of the possible thickness of the growths range to 6 inches. A relative roughness of

$$K_s/D = \frac{6}{360} = 1700 \times 10^{-5}$$

falls well beyond the 900×10^5 used in determining the percentage of friction to form drag. A curve for a roughness of 2000×10^{-5} indicates the total drag would not be materially affected except by the increase in total projected area and in the turbulence level of the flow around the surface of the pipe, Figure 6.6. A generalization of the effect of roughness on the drag coefficients for cylinders has been made for higher Reynolds numbers (1×10^5 to 6×10^6). The C_D values range from about 0.58 for the smooth cylinder to 1.1 for the roughest cylinder. 6.6/

A steady current may occur at times in flow passing the pipeline. The drag force will not be steady on a suspended pipe because of vortex shedding but experimental mean drag coefficients have been determined for a fixed cylinder. Assuming this condition, then the range of drag coefficient C_D most probably would be from 0.25 to 1.3. The 0.25 occurs in the "critical range" of the shift of the flow pattern from

---

6.6/ Ippen, A. T., Ed., "Estuary and Coastline Hydrodynamcis," Eng. Soc. Monographs, McGraw-Hill Book Co., Inc., page 362, Figure 8.11

partially to fully spearated flows. The value of about 1.2 to 1.3 occurs at Reynolds numbers both higher and lower than the critical range between about 3×10^5 to 2×10^6.

The use of a C_D value of about 1.2 would be indicated for computing the maximum total form drag for a steady current at Reynolds numbers greater than about 1×10^4, Figure 6.4.

Currents passing at an angle to the cylinder centerline produce larger drag forces than currents perpendicular to the center. Small amounts of data are available from a 1.5-inch cylinder showing ranges of coefficient from

$$C_D = 1 \text{ at } 90° \text{ to } 3 \text{ at } 45° \quad 6.7/$$

(The undisturbed angular velocity was used in the computation).

Changes in drag coefficient on a smooth upstream or downstream cylinder in a pair show a wide variation for the small Reynolds number range of the study. 6.7/ The spacing between cylinders and distance from a boundary both affected the ~~lift~~ drag force, Figure 6.7.

6.7/ Wilson, J. F., Caldwell, H. M., "Force and Stability Measurements on Models of Submerged Pipelines," Transactions of the ASME, Journal of Engineering for Industry, November 1971, pp 1290 - 1298.

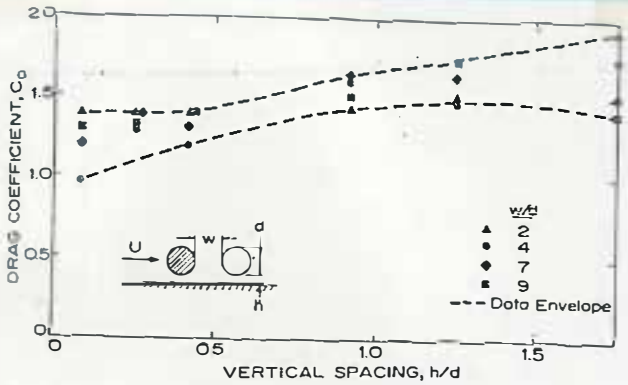

Fig. 5 Proximity effects on drag of the upstream cylinder at R = 33,200 and θ = 90 deg

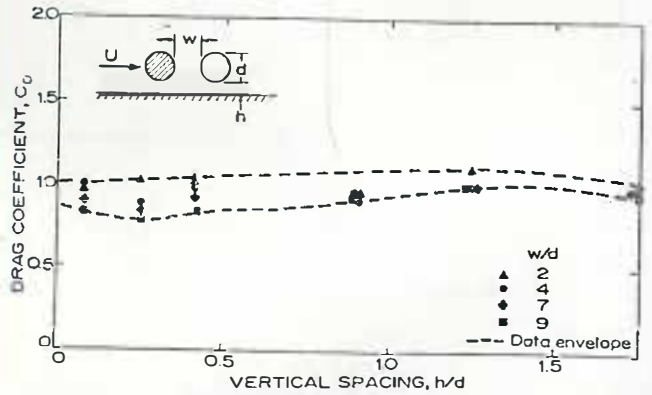

Fig. 6 Proximity effects on drag of the upstream cylinder at R = 56,600 and θ = 90 deg

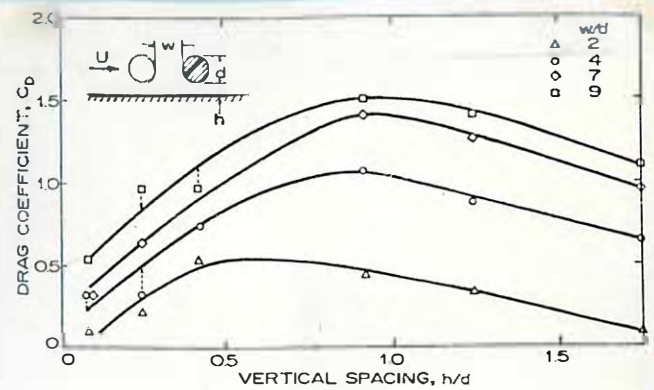

Fig. 7 Proximity effects on drag of the downstream cylinder at R 33,200 and θ = 90 deg

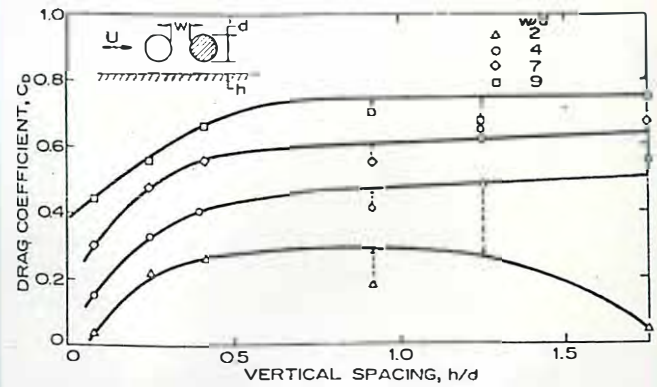

Fig. 8 Proximity effects on drag of the downstream cylinder at R 56,600 and θ = 90 deg

Figure 6.7 - Drag coefficients for paired cylinders. Reference 6.7/

Lift Force - Buoyant Concept

A suspended cylinder experiences no lift force in potential flow. In separated flow a periodic upward and downward force is imposed by the periodic shedding of vortices, that is, changes in the lift force.

A downward force (negative lift) is imposed on the pipe in an assymmetrical flow produced by a flat boundary near one side of the cylinder. Velocities are increased between the pipe and boundary producing an

---

6.7/ Op cit

unbalance of pressure toward the boundary. Analytical and experimental evaluations have been made of the change of the lift coefficient for single and paired cylinders adjacent to boundaries. 6.7/ 6.8/

Lift coefficients (negative, that is toward the boundary) resulting from the experimental data for two pipe Reynolds numbers, 33,200 and 56,6000, brackets in part, analytical data and experimental data for a Reynolds number of 150,000, Figure 5. 6.7/

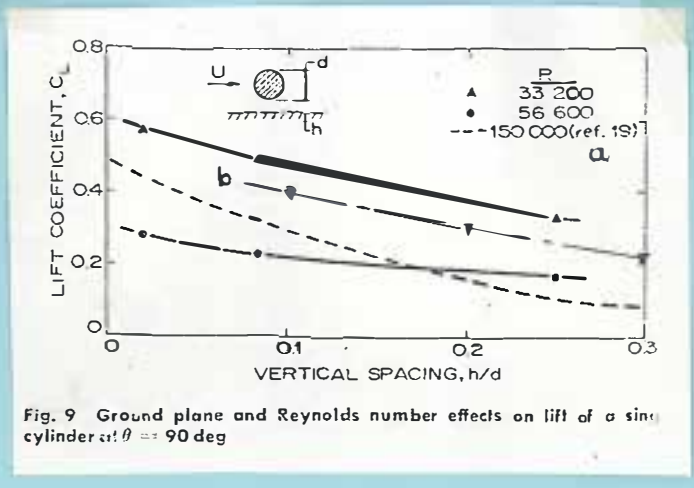

Fig. 9 Ground plane and Reynolds number effects on lift of a sin cylinder at θ = 90 deg

Figure 6.8 - Lift coefficients for single cylinder. 6.7/

(a) Reference 19, Rouse, H., Ed. Engineering Hydraulics, Wiley, N. Y., 1950, page 130 (b) from Reference 6.8

6.7/ Op cit

6.8/ "Ocean Environment and Design Considerations in a Prereconnaissance Study of a California Underseas Aqueduct," Contract No. 14-06-D-6780, Litton Systems, AMTD,. June 13, 1969.

The lift on an upstream cylinder is increased by the presence of a cylinder on the downstream side for small models and low Reynolds numbers. 6.7/ The lift coefficients reflect the proximity of both an adjacent boundary and the distance between two cylinders, Figure 6.9.

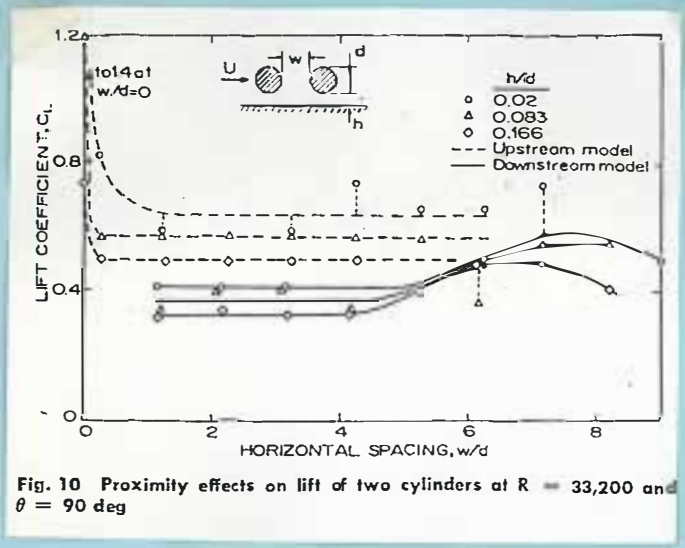

Fig. 10 Proximity effects on lift of two cylinders at R = 33,200 and θ = 90 deg

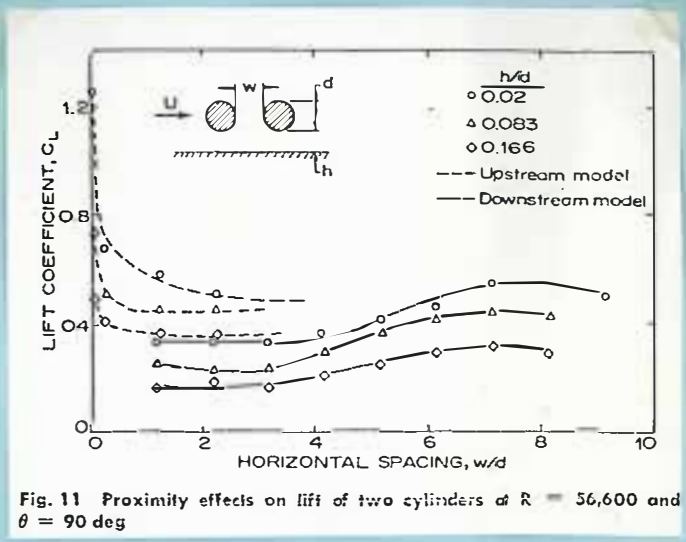

Fig. 11 Proximity effects on lift of two cylinders at R = 56,600 and θ = 90 deg

Figure 6.9 - Boundary and spacing effect on paired cylinder lift coefficients 6.7/

Oscillating Forces - Buoyant Concept

A primary characteristic of the flow past a stationary cylinder is the lateral pendulation of the separation zone as a vortex is shed from alternating sides of the flow centerline, Figure 6.3. Experiments have generalized the characteristics of the shedding frequency in terms of the cylinder Reynolds number and the Strouhal number (S) Prevously cited.

6.7/ Op cit

An abundant amount of information is available on vortex frequency but application of the results may be limited by the large magnitude scaling from model to aqueduct pipeline. Strouhal numbers range from about 0.2 to 0.45 for Reynolds numbers 1 x 10^4 to 1.5 x 10^6, Figure 6.4. Measurements at higher Reynolds numbers indicate a decrease in Strouhal number to about 0.25, Figure 6.10

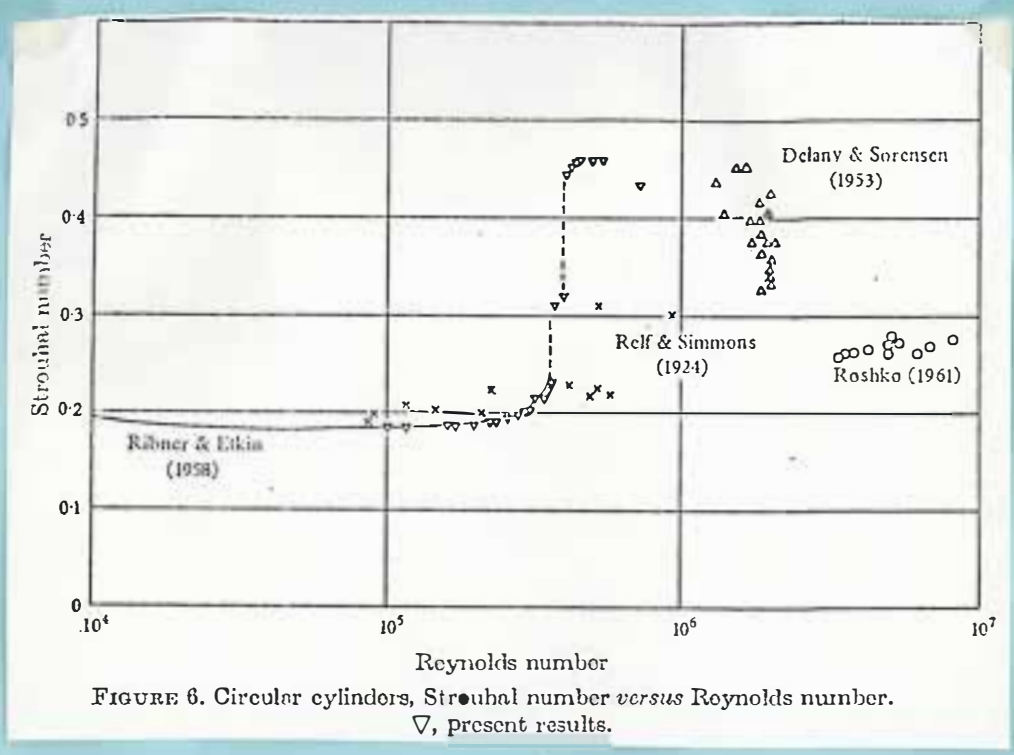

FIGURE 6. Circular cylinders, Strouhal number *versus* Reynolds number. ▽, present results.

Figure 6.10- Variation of Strouhal number for circular cylinders, 6.9/

6.9/ Bearman, P. W., "Vortex Shedding From a Circular Cylinder," J. Fluid Mechanics, Vol 37, part 3, July 1969, page 584.

Selection of a Strouhal number from these small model data to apply to the large aqueduct may be difficult. Additional study on larger cylinders in a stationary position may show the correspondence between the model and aqueduct pipeline. Solving the Strouhal number equation using the natural bending frequency of the pipeline would indicate a critical Strouhal number. Coincidence of the number with one in the range indicated by experimental investigations would be cause for an extensive study of the possible oscillation of the aqueduct.

Forced oscillation of a flexible cylinder, e.g. a tethered aqueduct pipeline by waves could cause serious bending moments if the natural period of elastic oscillation is in resonance with the vortex and wave velocity periods. The force exerted by the water on the moving pipeline contains two parts, one depending on the form drag, and the other depending on the displaced water.

The direct and fundamental approach represents the total force on the cylinder as the sum of the drag and inertia force components

$$dF_T = dF_D + dF_I \quad \text{(Morison Formula)}$$

The components dF_T and dF_I are defined

$$dF_D = C_D \rho D \frac{u|u|}{2} ds$$

$$dF_I = C_I \rho \frac{\pi D^2}{4} \dot{u} ds$$

where ρ = density of water

u = instantaneous horizontal velocity of water particle

$\dot{u}$ = instantaneous horizontal acceleration of water particle

C_D = hydrodynamic force coefficient, the drag coefficient

C_m = hydrodynamic force coefficient, the inertia or mass coefficient

The equation for the drag force component is the usual representation of the force resulting from the steady flow discussed in the previous section on drag. The absolute value symbols in the F_D equation insure that the drag force component is in the same direction as the velocity.

Measurements of drag forces on cylinders subject to wave velocities show a large scatter apparently caused by turbulence near the cylinder. A steady state vortex shedding period cannot occur because of the oscillating nature of the wave velocity. Thus in the presence of a current and oscillating wave velocity, wide variations occur in the drag force, Figure 6.11.

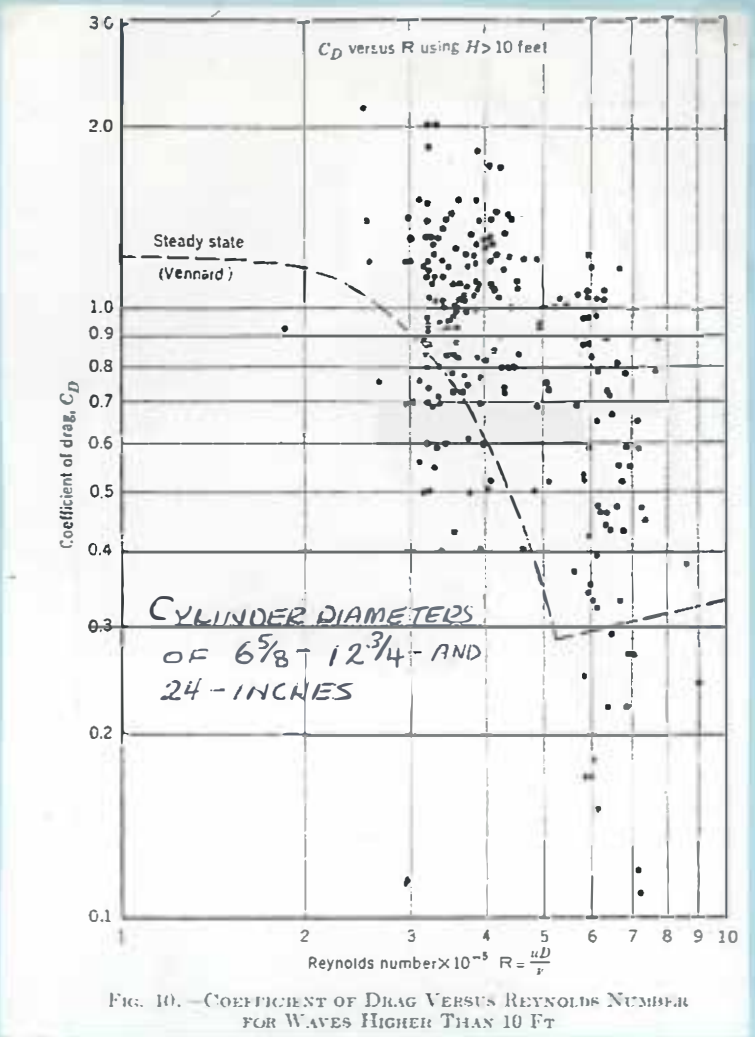

FIG. 10.—COEFFICIENT OF DRAG VERSUS REYNOLDS NUMBER FOR WAVES HIGHER THAN 10 FT

Figure 6.11- Drag coefficients for unsteady velocities caused by waves. 6.10/

Flow patterns resulting from the movement of a cylinder in the surrounding water in unsteady and oscillating flows are related through the "inertia" or "mass" coefficient. Because of the oscillating motion of both the pipe and water, the effects of such motion are not well known.

6.10/ Weigel, R. L., Beebe, K. E., Moon, J., "Ocean Wave Forces on Circular Cylindrical Piles" ASCE Transaction, Volume 124, pages 89-116, 1959.

An early theoretical and experimental study resulted in agreement of the computed and measured forces on a cylinder in a wave tank. 6.11/ The Morison type equation was used to find the total force on the cylinder. No steady or unsteady currents were imposed on the simple sinusoidal currents in a rectangular basin.

Studies were extended in later years by investigating the forces on single and paired cylinders in laboratory and ocean condition. 6.12/ 1.13/ 1.14/ 6.15/. The studies further reinforced the doubt of assuming a C_D-value applied to a cylinder in reversible accelerating flow, as in wave action, would be the same as a C_D value for steady flow. The wide variance of values for both C_D and C_M indicate caution should be exercised in using the information in a model to aqueduct conformance, Table 6.2.

6.11/ Kuelegan, G. H., and Carpenter, L. H., "Forces on Cylinders and Plates in an Oscillating Fluid," Research of the National Bureau of Standards, Vol 60, No. 5, May 1958, Res. Paper 285, pp 423-440.

6.12/ Laird, A. D. K., Johnson, C. A., and Walker, R. W., "Water Forces on Accelerated Cylinders," Jour. of Waterways and Harbors Div., ASCE WW1, March 1959, pp 99-119.

6.13/ Beckmann, H., and Thibodeaux, M. H., "Wave Force Coefficients for Offshore Pipelines," Jour. Waterways and Harbors Div., ASCE, WW 2, May 1962.

6.14/ Laird, A. D. K., "Water Forces on Flexible Oscillating Cylinders," Jour. of Waterways and Harbors, Div., Proc. ASCE, August 1962, Vol 88 pp125-137

6.15/ Surry, David, "Some Effects of Intense Turbulence on the Aerodynamics of a Circular Cylinder at Subcritical Reynolds Number," Jour. Fluid Mech., 1972, Vol 52, part 3, pp 543-563.

TABLE 6.2

Summary of C_D and C_M Coefficients for Cylinders 6.4/

Table 8.1 Drag and Inertial Coefficient Values for Circular Cylinders in Accelerating Flows (from [6])

Authority and date	Nature of experiments	Cylinder diameter (inches)	Coefficient value		Type of flow (remarks)
			C_D	C_M	
(1)	(2)	(3)	(4)	(5)	(6)
Crooke, 1955	Model	2, 1, ½	1.60	2.30	Oscillatory
Keulegan and Carpenter, 1956	Model	3, 2½, 2	1.34	1.46	Oscillatory (av. of 29 tabulated values)
		1½, 1¼	1.52	1.51	(Av. of 57 tabulated values)
Keim, 1956	Model	1, ½	1.00	0.93	Accelerated, nonoscillatory
Dean, 1956	Model	3	1.10	1.46	Accelerated, nonoscillatory
Wiegel et al., 1956	Prototype	24	1.00	0.95	Ocean waves, west coast (based on their Fig. 15)
Reid, 1956	Prototype	8¾	0.53	1.47	Ocean waves, Gulf of Mexico
Bretschneider, 1957	Prototype	16	0.40	1.10	Ocean waves, Gulf of Mexico
Wilson, 1957	Prototype	30	1.00	1.45	Ocean waves, Gulf of Mexico

An average value of $\bar{C}_D$ = 1.05 and $\bar{C}_m$ = 1.40 from Table 6.2 would be a first approximation in a preliminary design of the buoyant aqueduct. A mean value of C_m = 2.5, standard deviation of 1.2, and a skewness of about zero was calculated from data associated with drag coefficients of Figure 6.10. 6.10/ This mean, in a range of C_m values from 0.7 to 5.5, indicates a much larger "inertia" effect than the average from Table 6.2. Thus, a maximum C_m value appears to be greater than 5 or about 2.5 times the theoretical value of 2. Information reviewed generally indicates that an "inertia" coefficient value C_m = 2 should be used in the appraisal study of the aqueduct.

Additional investigation of larger models or analysis of reported results may be necessary before design forces on a large aqueduct can be calculated with confidence. Further investigation may resolve the inconsistencies by rigorous control of experimental facilities.

6.4/ Op cit
6.10/ Op cit

This area of the hydrodynamic design of structures in the ocean has been reviewed by several organizations and their publications offer valuable reference information. 6.6/ 6.8/ 6.16/ 6.17/ This part of the design study of the buoyant concept of the aqueduct should be given comprehensive study because of the modes of movement possible from a semirigid structure. Forces varying in magnitude and direction at sections of the pipe throughout the length could produce a highly complex dynamic behaviour of the aqueduct.

6.16/ ~~Skalak, Richard, Ed.~~ WEIGEL, ROBERT L., Oceanographical Engineering, Prentice-Hall series in Fluid Mechanics, 1964.

6.17/ Meyers, J. J. Ed., Handbook of Ocean and Underwater Engineering, McGraw-Hill Book Company, 1969.

Drag, Lift, and Oscillatory Forces - Cylinder in Contact or Partly Embedded in Boundary

A design of the aqueduct may require the pipe to be restrained in contact or partly buried in the ocean floor.

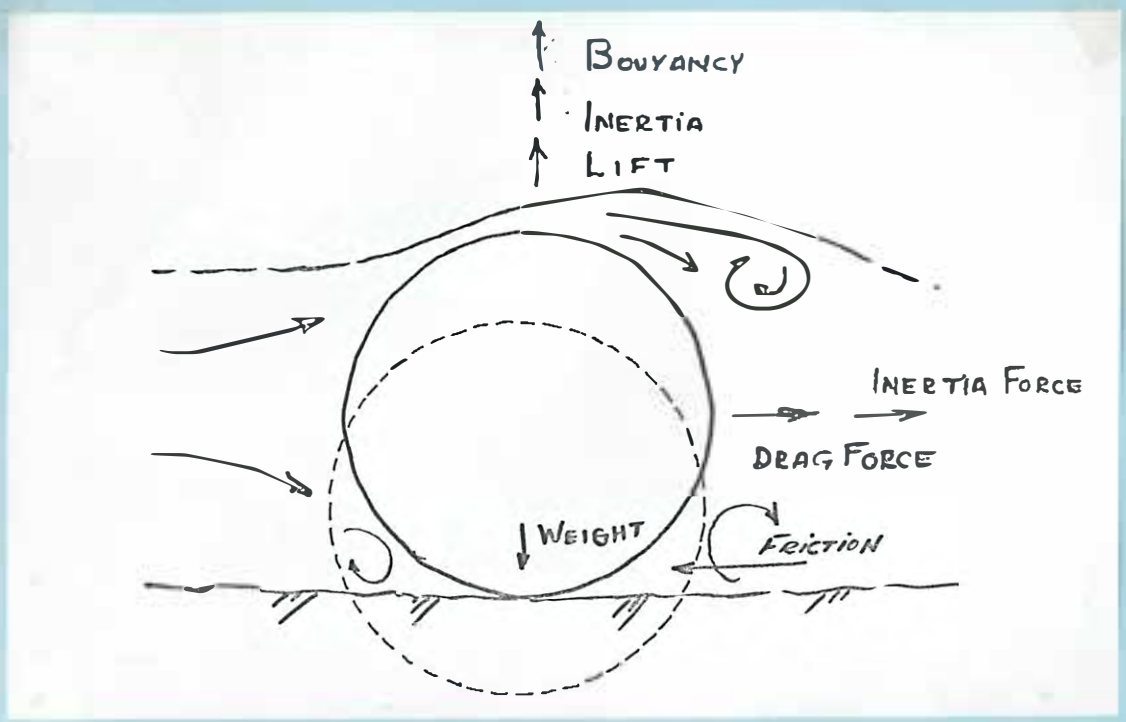

Figure 6.12 - Force on cylinder in contact or partly embedded in boundary.

Asymmetry of flow will produce forces of lift, drag, and oscillation to be balanced by the restraining structure. Studies of forces for

the pipe configurations of boundary contact and partly buried appear to have been minimal 6.13/ 6.18/.

A discussion of Reference 6.13/, 6.4/, suggests that the values of C_D, C_L, and C_M recommended from the studies are too low. Values of $C_D = 0.5$, $C_L = 0.5$, and $C_M = 1.5$ appear to have been used in the analysis but the discussers suggest larger values of $C_D \geq 1$, $C_L \geq 1$, and $C_M \geq 2.5$.

Six- and ten-inch cylinders were used in a Venturi-shaped flume for an ivestigation of lift and drag coefficients 6.18/. Pressures were

---

6.4/ Op cit

6.13/ Op cit

6.18/ Brown, R. J., Hydrodynamic Forces on Submarine Pipeline, Jour. of Pipeline Division, ASCE, PL1, March 1967, pp 9-19, and Discussions PL3, November 1967, pp 75-81.

6.19/ Wilson, B. W., and Reid, R. O., Wave Force Coefficients for Offshore Pipelines, Jour. Waterways and Harbors, ASCE, WW1, February 1963, pp 61-65.

measured at the cylinder surface and velocities in the surrounding flow. Values of C_D in the range 0.9 to 0.55, and C_L in the range 1.3 to 0.8 for Reynolds numbers ranging from 0.6×10^5 to 3×10^5 resulted from the investigation. No "inertia" or"mass" coefficient information was included in the results.

Additional experiments 6.20/ resulted in drag and lift coefficients of $C_D = 0.85$ to 0.93 and $C_L = 1.48$ to 1.11 for a Reynolds number range of 0.97×10^5 to 0.53×10^5.

The lift and drag force exerted on the cylinder will be oscillatory. Vortex formation in the wake of the cylinder will be periodic. The period of the force may be inferred from the investigations of vibrating cylinders having different natural vibrating frequencies and cylinder material to fluid mass ratios M, Figure 6.13.

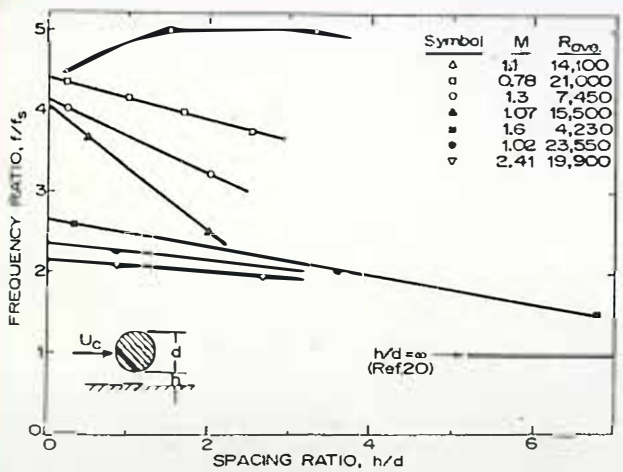

Fig. 13 Frequency of impending vibrations for a single cylinder near a ground plane

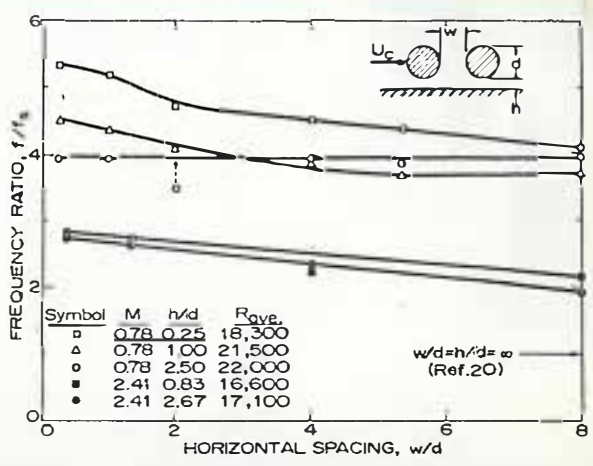

Fig. 14 Frequency of impending vibrations for two cylinders near a ground plane

Figure 6.13 - Oscillating tendencies of cylinders 6.20/

(Reference 20 6.6/.

6.20/ Font. Juan B., Discussion of Reference 13 in J. of Pipeline Division, ASCE, PL3, November 1967, pp 77-80.

6.6/ Op cit

Allowing h to become zero simulates contact of the cylinder with the boundary. A ratio of the natural to impending frequency of vibration can be inferred from the measurements on single and paired cylinders. Care should be exercised in selecting the frequency ratio because the minimum boundary spacing to diameter ratio is 0.25. Extrapolations of the curves have been made for the single cylinder, none have been made for two cylinders.

Reynolds numbers for measuring the frequency ratios were small, the largest being about 2.5×10^4. Mass ratios were scaled to represent steel pipes carrying oil, $1<M<3$. The model ratio ranged from $0.78 \leq M \leq 2.4$. and the natural frequency from about 4.5 to 24.5 cps. The stiffness of the model was increased thus increasing the natural frequency, over a Reynolds number range of 3×10^3 to 2.5×10^4.

The model to aqueduct conformance is not well established between 1.5-inch cylinders and 30-foot-diameter pipelines in contact or partly embedded in a boundary. One conclusion indicated that the natural bending frequency of the cylinder (aqueduct pipeline) or segment between anchor blocks should exceed 5 f_s to avoid significant midspan deflections.

$$f_n/f_s = 5.$$

Paired cylinders showed a frequency ratio greater than 5 as the cylinders were placed 0.25 of the diameter from the boundary. The natural frequency of the cylinders should be in excess of f_s by at least the factor given by the curves. The shape of these curves at $^d/_h$ values less than 0.25 is indefinite.

Available information on drag, lift, and inertia coefficients is meager for a cylinder on or embedded in a boundary. Extensive investigations are needed on larger cylinders near boundaries to improve the reliability of drag, lift, and inertia force coefficients. These studies should include thorough investigation of the interaction of the pipe moving in an oscillating flow of water.

Effect of Currents at an Angle to Cylinder - Buoyant or in Contact with Boundary

Currents flowing past a cylinder at an angle will take place for the buoyant, in contact, and partly embedded concepts of aqueduct construction. A small amount of information was available for a cylinder remote from a boundary 6.21/ 6.22/

6.21/ Chiu, W. S., and Lienhard, J. H., On Real Fluid Flow Over Yawed Circular Cylinders, ASME, Jour. of Basic Engineering, December 1967, pp 851-857.

6.22/ Schlichting, H., Boundary-layer Theory, 6th ed McGraw-Hill, New York, 1968, pp 241-242.

Chiu and Lienhard concluded that the separation along a cylinder was independent of the flow angle and would occur beyond the separation point of the flow component across the cylinder. Thus, particles in the cylinder wake were counterrotating corkscrew paths within the upper and lower rows of the vortex paths. The Strouhal number and pressure drag coefficient were evaluated for the crosswise component as though the spanwise flow did not exist. Strouhal numbers measured for Reynolds numbers between 3.9×10^3 and 2.1×10^4 show a gradually diminishing number as the current angle increases Figure 6.14.

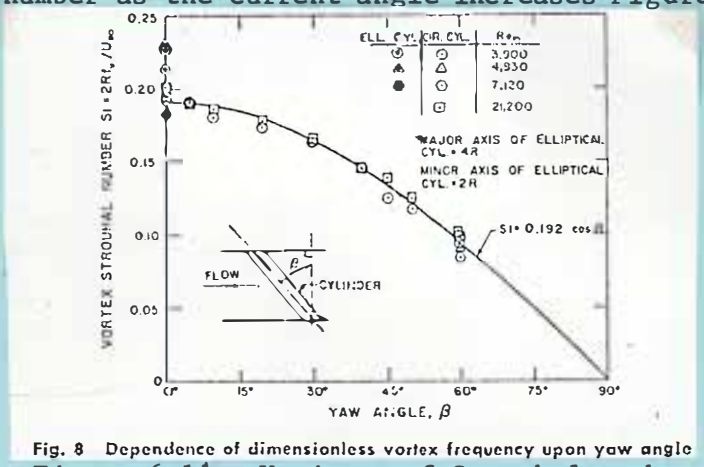

Fig. 8 Dependence of dimensionless vortex frequency upon yaw angle

Figure 6.14. Variance of Strouhal number with increased current angle 6.21/

The Strouhal number of about 0.1 at a 60° current angle and Reynolds number of 2×10^4 is slightly less than the 0.12 for a 2:1 ellpitical cylinder at 5×10^5 and a 90° current angle 6.3/.

6.21/ Op. cit.,

6.3/ Op. cit.,

Drag coefficients for yawed cylinders at angles between 45° and 90° show a variance range from about 1 to 3 Figure 6.14.

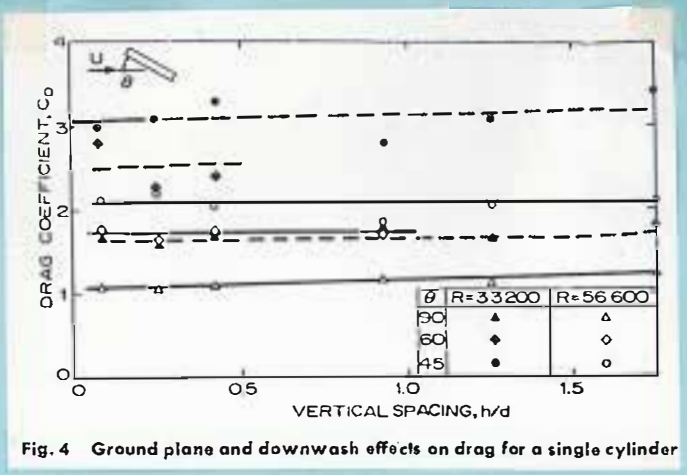

Fig. 4 Ground plane and downwash effects on drag for a single cylinder

Figure 6.14. Variance of drag coefficient with increased current angle 6.7/.

The direction of the drag force is the same as the undisturbed velocity.

Slight decreases in the coefficient were indicated as the space was decreased between the cylinder and the boundary. Average values of drag coefficient were calculated in this study.

Information was not available for evaluating a drag and "mass" or "inertia" coefficient in the Morison equation for cylinders inclined to the current direction.

6.7/ Op. cit. (Wilson/Caldwell).

SECTION 7

WATER MOVEMENT CAUSED BY WAVES AND EFFECT UPON THE CONDUIT

Introduction

Ocean waves occur in irregular shapes and patterns. Wave profiles may have a widely variable shape as shown in Figure 7.1. In a wave train there can be large and small waves and a wide range of wave heights and lengths.

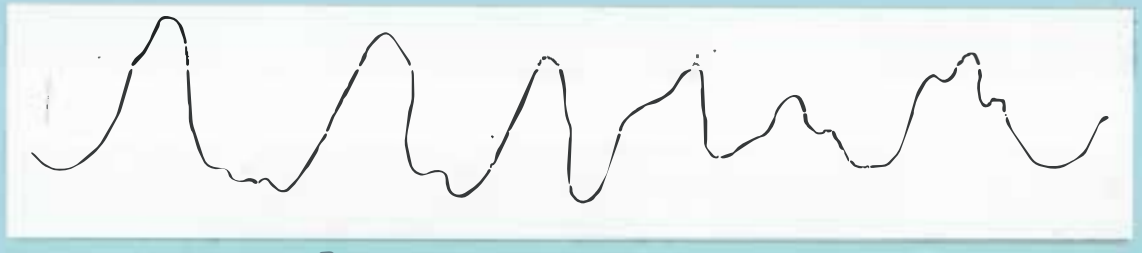

Figure 7.1 - Wave profiles of a wave train

A mathematical theory has not been developed that precisely describes all the diverse features of natural wave action in water. Many theories of varying complexity and difficulty have been developed to describe water movement caused by waves. For engineering purposes the Airy Equations 7.1/ are often used. A description of the theoretical derivation of the Airy Equations is given in Reference 7.1 /. These equations were selected for use in the hydrodynamics study because (1) these equations are the most convenient to use, and (2) for defining velocities occurring within the lower half of the water depth, the results appear as dependable as those from other theories (Appendix I).

7.1/ Ippen, A. T., Estuary and Coastline Hydrodynamics, McGraw-Hill Book Company, Inc., 1966, pp 14-20.

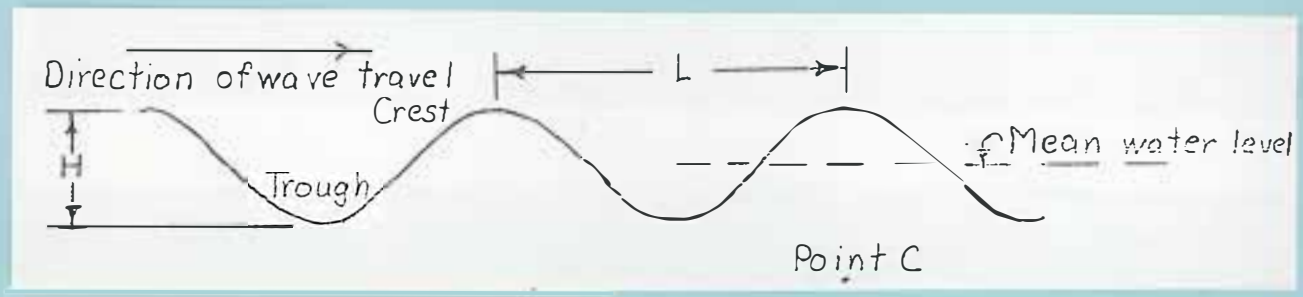

Figure 7.2 - Shape of the Airy curve

The wave profile shape as formulated by the Airy Equation is that of a sine curve, Figure 7.2. This profile is regular and easier to define than that of Figure 7.1. The wave length (L) is the horizontal distance between wave crests, and the wave height (H) the vertical distance from trough to crest. The wave period (T) is the time required for a wave crest to travel the distance of one wave length.

Waves are classified in the literature according to the relative depth:

Deep water wave	Intermediate depth wave	Shallow water wave
$d/L \geq \frac{1}{2}$	$\frac{1}{2} > d/L > 1/20$	$d/L \leq 1/20$

d/L = relative depth

where

d = depth of water to bottom (measured from mean water level)

L = wave length

As waves travel along the water surface the water particles beneath the waves experience an orbital motion. For example, the displacement

of a particle of water about point C in Figure 7.2 has an orbital path during the time of one wave period. FIGURE 7.3.

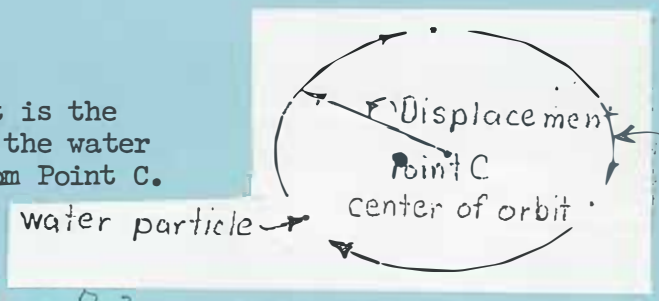

Figure 7.3 - Orbital path of a water particle under a wave for one wave period

The water particle travels once around the orbit path during the wave period T. The magnitude of the displacement, and shape of the orbital path, vary with distance below the water surface and relative water depth.

The orbital paths change as a wave progresses toward the shore, Figure 7.4. For a deep water wave (d/L = 1), the orbits are circular, and displacement magnitude is smaller with increasing depth below the water surface. For this case oscillatory motion caused by the waves is negligible at the bottom. For an intermediate depth wave (d/L = 1/2) orbital motion extends to the bottom. At the bottom, downward movement of the orbital water motion is inhibited, and the oscillatory motion is mainly linear, and in a horizontal direction. Progressing upward from the bottom the orbiting motion is elliptical and may be circular near the water surface. For waves moving into shallower water the major axis of the

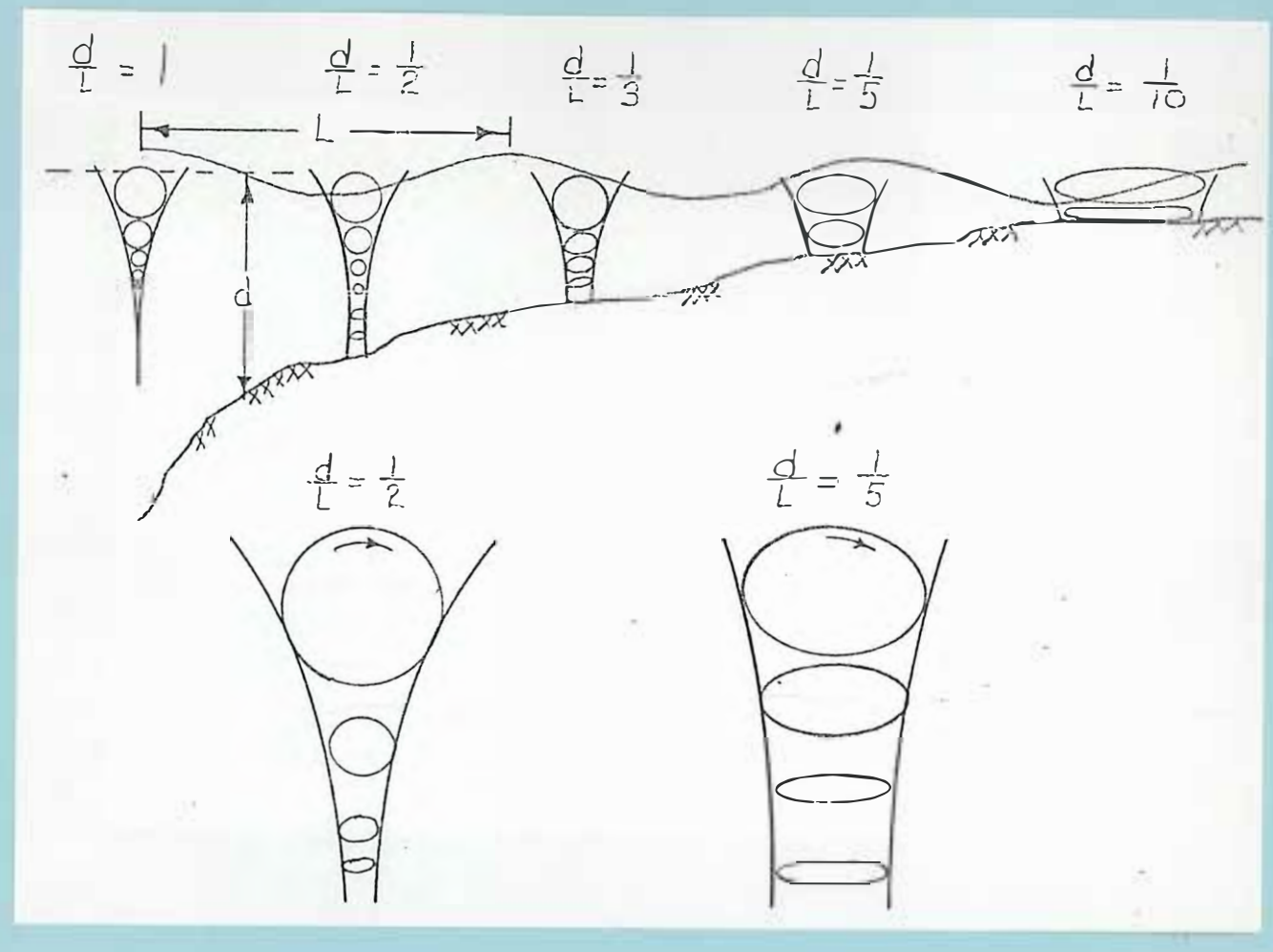

Figure 7.4 - Variation of orbital motion with respect to relative depth $\frac{d}{L}$.

elliptical orbit becomes larger (d/L = 1/5 and d/L = 1/10 of Figure 7.4). In shallow water there is less change in the horizontal portion of the displacement magnitude with decreasing depth.

The Airy Equations

Nomenclature and Symbols. - The California Undersea Aqueduct, constructed on the ocean bottom or above the bottom, will be subjected to forces of wave action. The Airy Equations mathematically describe the water movements and wave action causing the forces on the pipe. Following is a list, brief explanation, and definition sketch (Figure 7.5) of symbols used in the Airy Equations:

x - horizontal coordinate, ft

y - vertical coordinate, ft

d - water depth, distance from mean water level to the bottom, ft

η - vertical distance or displacement of the water surface from mean water level, ft

H - wave height, ft

a - wave amplitude, $a = H/2$, ft

L - wavelength, ft

T - wave period, sec

C - wave celerity, ft/sec

g - acceleration of gravity, ft/sec^2

t - time measured from the instant that a wave crest is located at $x = 0$, sec

θ - phase, angle $\theta = 2\pi(x/L - t/T)$, radians

ξ_x, ξ_y - particle displacements in the x and y directions, ft

V_x, V_y - particle velocities in the x and y directions, ft/sec

A_x, A_y - particle accelerations in the x and y directions, ft/sec^2

k - radian "wave number," $k = 2\pi/L$

σ - radian "wave frequency," $\sigma = 2\pi/T$

p - pressure, lb/ft^2

γ - specific weight, lb/ft^3

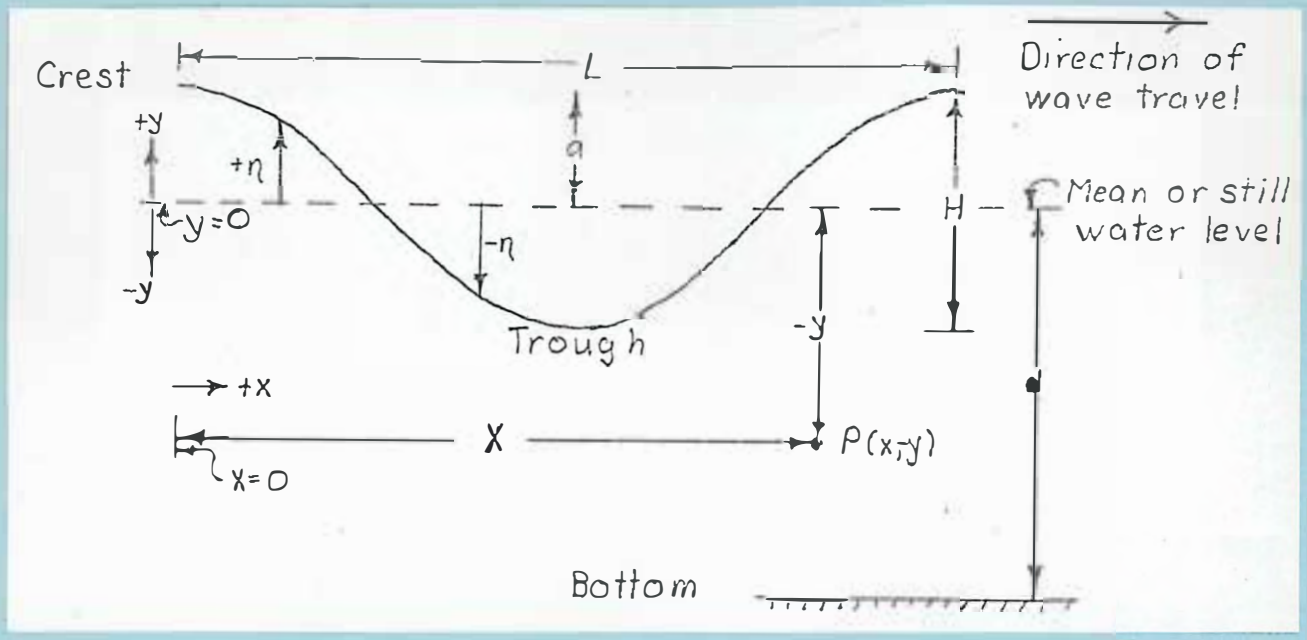

Figure 7.5 - Wave definition

The Equations

$$\theta = 2\pi\left(\frac{x}{L} - \frac{t}{T}\right) \qquad (7.1)$$

$$\eta = a(\cos\theta) \qquad (7.2)$$

$$C = \frac{L}{T} \qquad (7.3a)$$

$$C^2 = \frac{g}{d}\tanh(kd) \qquad (7.3b)$$

$$\varepsilon_x = -a\left[\frac{\cosh k(d+y)}{\sinh kd}\right]\sin\theta \qquad (7.4a)$$

$$\varepsilon_y = a\left[\frac{\sinh k(d+y)}{\sinh kd}\right]\cos\theta \qquad (7.4b)$$

$r \sin\theta$

$$h = \frac{1}{2}\sin 180t$$

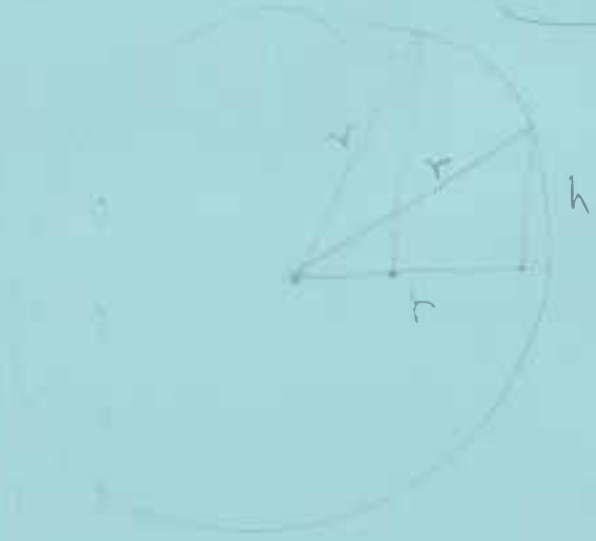

$$\frac{360}{2}$$

$$\frac{\theta}{360} \; 2 = t$$

$$\frac{\theta}{180} = t$$

$$\theta = 180t$$

$$V_x = a\left(\frac{2\pi}{T}\right)\left[\frac{\cosh k(d+y)}{\sinh kd}\right]\cos\theta \qquad (7.5a)$$

$$V_y = a\left(\frac{2\pi}{T}\right)\left[\frac{\sinh k(d+y)}{\sinh kd}\right]\sin\theta \qquad (7.5b)$$

$$A_x = a\left(\frac{2\pi}{T}\right)^2\left[\frac{\cosh k(d+y)}{\sinh kd}\right]\sin\theta \qquad (7.6a)$$

$$A_y = -a\left(\frac{2\pi}{T}\right)^2\left[\frac{\sinh k(d+y)}{\sinh kd}\right]\cos\theta \qquad (7.6b)$$

$$p = \gamma\left[a\frac{\cosh k(d+y)}{\cosh kd}\cos\theta - y\right] \qquad (7.7)$$

Combining Terms to Simplify the Equations. - The following terms were combined to present the equations in a simplified form. The functions Ux and Uy are presented in graph form and will be discussed later in the text. Let

$$Ux = \frac{\cosh k(d+y)}{\sinh kd} \qquad (7.8a) \qquad Uy = \frac{\sinh k(d+y)}{\sinh kd} \qquad (7.8b)$$

and

$$\varepsilon_{xm} = aUx \qquad (7.9a) \qquad \varepsilon_{ym} = aUy \qquad (7.9b)$$

Then

$$\varepsilon_x = \varepsilon_{xm}(-\sin\theta) \qquad (7.10a) \qquad \varepsilon_y = \varepsilon_{ym}\cos\theta \qquad (7.10b)$$

$$V_x = \frac{2\pi}{T}\varepsilon_{xm}\cos\theta \qquad (7.11a) \qquad V_y = \frac{2\pi}{T}\varepsilon_{ym}\sin\theta) \qquad (7.11b)$$

$$A_x = \left(\frac{2\pi}{T}\right)^2\varepsilon_{xm}\sin\theta \qquad (7.12a) \qquad A_y = \left(\frac{2\pi}{T}\right)^2\varepsilon_{ym}(-\cos\theta) \qquad (7.12b)$$

Explanation for Visualization of Water Movement as Formulated by the Airy Equations

Phase Angle. - Wave action formulated by the Airy Equations is periodic in nature. A cycle of wave action occurs over and over again. The phase angle is defined:

$$\theta = 2\pi\left(\frac{x}{L} - \frac{t}{T}\right) \qquad (7.1),$$

and can vary between values, or multiples, of 0 to 2π. The sine and cosine of the phase angle perform a cycling function to parameters of wave action. These parameters are wave profile, particle orbit, particle velocity, and particle acceleration. Note that θ appears in many of the equations (7.1) through (7.12). Thus one cycle of wave action occurs as the phase angle varies from 0 to 2π. In a sense the phase angle may be viewed as a "bookkeeper" to keep account of these continuous cycles. "x" and "t" are variables of the phase angle and are used to obtain the correct relative location within the cycle for a given event.

Simplifications can be made to variables of the phase angle. For example, if the wave acts perpendicular to the pipe the pipe centerline can be located at $x = 0$. The phase angle will then be $\theta = 2\pi\left(-\frac{t}{T}\right)$. Another simplification is to state the variable t in terms of the wave period T. For example, if T is divided into 8 equal parts, the sequence of phase angles will be as follows:

$$t = \frac{T}{8}, \frac{T}{4}, \frac{3T}{8}, \frac{T}{2}, \frac{5T}{8}, \frac{3T}{4}, \frac{7T}{8}, T$$

$$\theta = \frac{-\pi}{4}, \frac{-\pi}{2}, \frac{-3\pi}{4}, -\pi, \frac{-5\pi}{4}, \frac{-3\pi}{2}, \frac{-7\pi}{4}, -2\pi \text{ radians}$$

$$\theta = -45°, -90°, -135°, -180°, -225°, -270°, -315°, -360°$$

By convention a negative angle varies as shown in Figure 7.6 . From Equation (7.1), the phase angle θ varies in a negative direction for the variable t and in a positive direction for the variable x.

Wave Profile. - The equation

$$\eta = a(\cos \theta) \qquad (7.2)$$

describes the wave profile on the water surface. Variation of the water surface with respect to time is shown in Figure 7.7a for x = 0 and $0 < t < T$. Since values of θ, in terms of t, are negative, these values are plotted in the negative direction on Figure 7.7a. The wave profile progresses to the right. For example, the reader may imagine himself located at point P of Figure 7.7a and mentally move a complete wave profile past himself. One wave passes over the pipe. One cycle of wave action occurs as the phase angle varies from 0 to 2π.) Figure 7.7a shows the location of the water surface above the pipe for given times of t.

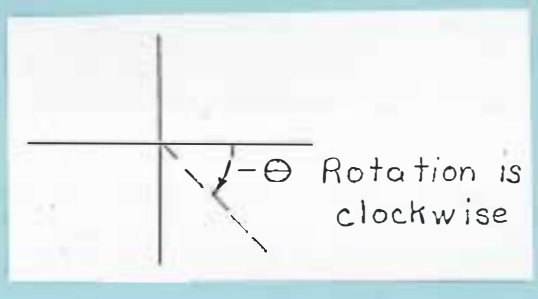

Figure 7.6 . - Variation of θ in the negative direction

The abscissa scale of the wave profile may be viewed as distance along the x axis with respect to the wavelength L. If the wave crest is traveling parallel longitudinally with respect to the pipe, then the solid line of Figure 7.7b shows the wave profile at the instant t = 0. After passage of time T/8 the wave profile has traveled an x distance to the right, dashed line in Figure 7.7b .

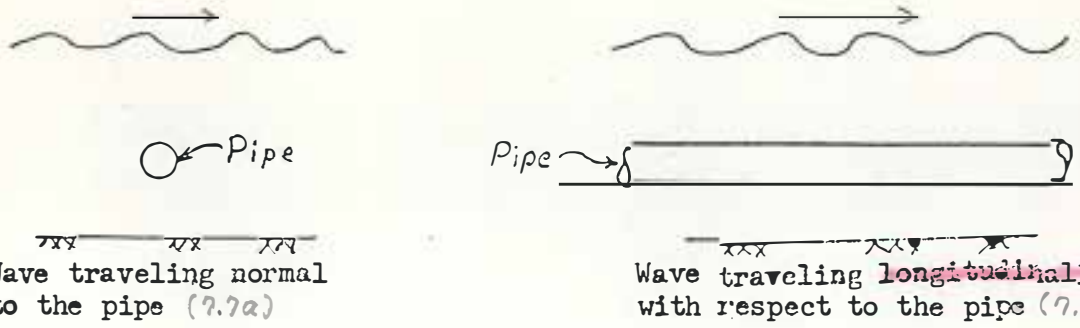

Wave traveling normal to the pipe (7.7a)

Wave traveling longitudinally with respect to the pipe (7.7b)

parallel

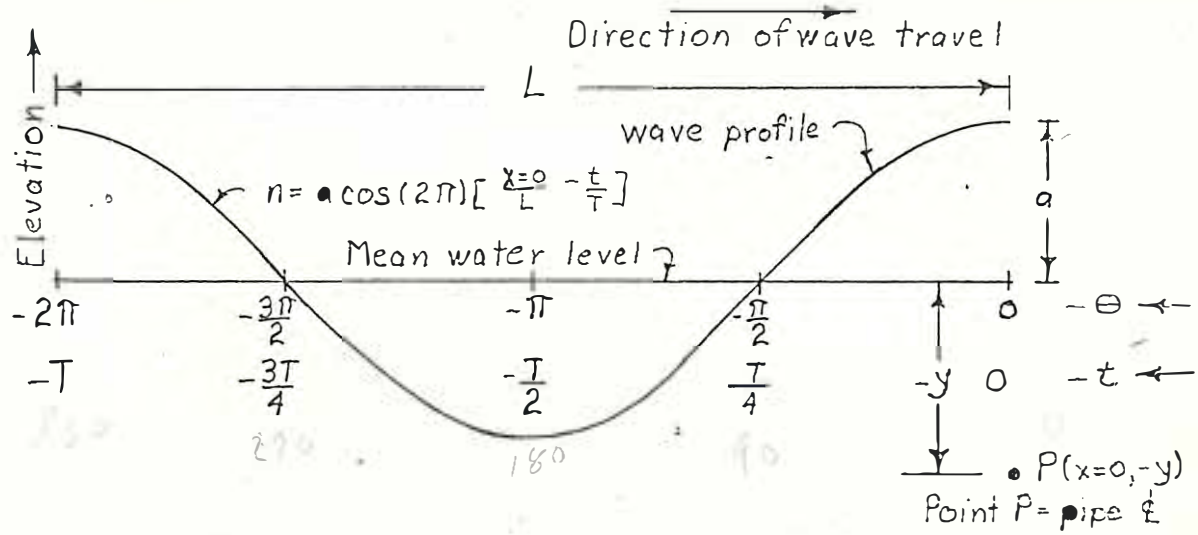

Figure 7.7a - Variation of the water surface with time

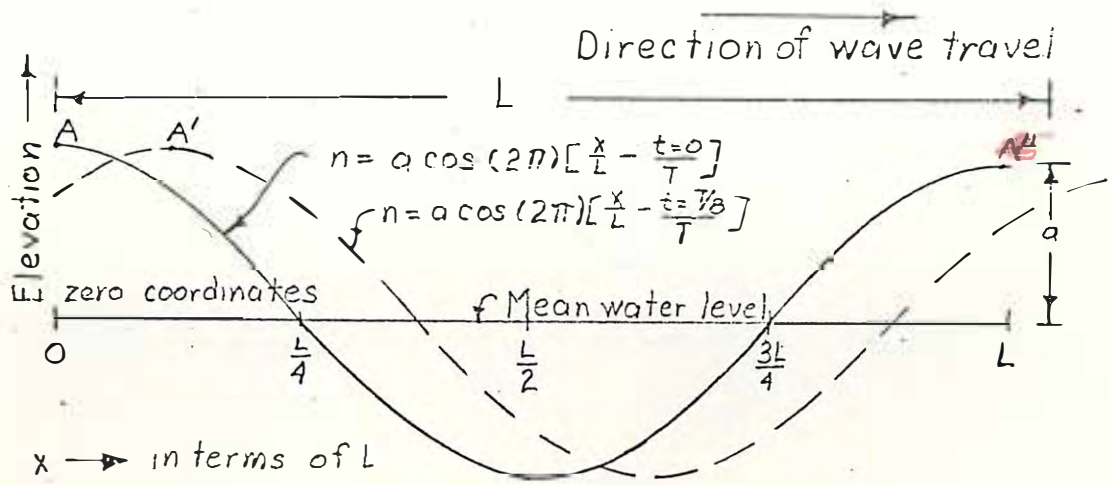

Figure 7.7b - Variation of the water surface with distance

Figure 7.7 - The Water Surface Profile

Wave Celerity. - Wave celerity is the velocity at which the wave travels across the water surface. For example, note point A on the wave crest of Figure 7.7b . After the passage of time (t = T/8) the crest has traveled to point A' (dashed line). By definition the wave celerity is

$$C = \frac{L}{T} \quad (7.\ \ ),$$

and the actual wave celerity could be computed if wave parameters L and T are known. The wave celerity formulated by the Airy Equations is

$$C^2 = \frac{g}{d} \tanh(kd) \qquad (7.3b)$$

Particle Orbit. - The Equations

$$\xi_x = \xi_{xm} (-\sin \theta) \quad (\ .10a) \text{ and } \xi_y = \xi_{ym} \cos \theta \quad (\ .10b)$$

describe the particle orbit path around a given point below the mean water level. For example, consider how water oscillates around the point P(x = 0,-y) of Figure 7.7a as one wave travels past this point. Figure 7.8a shows the orbit path for a given particle of water. Numbered points on the orbit path show location on the particle at the corresponding times of t_1, t_2, t_3, etc. As the phase angle varied from 0 to 2π the particle traveled through a complete orbit from point 0 to point 8. Point 0 and point 8 are at the same location.

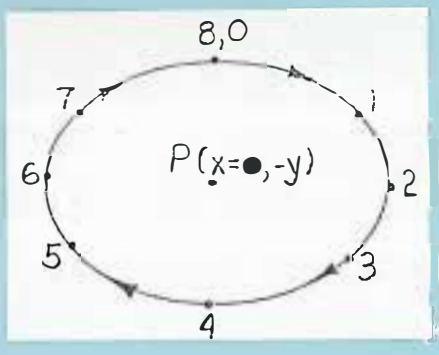

Figure 7.8a. Particle orbit path during the time of one wave period T. $\Delta t = \frac{T}{8}$ and $t_1 = \frac{T}{8}$, $t_2 = \frac{T}{4}$, $t_3 = \frac{3T}{8}$, etc.

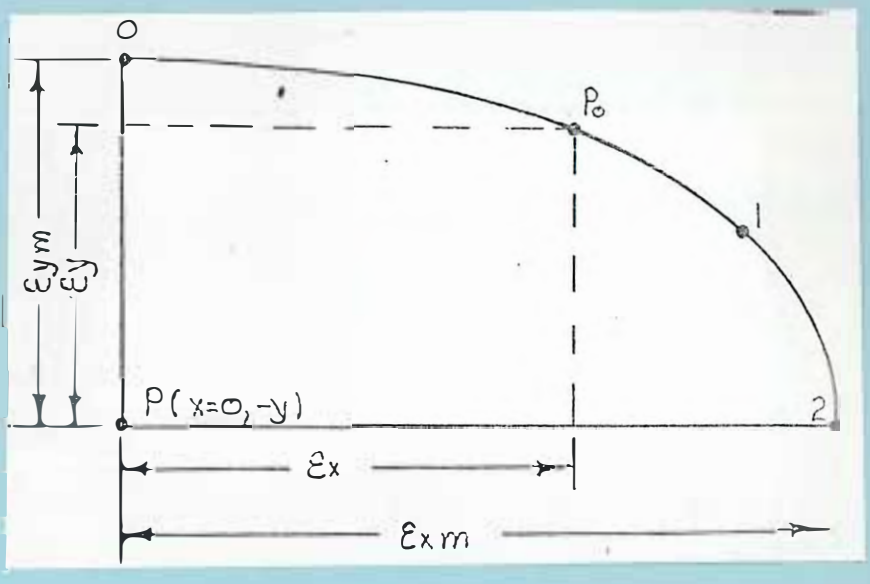

Figure 7.8b. Displacement of particle Po and graphical description of symbols in Equations 7.10a and 7.10b.

Figure 7.8. The wave orbit

Figure 7.8b is an enlargement of one-quarter of the orbit. The displacement of Particle P_o from point P(x = 0,-y) is defined by ε_x and ε_y. The designations ε_{xm} and ε_{ym} were used for lengths of the semi-major and semi-minor axis. As the particle travels around the orbit the displacements ε_x and ε_y are some fraction (between 0 and 1) of the axis ε_{xm} and ε_{ym}. For a pipe free to move with the oscillating water, the orbit path would ~~describe the required distances needed for such~~ provide some measure of the movement, that needs to be considered in design.

Particle Velocities. - The Equations

$$Vx = \frac{2\pi}{T} \varepsilon_{xm} \cos \theta \quad (7.11a) \quad \text{and} \quad Vy = \frac{2\pi}{T} \varepsilon_{ym} \sin \theta \quad (7.11b)$$

describe water movement beneath the waves. There are two methods of visualizing the water movement. The choice of which method is used depends on whether waves are traveling normal or parallel to the conduit.

If the waves are traveling normal to the pipe centerline, P(x=0,-y) should be used as the point of interest. In this case the water motion is of the orbital type as shown by Figures 7.9a and 7.9b. The particle velocity V_p is tangential to the orbit path (Figure 7.9a) and is defined by the component velocities V_x and V_y. Thus during one cycle of wave action the particle velocity changes direction 360°, Figure 7.9b. Velocities V_1 through V_8 can be considered acting at P(x = 0,-y) as shown in Figure 7.9c. When viewing velocities in this manner (normal to the pipe), one imagines himself stationary at a given point and observing direction and magnitude of the velocity for a given time interval. Thus in the equation for phase angle θ only the variable t is used because x = 0.

If the waves are traveling parallel to the pipe, water velocities should be viewed as shown in Figure 7.9d. The velocity V_p is still defined by the component velocities V_x and V_y, but in this case (the solid line curve) variable x is used in the phase angle equation and t = 0. Values of x are stated in terms of the wavelength L. After a given time interval the wave profile has traveled to the right. The

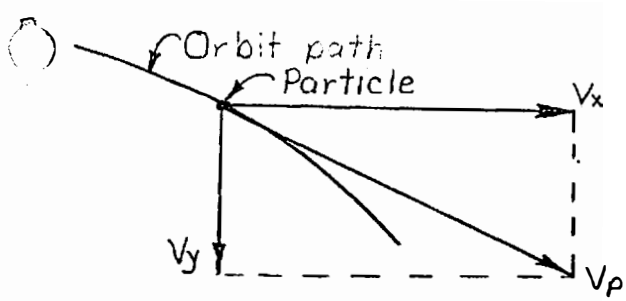

Fig. 7.9a
Particle velocity

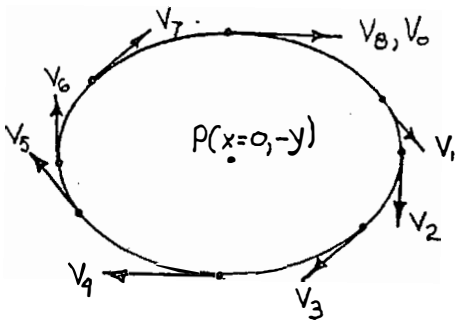

Fig. 7.9b
Directional variation of the particle velocity during the time of one wave period T.
$\Delta t = \frac{T}{8}$, $t_1 = \frac{T}{8}$, $t_2 = \frac{T}{4}$, $t_3 = \frac{3T}{8}$, ect.

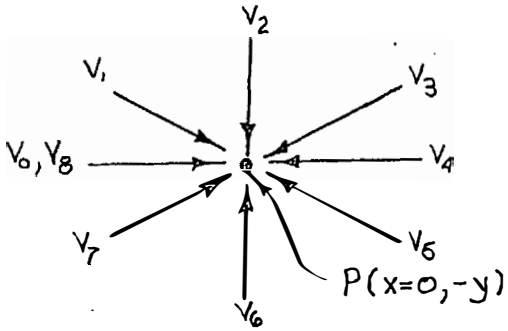

Fig. 7.9c
Directions of the velocity acting on point P(x=0,-y) during the time of one wave period T.

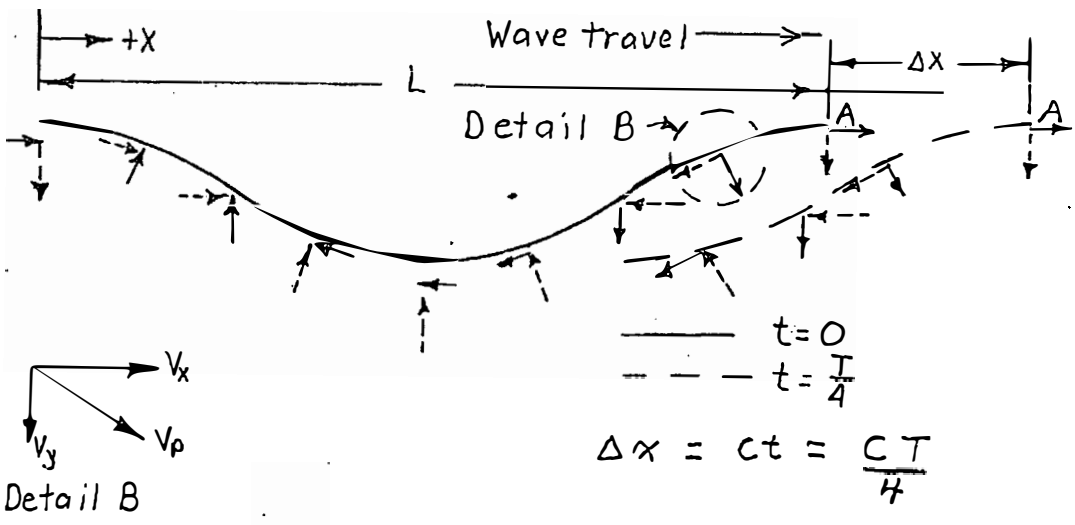

Fig 7.9d
Direction of the water velocity with respect to the wave profile. Heavy lined arrows are velocity and dotted arrows acceleration.

Figure 7.9 - Methods of Viewing Particle Velocity

wave profile of the dashed line in Figure 7.9d is for a time t = T/4. For the t = T/4 wave profile both variables x and t are considered in the phase angle. Another method for obtaining the velocity pattern of the t = T/4 wave would be to transpose velocities of the t = 0 wave to the right a distance Δx.

Particle Acceleration. - The Equations

$$A_x = \left(\frac{2\pi}{T}\right)^2 \mathcal{E}_{xm} \sin\theta \quad (7.12a) \quad \text{and} \quad A_y = \left(\frac{2\pi}{T}\right)^2 \mathcal{E}_{ym} (-\cos\theta) \quad (7.12b)$$

describe particle acceleration in the orbit. The particle acceleration A_p acts inward from the orbit (Figure 7.10a) and is defined by component accelerations A_x and A_y. During one wave cycle the particle acceleration changes direction 360°, similar to velocities of Figures 7.9b and 7.9c, etc., but precedes the velocity as shown in Figure 7.10b.

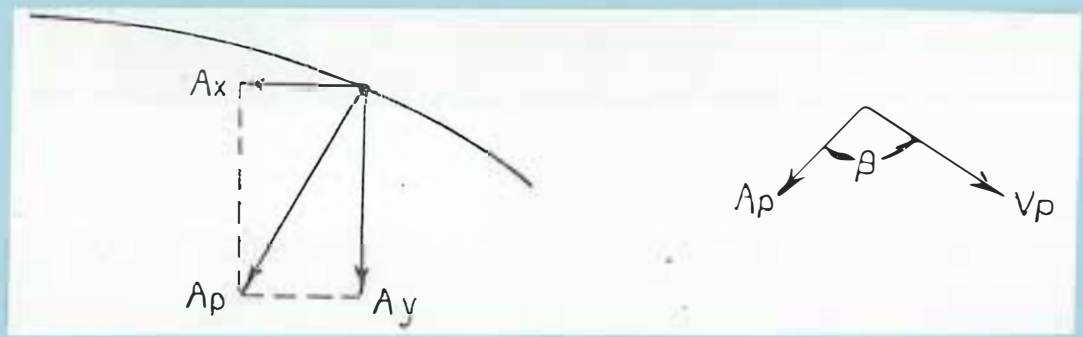

Figure 7.10a - Particle Acceleration Figure 7.10b - Acceleration precedes the velocity

Figure 7.10 - Particle Acceleration

Note the relation of sine and cosine terms for the phase angle θ of equations 7.11 and 7.12. For the x direction the relation is cosine versus sine and for the y direction the relation is sine versus -cosine. With the trigonometric identity sine θ = cos (90° - θ) a 90° shift of the sine equals the cosine. Thus, in wave literature the acceleration

acts 90° out of phase with respect to the velocity. But one must be careful to view this 90° shift with degrees used in the phase angle θ, and not that the angle β, shown in Figure 7.10b, equals 90°, because for elliptical orbits the actual angle β between A_p and V_p can be greater or less than 90°.

Development of Proportionate Vectors to Describe Orbit Parameters

General. - Proportionate vectors are developed describing parameters of orbit displacement, particle velocity, and particle acceleration. Later in the text the vectors will be used to construct a diagram of the force acting on a pipe rigidly fixed above the ocean bed. In development of these proportionate vectors, graphical constructions showing the various orbit parameters are used. This graphical presentation more clearly shows how the Airy Equations formulate the "physical" motion of the water, and how the proportionate vectors can describe the orbit parameters.

Wave Profile. - The initial layout in preparing for construction of the wave profile is shown in Figure 7.11a. In this example one cycle of the phase angle ($0 \leq \theta \leq 2\pi$) is divided into 12 equal increments. This division is shown on the abscissa scale of the wave profile and also on the circle to the right. The length of the abscissa scale represents either one wave period T or one wave length and the radius of the circle represents the wave amplitude a. For convenience of explanation and construction of the wave profile, incremental points are consecutively numbered for both the abscissa scale and generating

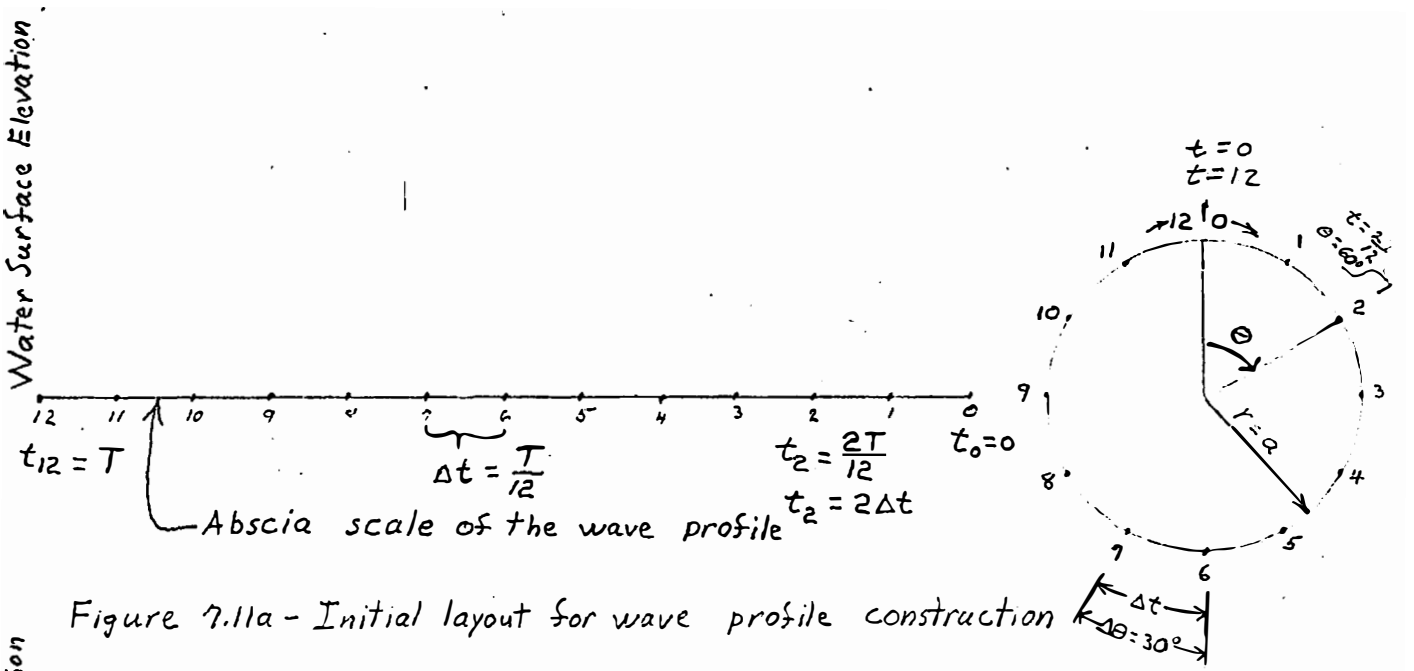

Figure 7.11a - Initial layout for wave profile construction

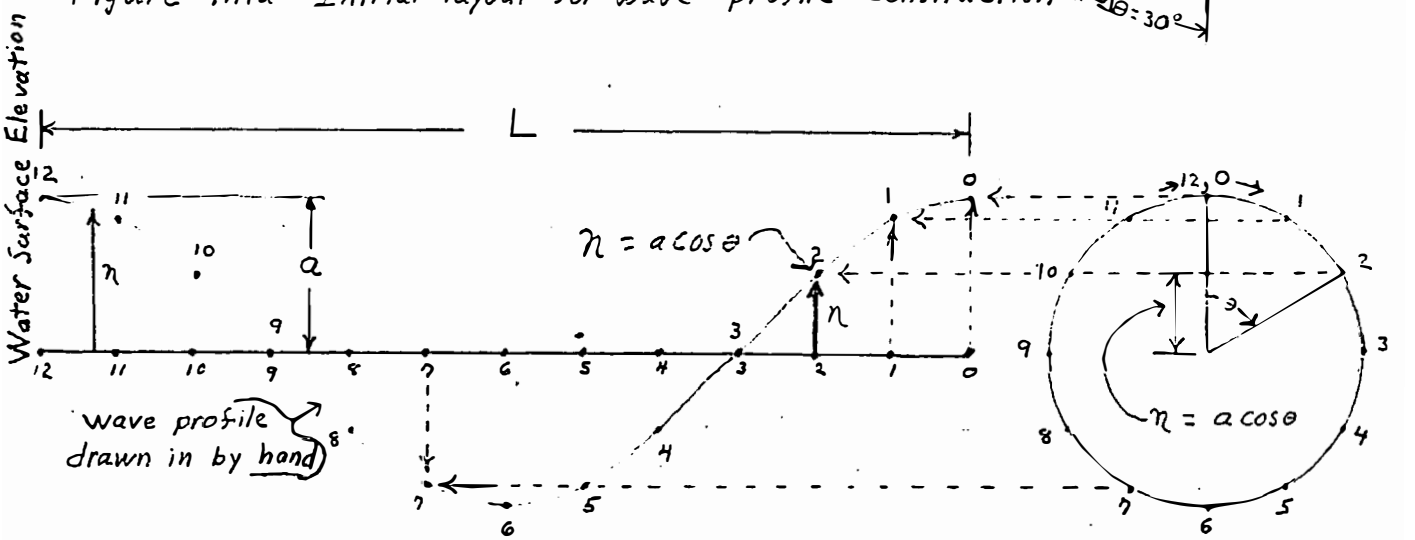

Abscissa Scale of Wave Profile

Note - The abscissa scale may either be in units of time or length. See Figures 6a and 6b.

Figure 7.11b - Constructed wave profile

Figure 7.11 - Method of Constructing the Wave Profile

circle. Values of corresponding points between the abscissa scale and circle are noted on Figure 7.11a. The zero numbered point should be located carefully because the location can be different for the wave parameters (wave profile, orbit, velocity, and acceleration).

The constructed wave profile is shown in Figure 7.11b, and the method of construction is as follows. Start at point zero on the generating circle. Horizontally project the point to the left until it intersects the vertical projection of point zero above the abscissa scale. At this intersection, make a dot and label it zero. Go back to the generating circle and move clockwise to point No. 1. Horizontally project point No. 1 left to the correct location and at this intersection make a dot and label it 1. Repeat the above process with the other points on the generating circle moving in a clockwise direction around the circle. The wave profile is drawn through the labeled intersection points.

The generating circle performs the operation of multiplying the wave amplitude a by the cos θ (note point No. 2 on the generating circle of Figure 7.11b). Generating circles to perform cos θ and sine θ multiplying operations are used in following construction of particle properties.

Particle Orbit. - Construction of the particle orbit path is shown in Figure 7.12. In this case, two generating circles are needed. The circle on the right is for the semi-minor axis of the orbit path and

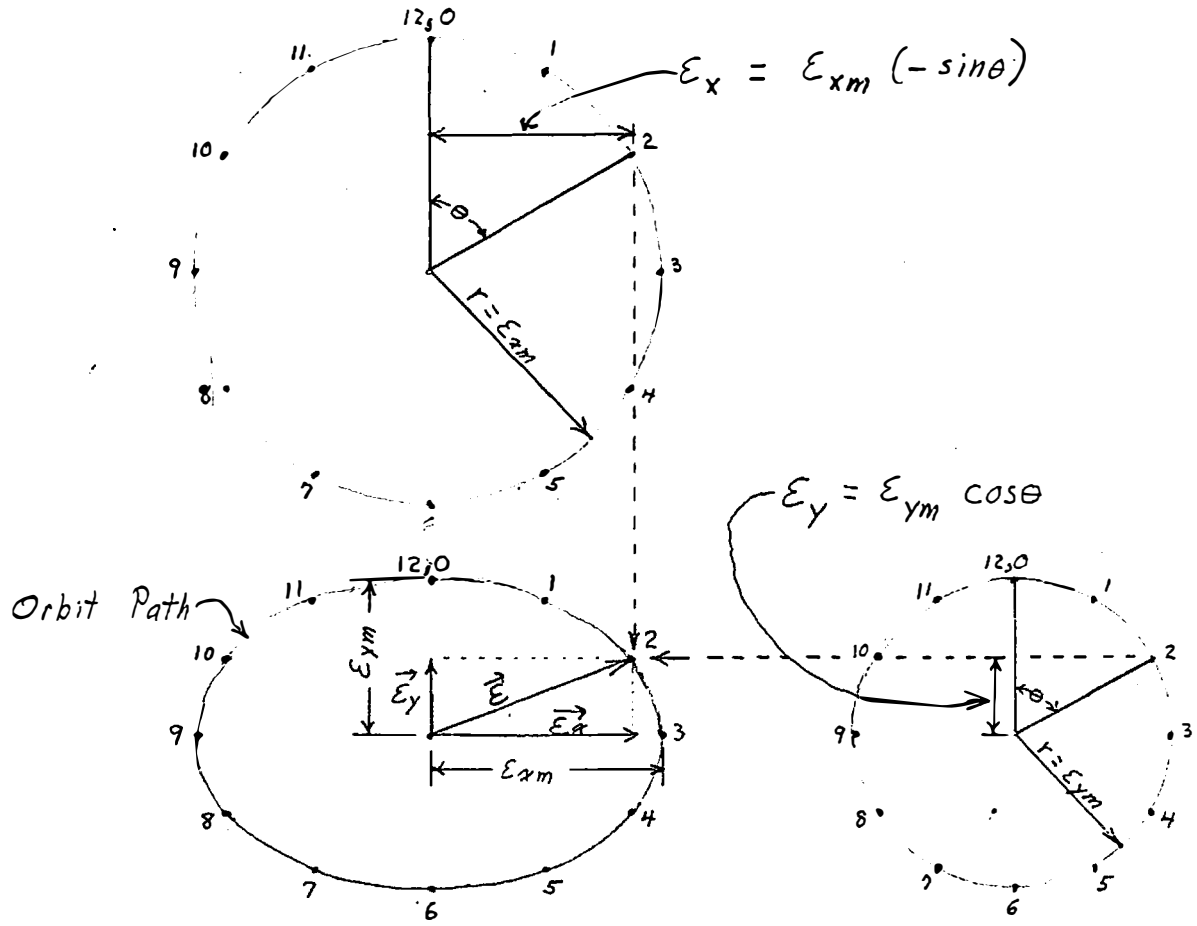

Figure 7.12 - Constructed orbit path

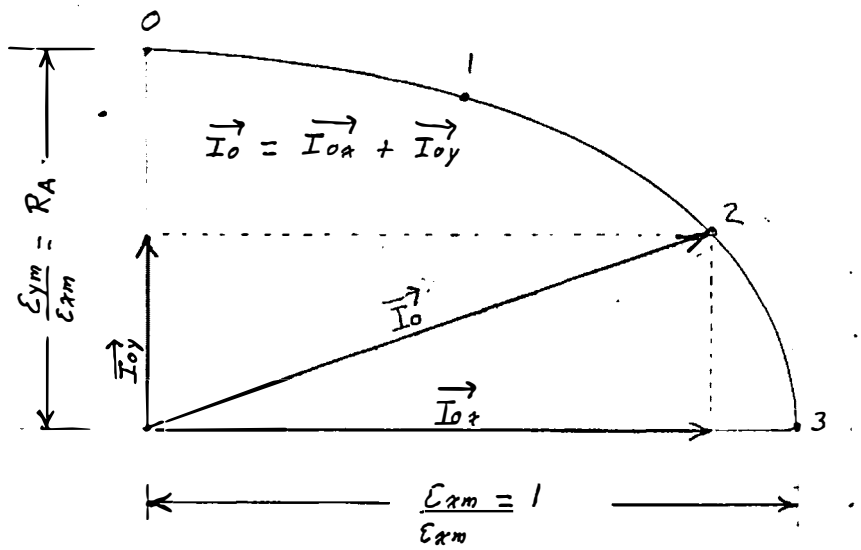

Figure 7.13 - Diagram showing establishment of the proportionate orbit vector $\vec{I_o}$

the radius of this circle is $\mathcal{E}_{ym}$. The upper circle is for the semi-major axis of the orbit path and the radius of this circle is $\mathcal{E}_{xm}$. For point No. 2, the values of $\mathcal{E}_x$ and $\mathcal{E}_y$ are shown on the respective circles. Dotted lines from points No. 2 on the circles show how point No. 2 on the orbit path is located by the intersection of the $\mathcal{E}_x$ and $\mathcal{E}_y$ projections. In like manner, points 0 through 12 are located for the orbit path and then the orbit path can be drawn in.

In Figure 7.13 establishment of the proportionate orbit vector $\vec{I}_o$ is shown. The objective was to have a vector ($\vec{I}_o$) somewhat similar to a unit vector. This was accomplished by the following steps:

(1) Divide the semi-major axis $\mathcal{E}_{xm}$ by $\mathcal{E}_{xm}$ which sets the semi-major axis equal to unity.

(2) Divide the semi-minor axis $\mathcal{E}_{ym}$ by $\mathcal{E}_{xm}$ ($R_A = \mathcal{E}_{ym}/\mathcal{E}_{xm}$), which sets the semi-minor axis as a ratio of the semi-major axis.

(3) Construct the particle orbit path as shown in Figure 7.12; but for the upper circle use a radius equal to 1, and for the right-hand circle use a radius equal to R_A.

Thus by this "proportioning technique" equation 7.13 is developed.

$$\vec{\mathcal{E}} = \mathcal{E}_{xm}\,\vec{I}_o \qquad (7.13)$$

where $\vec{I}_o = \vec{I}_{ox} + \vec{I}_{oy}$.

Equation 7.13 can be used to define the orbit path. The relationships of vectors shown in Figures 7.12 and 7.13 to Equations 7.10 are as follows:

$$\mathcal{E}_x = \mathcal{E}_{xm}(-\sin\theta) \quad (7.10a) \qquad \mathcal{E}_y = \mathcal{E}_{ym}\cos\theta \quad (7.10b)$$

$$\vec{\mathcal{E}}_x = \mathcal{E}_{xm}\,\vec{I}_{ox} \qquad \vec{\mathcal{E}}_y = \mathcal{E}_{xm}\,\vec{I}_{oy}$$

In a sense, vectors $\vec{I}_{ox}$ and $\vec{I}_{oy}$ are $(-\sin\theta)$ and $\cos\theta$ functions; however, because of proportioning the orbit, the vector $\vec{I}_{oy}$ is more useful. It should be noted that in equation $\vec{\mathcal{E}}_y = \mathcal{E}_{xm}\,\vec{I}_{oy}$ the $\mathcal{E}_{ym}$ term does not appear, but has been replaced by a $\mathcal{E}_{xm}$ term, which allows the formation of equation 7.13:

$$\vec{\mathcal{E}} = \vec{\mathcal{E}}_x + \vec{\mathcal{E}}_y = \mathcal{E}_{xm}(\vec{I}_{ox} + \vec{I}_{oy}) = \mathcal{E}_{xm}\,\vec{I}_o \quad (7.13)$$

In showing this replacement, the I_{ox} vector is

$$\vec{I}_{ox} = (-\sin\theta)\ (\text{semi-major axis of Figure } 7.13)$$

$$\vec{I}_{ox} = (-\sin\theta)\left(\frac{\mathcal{E}_{xm}}{\mathcal{E}_{xm}}\right);$$

and the $\vec{I}_{oy}$ vector is

$$\vec{I}_{oy} = (\cos\theta)\ (\text{semi-minor axis of Figure } 7.13)$$

$$\vec{I}_{oy} = (\cos\theta)\,R_A = (\cos\theta)\left(\frac{\mathcal{E}_{ym}}{\mathcal{E}_{xm}}\right), \text{ and}$$

$$\text{then } \vec{\mathcal{E}}_y = \mathcal{E}_{xm}\,\vec{I}_{oy} = \mathcal{E}_{xm}\left[(\cos\theta)\left(\frac{\mathcal{E}_{ym}}{\mathcal{E}_{xm}}\right)\right] = \mathcal{E}_{ym}(\cos\theta)$$

While replacement of the $\mathcal{E}_{ym}$ term with the $\mathcal{E}_{xm}$ term in equation (7.10b) may appear inconsequential, it will later prove very beneficial for easier manipulation of the equations when constructing a force diagram of the orbiting water acting upon the pipe.

This "proportioning technique" will also be used to establish proportionate vectors for both velocity and acceleration.

Particle Velocity. - Construction of the proportionate velocity vector $\vec{I}_v$ is shown in Figure 7.14. Constructing the diagram is similar to that of Figure 7.12. But in this case the zero-numbered points on the generating circles are located 90° clockwise from the top of the circles. Also the radius of the circles are different than those of Figure 7.12 in that the radius of the upper circle is 1 and the radius of the right-hand circle is $R_A = \mathcal{E}_{ym}/\mathcal{E}_{xm}$. The relationship of vectors noted in Figure 7.14 to velocity equations 7.11 is as follows:

$$V_x = \frac{2\pi}{T}\,\mathcal{E}_{xm}\cos\theta \qquad (7.11a) \qquad V_y = \frac{2\pi}{T}\,\mathcal{E}_{ym}\sin\theta \qquad (7.11b)$$

$$\vec{V}_x = \left(\frac{2\pi}{T}\right)\mathcal{E}_{xm}\,\vec{I}_{vx} \qquad \vec{V}_y = \left(\frac{2\pi}{T}\right)\mathcal{E}_{xm}\,\vec{I}_{vy}$$

$$\vec{V}_p = \vec{V}_x + \vec{V}_v$$

$$\vec{I}_v = \vec{I}_x + \vec{I}_y$$

and

$$\vec{V}_p = \left(\frac{2\pi}{T}\right)\mathcal{E}_{xm}\,\vec{I}_{vx} + \left(\frac{2\pi}{T}\right)\mathcal{E}_{xm}\,\vec{I}_{vy} = \left(\frac{2\pi}{T}\right)\mathcal{E}_{xm}\,\vec{I}_v \qquad (7.14)$$

Particle Acceleration. - Construction of the proportionate acceleration vector $\vec{I}_a$ is shown in Figure 7.15. Location of the zero point for the generating circles is at the bottom of the circles. The relationships of the vectors noted in Figure 7.15 to the acceleration equations 7.12 are as follows:

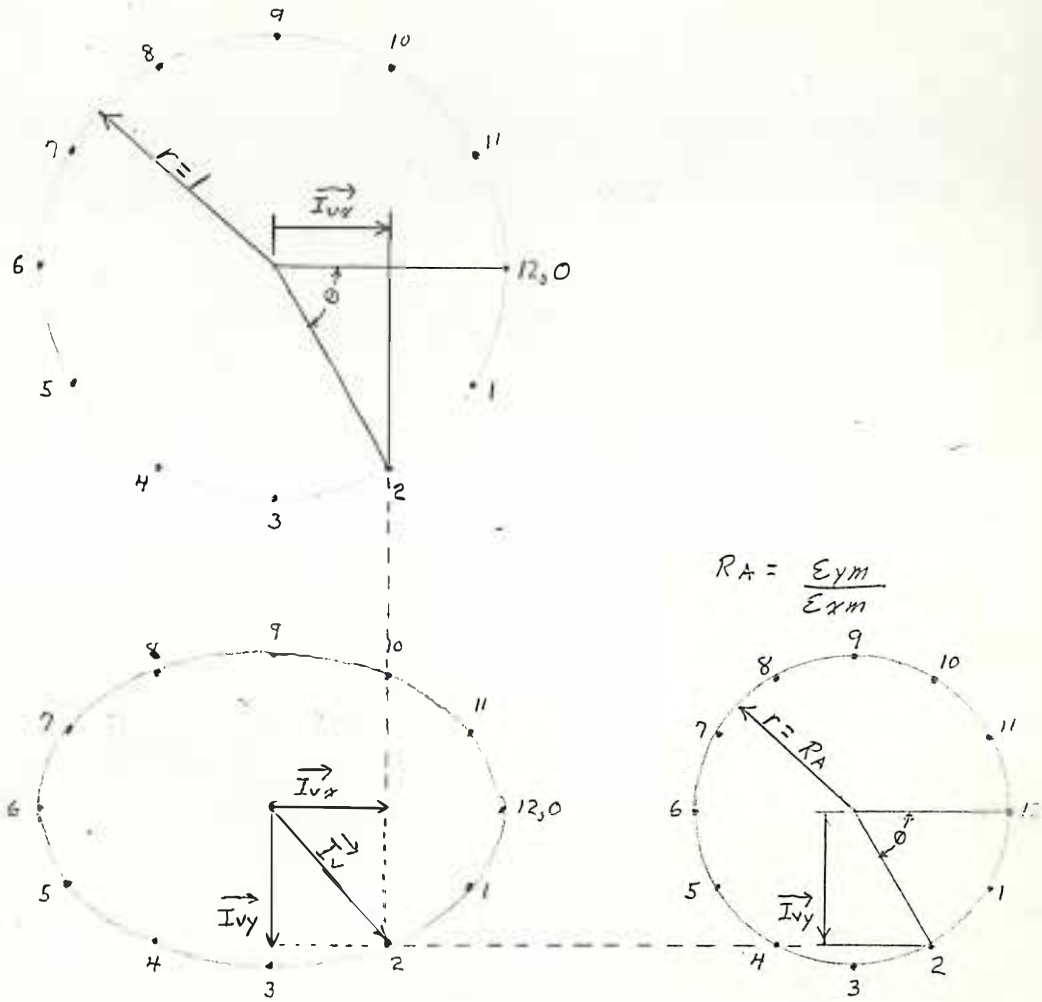

$$\vec{I}_v = \vec{I}_{vx} + \vec{I}_{vy}$$

Figure 7.14 Construction and establishment of the proportionate velocity vector $\vec{I}_v$.

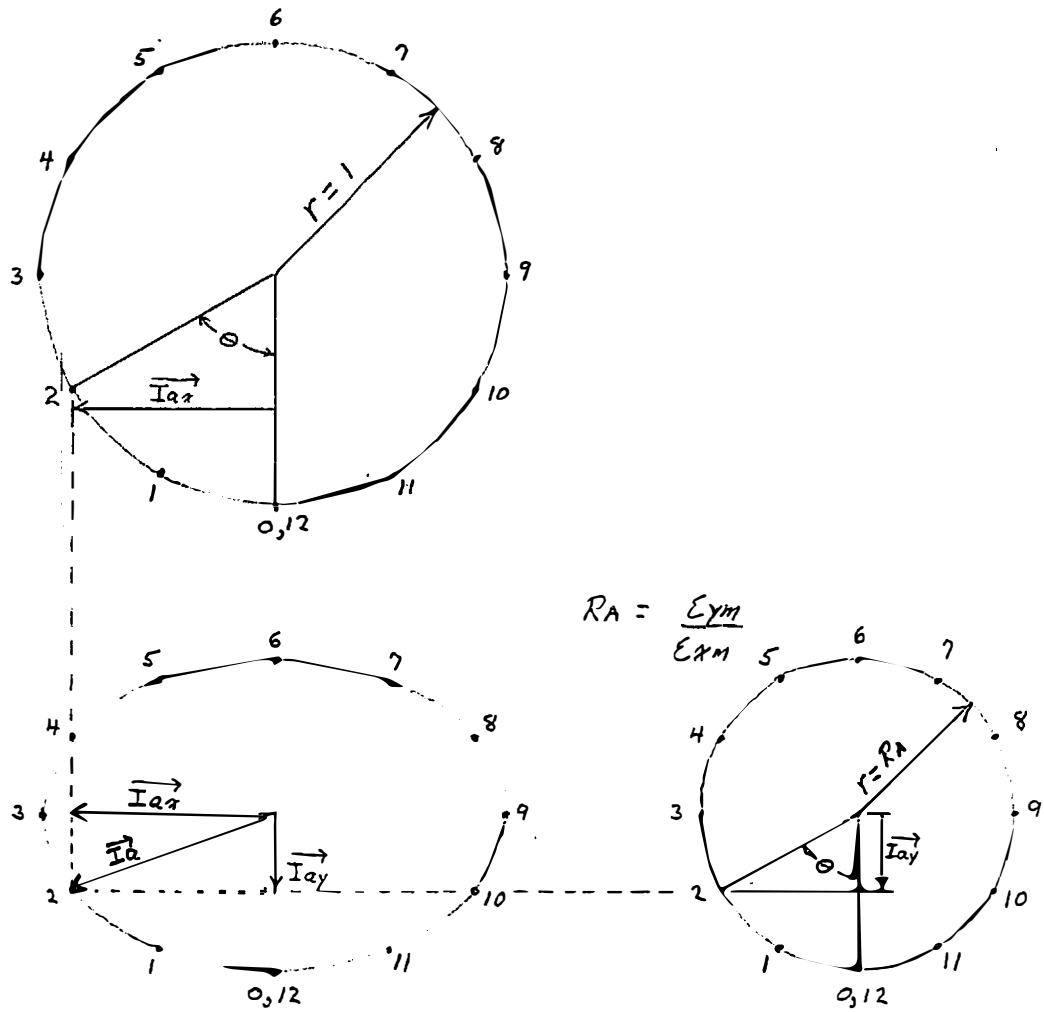

$$\overrightarrow{I_a} = \overrightarrow{I_{ax}} + \overrightarrow{I_{ay}}$$

Figure 7.15- Construction and establishment of the proportionate acceleration vector $\overrightarrow{I_a}$

$$A_x = \left(\frac{2\pi}{T}\right)^2 \zeta_{xm} \sin\theta \qquad (7.12a) \qquad A_y = \left(\frac{2\pi}{T}\right)^2 \zeta_{ym} (-\cos\theta) \qquad (7.12b)$$

$$\vec{A}_x = \left(\frac{2\pi}{T}\right)^2 \zeta_{xm} \vec{I}_{ax} \qquad A_y = \left(\frac{2\pi}{T}\right)^2 \zeta_{xm} \vec{I}_{ay}$$

and

$$\vec{A}_p = \left(\frac{2\pi}{T}\right)^2 \zeta_{xm} \vec{I}_a \qquad (7.15)$$

Review of Wave Property Diagrams. - With respect to time t, the wave profile diagram (Figure 7.11b) shows location of the water surface, the orbit diagram (Figure 7.13) shows particle displacement, the velocity diagram (Figure 7.14) shows direction of the velocity, and the acceleration diagram (Figure 7.15) shows direction of the acceleration. These four diagrams are consolidated in Figure 7.16 . As an example, consider what is occurring at point P(x,-y) (centerline location of the pipe below the mean water level) when $t = t_2$. Point No. 2, Figure 7.16 , of the four diagrams gives the answer. In Diagram 7.16a the water surface is one-half the wave amplitude above the mean water level. Orbit properties from the remaining three diagrams are illustrated in Figure 7.17 . Actually the velocity V_p, and acceleration A_p, acting at P_2 could be transposed to P(x,-y) and considered as acting on the pipe centerline. This would be for the condition where the pipe is rigidly fixed at the location P(x,-y).

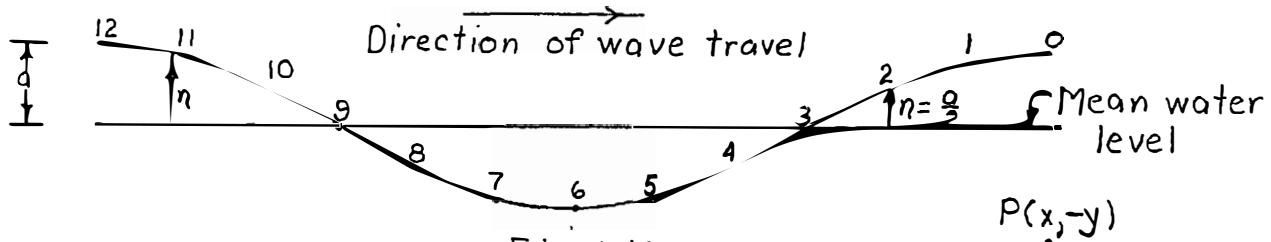

Fig. 7.16a
Wave profile diagram

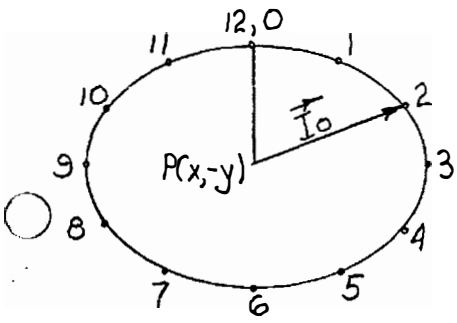

Fig. 7.16b
Orbit diagram
$\mathcal{E} = \mathcal{E}xm\ Io$

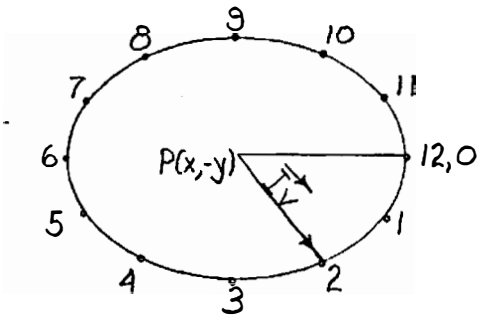

Fig. 7.16c
Velocity diagram
$Vp = \left(\frac{2\pi}{T}\right)\mathcal{E}xm\ IV_x$

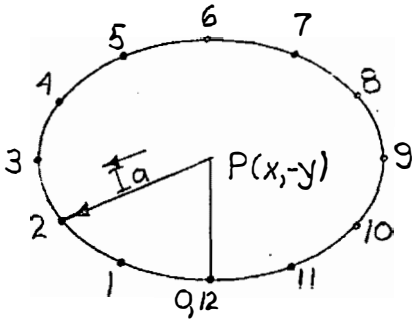

Fig. 7.16d
Acceleration diagram
$Ap = \left(\frac{2\pi}{T}\right)^2\mathcal{E}xm\ Ia$

Figure 7.16
Relationship of the wave properties for one cycle of wave action

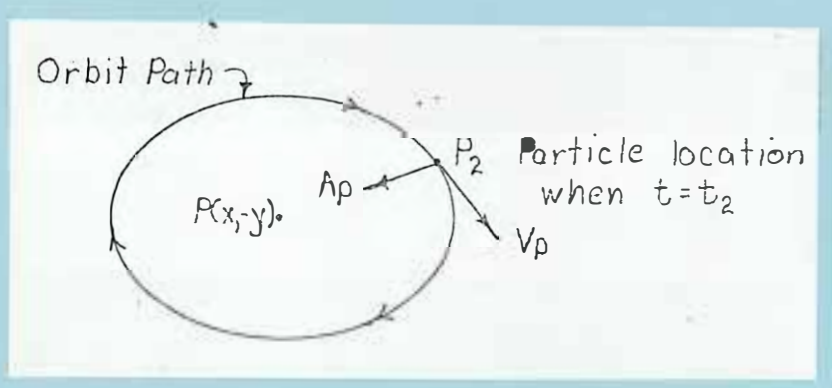

Figure 7.17 - Orbit properties when $t = t_2$

Notice in Figure 7.16 the three diagrams, b through d, have the same size and shape. Only the location of the numbers is different, which reflects the phase angle θ difference between the various orbit properties. Actually one diagram is sufficient for the three proportionate vectors $\vec{I}_o$, $\vec{I}_v$, and $\vec{I}_a$. Therefore, to obtain the proportionate vectors, only one orbital diagram is constructed, but careful and correct observation of phase angle difference is required when using the vectors.

Values of the proportionate vectors can be used in equations 7.13, 7.14, and 7.15 for computing values of the orbital properties. More information about use of the proportionate vectors will be given in a later section.

Force of the Oscillating Water Acting upon the Conduit

The Morison Formula. - The Morison Formula is selected for computing hydrodynamic forces, resulting from wave action, that act upon the pipe. The hydrodynamic forces are composed of two parts. One part considers drag force created by velocity of water flowing by the pipe and the second part considers the force of the accelerating water acting upon the pipe. The formula is

$$F = \overbrace{\frac{1}{2}\rho C_D D V^2}^{\text{drag}} + \overbrace{\frac{\pi}{4}\rho C_m D^2 A}^{\text{acceleration}} \qquad (7.16a)$$

where F = force per unit length of pipe, lbs/ft

ρ = density of the water, slug/ft^3 or lb-sec^2/ft^4

D = pipe diameter, ft

V = velocity of water flowing by the pipe, ft/sec

A = acceleration of water acting on the pipe, ft/sec^2

C_D = drag coefficient, see Section 6

C_m = inertial coefficient, see Section 6

Combining and Rearranging Terms

Equation 7.16a is ~~viewed as being~~ composed of constant and variable terms. The variable terms are velocity V and acceleration A acting upon the pipe. Then Equation 7.16a can be stated

$$F = K_D V^2 + K_A A \qquad (7.16b)$$

where $K_D = \frac{\rho C_D D}{2}$ (7.17) and $K_A = \frac{\pi \rho C_m D^2}{4}$ (7.18)

Entering Proportionate Vectors I_v and I_a into the Formula. - Equation 7.16b should be stated in vector form because in wave motion the velocity and acceleration may not act in the same direction at a given instant, and may also vary during the time period T. The vector form is

$$\vec{F}_T = \vec{F}_D + \vec{F}_A = K_D(\vec{V}_p^{\,2}) + K_A\vec{A}_p \qquad (7.16c)$$

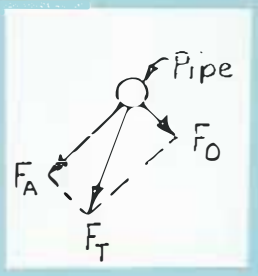

where $\vec{F}_T$ = total force vector

$\vec{F}_D$ = drag force vector

$\vec{F}_A$ = acceleration force vector.

Equations

$$\vec{V}_p = \left(\frac{2\pi}{T}\right)\varepsilon_{xm}\vec{I}_v \qquad (7.14) \qquad \vec{A}_p = \left(\frac{2\pi}{T}\right)^2\varepsilon_{xm}\vec{I}_a \qquad (7.15)$$

or $$\vec{V}_p^{\,2} = \left(\frac{2\pi}{T}\right)^2\varepsilon_{xm}^{\,2}(\vec{I}_v^{\,2})$$

were substituted into equation 7.16c to obtain

$$\vec{F}_T = K_D(\vec{V}_p^{\,2}) + K_A\vec{A}_p = K_D\left(\frac{2\pi}{T}\right)^2\varepsilon_{xm}^{\,2}(\vec{I}_v^{\,2}) + K_A\left(\frac{2\pi}{T}\right)^2\varepsilon_{xm}\vec{I}_a$$

$$\vec{F}_T = \left(\frac{2\pi}{T}\right)^2\varepsilon_{xm}\left[K_D\varepsilon_{xm}(\vec{I}_v^{\,2}) + K_A\vec{I}_a\right] \qquad (7.16d)$$

and equation 7.16d was altered further by entering

$$K_R = \frac{K_A}{K_D} = \frac{\frac{\pi\rho C_m D^2}{4}}{\frac{\rho C_D D}{2}} = \frac{\pi C_m D}{2C_D} \qquad (7.19), \qquad K_D = \frac{K_A}{K_R}.$$

Then the force of drag and acceleration acting upon the pipe due to wave action becomes

$$\vec{F_T} = \left(\frac{2\pi}{T}\right)^2 \varepsilon_{xm} \left[\frac{K_A}{K_R} \varepsilon_{xm} (\vec{I_v}^2) + K_A \vec{I_a} \right]$$

$$F_T = \left(\frac{2\pi}{T}\right)^2 \varepsilon_{xm} K_A \left[\frac{\varepsilon_{xm}}{K_R} (\vec{I_v}^2) + I_a \right] \qquad (7.16e)$$

An example problem showing the use of equation 7.16e will be given later in the text.

U_x and U_y Functions

The hyperbolic sine and hyperbolic cosine terms, in the Airy cosine terms vary depending upon the values of k, d, and y contained within the terms. Since these hyperbolic terms are common in the equations, they are combined in the U_x and U_y Functions of equations 7.8,

Equations 7.4 thru 7.6,

$$U_x = \frac{\cosh k(d+y)}{\sinh kd} \qquad (7.8a) \qquad U_y = \frac{\sinh k(d+y)}{\sinh kd} \qquad (7.8b)$$

The U_x and U_y Functions are shown in graphical form, Figures 7.18 and 7.19. These figures show (1) function values which are given on the abscissa scale, (2) proportionate depth given on the ordinate scale, and (3) a family of relative depth (d/L) curves. Proportionate depth is a ratio of distance above the ocean bottom to the depth d, and is shown in Figure 7.20. The term (d+y) is the distance of the pipe centerline above the ocean bottom.

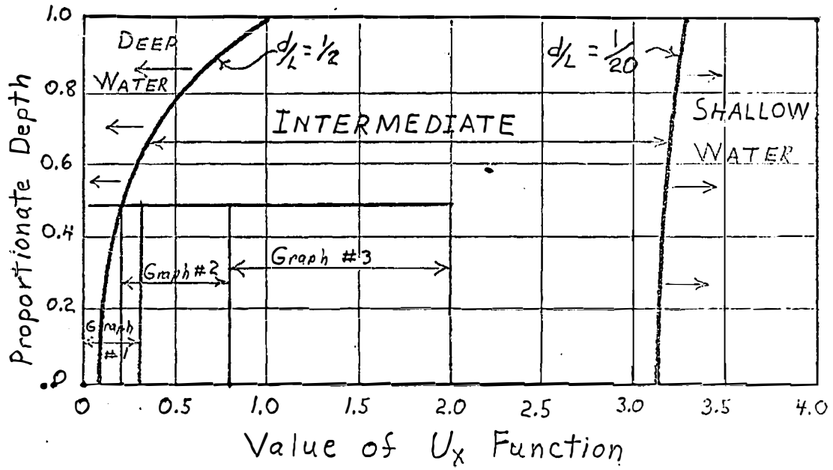

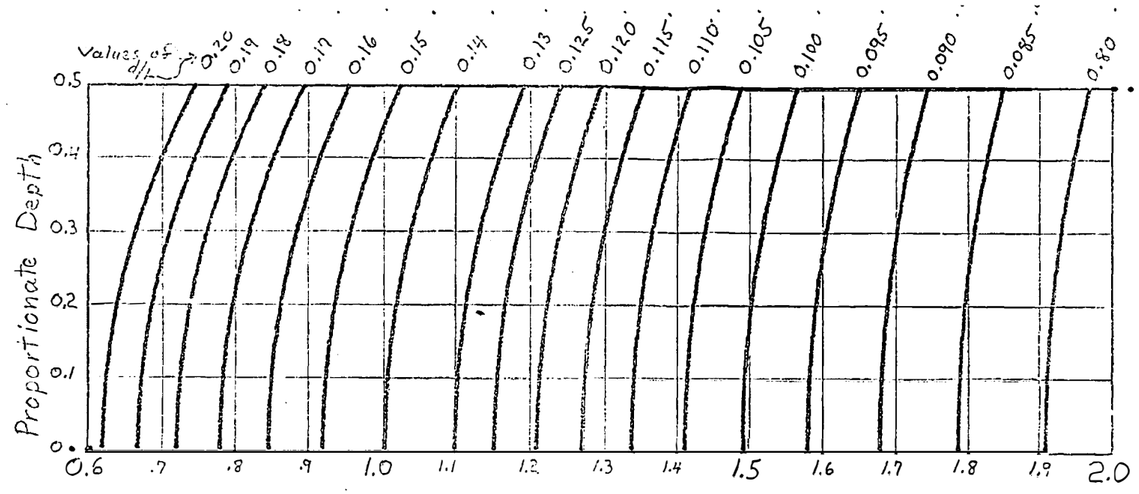

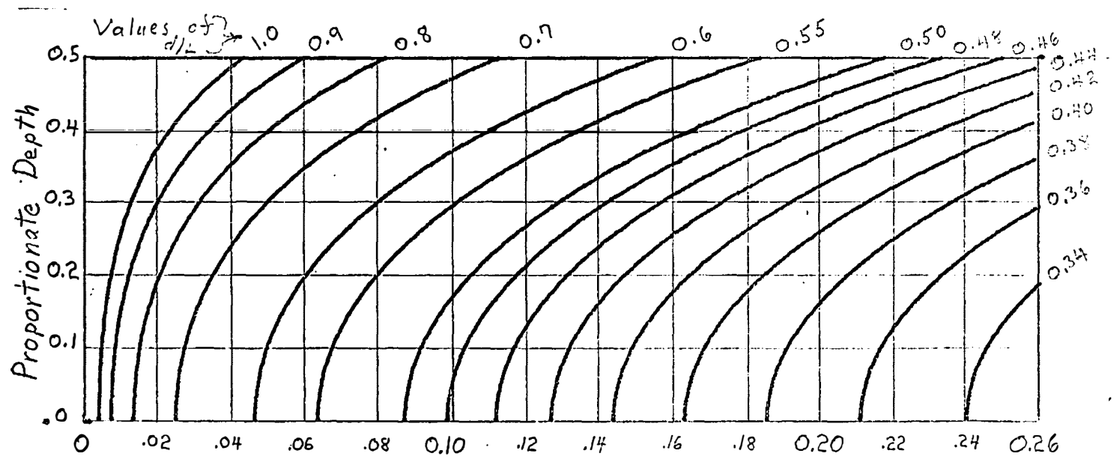

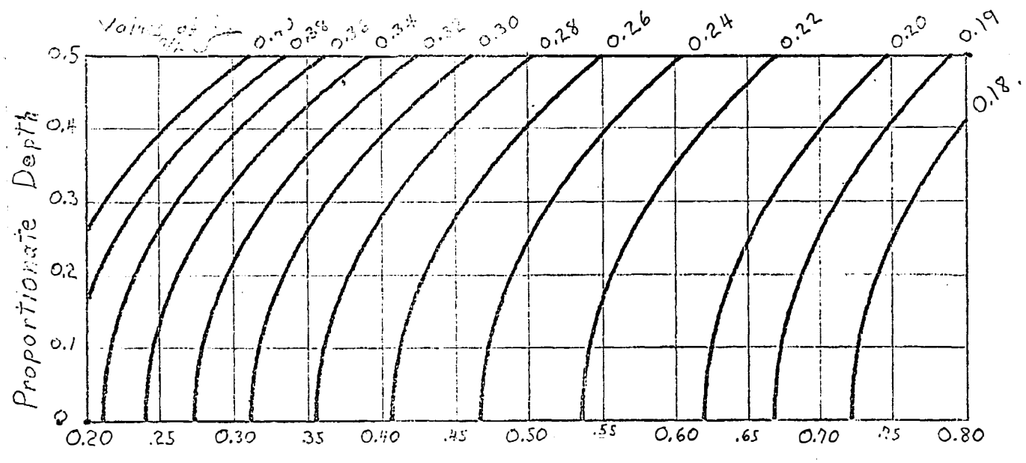

Figure 7.18 - U_X Function

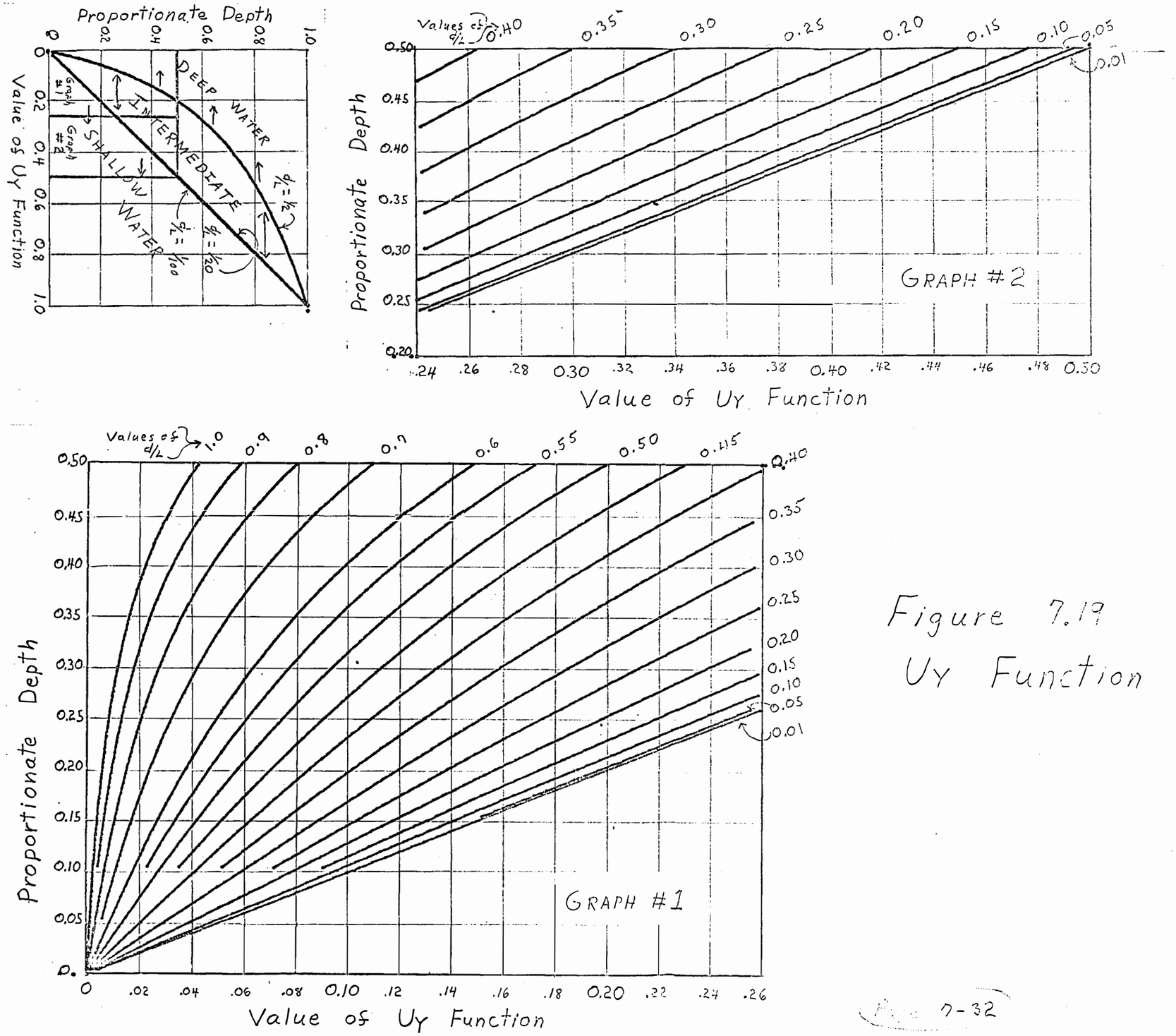

Figure 7.19
Uy Function

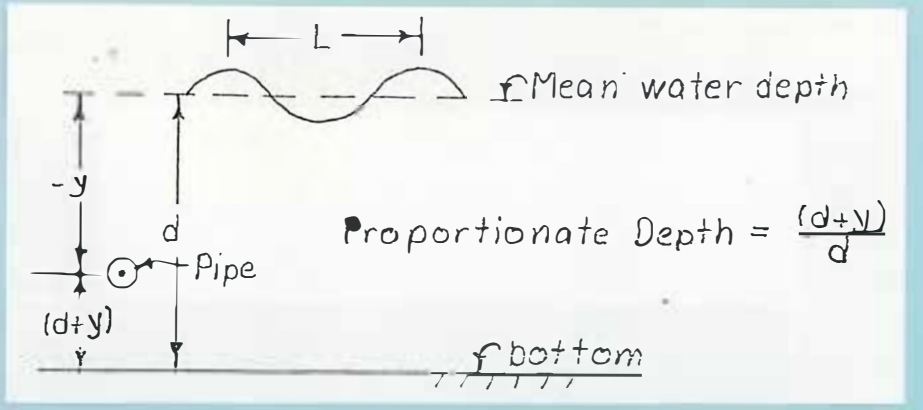

Figure 7.20 - Definition sketch of proportionate depth

Example Problem

General. - An example problem will be worked and a pipe force diagram obtained for one cycle of wave action. The force diagram is schematic and gives a visual presentation of the formulated wave forces acting on the pipe. This example problem will illustrate the use of the U_x and U_y Functions, construction of the proportionate vectors diagram, and use of the $\vec{I}_v$ and $\vec{I}_a$ proportionate vectors in the Morison Formula. A sequence of steps is given that lead to the "graphic" construction of the force diagram.

Graphically constructing a force diagram should be viewed as a visual aid in designing the undersea aqueduct, and provides insight about the oscillating force acting on the pipe. The intent of the method is to provide a mental picture of forces acting on the pipe due to the movement of water by wave action. This mental picture should prove useful when the equations are used to formulate a computer program for solving the undersea aqueduct problem.

Conditions of the Problem. - Conditions of this problem were taken from Reference 7.2/, pages 3-33 to 3-35. However, in this example

problem a fixed wave length of L = 685 feet is used for all three water depths. (In Reference 7.2/, L = 730 feet for the 300-foot depth and L = 736 feet for the 400-foot depth. More discussion about this will follow after working the example problem.)

The pipe is 30 feet in diameter with the centerline located 40 feet above the ocean bottom. The requirement is to obtain force diagrams for ocean depths of 180 feet, 300 feet, and 400 feet.

Wave parameters: H = 50 feet L = 685 feet T = 12 sec

Density: $\rho = 1.994 \approx 2.0$, drag coefficient $C_D = 1.0$,

and inertial coefficient $C_m = 2.0$.

Schematic of Problem Conditions. -

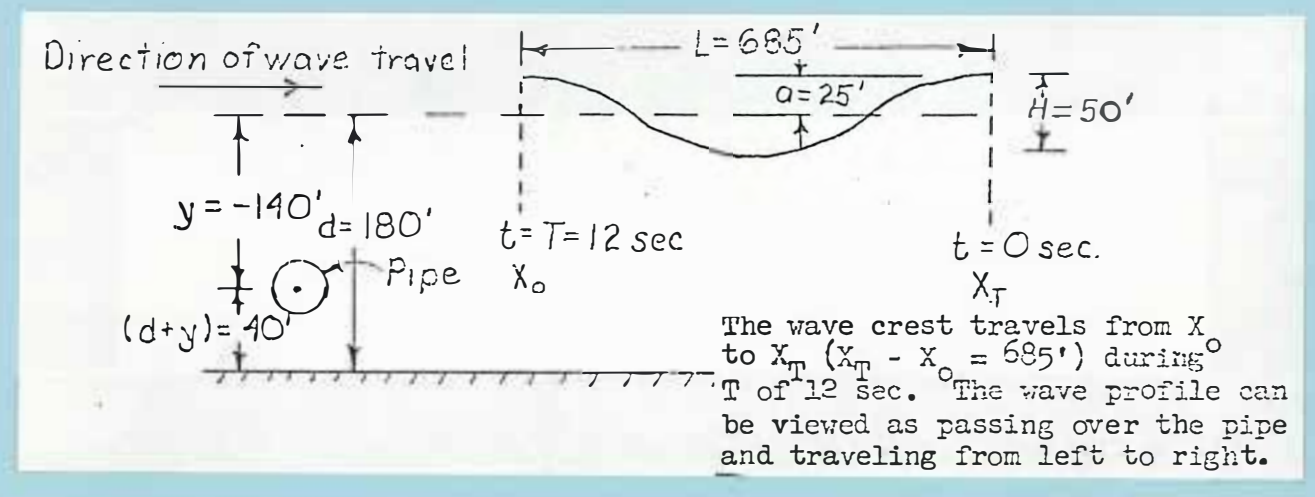

x and y coordinates for pipe centerline
$P_{\mathbb{C}}$ (x = o, y = -140) and
pipe is rigidly fixed (not free to move)
at these coordinates.

Figure 7.2 - Problem definition sketch

7.2/ Ocean Environment and Design Considerations in a Prereconnaissance Study of a California Undersea Aqueduct, Litton Systems Advanced Marine Technology Division, May 16, 1969.

Steps in Obtaining the Force Diagram

Step 1 - Compute relative depth and proportionate depth

Relative depth $d/L = 180/685 = 0.263$

Proportionate depth $(d+y)/d = (180 + 140)/180 = 0.222$

Step 2 - Determine U_x and U_y function values

Using the proportionate depth (0.222) and relative depth (0.263) the function values are obtained from Figures 7.18 and 7.19.

$$U_x = 0.42 \qquad U_y = 0.15$$

Step 3 - Compute semi-major and semi-minor axes for the orbital path about point $P_{\mathcal{L}}$ $(x = 0, y = -140)$

From equation 7.9a $\mathcal{E}_{xm} = aU_x = (25)(0.42) = 10.5$ ft

From equation 7.9b $\mathcal{E}_{ym} = aU_y = (25)(0.15) = 3.75$ ft

Step 4 - Constructing the proportionate vectors diagram

Compute $R_A = \dfrac{\mathcal{E}_{ym}}{\mathcal{E}_{xm}} = \dfrac{3.75}{10.5} = 0.36$

For this example the phase angle θ is divided into 12 equal increments. $\Delta\theta = 30°$ and $\nabla t = T/12 = 1$ sec. If a more detailed diagram is desired, the phase angle could be divided into more increments.

The Proportionate Vectors Diagram (ellipse of Figure 7.22) is constructed by the process shown in Figure 7.12, but with the radius of the upper generating circle equal to 1, and the radius

of the right generating circle equal to R_A = 0.36. When construct-int the actual diagram a larger figure should be made.

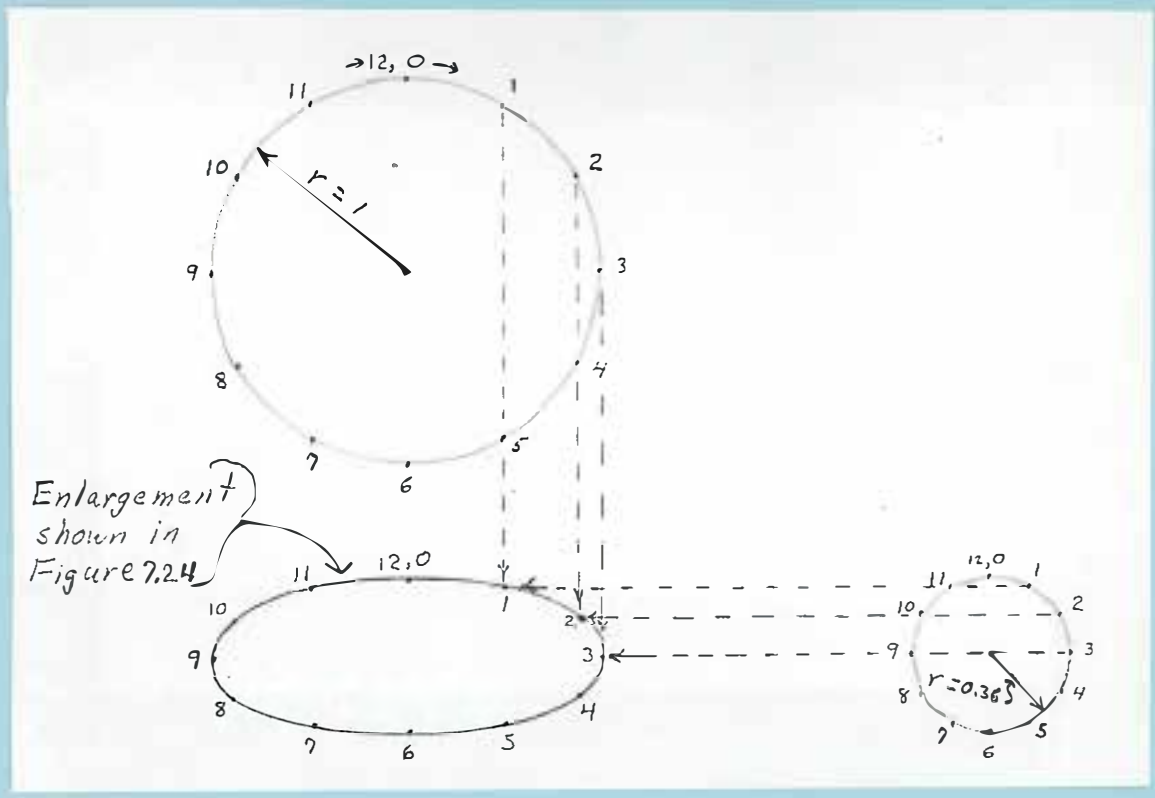

Figure 7.22 - Constructing Proportionate Vectors Diagram for Example Problem

Values of the proportionate vectors $\vec{I}_o$, $\vec{I}_v$, and $\vec{I}_a$ are obtained for times t_o, t_1, t_2, etc., from the Proportionate Vectors Diagram; but the correct numbered point for the desired vector must be used when accounting for the phase angle difference between the vectors. For a review of this phase angle difference the reader should refer to Figure 7.16, Diagrams 7.16b through 7.16d. Note the location of the zero numbered point on each diagram.

There is a 90° phase angle difference between each successive diagram. The location of each proportionate vector when $t = t_2$ is shown in Figure 7.23 for this example problem.

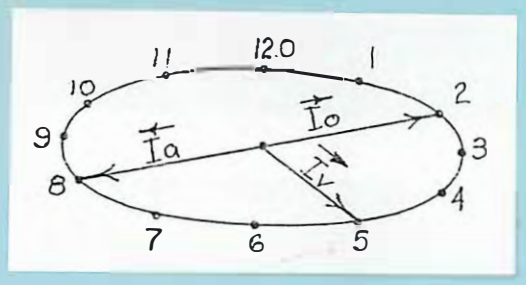

For this example problem $\Delta t = T/12$ and $\Delta\theta = 360°/12 = 30°$, then three time increments equal a 90° phase angle difference ($3\Delta\theta = 90°$). In this diagram the point numbering is for the orbit path, therefore the correct numbered point for $\vec{I}_v$ precedes $\vec{I}_o$ by 3 points (2+3 = 5), and I_a precedes I_o by 6 points (2+6 = 8).

Figure 7.23 - Proportionate vectors for $t = t_2$ of example problem.

The large-scale Proportionate Vectors Diagram is shown in Figure 7.24. Points of the respective time increments are numbered clockwise around the diagram. Below the point number the value of the proportionate vector is given within the parentheses. This value is the measured distance from the center of the ellipse to the perimeter and is measured with a scale. An example of this measurement is shown for point 2 on Figure 7.24. The relationship of the proportionate vectors to orbit properties at t_2 is shown in Figure 7.25.

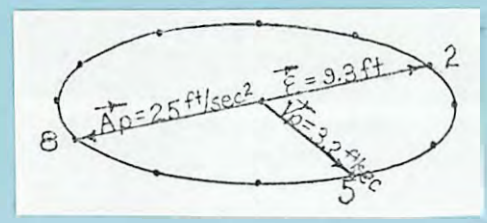

Figure 7.25 - Orbit properties at t_2.

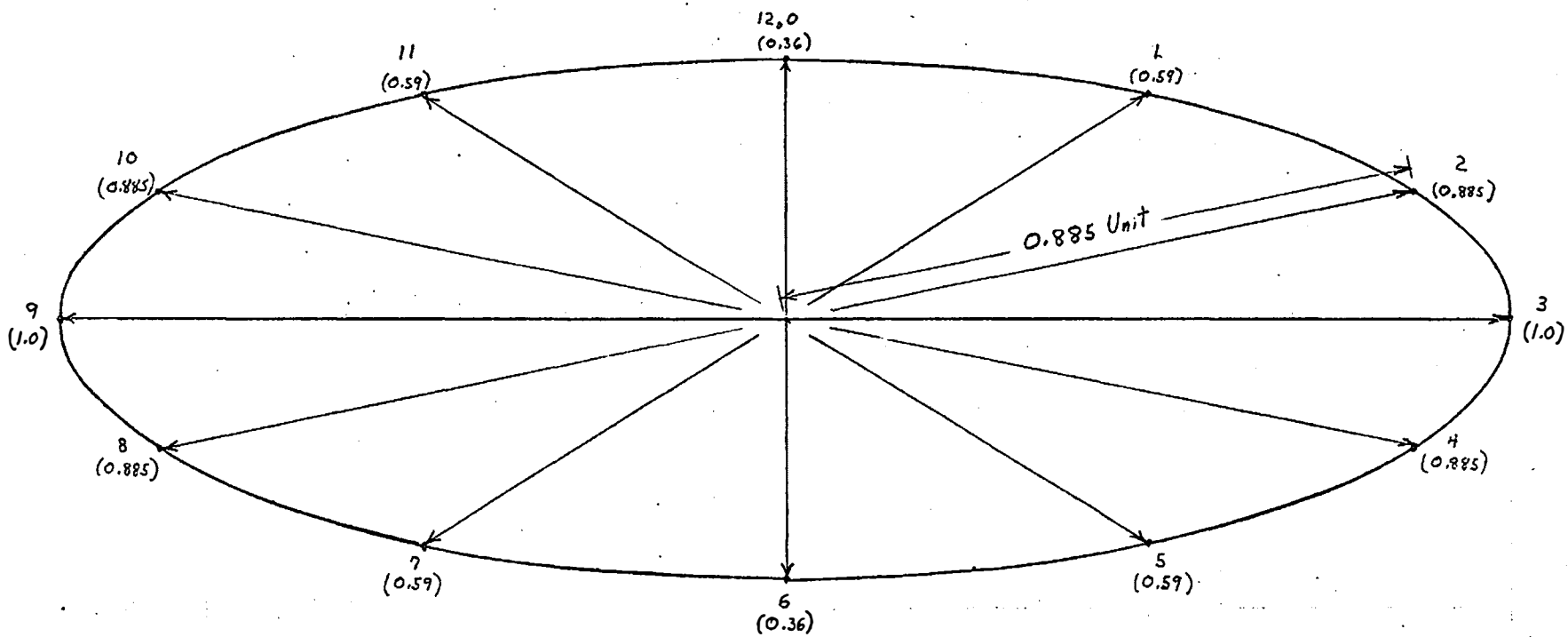

Figure 7.24 - Large scale Proportionate Vectors Diagram

Page 7-38

The mathematical computation for orbit properties shown in Figure 7.25 and how to use the proportionate vectors are given. Values of the vectors $\vec{I}_o = 0.885$ (Point 2), $\vec{I}_v = 0.59$ (Point 5), and $\vec{I}_a = 0.885$ (Point 8) were obtained from Figure 7.24 and were substituted into numbered equations as shown.

$$\left(\frac{2\pi}{T}\right) = \left(\frac{2\pi}{12}\right) = 0.524 \qquad \left(\frac{2\pi}{T}\right)^2 = 0.274$$

$$\mathcal{E} = \mathcal{E}_{xm}\,\vec{I}_o = 10.5\,\vec{I}_o = 10.5(0.885) = 9.3 \text{ ft} \qquad (7.13)$$

$$V_P = \left(\frac{2\pi}{T}\right)\mathcal{E}_{xm}\,\vec{I}_v = 0.524\,(10.5)\,\vec{I}_v = 5.50\,\vec{I}_v = 5.50(0.59) = 3.2 \text{ ft/sec} \qquad (7.14)$$

$$A_P = \left(\frac{2\pi}{T}\right)^2 \mathcal{E}_{xm}\vec{I}_a = 0.274(10.5)\vec{I}_a = 2.88\,\vec{I}_a = 2.6 \text{ ft/sec}^2 \qquad (7.15)$$

Step 5 - Substitute problem values into the force equations

$$\vec{F}_T = \left(\frac{2\pi}{T}\right)^2 \mathcal{E}_{xm}\,K_A\left[\frac{\mathcal{E}_{xm}}{K_R}\,(\vec{I}_v^{\,2}) + \vec{I}_a\right] \qquad (7.16e)$$

$$K_A = \frac{\pi\rho C_m D^2}{4} = \frac{\pi(2)(2)(30)^2}{4} = 2830 \qquad (7.18)$$

$$K_R = \frac{\pi C_m D}{2C_D} = \frac{\pi(2)(30)}{(1)(2)} = 94.2 \qquad (7.19)$$

$\mathcal{E}_{xm} = 10.5$ ft from Step 3

Then

$$\vec{F}_T = (0.274)(10.5)(2830)\left[\frac{10.5}{94.2}\,(\vec{I}_v^{\,2}) + \vec{I}_a\right]$$

$$\vec{F}_T = 8140\left[0.111\,(\vec{I}_v^{\,2}) + \vec{I}_a\right]$$

This is the force equation for conditions of the example problem.

Notes - (1) The lighter lined vectors which are designated by [3] thru [9] are proportionate vectors of Figure 7.24 which were viewed through the transparent sheet.
(2) The dotted lines, from points 0' to 0, 1' to 1, 2' to 2, and 3' to 3, relate to the vector addition explained in Steps 6b thru 6e.

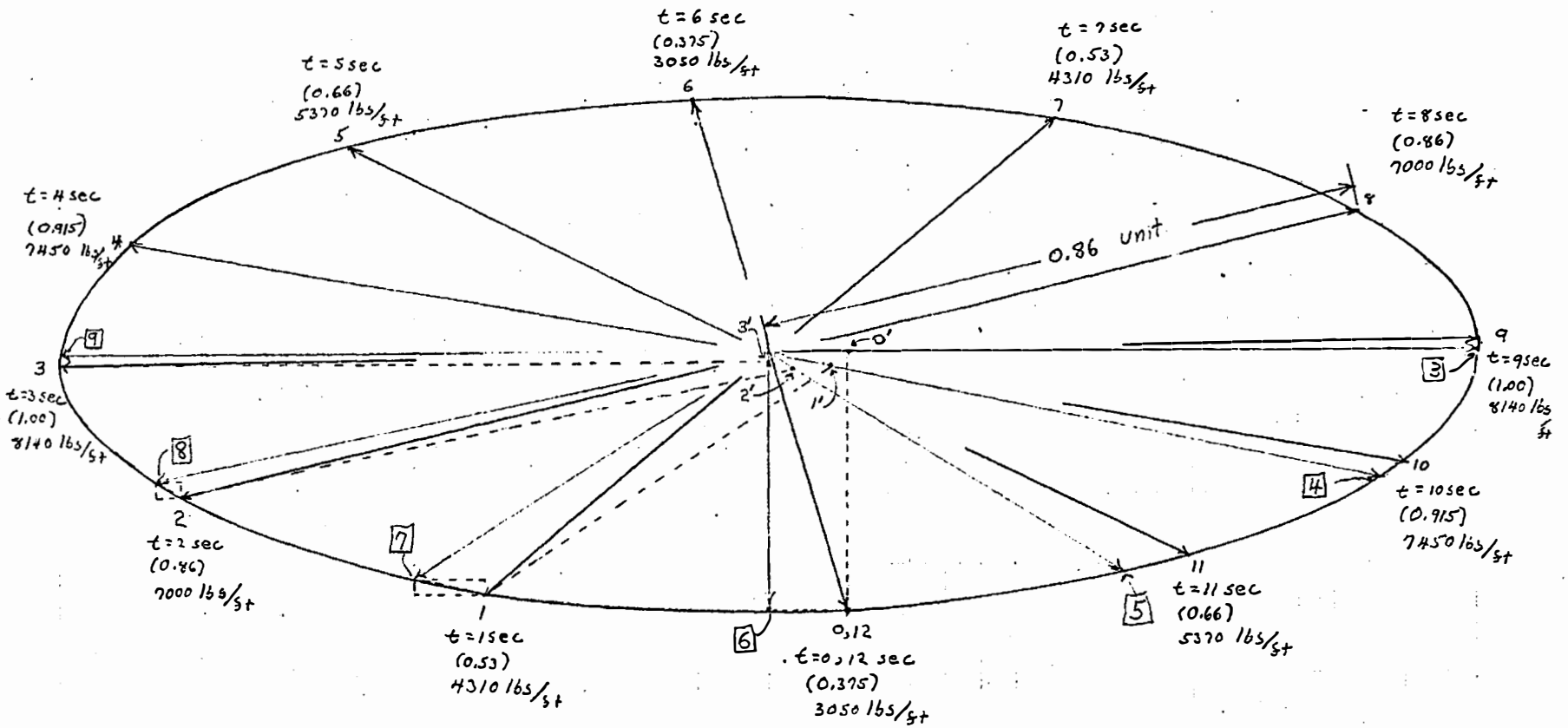

Figure 7.26 - Force Diagraime

Step 6 - Constructing the Force Diagram

Values of the proportionate velocity vector $\vec{I}_v$ and the proportionate acceleration vector $\vec{I}_a$ are substituted into the force equation. A graphic method is involved in making the vector addition as required by the force equation. The completed Force Diagram is shown in Figure 7.26. Before explaining the graphic vector addition an illustration of drag and acceleration force acting upon the pipe will be given, and shown in Figure 7.27. Then in Figure 7.28 the operation of adding vector forces F_D and F_A is shown, but where the addition actually occurs using the proportionate vectors $\vec{I}_v$ and $\vec{I}_a$. Afterwards Steps 6a through 6g are given which explain how the graphic construction of the force diagram shown in Figure 7.26 was done.

The drag and acceleration forces acting upon the pipe for times t_o, t_1, t_2, and t_3 are given in the table below:

Table of Drag and Acceleration Forces for Example Problem

	t_o	t_1	t_2	t_3
$\vec{I}_v$	1.0	0.885	0.59	0.36
$\vec{I}_a$	0.36	0.59	0.885	1.0
$\vec{V}_P$	5.50	4.87	3.24	1.98
$\vec{A}_P$	1.04	1.70	2.55	2.88
$\vec{F}_D$	908	712	315	118
$\vec{F}_A$	2940	4810	7220	8150

The formulas from Step 4,

$$\vec{V}_P = 5.59\ \vec{I}_v \text{ ft/sec} \quad \text{and} \quad \vec{A}_P = 2.88\ \vec{I}_a \text{ ft/sec}^2$$

were substituted into the following equations

$$\vec{F}_D = K_D\left(\vec{V}_p^{\,2}\right) \quad \text{and} \quad \vec{F}_A = K_A\vec{A}_P$$

to obtain the drag force $\vec{F}_D$ and acceleration force $\vec{F}_A$. These vector forces are shown in Figure 7.27.

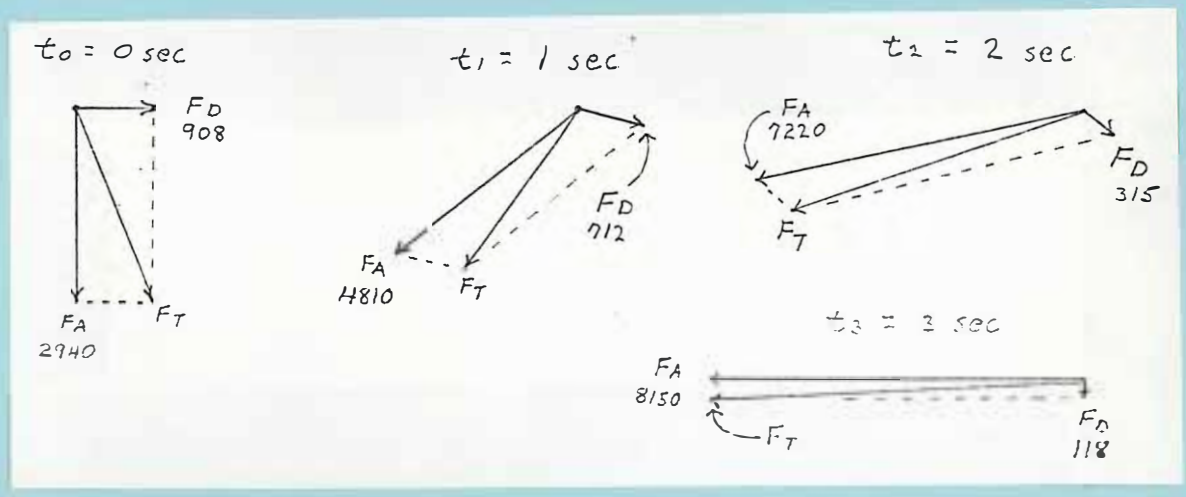

Figure 7.27. - Vector forces of F_D and F_A which must be added to obtain F_T defined by equation 7.16e.

The vector addition of the drag and acceleration forces is done with the $\vec{I}_v$ and $\vec{I}_a$ vectors that are within the brackets of equation

$$\vec{F}_T = 8140\left[0.111\left(\vec{I}_v^{\,2}\right) + \vec{I}_a\right]. \quad (7.16e, \text{ from Step 5})$$

For $t = t_o$ where $\vec{I}_v = 1.0$ and $\vec{I}_a = 0.36$, the operation of $\left[0.111\left(\vec{I}_v^{\,2}\right) + \vec{I}_a\right]$ is done as indicated in Figure 7.28. The same operation was done for times t_1, t_2, and t_3 as shown in Figure 7.28 b, c, and d.

Point 0 and 12 on Fig 7.26 is for $t = t_0$, $\vec{I}_v = 1.0$, and $\vec{I}_a = 0.36$

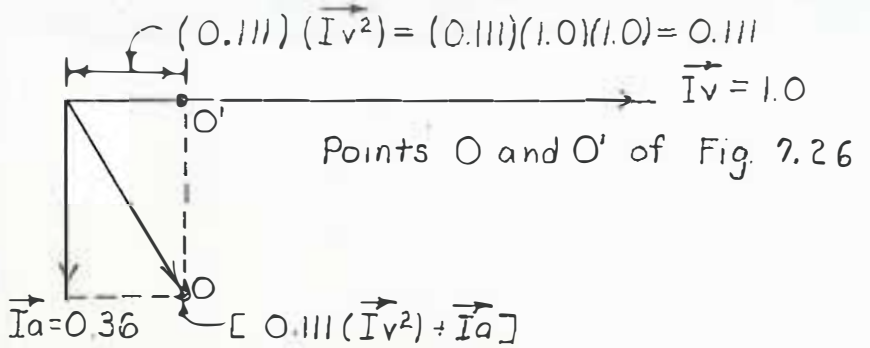

Points O and O' of Fig. 7.26

(Fig. 7.28 a)

Point 1 of Fig. 7.26 is for $t = t_1$, $\vec{I}_v = 0.885$, and $\vec{I}_a = 0.59$

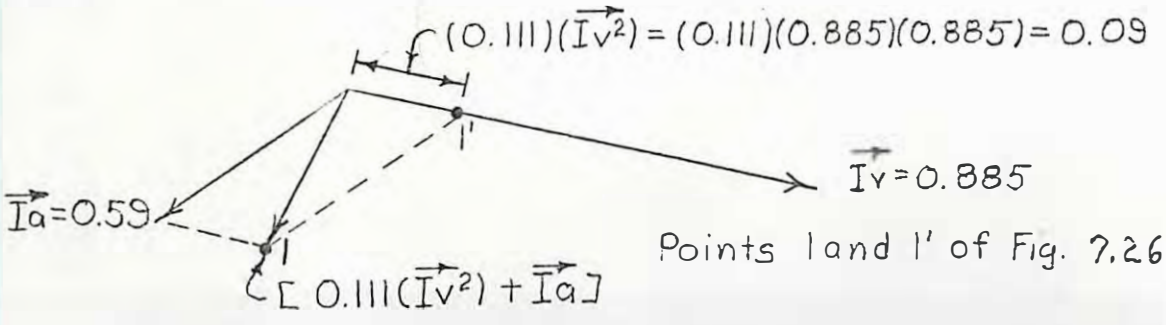

Points 1 and 1' of Fig. 7.26

(Fig. 7.28 b)

Figure 7.28, parts a and b

Point 2 of Fig. 7.26 is for $t = t_2$, $\vec{I}v = 0.59$, and $\vec{I}a = 0.885$

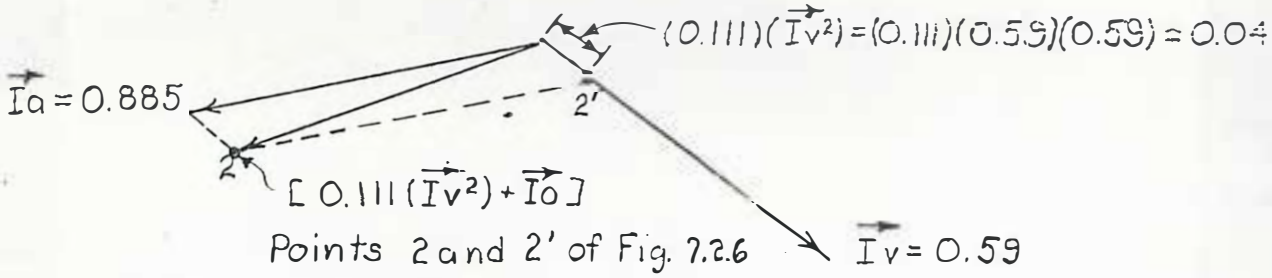

(Fig. 7.28c)

Point 3 of Fig. 7.26 is for $t = t_3$, $\vec{I}v = 0.36$, and $\vec{I}a = 1.0$

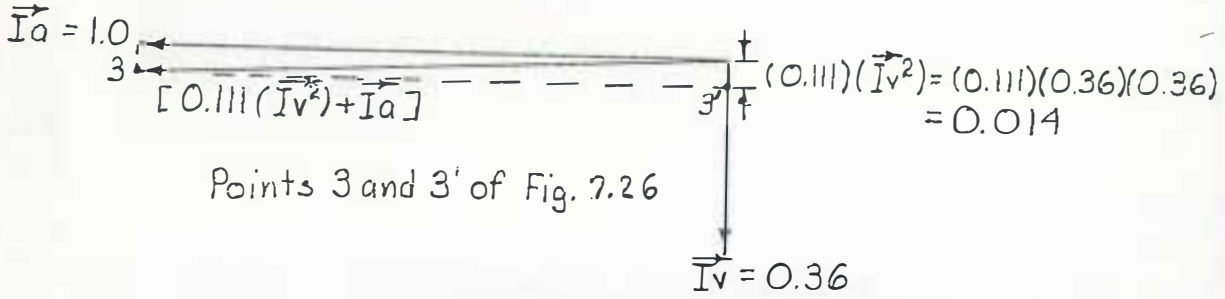

(Fig. 7.28 d)

Figure 7.28, parts c and d

Illustration showing the vector addition of
$[0.111(I_v^{\rightarrow 2}) + I_a^{\rightarrow}]$

The vector additions indicated in Figure 7.28 are accomplished during the graphic construction of the force diagram, Figure 7.26. The method of construction is as follows:

(a) A transparent sheet of graph paper is placed over the Proportionate Vectors Diagram of Figure 7.24. The lines, graph grids, and numbered points of the diagram should be easily seen through the transparent sheet. Construction of the force diagram is done on the transparent sheet (Figure 7.26).

(b) Select the proper $\vec{I}_v$ and $\vec{I}_a$ vectors that correspond to the times t_o, t_1, t_2, etc., when making the vector addition operation. Point numbering for the Proportionate Vectors Diagram is for the orbit displacement. The phase angle θ for the $\vec{I}_v$ and $\vec{I}_a$ vectors precedes the $\vec{I}_o$ vector (discussed in Step 4 and shown in Figure 7.23).

(c) Make computations for determining what portion of the $\vec{I}_v$ vector should be added. The portion of the $\vec{I}_v$ vector is

$$\frac{\mathcal{E}_{xm}}{K_R}\left(\vec{I}_v^{\,2}\right) \quad \text{from equation 7.16c}$$

and for the example problem is 0.111 $\left(\vec{I}_v^{\,2}\right)$. Examples of this computation are shown in Figure 7.28.

(d) Locate the $\vec{I}_v$ vector portion on the transparent sheet of paper. The points 0', 1', 2', and 3' on Figure 7.26 show the I_v vector portions for times t_o, t_1, t_2, and t_3. These points 0', 1', 2', and 3' are those shown on Figures 7.28a through 7.28d.

The method for locating these points on the transparent sheet is to measure the distance (0.11, 0.09, 0.04, 0.0014) with a scale for the respective vectors.

(e) Locate the numbered points on the Force Diagram. Using the points (0', 1', 2', 3') determine x and y components of the $\vec{I}_v$ vector portion and add these components to the $\vec{I}_a$ vector. An illustration of this vector addition is shown in Figure 7.29 for point 1.

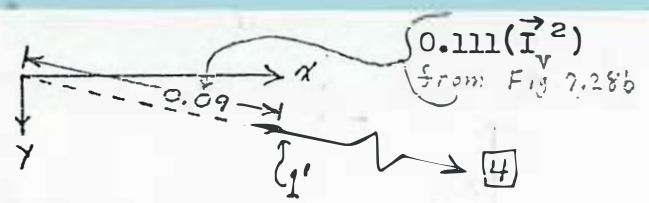

Fig 7.29a
Determine x and y component vectors

Points 1', 4, 7, and 1 are shown in Figure 7.26.

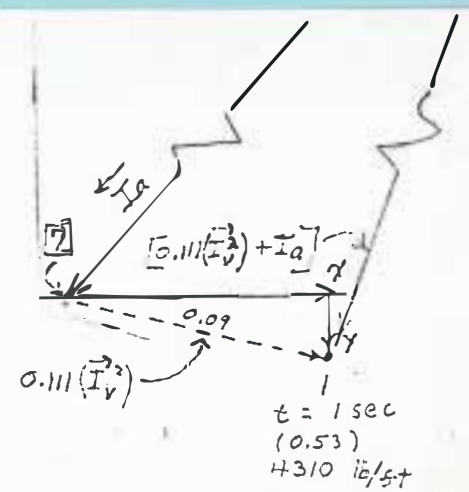

Fig 7.29b
Adding the x and y component vectors to the $\vec{I}_a$ vector

Figure 7.29 - Illustrating graphic vector addition of [0.111($\vec{I}_v^2$) + $\vec{I}_a$]. The x and y components are determined for the 0.111($\vec{I}_v^2$) portion, Figure 7.29a, and these same x and y components are added to the $\vec{I}_a$ vector, Figure 7.29b. The graphic vector addition operation is similar to that for t_1 shown in Figure 7.27, but which is done with the proportionate vectors as shown in Figure 7.28b. Thus the graphic vector addition is manually done on the transparent sheet (Force Diagram - Figure 7.26) by using the proportionate vectors (Proportionate Vectors Diagram - Figure 7.24) which can be viewed through the transparent sheet.

Using grid spaces that can be seen through the transparent sheet the x and y component vectors are determined by visual inspection. Then again by visual inspection the components are added to the $\vec{I}_a$ vector by use of the grid to perform the manual vector addition

$\left[0.111(\vec{I}_v^2) + \vec{I}_a \right]$. Point number 1 of the force diagram is then located and marked on the transparent sheet.

(f) Measure and note distance for numbered points. A scale is used to measure the distance from the center of the ellipse to respective points on the perimeter of the ellipse (see point 8 of Figure 7.26). These distances are noted in parentheses by the respective points of Figure 7.26 . The distance represents the magnitude value within the brackets of equation from Step 6

$$\vec{F}_T = 8140 \left[0.111(\vec{I}_v^2) + I_a \right].$$

(g) Compute the total force at times t_o, t_1, t_2, etc., and note the forces at respective points on the force diagram. Computation for some points are shown below. The values 0.375, 0.53, and 0.86 are from the force diagram (Figure 7.26) and are those from Step 6f.

For t_o $\quad \vec{F}_T = 8140\ (0.375) = 3050$ lbs/ft

For t_1 $\quad \vec{F}_T = 8140\ (0.53) = 4310$ lbs/ft

For t_2 $\quad \vec{F}_T = 8140\ (0.86) = 7000$ lbs/ft

The Force Diagram, Figure 7.26 , shows magnitude and direction of the force acting upon the pipe for the 12 incremental times of the wave period T.

$$\frac{\frac{\cosh k(d+y)}{\sinh kd}}{\frac{\sinh k(d+y)}{\sinh kd}}$$

$$\tanh k(d+y)$$

$$\tanh \left(\frac{2\pi}{L}\right)(d+y)$$

$$d\left(1+\frac{y}{d}\right) = d+y$$

$$\tanh (2\pi)\left(\frac{d}{L}\right)$$

Example Problem Continued for 300- and 400-foot Depths

	300-foot depth	400-foot depth
Step 1		
Relative depth	$\frac{d}{L} = \frac{300}{685} = 0.438$	$\frac{d}{L} = \frac{400}{685} = 0.584$
Proportionate depth	$\frac{40}{300} = 0.133$	$\frac{40}{400} = 0.100$
Step 2 From Figures 7.18 and 7.19		
	$U_x = 0.138$	$U_x = 0.054$
	$U_y = 0.048$	$U_y = 0.020$
Step 3		
	$\mathcal{E}_{xm} = 25\ (0.138) = 3.45$ ft	$\mathcal{E}_{xm} = 25\ (0.056) = 1.40$ ft
	$\mathcal{E}_{ym} = 25\ (0.048) = 1.20$ ft	$\mathcal{E}_{ym} = 25\ (0.020) = 0.36$ ft

Step 4

$$R_A = \frac{\mathcal{E}_{ym}}{\mathcal{E}_{xm}} = \frac{aU_y}{aU_x} = \frac{U_y}{U_x} = \frac{\frac{\sinh k(d+y)}{\sinh kd}}{\frac{\cosh k(d+y)}{\sinh kd}} = \tanh k(d+y)$$

Since the $(d+y) = 40$ the ratio R_A does not change for the 300- and 400-foot depths. Thus the same proportionate vectors diagram (Figure 7.24) was used.

Step 5

$$\vec{F_T} = \left(\frac{2\pi}{T}\right)^2 \mathcal{E}_{xm} K_A \left[\frac{\mathcal{E}_{xm}}{K_R}(\vec{I_v}^2) + \vec{I_a}\right] = 0.274\ (3.45)\ 2830 \left[\frac{3.45}{94.2}(\vec{I_v}^2) + \vec{I_a}\right]$$

$\vec{F_T} = 2675\ [0.037(\vec{I_v}^2) + \vec{I_a}]$ 300-foot depth

$\vec{F_T} = 1086\ [0.015(\vec{I_v}^2) + \vec{I_a}]$ 400-foot depth

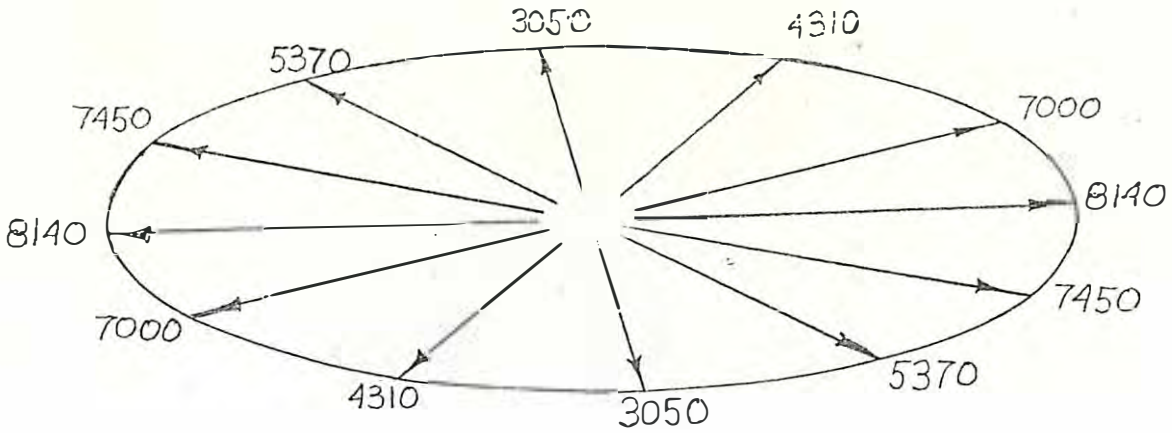

Water depth 180 feet

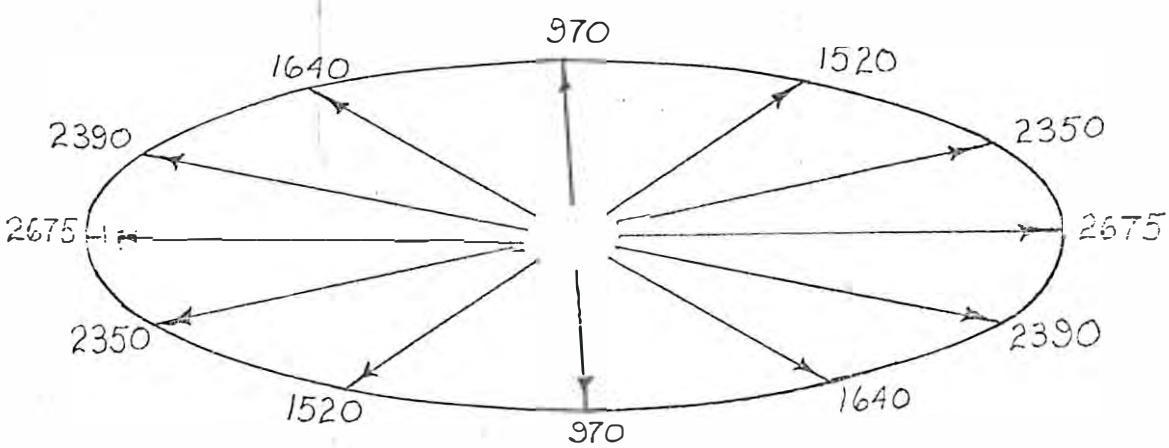

Water depth 300 feet

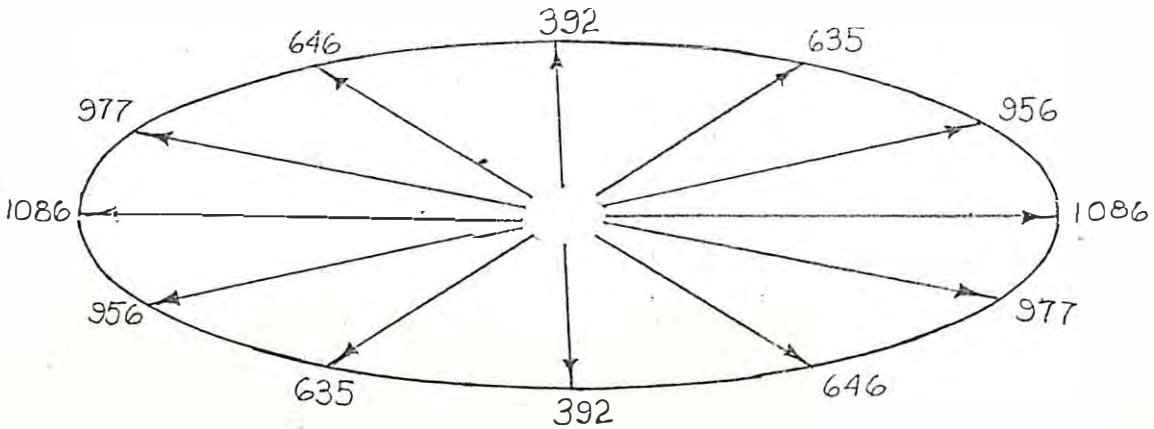

Water depth 400 feet

Figure 7.30 - Comparison of force diagrams, for 180, 300, and 400-foot depths for waves (H = 50', L = 685', T = 12 sec.) Numbers on force diagrams are lbs/ft

Step 6 - Construct the Force Diagrams

Force diagrams are constructed for the 300- and 400-foot water depths and are shown in Figure 7.30. Note that deeper water has a sheltering effect upon the conduit. Forces acting on the conduit at a 400-foot depth are approximately one-eighth those of the 180-foot depth for the given wave. Thus locating the conduit in deeper water decreases wave action forces acting on the conduit.

In the example problem a process is used where wave parameters (H, L, and T) are taken for a 180-foot water depth. These same wave parameters are used for the 300- and 400-foot water depths. Care must be taken when reversing the process and using a 400-foot depth in succeedingly shallower depths, because high waves in shallow water tend to break, Figure 7.31. References 7.3 and 7.1 give information about breaking waves. Another danger of the reverse process is that wave parameters of H and L may be reduced as a big wave moves from gradually deeper to shallower water. Thus, wave lengths in Reference 7.2 / were different for the 300- and 400-foot depths. In their example problem the "reverse process" was used by modifying the wave length L.

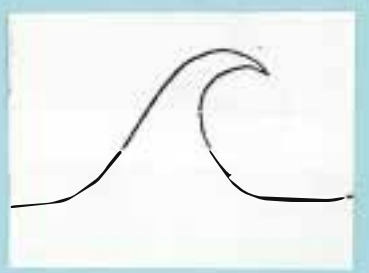

Figure 7.31. - Breaking wave

7.3 / Wiegel, R. L., Oceanographical Engineering, Prentice-Hall, Inc., pages 173 to 177.

7.1 / Ippen, A. T., Estuary and Coastline Hydrodynamics, McGraw-Hill Book Company, Inc., 1966, page 114, Figure 2.11.

Additional information about modifying deep water waves to somewhat shallower depths is given in Reference 7.4/.

Buoyant Concept

Suspension of the Conduit. A schematic sketch of the conduit in suspension is shown in Figure 7.32.

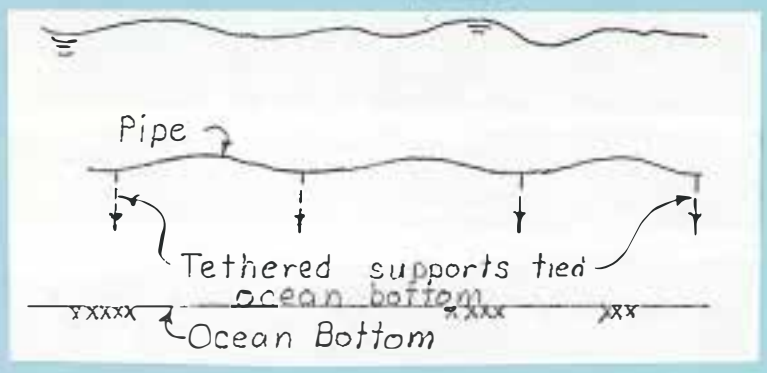

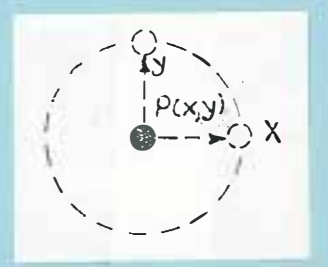

Pipe tethered at $P_{(x,y)}$ but has some freedom of movement

Figure 7.32. - Conduit suspended above ocean bottom

The pipe is suspended above the ocean bottom and is not rigidly confined at specific x and y coordinates. The pipe is viewed somewhat analogous to a suspension bridge with vertical forces on the bridge acting in an upward direction. Due to density difference between salt and fresh water there is a buoyant force acting upward on the pipe. Tethers are spaced longitudinally along the pipe to restrict the amount of pipe movement and counteract forces acting on the pipe.

Envisioned Manner of Wave Oscillatory Forces Acting on the Conduit. - The pipe when rigidly fixed is subjected to the full action of the orbiting water. If the pipe moves freely (Figure 7.33g) the orbiting water exerts a minimum drag and acceleration force, because velocity and acceleration

7.4/ Myers, Holm, and McAllister, Handbook of Ocean and Underwater Engineering, McGraw-Hill Book Company, 1969, pages 12-29 and 12-39 to 12-41, and Figures 12-20, 12-35, and 12-36.

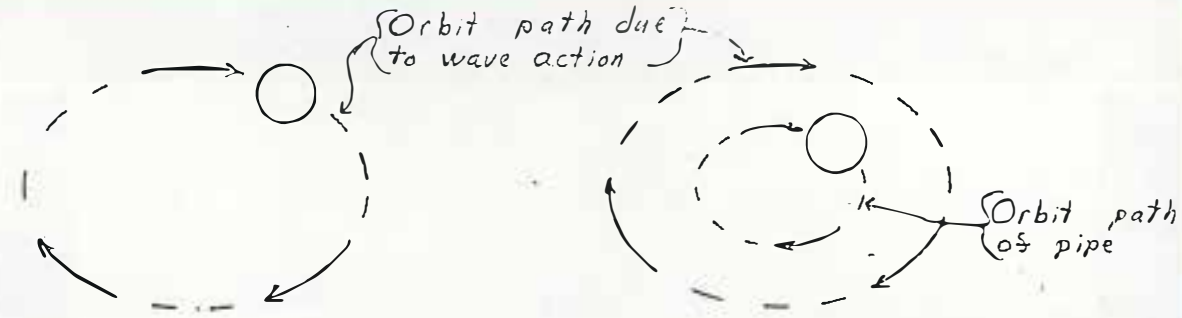

Figure 7.33 a - Pipe completely free to move with orbiting water

Figure 7.33 b - Pipe moves with orbiting water but tethers restrain the pipe orbit path

Figure 7.33 - Idealized action of buoyant pipe.

of water relative to the pipe are small since the pipe moves with a similar speed as the surrounding water. However, the tethered pipe will not be free to move with the orbiting water, Figure 7.33b. In this case the pipe is not subjected to the full action of the orbiting water. The important factor is that drag and acceleration forces acting on the pipe are produced by velocities and accelerations relative to the pipe. As shown in Figure 7.33b the relative velocity and acceleration are less than if the pipe were rigidly fixed; this assumes pipe movement is in phase with the movement of the orbiting water. Most likely, pipe movement will be out of phase as compared to the idealized condition of Figure 7.33b. The pipe movement may be only slightly out of phase or greatly out of phase as shown in Figure 7.34.

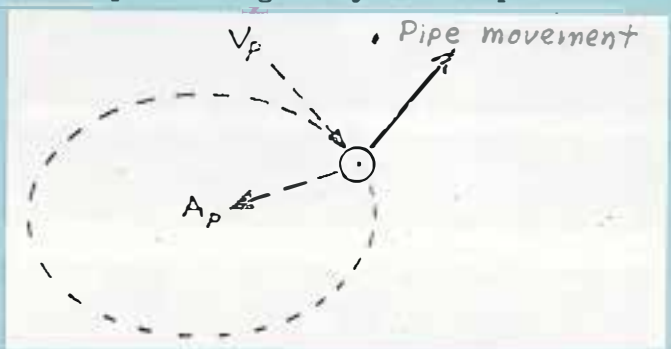

Figure 7.34 - Schematic showing movement of the pipe which is out of phase with velocity and acceleration of the orbiting water.

Use of the Morison Formula. - When there is pipe movement relative velocity and acceleration should be used in the Morison Formula

$$\vec{F}_T = K_D(\vec{V}_R^2) + K_A\vec{A}_R \qquad (7.16C)$$

$$K_D = \frac{\rho C_D D}{2}, \quad K_A = \frac{\pi \rho C_m D^2}{4} .$$

The relative velocity and acceleration are

$$\vec{V}_R = \vec{V}_p - \vec{V}_c \qquad (7.20) \quad \text{and} \quad \vec{A}_R = \vec{A}_p - \vec{A}_c \qquad (7.21)$$

where

$\vec{V}_R$ = relative velocity vector,

$\vec{V}_p = \vec{V}_x + \vec{V}_y$ = particle velocity vector,

$\vec{V}_c$ = conduit velocity vector due to pipe movement,

$\vec{A}_R$ = relative acceleration vector,

$\vec{A}_p = \vec{A}_x + \vec{A}_y$ = particle acceleration vector,

$\vec{A}_c$ = conduit acceleration vector due to pipe movement.

One difficulty is determining what $\vec{V}_c$ and $\vec{A}_c$ values to use in the Morison Formula when computing the force acting upon the pipe. Forces of wave action flex and move the pipe; this movement is in turn structurally transferred to the tethered supports, and the tethered supports respond by providing a restoring force which moves the pipe. Thus to determine pipe movement the force acting on the pipe must be known, yet force acting on the pipe is interrelated with and a function of pipe movement.

Fluid shear at the sediment boundary, lift, and turbulence are considered the main forces that initiate the transport of sediment. To determine average shear, velocity distributions need to be known. Turbulence is described as statistical distributions of eddy sizes and velocity fluctuations. Turbulence causes random fluctuation of shear, lift, and drag forces acting on the sediment particles. Particles can slide, roll, bounce, move as bed form waves, or travel in suspension. The statistical nature of turbulence, sediment, and its movement is the reason why Einstein 8.1/ used probablistic models in developing his sediment transport theory and functions.

Structures have various sizes and shapes that accelerate the main flow and change the turbulence characteristics of the flow near the structure. Scour near structures is almost exclusively studied by models requiring compromising model distortions that apply only to cohesionless sediment. No distortion laws are known for moedling scour with cohesive soils. Our knowledge of sediment transport, bed forms, scour, and deposition is rather limited and comes mostly from experience with channelized flow with fresh water rather than seawater.

For the ocean environment there is very little documented experience and our capability of predicting scour on the ocean bottom is further limited by the complicated reversing and oscillating flows caused by tides and surface waves that are superimposed on the main ocean currents.

8.1/ Op cit

Organization. - The organization and the material contained in the scour section is tempered by the probable amount and quality of data that the designers will have available at the appraisal stage of planning. First relative scour in terms of soil classification is discussed. Then critical velocity and tractive force criteria in terms of some specific soil properties are considered.

Hopefully at this point in the appraisal, further worry or concern with scour may have been eliminated. Theoretically scour near a structure can be determined by before and after implacement calculations of transport. Therefore transport equations are discussed for both unidirectional and oscillatory flows. Finally bridge pier data are presented that can be used to determine depth of scour near anchor blocks or other obstructions in and on the ocean bed.

Relative Scour Resistance in Terms of Soil Classification

Ranking by unified soil classification groups. - Through experience engineers have developed concepts of relative resistance of soils by categories to erosion. For example, Bureau of Reclamation Soils Engineers have ranked 8.2/ the relative resistance of different soil types in Figure 8.1. This ranking is for canals where the embankments have been compacted or consolidated. The degree of compaction in ocean sediment is one of the more important unknowns when appraising scour. However, the ranking in Figure 8.1 is probably adequate for cohesionless soils and consolidated cohesive soils.

8.2/ Report EM-643, H. J. Gibbs, U.S. Bureau of Reclamation

MAJOR DIVISIONS OF SOILS			TYPICAL NAMES OF SOIL GROUPS	GROUP SYMBOLS	EROSION RESISTANCE
COARSE GRAINED SOILS More than half of material is larger than No. 200 sieve size (The No. 200 sieve size is about the smallest particle visible to the naked eye)	GRAVELS More than half of coarse fraction is larger than No. 4 sieve size (For visual classifications, the ¼" size may be used as equivalent to the No. 4 sieve size)	CLEAN GRAVELS (Little or no fines)	Well graded gravels, gravel-sand mixtures, little or no fines	GW	2
			Poorly graded gravels, gravel-sand mixtures, little or no fines	GP	3
		GRAVELS WITH FINES (Appreciable amount of fines)	Silty gravels, poorly graded gravel-sand-silt mixtures	GM	5
			Clayey gravels, poorly graded gravel-sand-clay mixtures	GC	4
			Gravel with sand-clay binder	GW-GC	1
	SANDS More than half of coarse fraction is smaller than No. 4 sieve size (For visual classifications, the ¼" size may be used as equivalent to the No. 4 sieve size)	CLEAN SANDS (Little or no fines)	Well graded sands, gravelly sands, little or no fines	SW	8
			Poorly graded sands; gravelly sands, little or no fines	SP	9 coarse
		SANDS WITH FINES (Appreciable amount of fines)	Silty sands, poorly graded sand-silt mixtures	SM	10 coarse
			Clayey sands, poorly graded sand-clay mixtures	SC	7
			Sand with clay binder	SW-SC	6
FINE GRAINED SOILS More than half of material is smaller than No. 200 sieve size (The No. 200 sieve size is about the smallest particle visible to the naked eye)	SILTS AND CLAYS Liquid limit less than 50		Inorganic silts and very fine sands, rock flour, silty or clayey fine sands with slight plasticity	ML	—
			Inorganic clays of low to medium plasticity, gravelly clays, sandy clays, silty clays, lean clays	CL	11
			Organic silts and organic silt-clays of low plasticity	OL	—
	SILTS AND CLAYS Liquid limit greater than 50		Inorganic silt, micaceous or diatomaceous fine sandy or silty soils, elastic silts	MH	—
			Inorganic clays of high plasticity, fat clays	CH	12
			Organic clays of medium to high plasticity	OH	—
HIGHLY ORGANIC SOILS			Peat and other highly organic soils	Pt	

**Numbers above indicate the order of increasing values for the physical property nom indicate relative suitability (1 = best)

Figure 8.1

FIGURE 8.1 SOIL CLASSIFICATION 8.2/

Ranking in terms of soil plastic properties. - For soils with over 50 percent of their grain diameters less than .074 mm, plastic properties can contribute to erosion resistance in varying degrees from just slightly adding to being the dominant source. Plastic soil properties are expressed by the Atterberg limit as follows:

1. The Liquid Limit (LL), the water content percent dry weight that marks the separation between acting like a liquid or plastic.

2. The Plastic Limit (PL), the boundary between acting like a plastic or solid.

3. The Plastic Index (PI), which is the difference between (LL) and (PL) and is the range of water content through which the soil has plastic characteristics.

Figure 8.2 taken from 8.2/ shows the relative resistance of cohesive soils in terms of the Liquid Limit (LL) and the Plastic Index (PI). The "A-line" separates the clays above it from the silts below. It should be remembered that the ranking in this chart applies to soils that were compacted to 90 pcf (pounds per cubic foot).

8.2/ Op cit

Table 8.1

from Lee and Valent

California Division of Mine and Geology Classification	Percent Occurrence 3-mile limit	Unified soil classification
Rock (Rx)	37	
Gravel (G)	21	SW, SP, GW, GP
SAND (CS)(S)		
Fine Sand (FS)	33	
Mud (M)	7	CH, CL, MY, ML*, SM
Shell (SH)	2	

* Most common on shelf near shore.

Critical Scour Criteria

Background. - In order to formulate and quantify scour and transport criteria, the engineer must relate soil types or soil properties to flow dynamic properties. For cohesionless soils it is generally accepted that the weight (W) of the largest sediment grain transported is proportionally related to velocity (V) as follows:

$$W \propto V^6 \quad \ldots\ldots\ldots\ldots\ldots\ldots \quad (8.1)$$

The quantity of sediment transported (q_s) is proportionally related 8.5/ as follows:

$$q_s \propto V^{\eta} \quad \ldots\ldots\ldots\ldots\ldots\ldots \quad (8.2)$$

where the exponent (η) is approximately equal to 1/4. Equation (8.1) suggests the possibility of a critical velocity (V_{cr}) that will just move a particle of diameter (d). If all the particles are assumed to be spheres with constant specific weight, then we can write

$$W \propto d^3 \quad \ldots\ldots\ldots\ldots\ldots\ldots \quad (8.3)$$

and combining with equation (8.1) results in

$$V_{cr} \propto d^{\frac{1}{2}} \quad \ldots\ldots\ldots\ldots\ldots\ldots \quad (9.4)$$

$$V_{cr} = f_1 (d) \quad \ldots\ldots\ldots\ldots\ldots\ldots \quad (9.5)$$

8.5/ Myers, Holm and McAllister, et al, Handbook of Ocean and Underwa Engineering, McGraw-Hill, 1969.

Shear and shear fluctuations at the sediment boundary are considerd the dominant factors in initiating sediment movement. For flow in canals and rivers, average shear can ~~most~~ easily be determined from a free body diagram and assuming normal flow. Then

$$\tau = \gamma_f D S \quad \ldots\ldots\ldots\ldots\ldots\ldots \quad (8.6)$$

where

τ = the boundary shear #/ft^2

D = depth (ft)

S = slope of bed or energy gradient

γ = specific weight #/ft^3

f = subscript denoting fluid

Sometimes the effects of cohesion are incorporated into an analysis subtly by assuming that it is defined by grain size only. Sometimes more complicated approaches will include all or part of the following:

d50 = mean grain size

S_d = standard deviation grain size

K_d = skewness of grain size

ϕ = void ratio

%C = percent compaction

Svs = vane shear strength

C_s = compressive strength

PI = plastic index

LL = liquid limit

and others

Turbulence contributes in initiating movement and is very important in keeping particles in suspension once suspended. Turbulent intensity (ε_t) is expressed as

$$\varepsilon_t = \frac{\sqrt{\overline{V'^2}}}{V_m} \quad \ldots\ldots\ldots\ldots\ldots\ldots \quad (8.9)$$

where (V') is velocity fluctuation about (V_m) the mean velocity. Values of (ε_t) have been measured from 0.03 up to 0.07 and 0.1 is considered the

Excepting turbidity and density currents, flow is not necessarily in the direction of the bottom slopes. Therefore, in the ocean no energy slope (S) can be easily assigned to a particular portion of the bed. Shear must be obtained from a velocity distribution law and at least two measured velocities at different elevations above the bed are required. Boundary shear can then be expressed as

$$\tau = \rho \left[\frac{V_2 - V_1}{5.75 \log 10 \frac{Z_2}{Z_1}} \right]^2$$

where (Z_1) and (Z_2) are elevations above the bed corresponding to (V_1) and (V_2). Equations 8.6 and 8.7 indicate that tractive force is proportional to the square of velocity. Also equations 8.6 and 8.7 suggest the possibility of a critical tractive force (τ_{cr}) or shear that will just move a particle of diameter (d) and we can write

$$\tau_{cr} = f_2 (d) \quad . \quad . \quad . \quad . \quad . \quad . \quad . \quad . \quad . \quad . \quad . \quad (8.8)$$

When over 50 percent of soil particles are less than 0.074 mm then cohesion (C_o) must be considered. Equations 8.5 and 8.8 are modified to read

$$V_{cr} = f_1 (d, C_o) \quad . \quad . \quad . \quad . \quad . \quad . \quad . \quad . \quad . \quad . \quad (8.5a)$$

$$\tau_{cr} = f_2 (d, C_o) \quad . \quad . \quad . \quad . \quad . \quad . \quad . \quad . \quad . \quad . \quad (8.8a)$$

value at which the velocity fluctuation can no longer be considered part of the main flow. 8.6/ Panicker 8.7/ compares the particle settling velocity to upward turbulent velocity fluctuation intensity and roughly estimates the mean velocity of turbidity flows and their depths.

Velocity fluctuations are normally distributed about the mean velocity (V_m) and therefore the largest fluctuation to be expected would be nearly (3σ) where (σ) is the standard deviation. Kalinski 8.8/ found that near the bed

$$V_{mb} \approx 4\sigma \quad \ldots\ldots\ldots\ldots\ldots\ldots \quad (8.10)$$

The normal distribution and equation (8.10) indicates that the maximum instantaneous velocity (V_{mb}) near the bed can be 1.75 times the average velocity. Since (τ) is proportional to velocity squared, then maximum instantaneous shear can be about three times the average shear. 8.9/

8.6/ Bird, Stewart, Lightfoot, Transport Phenomena, Wiley 1960.

8.7/ V. N. Panicker, Prediction of Bottom Current Velocities from Sediment Deposits, California University, Berkeley Hydraulic Engineering Laboratory, 1969

8.8/ A. A. Kalinski, "Movement of Sediment as Bed Load in Rivers." Trans. Am. Geophys. Union, Vol 28, #4

8.9/ W. H. Graf, "Hydraulics of Sediment Transport." 1971

Critical tractive force versus grain size for noncohesive soils. - Lane 8.~~12~~[10]/ summarizes a considerable number of the investigations concerning critical scour criteria, Tables 8.2 to 8.6, were taken from his work. The critical tractive force for noncohesive soils versus mean grain diameter is plotted in Figure 8.4. This figure also shows that clear water has more scouring power.

8.~~12~~[10]/ E. W. Lane. Progress Report on The Design of Stable Channels," Bureau of Reclamation Report. HYD 352, 1952

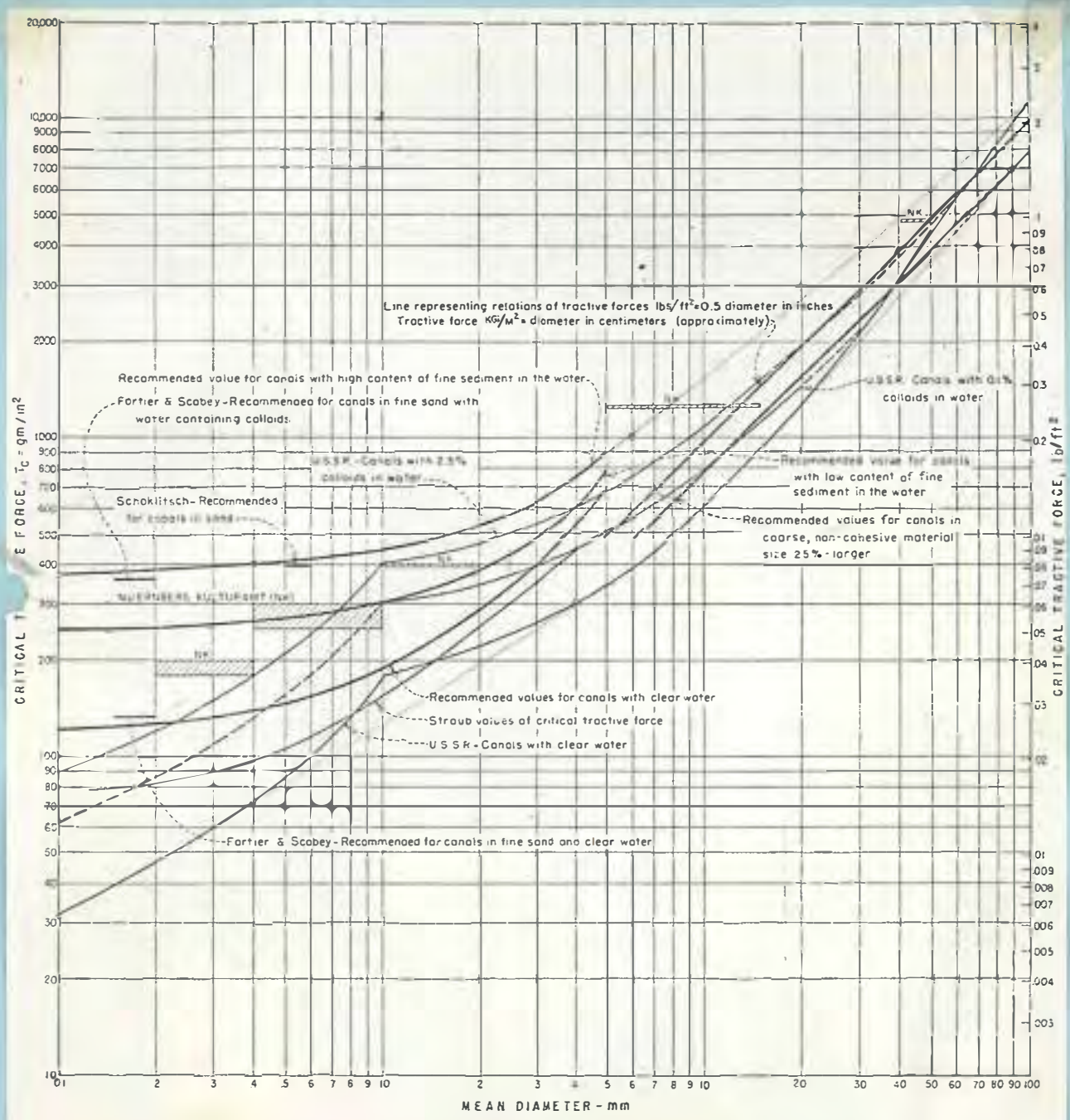

LIMITING TRACTIVE FORCES
RECOMMENDED FOR CANALS
AND
OBSERVED IN RIVERS

FIGURE 8.4 TRACTIVE FORCES (FIGURE H-8.10)

TABLE 8.5 8.10

Table 6

USSR CORRECTIONS OF PERMISSIBLE VELOCITY FOR DEPTH
Noncohesive Material

Average depth							
Meters	0.30	0.60	1.00	1.50	2.00	2.50	3.00
Feet	0.98	1.97	3.28	4.92	6.56	8.20	9.84
Correction factor	0.8	0.9	1.00	1.1	1.15	1.20	1.25

TABLE 8.6 8.19

Table 7

USSR LIMITING VELOCITIES AND TRACTIVE FORCES IN COHESIVE MATERIAL

Compactness of bed													
Descriptive term	Loose		Fairly						Very				
Descriptive term	loose		compact		Compact				compact				
Voids ratio	2.0-1.2		1.2-0.6		0.6-0.3				0.3-0.2				
Principal cohesive Material of bed	Limiting mean velocity ft/sec and limiting tractive force lb/sq ft												
	Ft/sec	Lb sq ft	Ft sec	Lb sq ft	Ft sec	Lb sq ft	Ft sec	Lb sq ft	Ft sec	Lb sq ft	Ft sec	Lb sq ft	
Sandy clays (sand content less than 50 percent)	1.48	0.040	2.95	0.157	4.26	0.327	5.90	0.630					
Heavy clayey soils	1.31	0.031	2.79	0.141	4.10	0.305	5.58	0.563					
Clays	1.15	0.024	2.62	0.124	3.94	0.281	5.41	0.530					
Lean clayey soils	1.05	0.020	2.30	0.096	3.44	0.214	4.43	0.354					

Fig. 7-11. Permissible unit tractive forces for canals in cohesive material as converted from the U.S.S.R. data on permissible velocities.

The dimensionless entrainment function of Schields 8.~~18~~/ has been commonly accepted for uniform soils or single grain sizes. Schields' curve in Figure 8.9 from Rouse 8.~~19~~/ besides giving a yes-no determination of bed transport, provieds indication of bed form and transport mode that will occur. The dimensionless shear parameter $[\tau/(S-1)d]$ must be expressed as $[\tau/(\gamma_s - \gamma_s)d]$ for use in sea water. The term $(d\sqrt{\tau/\rho_f}/\nu)$ is a grain shear Reynolds number. Outside of the laminar flow range, Schields' dimensionless shear data vary from 0.03 to 0.06. After a critical Reynolds number of 400 is reached, the dimensionless shear remains at 0.06. Vanoni 8.~~20~~/ added an auxiliary scale, Figure 8.10, with sloping lines to facilitate the determination of (τ) when (γ_s), (γ_f), and (ν) are known. In Figure 8.10 $\sqrt{\tau/\rho_f}$ is expressed as (u^*) and is called shear velocity.

Figure 8.9 - Schields Dimensionless Shear Function 8.~~19~~/

8.~~18~~/ Schields, A. (1936): Anwendung der Ähnlichkeitsmechanik und Turbulenzforschung auf die Geschiebebewegung, Mitteil. Preuss. Versuchsanst. Wasser, Erd, Schiffsbau, Berlin, no 26.

8.~~19~~/ H. Rouse, Engineering Hydraulics, Wiley, 1950

8.~~20~~/ V. A. Vanoni, Measurement of Critical Shear Stress for Entraining Fine Sediments in a Boundary Layer, Report No. KH-R-7, W. M. Keck Laboratory, California Institute of Technology Pasadena, California, 1964.

TABLE 8.2 8.10/

Table 3

COMPARISON OF ETCHEVERRY'S MAXIMUM ALLOWABLE VELOCITIES AND TRACTIVE FORCES

Material	Value of Manning's n used	Velocity ft/sec	Tractive force lb/sq ft
Very light pure sand of quicksand character	0.020	0.75-1.00	0.006-0.011
Very light loose sand	.020	1.00-1.50	0.011-0.025
Coarse sand or light sandy soil	.020	1.50-2.00	0.025-0.045
Average sandy soil	.020	2.00-2.50	0.045-0.070
Sandy loam	.020	2.50-2.75	0.070-0.084
Average loam, alluvial soil, volcanic ash soil	.020	2.75-3.00	0.084-0.100
Firm loam, clay loam	.020	3.00-3.75	0.100-0.157
Stiff clay soil, ordinary gravel soil	.025	4.00-5.00	0.278-0.434
Coarse gravel, cobbles and shingles	.030	5.00-6.00	0.627-0.903
Conglomerate, cemented gravel, soft slate, tough hardpan, soft sedimentary rock	.025	6.00-8.00	0.627-1.114

8.10/

TABLE 8.3 8.10/

Table 4

COMPARISON OF FORTIER AND SCOBEY'S LIMITING VELOCITIES WITH TRACTIVE FORCE VALUES

Straight Channels After Aging

Material	n	For clear water		Water transporting colloidal silts	
		Velocity ft/sec	Tractive force lb/sq ft	Velocity ft/sec	Tractive force lb/sq ft
Fine sand colloidal	0.020	1.50	0.027	2.50	0.075
Sandy loam noncolloidal	.020	1.75	.037	2.50	0.075
Silt loam noncolloidal	.020	2.00	.048	3.00	0.11
Alluvial silts noncolloidal	.020	2.00	.048	3.50	0.15
Ordinary firm loam	.020	2.50	.075	3.50	0.15
Volcanic ash	.020	2.50	.075	3.50	0.15
Stiff clay very colloidal	.025	3.75	.26	5.00	0.46
Alluvial silts colloidal	.025	3.75	.26	5.00	0.46
Shales and hardpans	.025	6.00	.67	6.00	0.67
Fine gravel	.020	2.50	.075	5.00	0.32
Graded loam to cobbles when noncolloidal	.030	3.75	.38	5.00	0.66
Graded silts to cobbles when colloidal	.030	4.00	.43	5.50	0.80
Coarse gravel noncolloidal	.025	4.00	.30	6.00	0.67
Cobbles and shingles	.035	5.00	.91	5.50	1.10

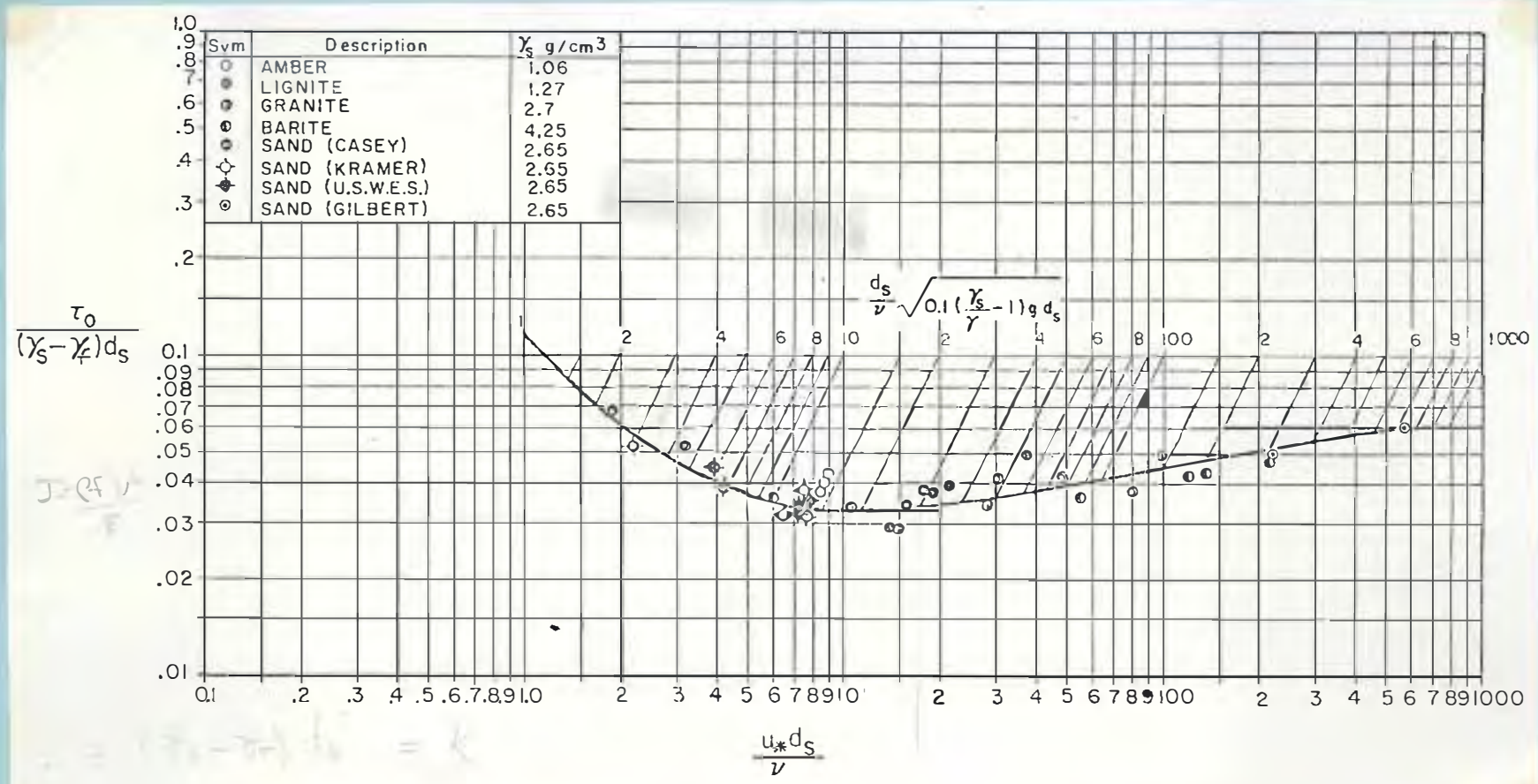

Fig. 1. Shields diagram for critical shear stress (ref. 1).

FIGURE 8.10 SHIELDS DIAGRAM WITH VANONI'S FACILITATION SCALE 8.13

Gessler ~~8.21~~ 14/ shows that the average bottom shear is equal to critical shear for a given grain size when the probability of remaining still (q) is 0.5. He then determines that this definition is independent of grain distributions or armoring. Then he presents a dimensionless Schields type shear plot in terms of grain, Reynolds Number, and the probability (q) of remaining still. His plot is shown in Figure 8.11. ~~In Figure 8.11~~ Gessler used (K) for grain size (q). He also shows a narrower range of dimensionless shear for turbulent flow from 0.033 to 0.047 for (q) of 0.5. Gesslers approach can be used to determine the percentage of a given fraction of a soil gradation that will remain on the bed or that will move.

~~8.21~~ 14/ Gessler, J. (1965): Der Geschiebetriebbeginn bei Mischungen untersucht an natürlichen Abpflästerungserscheinungen in Kanälen, Mitteil. VAWE, Eidgen, Techn. Hochschule, Zurich, no. 69. Translation T-5. W. M. Keck Laboratory, California Institute of Technology, Pasadena, California

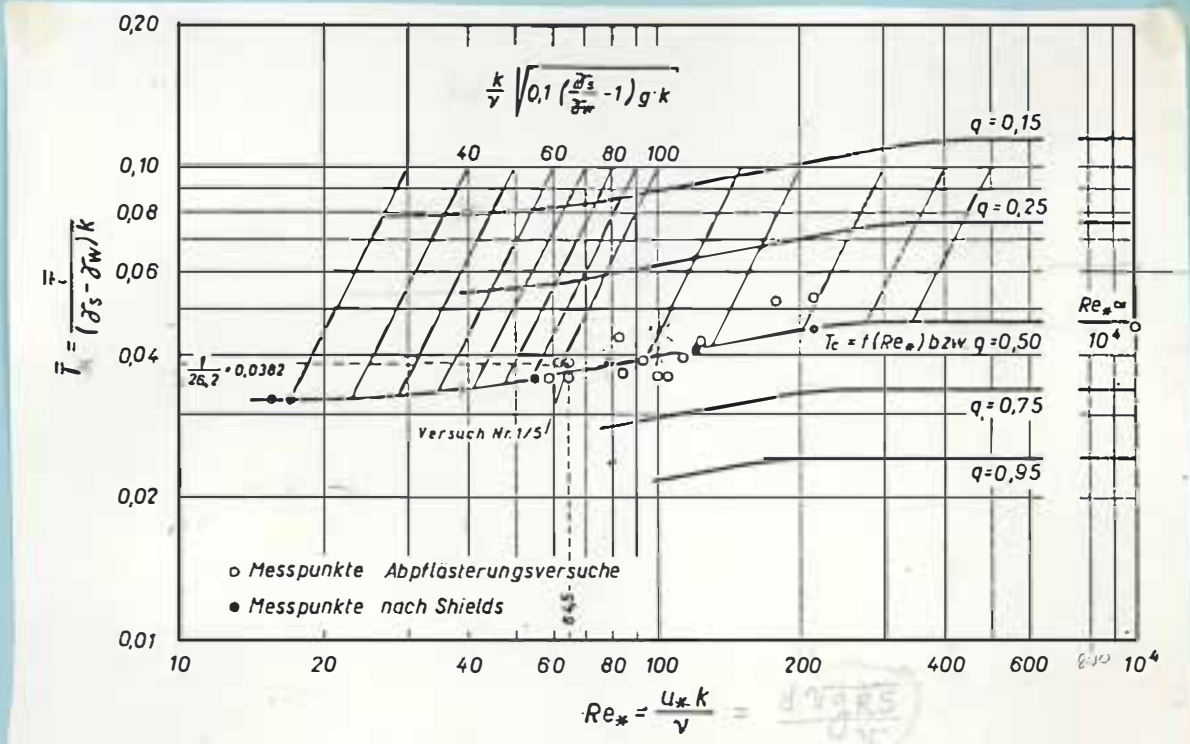

Figure 8. Dimensionless critical shear stress as a function of the Reynolds number of the grains. In the range of measurements made the curve for q = 0.5 is drawn (calculated on the basis of a standard deviation, $\sigma = 0.57$).

Figure 8.11 - Gessler's Extension of Schields Diagram to nonuniform soils, armoring and probability (q) of a particle remaining still (K = d). 8.14

Critical tractive force for cohesive soils. - Chow 8.13/ presented the USSR data Table 8.6 from Lane 8.10/ in graphical form that clearly shows the effect of compaction and/or voids ratio on the value of critical tractive force for various clay soil types, Figure 8.12. Gibbs 8.2/ gave tractive force values for plastic soils plotted along the A-Line of the plastic index line. The data shown in his plot of Figure 8.8 are for soil densities near 90 #/ft^3. Smerdon and Beasley 8.14/ and Enger, et al, 8.15/ and others have made linear correlations in terms of several cohesive, grain size, and density properties of soils. Smerdon shows that plastic-index is an important property. Lyle, et al, 8.16/ shows that some form of compaction variable should be incorporated in relating to tractive forces. Flaxman 8.17/ relates tractive force to unconfined compressive strength. Enger, et al, did various multiple correlations of several variables. It is doubtful that a sufficient number of the soil properties will be known to apply the multiple correlations during the appraisal stage of the undersea aqueduct design. All of the approaches mentioned in this paragraph are discussed more thoroughly by Graf 8.9/.

8.13/ Chow, Open Channel Hydraulics, McGraw-Hill, 1959.

8.14/ Smerdon and Beasley, The Tractive Force Theory Applied to the Stability of Open Channels in Cohesive Soils. Agriculture Experiment station Research Bulletin No. 715 Univ. Mo. Columbia, 1959

8.15/ Enger, et al, Canal Erosion and Tractive Study (correlation of laboratory test data) - LCCL Program USBR, Gen Report 26, 1960, 10 pg.

8.16/ Lyle, W. M., et al, Relation of Compaction and Other Soil Properties to Erosion and Resistance of Soils, Trans Am. Soc. Agri. Eng. vol 8, no.3, 1965.

8.17/ Flaxman, E. M. (1963), Channel Stability in Undisturbed Cohesive Soils, Proc Am. Soc. Civil Engrs., vol. 89, no. HY2.

Figure 8.6 - Cohesive material tractive force.

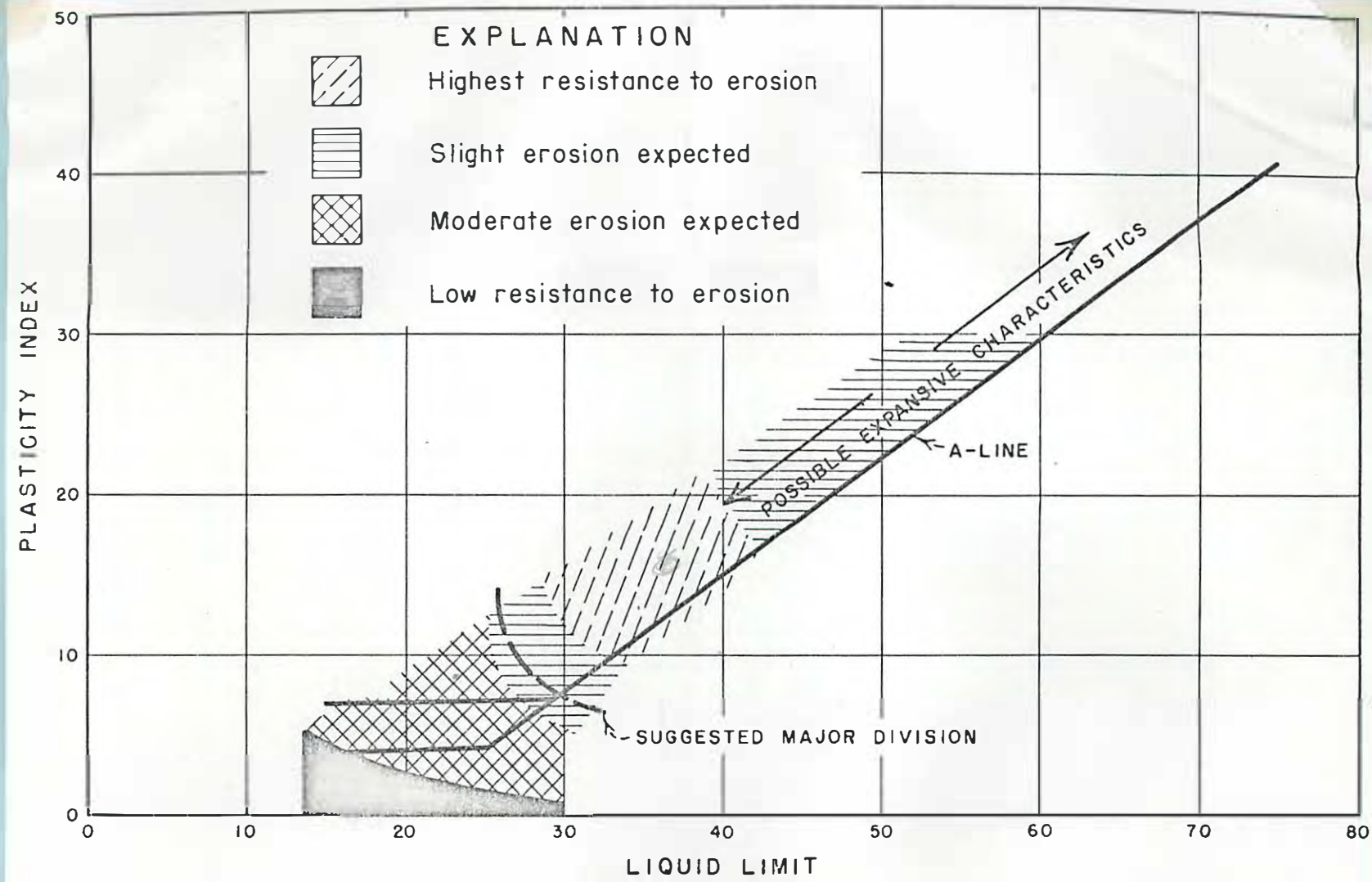

SUGGESTED TREND OF EROSION CHARACTERISTICS FOR FINE-GRAINED COHESIVE SOILS WITH RESPECT TO PLASTICITY

FIGURE 8.2 COHESIVE SOIL EROSION CHARACTERISTICS 8.21

Types of Soil on the Continental Shelf

To apply Figures 8.1 and 8.2 soil samples must be obtained at the site or existing sampling records must be used. There is not much information about continental shelf sediments. Table 8.1 was taken from Lee and Valent. 8.3/ Their table shows the distribution of soil types within the 3-mile limit according to the California Division of Mines and Geology Classification System. Because the California system is not as discriminatory as the Unified System, the suggested equivalent "Unified Soil Classification Grouping" is also shown on Table 1.

Bara 8.4/ in his summary report on foundations followed the 60-foot and 300-foot contour lines on the continental shelf and estimated distribution of soil types along them.

8.3/ H. G. Lee and P. J. Valent, NCEL, Report No. 4, USBR Contract No. 14-06-D-7210 "Comparison of Soil Classification Data - California Coastal Region, including Foundation Design Applications, 1972.

8.4/ Summary Report on Marine Soils, Bara, USBR, California Undersea Aqueduct Study.

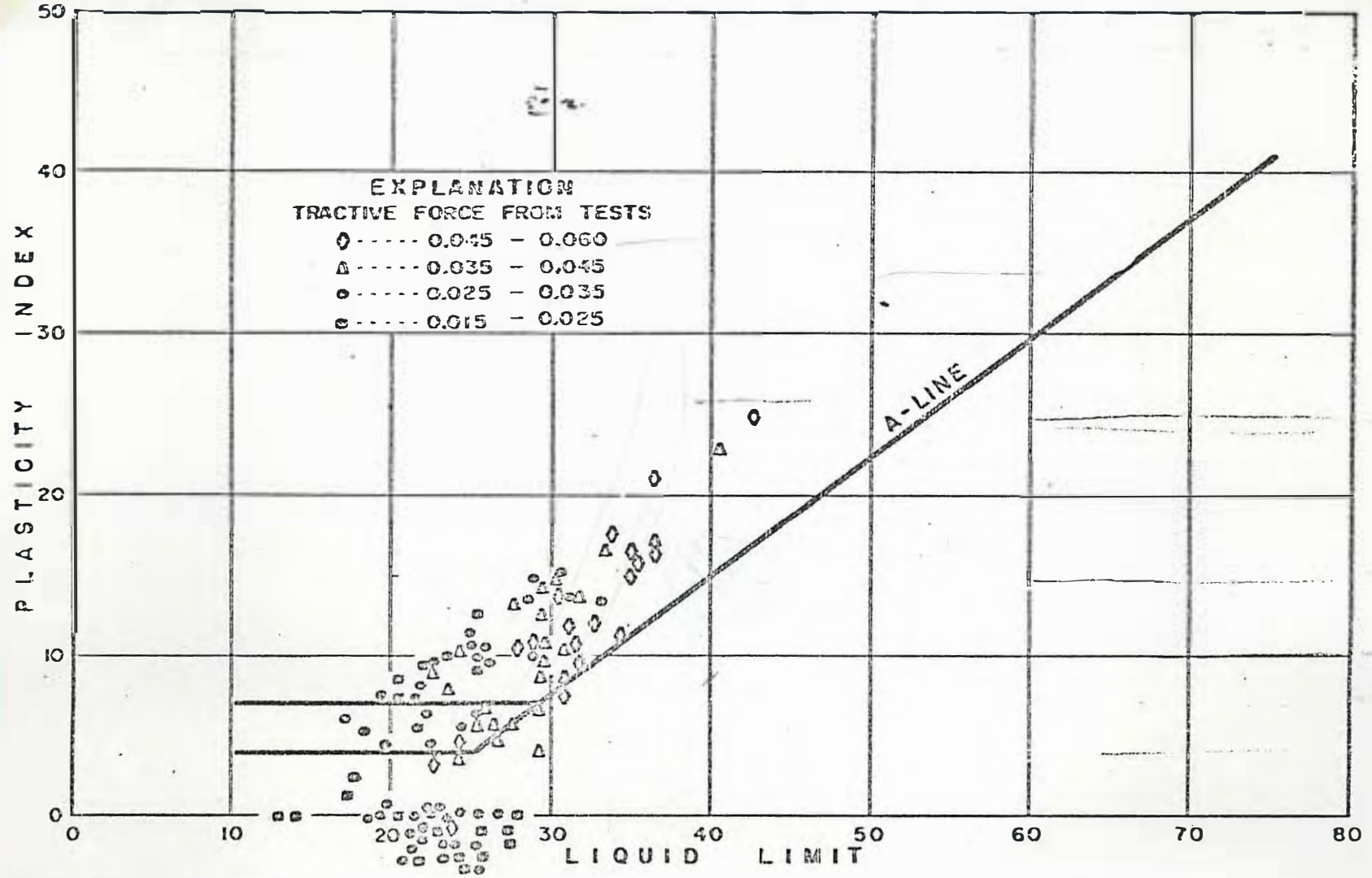

PLASTICITY CHARACTERISTICS WITH LABORATORY TRACTIVE FORCE VALUES ADJUSTED BECAUSE OF HIGH AND LOW DENSITY. SAMPLES WITH DENSITIES BELOW 80 PCF WERE RAISED IN VALUE AND SAMPLES WITH DENSITIES ABOVE 100 PCF WERE LOWERED IN VALUE

FIGURE 8.13 PLASTICITY CHARACTERISTICS 8.2

Critical velocity versus grain size. - The critical velocity curves of Sundborg plotted in 8.10/ were converted to feet per second and are plotted as solid lines in Figure 8.8. The intermediate solid line is the curve for critical velocities measured about 3 feet above the bed. Data of Hjulstrom 8.11/ for critical average velocity, all fall within the bounds of Sundborg. Kuenen 8.12/ critical velocity data is also plotted (dashed) for the portion outside of the bounds of the Sundborg curves and for maximum velocity for deposition. The Hjulstrom line for sedimentation agrees almost exactly with the Kuenen deposition curve. The zones denoted by "Erosion," "Transport," and "Sedimentation" shown on Figure 8.8 are those designated by Hjulstrom. The indication of consolidation of the fine soils is from Sundborg.

It is proper to consider the velocities along the unconsolidated line as those causing particles to be lifted from the bed and transported, and the Region A between this line and the "Deposition" line where particles will remain in suspension once they are already in suspension. The Region B between the consolidated line and the unconsolidated line shows the range of variation of resistance to erosion for soils with diameters less than 0.1 mm.

8.10/ NCEL "Environmental Factors Affecting the Emplacement of Seafloor Installation" 1971.

8.11/ Hjulstrom, 1935, "Morphological Activity of Rivers as Illustrated by River Fyris," Bulletin Geological Institute, Uppsala, Vol. 25, Chapter III.

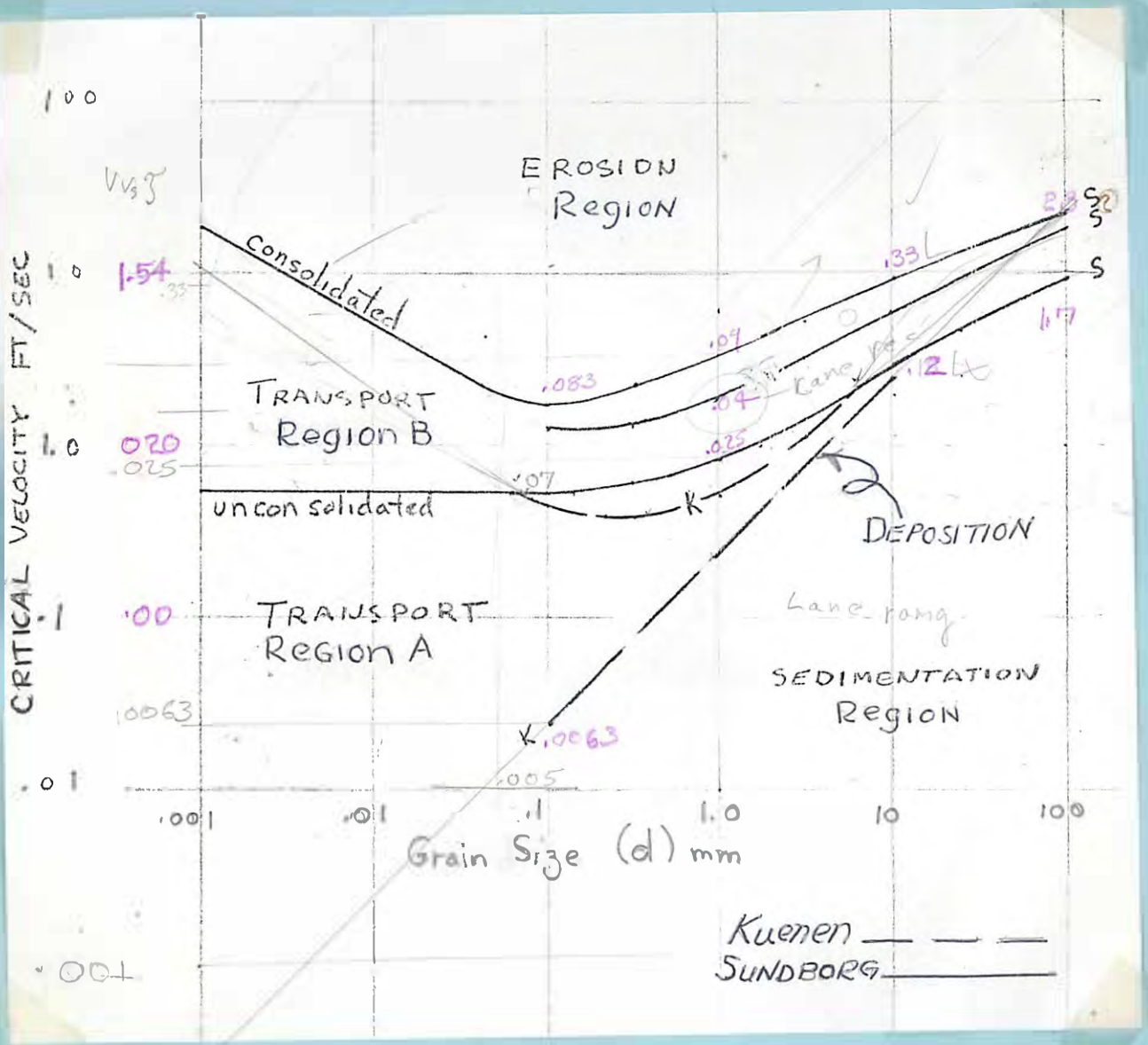

FIGURE 8.14 GRAIN SIZE AND CRITICAL VELOCITY RELATIONSHIPS

from Lane 8.10

Chow 8.~~13~~/ presented the USSR data in Table 8.6 in a graphical form that clearly shows the effects of compaction and/or voids ratio on the value of critical velocity for various clay soils, Figures 8.9.

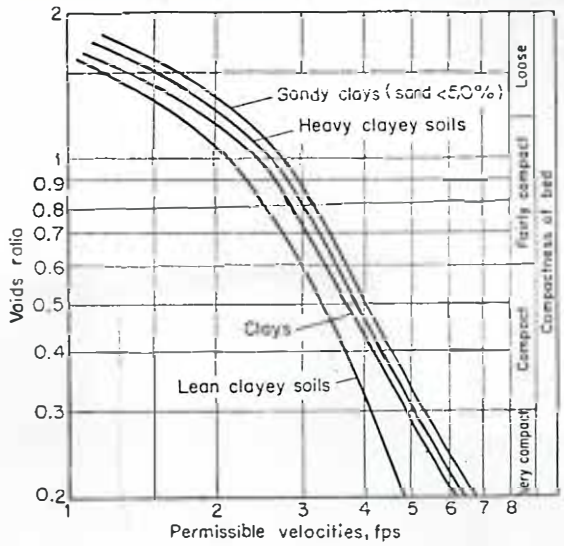

FIG. 7-4. Curves showing U.S.S.R. data on permissible velocities for cohesive soils.

V = 3.7 - 4.6

T = 0.21 - 0.37

Figure 8.9 - Cohesive soil critical velocity

8.~~13~~/ ~~Chow, "Open Channel Hydraulics," McGraw Hill, 1959.~~ Op cit

Linkage between critical velocity and critical tractive force. - Scour criteria are usually expressed in terms of grain diameter and critical tractive force because the force is generally considered to be the more appropriate than critical velocity. For example, the scour criteria data from Lane 8.12/ was stated in terms of tractive force and particle diameter (d) and came from canals and rivers data. In open channel flow it is useful to state erosion resistance in terms of critical tractive force, because fluid flow conditions of the channel can be related to boundary shear. But, probably for the undersea aqueduct, designers will not have sufficient information to determine what tractive forces are acting on the ocean bottom near the conduit. Most likely the designer will have just one value of water velocity above the bed.

An attempt to provide the designers with a rather crude linkage from critical tractive force to critical velocity is contained in Figure 8.5. Tractive force data along with a corresponding velocity measured at about 3 feet above the bed were available, and were plotted as velocity versus critical tractive force 8.12/. The solid data points and the dashed line are for soils with clays. The USSR data from Table 8.6 plotted as triangles in Figure 8.5, indicate that the compaction and/or voids ratio shifts the plotted values along the curve. The data for hard pan and shales to soft rock seem to be an extension of clay soil curve.

8.12/ E. W. Lane, "Progress Report on the Design of Stable Channels," Bureau of Reclamation Report, Hyd 352, 1952.

$$\tau = \frac{f \rho V^2}{8}$$

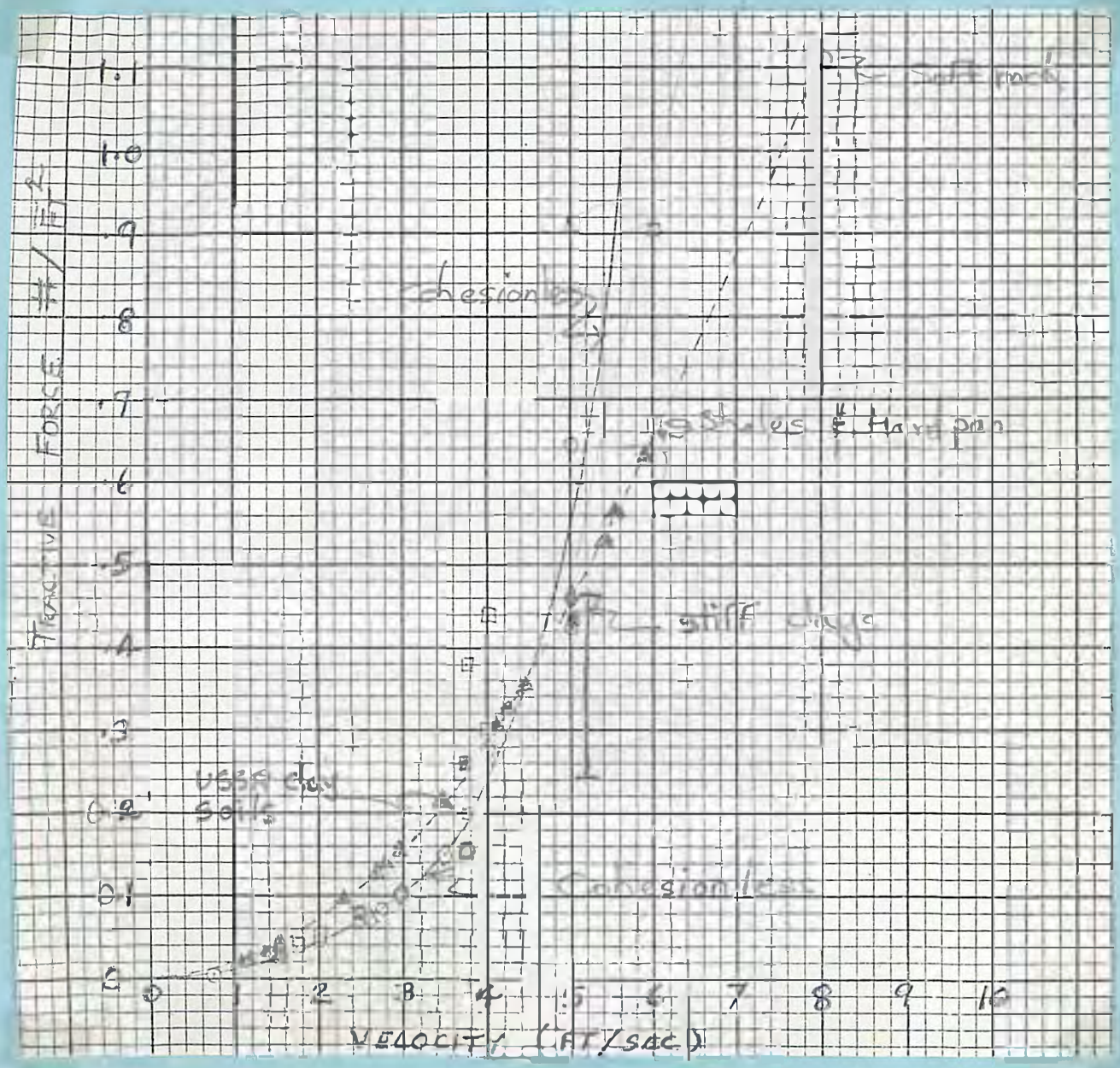

FIGURE B.14 — APPROXIMATE RELATIONSHIP OF TRACTIVE FORCE TO VELOCITY

Application and certain limitations of scour criteria. - Critical velocities and tractive forces should be considered as guides only. They do not always account for flow section shapes or turbulent fluctuations. All data were obtained from rivers or flume studies with fresh water rather than sea water. The elevations of velocities are not always clearly defined and the moment of initial movement is based on the decision of many different individual observers. The results usually are expressed in terms of single grain sizes or very uniform distribution of grain sizes. Those using these data for graded soils must select some characteristic grain size (50 percent size or larger) that could be assumed to effectively hide or protect the finer sizes. However, the dimensionless tractive force plots are self-correcting for water properties. The Gessler Function is recommended for noncohesive soils because it can be applied to soils with grain distributions and can be used to predict armoring. In any case, decisions made from scour criteria need be tempered by the engineer's experience and judgment.

Transport

Unidirectional bottom transport. - The amount of sediment being transported in the approach flow depends on the scour around structures. There are times where unidirectional transport equations can be applied to the ocean bed. Studies indicate that for (D/L) ratios greater than 0.5 waves do not produce significant oscillatory velocities on the bottom. The only reversing flows would be caused by the longer period tides. These reversing flows could be linearized to accomodate the use of unidirectional flows.

Bedload is probably the main mode of transport for the ocean near the aqueduct outside of beach areas and conyons. Bedload is the sediment that is traveling by sliding, rolling, and bouncing on the bed.

Graf 8.9/ has an excellent summary of various methods for computing bedload rates and shows the limitations of the method. He classifies bedload computations into three basic approaches that consider the relationship of:

1. Shear stress (du Boys)
2. Discharge (Schoklitsch)
3. Statistics of lift force variation (Einstein)

Graf compares four methods, Meyer-Peter et al 8.22/, Schoklitsch 8.23/, Kalinski 8.24/, and Einstein 8.25/. The values of transport were 288, 8.6, 290, and 350 kg/sec, respectively. Neglecting the extremely low value, there is about 20 percent variation about the mean of 312 kg/sec.

8.22/ Meyer-Peter, E. (1949), Quelques Problemes concernant le Charriage des Matieres solides, Soc. Hydrotechn. France, No. 2.

8.23/ Schoklitsch, A. (1930), "Handbuch des Wasserbaues," Spriner, Vienna (2d ed., 1950) English translation (1937) by S. Shulits.

8.24/ Kalinske, A. A. (1947), Movement of Sediment as Bed-Load in Rivers, Trans. Am. Geophys. Union, Vol 28, No. 4.

8.25/ Einstein, H. A., (1950), The Bed-load function for sediment transportation in open channel flows, U.S. Dept. of Agr. Tech. Bull. 1026, 70 p. (1951).

Einstein's method has been quite generally accepted and has been modified to compute the total load 8.26/ and 8.27/. The method requires some samples of suspended sediment however. Colby, et al, has compared various computational methods with actual measurements of total load. The modified Einstein method had deviations of sediment load running from 0.16 to 1.00 times the ~~true~~ measured load. The other methods had deviations as high as 3 to 10 times.

Oscillatory bottom transport. - Simplified models of transport of sand by water waves have been developed. Most are based on the Longuet-Higgins 8.~~31~~28/ equations of mass transport within the boundary layer for waves. Incipient motion criteria are established in terms of mass transport velocity, Eagleson 8.~~32~~29/ or in terms of some oscillatory Reynolds number, Manohar 8.~~33~~30/. These references are summarized in 8.~~8~~31/.

8.26/ Colby, et al, Computations of the Total Sediment Discharge Niobrara River near Cody, Nebraska, Geological Survey Water Supply Paper 1357, 1955, 187 pgs.

8.27/ Step Method for Computing Total Load by the Modified Einstein Procedure, USBR, 1955.

8.~~31~~28/ Longuet-Higgins, M. S., Mass transport in water waves, Phil. Trans. Roy. Soc., London (A) 245, No. 903, 585-91 (1953)

8.~~32~~29/ Eagleson, P. S. and Dean R. G., Wave-induced motion of bottom sediment particles, Proc. ASCE, 85, No. NY10, 53-79 (Oct. 1959)

8.~~33~~30/ Manohar, Madhao, Mechanics of bottom sediment movement due to wave action, U.S. Army Beach Erosion Board TM No. 75, 1955.

8.31/ RAUDKIVI A.J. LOOSE BOUNDARY HYDRAULICS, PERGAMON PRESS, 1967

Beach transport. - Where beaching action is occurring, erosion can be taking place at one point and deposition at another. For a constant wave, sorting of grain size occurs and continues until an equilibrium beach profile is formed. Figure 8.~~12~~ 17 shows a simplified equilibrium beach and segregation of soil sizes during a laboratory study with a direct on-shore wave 8.~~28~~ 32/.

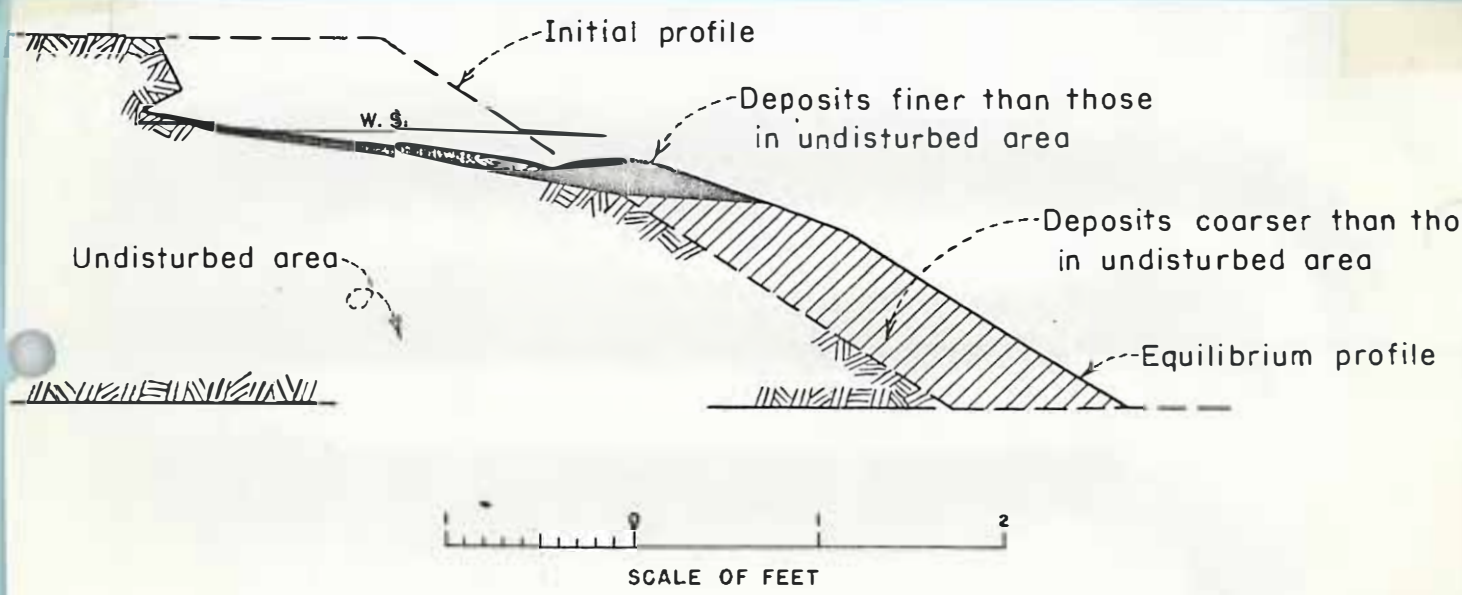

FIGURE 15
REPORT HYD. 475

CROSS-SECTION SHOWING SEGREGATION OF SOIL SIZES FOR WAVE NO. 1

Figure 8.~~12~~ 17 - Simplified Beach and Soil Size Segregation

8.~~28~~ 32/ USBR Report Hyd. No. 475.

Bascom 8.~~29~~ 33/ gives a more detailed description of grain segregation shown in Figure 8.~~13.~~ 18 The transport of sediment is complicated by wave direction, refraction, and focusing which cause coast-wise long-shore currents that carry sediment along the coast, feeding gullies and canyons that carry sediment out to deeper water. Water accumulates after successive waves, causing strong rip currents that can carry large amounts of suspended sediment, cut channels through the off-shore bars, and carry fines out to deeper water. Wave orbits described in Section 7 can continue to cause sediment movement out into deeper water. Vortex ripples have been found out to a depth of 170 feet. Wind-caused upwelling or tilt of the water surface can contribute to wave backwash currents. The backwash can be in or out of phase with mass transport of the wave. Wave steepness changes transport action and the beach can have a storm or winter profile versus a berm-type or summer profile. Tides change the still water level and cause currents. Both continually change sediment transport and bedform characteristics of the beach.

Trask 8.~~30~~ 34/ defines the active zone to a depth less than 30 feet, where sediment grain size increases with depth. He defines a more or less tranquil zone to a depth greater than 60 feet where there is very little movement and sediment grain size diminishes as depth decreases. In the beach area, the pipe should be buried out to at least the 60-foot depth. Between 30 to 60 feet there is occasional movement but grain size remains nearly constant.

8.~~29~~ 33/ Lascom, W. N., Relationships between sand sizes and beach face slope, Trans. Amer. Geophys. Union, 32, No. 6 866-74 (Dec. 1951)

8.~~30~~ 34/ Trask, P. D., Movement of sand around southern California promontories, U.S. Army Beach Erosion Board TM No. 76, 1955

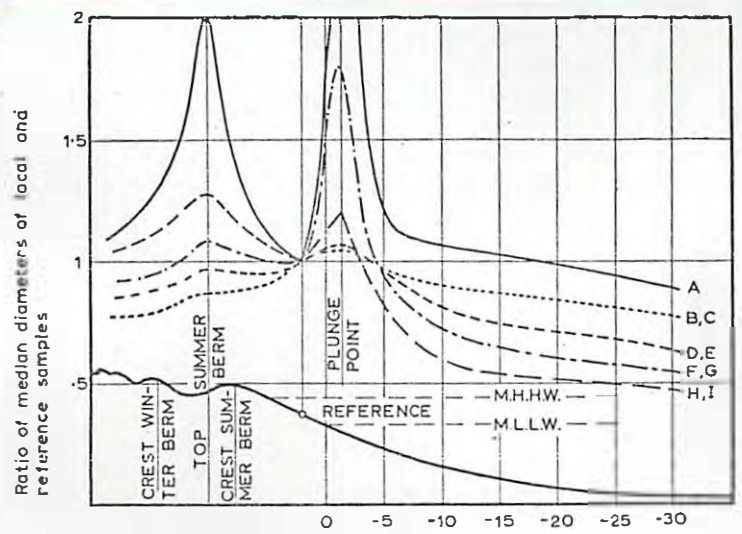

FIG. 14.29. Particle size distribution across a beach.

Location	*A*	*B*	*C*	*D* and *E*	*F*	*G*	*H*	*I*
Median diameter (in mm) of reference sample	0·42	0·22	0·19	0·35	0·44	0·40	0·36	0·30

Reference sample at mid-tide beach face used as 100 per cent. (From ref. 27, by permission of the American Geophysical Union.)

FIGURE 8.18 BEACH PARTICLE SIZE DISTRIBUTION
8.33

The difficulty of making transport load calculations and their lack of accuracy indicates that the designers should carefully apply critical velocity and critical tractive force criteria to eliminate the need to make these tenuous computations that are only rough estimates. Many of the wave transport models and computations need much further field comparisons and modifications for application to the more natural and complex beach situations. None of the transport computation methods apply to cohesive beds.

When there is general sediment transport in the approaching flow, dunes can travel along with the flow. ~~The effect dune height must be superimposed on the data Figure 8.36~~. Half the height of the largest expected dune should be added to the estimated equilibrium depth of scour determined from FIGURE 8.36 OR EQUATION 8.11 to predict the maximum probable depth. Traveling dunes or ripples 6 feet high have been reported in the oceans 8.41/.

Possible

~~The~~ limitations of this design method are:

1. data are for freshwater and for grain sizes ranging from 0.08 to 0.68 mm,
2. does not apply to cohesive soils.

The Reynold Number in Figure 8.18 is self-correcting for water properties. The equilibrium depth (d_{se}) may not need correction for difference in submerged weight.

A change of submerged weight could be considered tantamount to a change of diameter size and Chen et al 8.36/ show data that suggests that a change of grain size causes shift along the equation line in Figure 8.18. However, there is insufficient data to definitely eliminate the possibility of correcting for water density. A significant velocity will have to be defined to apply to Chen et al method to flow with wave oscillation.

8.41/ ~~Myers et al, Hand book of ocean and underwater Engineering,~~ McGraw & ~~Hill~~, 1969. op cit

8.5/ op cit

Time Rate of Local Scour. - Carstens provides considerable evidence that all local scouring relationships due to disturbances are of the form

$$\frac{S}{L} = f\left[\left(N_s^2 - N_{sc}^2\right)^{5/2}, \frac{d}{L}, \frac{Vt}{L}\right]$$

where the symbols not previously defined are

S = settlement or scour depth

L = fundamental dimension of structure = D for cylinder

t = time

V = reference velocity

$N_s = \frac{V}{\sqrt{(\gamma_s - \gamma_f)\, gd}}$

His dimensionless plots for both a vertical or horizontal cylinder are shown in Figures 8.19 and 8.20. Although Figure 8.19 suggests an asymtotic value for the vertical cylinder (S/D) of 1.5, at one time his data was as high as 2. The limit (S/D) for the horizontal cylinder of 1 is,of course, expected. The data for the horizontal cylinder are limited to ratios of length to diameters equal to 4.

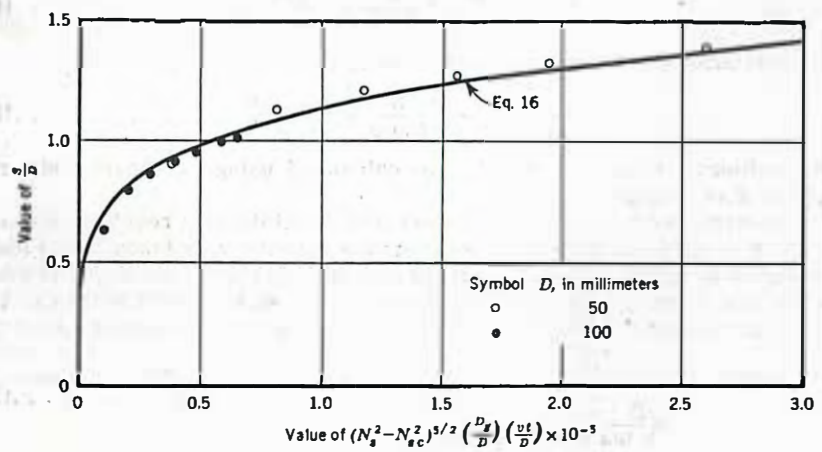

FIG. 10.—SCOUR DEPTH VERSUS TIME (VERTICAL CYLINDER) 8.39

$D_g = d$

FIGERE 8.19 SCOUR DEPTH VERSUS TIME

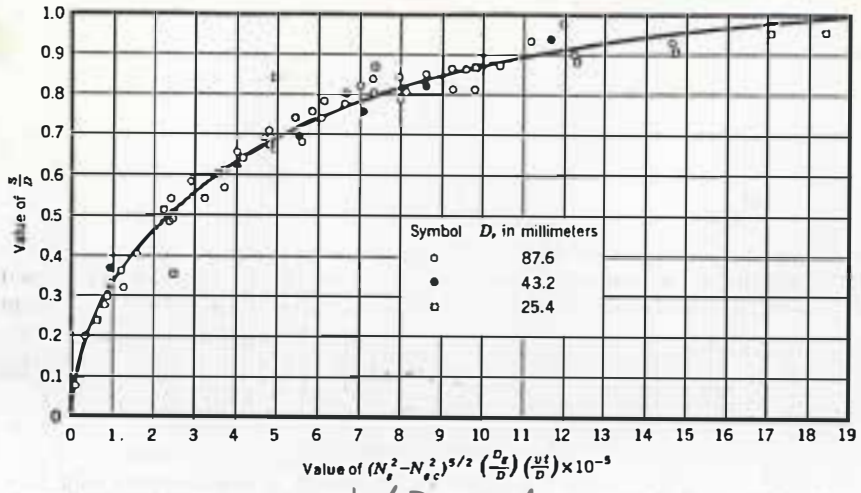

L/D = 4

FIG. 13.—SETTLEMENT VERSUS TIME (HORIZONTAL CYLINDER) 8.39

Figure 8.20.

Underflow Scour. - No information on local scour for long cylinders supported above or on the bed was found. The only method outside of model studies for the pipe above the bed is to estimate, by proportioning the approach flow OVER AND UNDER THE PIPE by potential theory, the increase of velocity under the pipe and check for critical velocity. If the velocity is above critical then assume a bed shape and find the depth of scour that will bring the velocity back to just below critical. It would probably be assumed that the slopes of the scour hole would be near the submerged angle of repose as Carsten 8.39 found for scour holes. Because of this tendency of local scour to form slopes at the submerged angle of repose, Figures 8.21 ~~and 8.22~~ WAS ~~were~~ taken from 8.10 to indicate the repose angle.

8.39 op. cit.

8.10 op cit.

Local Scour

Background. - Laursen 8.35/ essentially stated that the fundamental characteristics of local scour are:

1. The rate of scour is the difference between the rate of sediment supply approaching the scour area and the rate of local transport from the scour area.

2. The rate of scour will decrease as the scour hole enlarges and approaches an equilibrium shape that limits the extent of scour.

4. The limit of scour will be approached asymptotically with respect to time.

These statements imply that flow conditions are known before and after placing the structure. These statements also imply that methods are known for determining the sediment properties, for computing the transport before construction, and for computing the transport after placing the structure, and for determining the changing shape of the scour hole.

When a structure is placed in or on the bed, flow is accelerated and the turbulence is changed around parts of the structure. Wake vortices trailing vortices, and horseshoe vortices can be produced, Figure 8.14.

8.35/ Laursen, E. M. Progress Report of Model Studies of Scour Around Bridge Piers and Abutments, Research Report No. 13-B Highway Research Board, 1951.

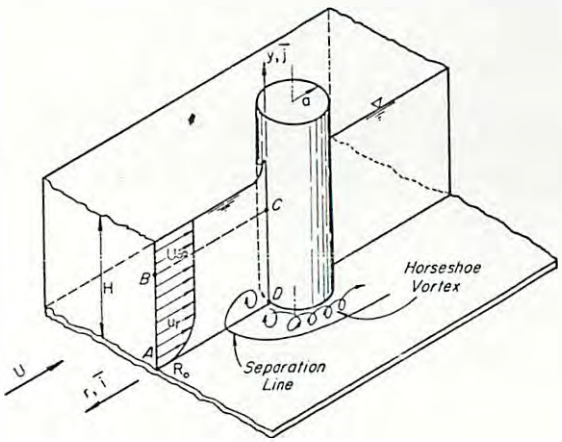

FIG. 2.—DEFINITION OF VARIABLES USED IN ESTIMATING STRENGTH OF HORSESHOE VORTEX

Figure 8.14. Horseshoe Vortex 8.36/

(from Shen et al)

Scour trend - Blunt-nose piers have maximum scour depth upstream in the stagnation zone and sharp-nose piers have the maximum scour downstream. Scour tendency patterns are shown in Figure 8.15 taken from reference 8.1/. The references relating to each case are shown under the respective diagram.

8.36/ Shen, H. W. et al, Local Scour around bridge piers, Journal of the Hydraulic Division, Proceeding ASCE, Vol 95, No. HY6, 1969.

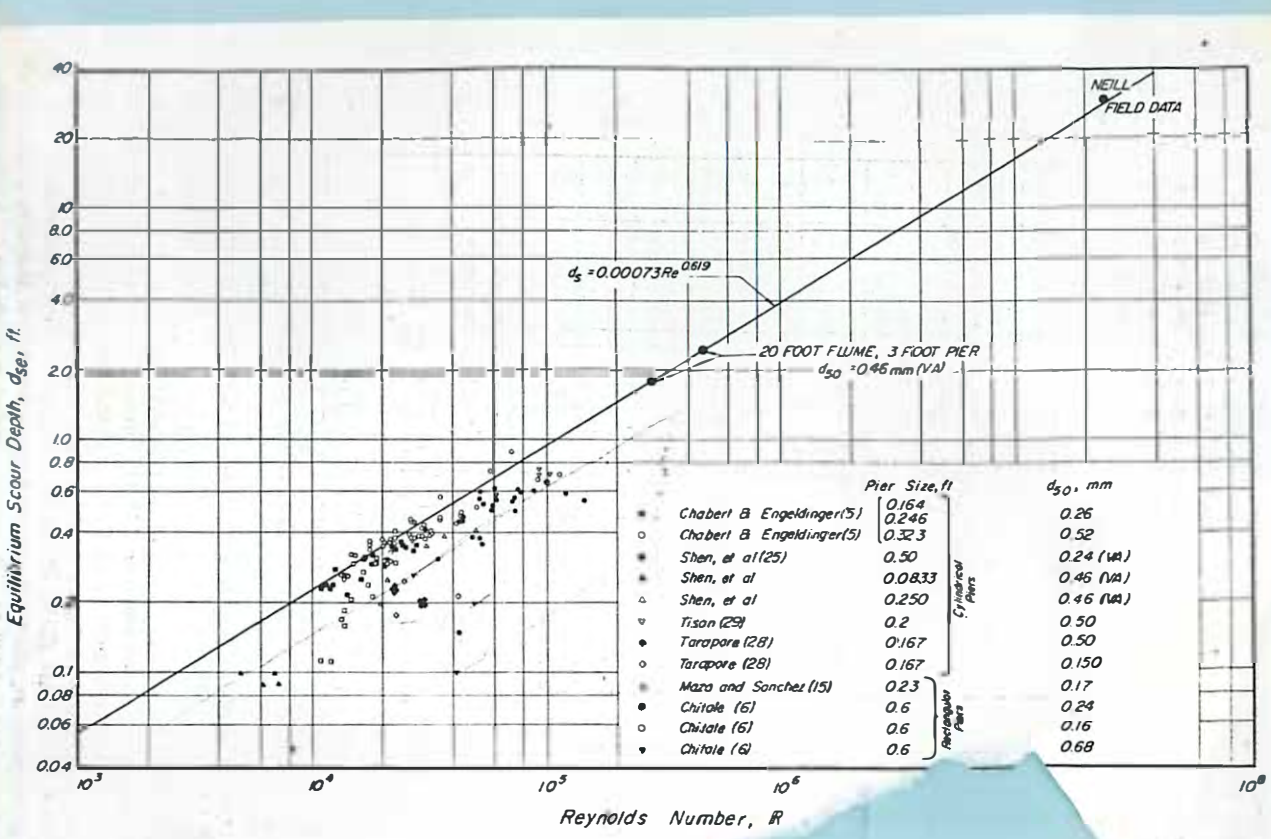

FIG. 6.—COMPARISON OF RESULTS FROM FIG. 5 W

8:36

Figure 8.18. - ENVELOPE OF SCOUR DEPTH VERSUS REYNOLDS NUMBER $\left(\frac{VD}{\nu}\right)$ FOR PIERS

the value read from Figure 8.18 [redacted]. The smallest value of the two should be used. Larras' equation is written as follows:

$$d_{se}^{*} = 1.42\ Kb^{0.75} \quad \ldots\ldots\ldots\ldots\ldots\ldots \quad (8.11)$$

where K = 1 for cylindrical piers

K = 1.4 for rectangular piers aligned with flow

d_{se}^{*} = depth of scour defined in Figure 9.17

b = diameter or width of projected plane normal to flow
= D for cylinder

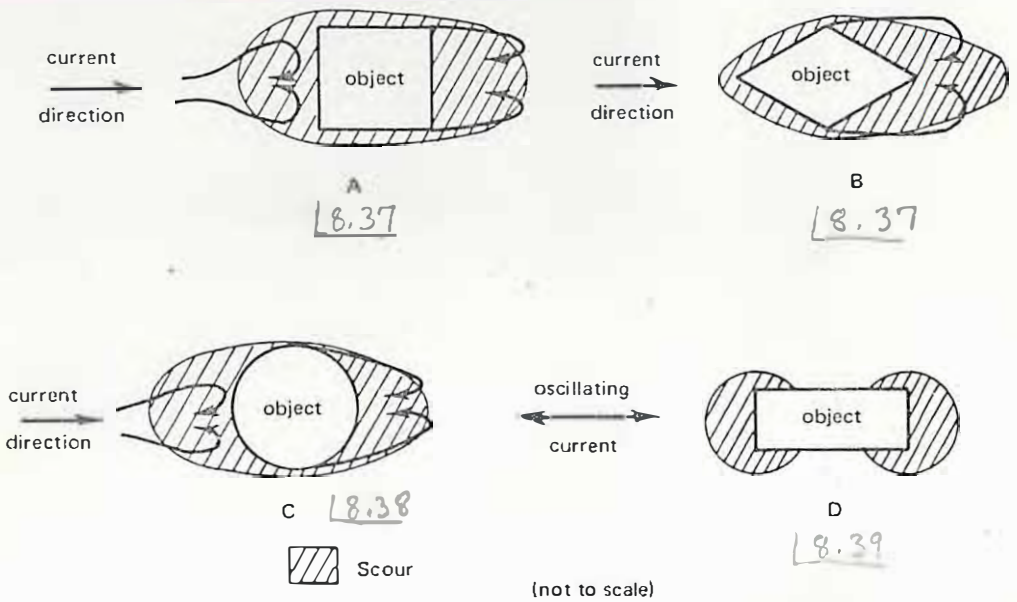

Figure 13. Areas of maximum local scour for objects of various geometries and flow conditions.

Figure 8.15. Scour Examples

8.37 Shen, H. W., Schneider, V. R., and Karaki, S. S. (1966). Mechanics of local scour, Engineering Research Center, Colorado State University, Report no CER 66HWS22, Fort Collins, Colorado, 1966.

8.38/ Shen, H. W., Ogawa, Y., and Karaki, S. S. (1965). "Time variation of bed deformation near bridge piers," in Proceedings, 11th Congress International Association for Hydraulic Research, Leningrad, Sept. 7-11, 1965, Vol. 3. Moscow, Committee for the USSR Participation in International Power Conferences, 1965, paper 3.14.

8.39/ Carstens, M. R. (1966). "Similarity laws for localized scour," American Society of Civil Engineers, Proceedings, Journal of the Hydraulics Division, vol. 92, no. HY3, May 1966, pp. 13-36.

Shen et al 8.36/ contrasts the clear water scour (ds) with scour with equilibrium scour (dse) in transport ~~with~~ respect to time, Figure 8.16 and with respect to velocity, Figure 8.17.

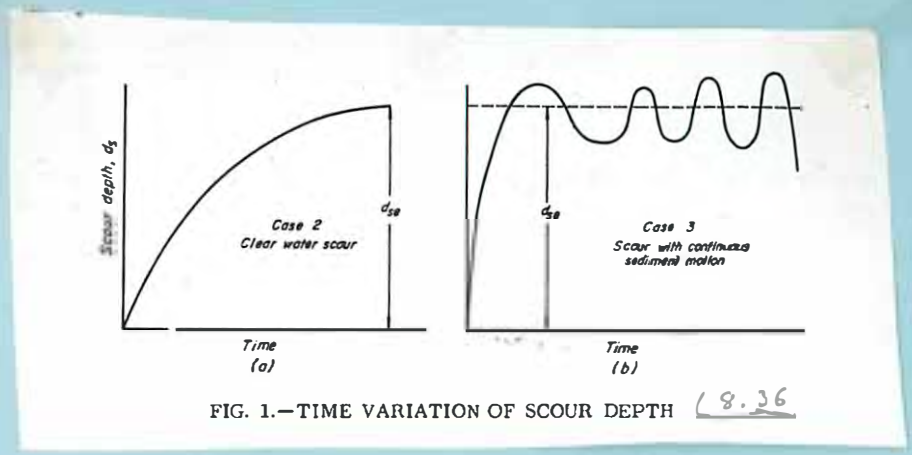

FIG. 1.—TIME VARIATION OF SCOUR DEPTH (8.36

Figure 8.16.- SCOUR VERSUS TIME

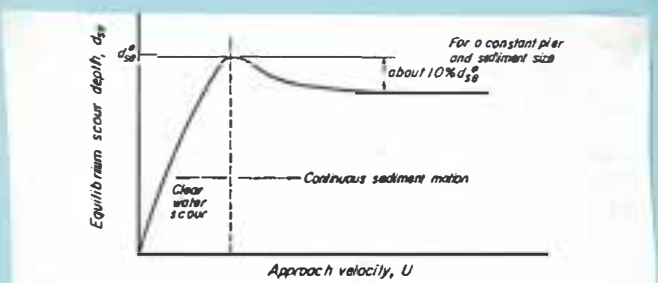

FIG. 4.—VARIATION OF SCOUR DEPTH WITH VELOCITY (8.36

Figure 8.17. - SCOUR VERSUS VELOCITY

Dimensionless Scour Depth Envelope. - For design Shen et al 8.36/ suggests that their equation and plot shown in Figure 8.18 be used as an envelope for clear water scour. If there is a continuous sediment transport in the approach flow then the value of equilibrium scour depth (d_{se}^*) should also be computed from Larras' 8.40/ equation and compared with

(8.40 Larras, J., "Profondeurs Maximales d'érosion des fonds mobiles autour des piles en rivière" ("Maximum Depth of Erosion in Shifting Beds Around River Piles"), *Annales des ponts et chaussees*. Vol. 133, No. 4, pp. 411–424.

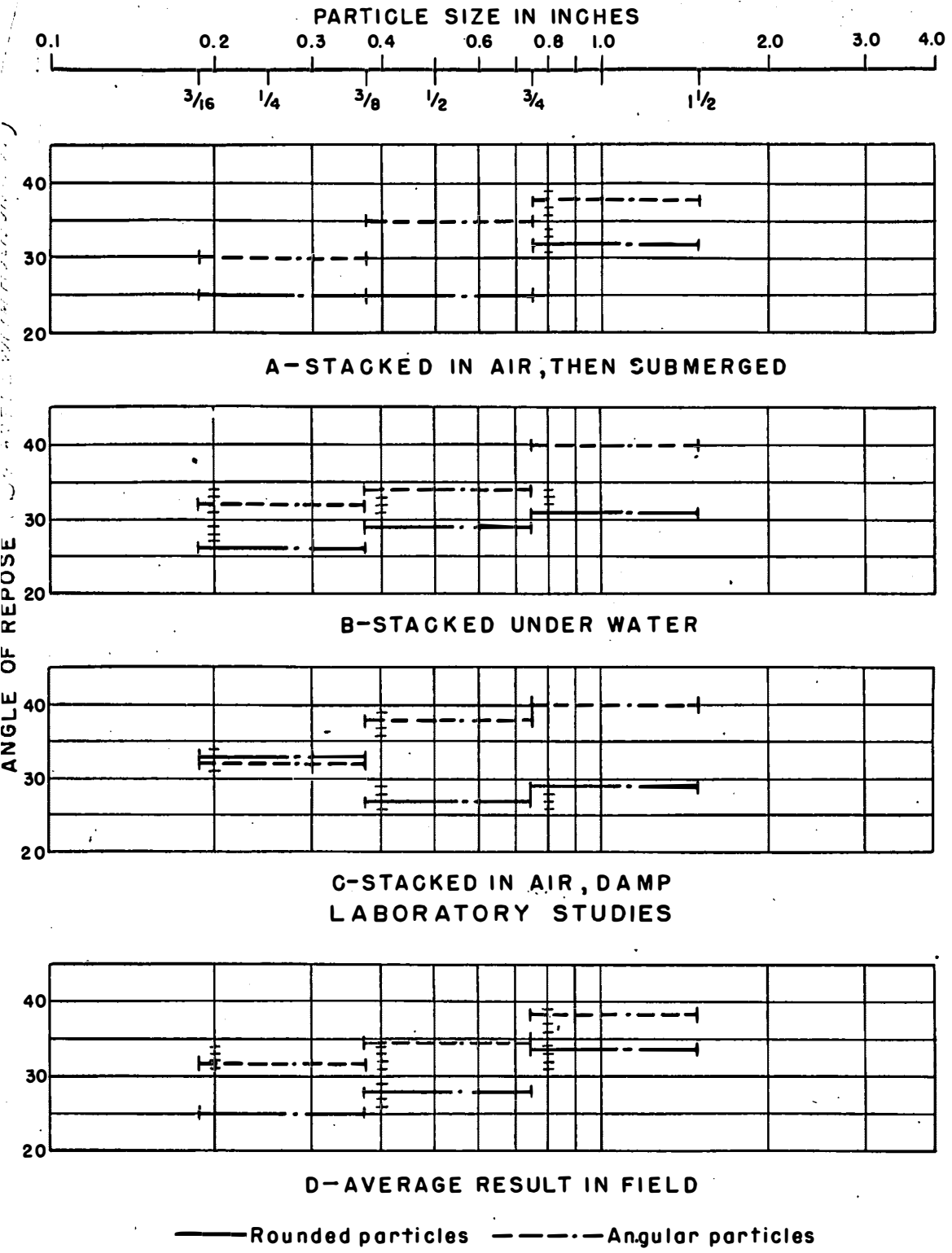

RESULTS OF OBSERVATIONS ON ANGLE OF REPOSE OF COARSE NON-COHESIVE MATERIAL

FIGURE 8.21 REPOSE ANGLE OF COARSE NON-COHESIVE MATERIAL

Long reaches of a pipe partially buried or resting on the bed can be easily underscoured and left unsupported. The pipes can either settle or rupture. No suitable information ~~for helping to account for~~ the amount of scour depth ~~has been~~ found to help compute, AND the required bridging strength. Wave oscillation and vortex trails can create pulsating forces on the bed or even produce alternating lifting of the pipe from the bed.

TP Scour by Fluidization. - Posey 8.41/ describes another mode of scour occurring around oil towers having many piles and braces disturbing the flow. For long-waves, pressures can be transmitted into permeable soils causing in and out flow. If this action ~~fluidizes~~ fluidizes the soil, the soil can move out. No suggestion for predicting this scour was made.

Scour in Cohesive Soil. - No information on local scour was found for cohesive soils in the consolidated, unconsolidated or the ooze form commonly found in the ocean. These unconsolidated forms HAVE virtually no resistance to scour. After foundation feasibility has been established, before and after tractive force values can be used to determine whether critical shear velocity ~~of~~ OR critical tractive force are exceeded. If critical values are exceeded, scour can not be predicted and scour protection such as riprap or anchoring into bedrock must be considered.

8.41/ Posey, C. J., "Protection of offshore structures against underscour ASCE Journal of the Hydraulic Division, Vol. 97, HY7, 1971, page 1011-1015.

Some limitations. - Virtually all the data included in the scour section is based on fresh water studies. The completely dimensionless approaches are self-correcting for seawater. Those studies that included some field checking were stressed. Bridge peer studies provide a source of local scour data but is usually presented in forms that include discharge, energy gradients, Fourde number, and depth of flow. Therefore, none can be easily applied to the ocean bottom. This is the reason that approaches of Chen et al 8.36/ and Carsten 8.39/ were stressed. However, their data must be ~~extended~~ used with care to ~~lower~~ obstructions where turbulence from the top might ~~affect~~ scour ~~significantly~~.

PROBABLISTIC APPROACHES*

The discussions and data contained in this section and in the remainder of this appendix were extracted as complete units without any internal editing from the more complete work done for the USBR by Dr. R. H. Riffenburgh. 1/

DEVELOPMENT OF METHODOLOGY FOR 100-YEAR EXTREMES

Suppose there exists a probability density $f_X(x)$ on a variate X. Let us use X = wave height (vertical component of trough-to-crest distance) in meters as an example throughout this section; other variates follow the same theory and methodology, but have different forms of $f_X(x)$. We are concerned with extreme values. In our example, we wish to predict the greatest wave height which will occur in the next hundred years. The first impulse is to find b such that

$$P[X \leq b] = \int_{-\infty}^{b} f(X)dX = 1 - \alpha,$$

and then to say, "We are $100(1 - \alpha)$ percent confident that the greatest value on X which will ever be observed is b." However, several objections occur in this approach. (1) Gumbel [1958] has shown that extreme values, or records, over a time period increase monotonically with the length of the time period, so that no "greatest . . . ever be observed" is possible to predict. (2) The physical circumstances which generate common values on X may be sufficiently different from those which generate record values so that influences found to be negligible in one may be important in the other and *vice versa*. Thus, the probability distribution for common occurrences may be different from that for extremes. (3) The difference between the true and assumed probability densities may become large in the tails. Consider figure 1. In this figure, f_X represents the assumed probability density, the one we can manipulate and calculate, and g_X represents the true density, which we can never know. If f_X should deviate very far from g_X, empirical frequency distributions of samples from g_X would so indicate in the region of the bulk of observations; herein lies the problem. The bulk of observations are in the central part of the curve. The reasonable agreement lies in the central region, not in the extremes. Traditional statistical methods study central parameters and variability about central parameters; the area under a tail is used only for measuring the separation between values of central location or central variability parameters. For example, in figure 1, the difference between the two curves, *i.e.*, the percent error in density in assuming f_X when g_X is true, is about 6 percent in the vicinity of the mean, but it is about 400 percent in the vicinity of point a.

1/ op cit

52/ Gumbel, E. J., (1958): "Statistics of Extremes," NY: Columbia University Press.

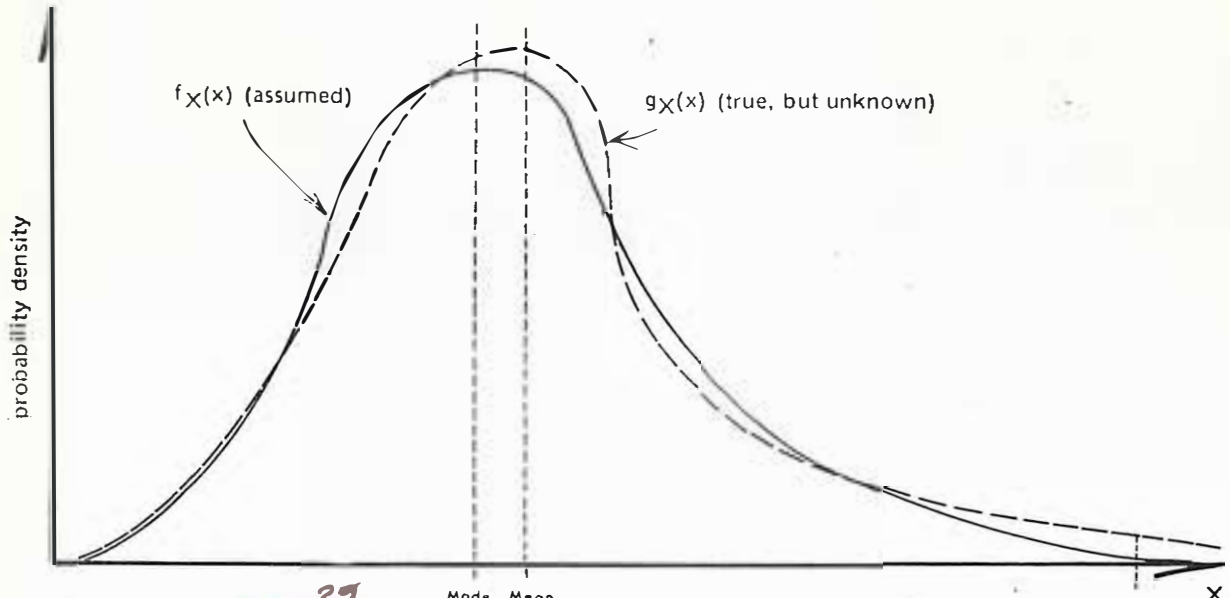

Figure 1. Examples of true and assumed probability distributions.

What we require is the probability distribution of extreme values. Gumbel [1958] and Borgman [1963] have derived probability distributions for the number of times an existing record will be exceeded during an ensuing time interval of given length, but they say nothing of the values of the exceedeness. Thompson [1969] proved that the distribution function of the values of the extremes follows the form

$$H_X(x) = e^{-e^{-(x-\beta)/\gamma}}$$

for the parameters

$$\beta = \text{mode } (x) \text{ and } \gamma = (\sqrt{6}/\pi) \times (\text{standard deviation of } x).$$

$h_X(x)$, the density associated with the distribution $H_X(x)$, is illustrated in figure 2 in its relation to g_X. Although Thompson has given the form of h_X, observations from h_X are not available to estimate the parameters of h_X, and we have been able to find no general development in the literature which allows observations from g_X to estimate h parameters. The analytic derivation of an approximation to h_X has appeared in the literature for only certain of the g_X forms we use, and even for those forms sample sizes and time interval relations prevent the approximation from being adequate in many cases. (For a review of such work, see Barlow and Singpurwalla [1972].) Since any analytic method developed must depend on the form of g_X, necessitating a new development for each form of g_X, we developed a simulation algorithm to be utilized on a computer so that the same program could be used for any g_X. Steps in the simulated algorithm are listed on page 10.

53/ Borgman, L. E., (1961): "The exact frequency distribution by near extremes," presented Pacific Southwest Regional Meeting, American Geophysical Union, January 26, 1961, Berkeley, California.

54/ Thompson, William A., (1969): "Applied Probability," NY: Holt, Reinhart, and Winston.

55/ Barlow, Richard E. and Singpurwalla, Nozer D., (1972): "Averaging Time and Maxima for Dependent Observations," Proceedings of the Symposium on Statistical Aspects of Air Quality Data. Triangle Universities Consortium on Air Pollution and Division of Meteorology. Environmental Protection Agency, Chapel Hill, November 1972. In press.

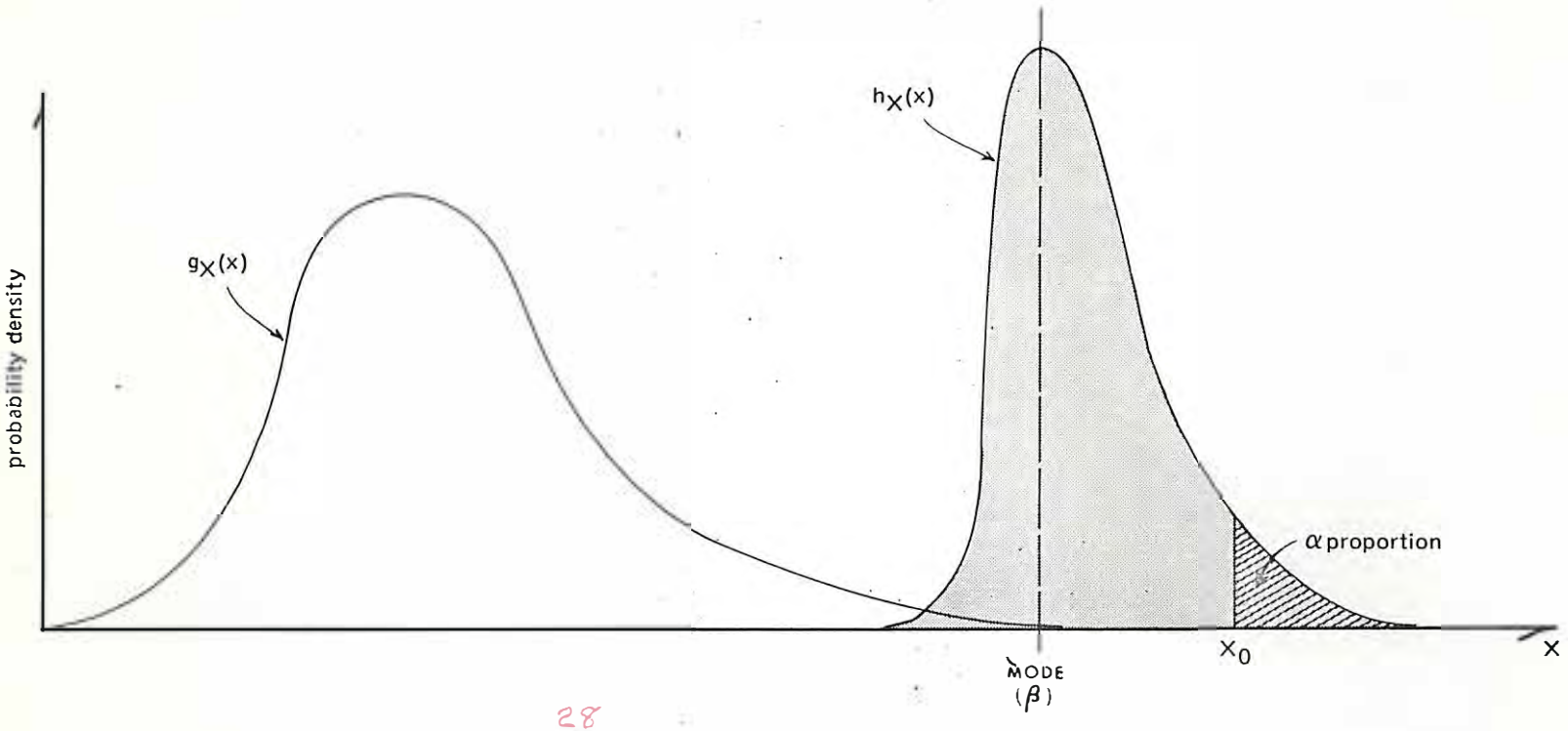

28

Figure 2. The Thompson extreme distribution h_X on the tail of g_X.

1. Obtain observations (x) on X. Desirably, x can appear only at discrete time intervals of, say, t_0 in length. For example, if X is the wave height during a storm and there are about three storms per year, then t_0 is about 4 months. Alternatively, X may be continuous, in which case x_t (x at time t) may be correlated with $x_{t+\epsilon}$ (ϵ small and positive) because of continuity constraints of the physical process. Worse, a simulation sampling can yield an arbitrarily large extreme because any size sample may be taken from any nonzero time interval. As an *ad hoc* solution for CUA purposes, an arbitrary time period, say t_0, was taken in continuous cases, and the midinterval or largest x in this interval was used as a datum. t_0 was chosen large enough to damp out the autocorrelation. An example of such a variable is the density of seawater, which exists and is measurable at any moment at any place in the sea.

2. Predict by f_X the functional form of g_X, and verify by goodness-of-fit tests on the empirical frequency function, which is illustrated in figure 3. Estimate parameters of f_X from data.

3. Using a computer, take a randomly chosen sample of n values drawn from the fitted f_X; record the largest of the n values. Suppose we wish to predict the most extreme values on X to appear in the time interval t_1 ($> t_0$); for CUARO, t_1 = 100 years. Then $n = t_1/t_0$. This procedure provides one observation on X drawn from h_X, and satisfies objection 1. Steps 1 and 3 together satisfy objection 2.

4. Repeat step 3 m times (m = 500 for the CUA study), and use these m data from h_X to estimate the parameters β and γ of h_X. This step satisfies objection 3.

5. Find an x_0 so that $H_X(x) = 1 - \alpha$ by

$$x_0 = -\gamma \ell\eta[-\ell\eta(1-\alpha)] + \beta \qquad (4)$$

to compute a $100(1 - \alpha)$ percent confidence bound on the greatest value of X to be observed in time period t_1. This bound, x_0, is shown in figure 2.

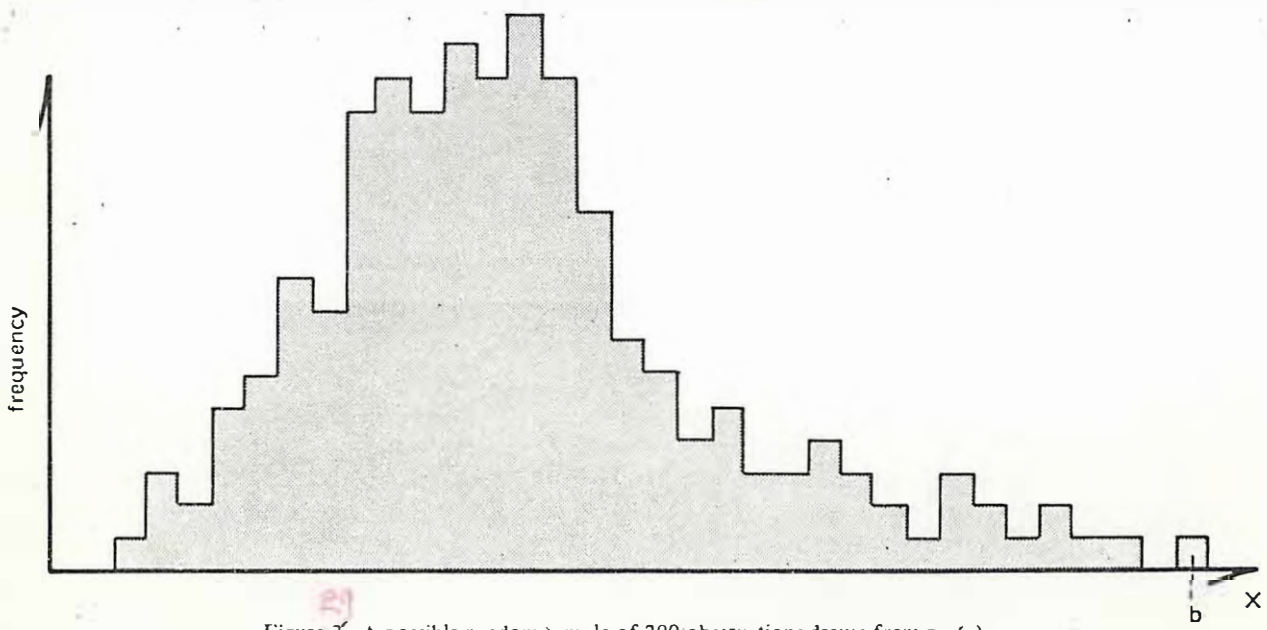

Figure 3. A possible random sample of 200 observations drawn from $g_X(x)$.

PROBABILITIES OF CONFLUENCES OF SURVIVAL THREATS TO THE CUA

Suppose we have two independent events, random in time, with variables t and w representing their beginning points. (The events may be tsunami bottom surge and wind wave bottom surge, or they may be any general events.) Let us use the following symbols.

Symbol	Meaning
ℓ_t	Length of occurrence of t event
ℓ_w	Length of occurrence of w event
$f_t(t)$	Probability density of t event
$f_w(w)$	Probability density of w event
Ω_t	Time interval(s) in which t may occur
Ω_w	Time interval(s) in which w may occur
$\Omega_{t_1}, \Omega_{t_2}, \ldots, \Omega_{t_{k_t}}$	Possible starting points of t if Ω_t is composed of k_t separated intervals
$\Omega_{w_1}, \Omega_{w_2}, \ldots, \Omega_{w_{k_w}}$	Possible starting points of w if Ω_w is composed of k_w separated intervals
CE	Confluence of events

The probability of a confluence of the two events is the probability that the two intervals $[t,t+\ell_t)$ and $[w,w+\ell_w)$ overlap, or

$$P\{CE(w,t)\} = \int_{\Omega_t \cap \Omega_w} f_w(w) \int_{w-\ell_t}^{w+\ell_w} f_t(t)\,dt\,dw. \tag{16}$$

In particular, if the events are as likely at any one moment as any other when they are possible to occur, which will be assumed in this report, the f's are uniform distributions and

$$\begin{cases} f_t(t) = \lambda_t^{-1}, & t \in \sum_{i=1}^{k_t} \Omega_{t_i}, \\ f_w(w) = \lambda_w^{-1}, & w \in \sum_{i=1}^{k_w} \Omega_{w_i}, \end{cases} \tag{17}$$

where the λ's are constants. In this case, Eq. (16) becomes

$$P\{CE(w,t)\} = \int_{\Omega_t \cap \Omega_w} \int_{w-\ell_t}^{w+\ell_w} (\lambda_t \lambda_w)^{-1} \, dt\,dw = \frac{\ell_t + \ell_w}{\lambda_t \lambda_w} \int_{\Omega_t \cap \Omega_w} dw. \quad \ldots\ldots (18)$$

Let us consider the case of confluence of three independent events, adding a new variable c with definitions equivalent to those of t and w. $P\{CE(w,c,t)\}$ is given by the probability that all of $[w, w+\ell_w)$, $[c, c+\ell_c)$, and $[t, t+\ell_t)$ overlap, or

$$P\{CE(w,c,t)\} = \int_{\Omega_c \cap \Omega_w \cap \Omega_t} f_c(c) \int_{c-\ell_w}^{c+\ell_c} f_w(w) \int_{c-\ell_t}^{c+\ell_c} f_t(t) dt\, dw\, dc. \quad (19)$$

In particular, for uniform probability densities,

$$P\{CE(w,c,t)\} = \int_{\Omega_c \cap \Omega_w \cap \Omega_t} \int_{c-\ell_w}^{c+\ell_c} \int_{c-\ell_t}^{c+\ell_c} (\lambda_t \lambda_w \lambda_c)^{-1} \, dt\, dw\, dc$$

$$= \frac{(\ell_c + \ell_w)(\ell_c + \ell_t)}{\lambda_t \lambda_w \lambda_c} \int_{\Omega_c \cap \Omega_w \cap \Omega_t} dc. \quad (20)$$

Let t, w, and c denote the start times of the century's greatest tsunami, wind wave bottom surge, and bottom current, respectively. Let us make the following assumptions, where the scale of all variables is measured in hours.

A tsunami wave train's largest portion will last 3 hours; $\ell_t = 3$. The largest portion of the wave train of the century's worst storm will last 3 days; $\ell_w = 72$. A century's worst current will last during either the ebb or flood (depending on direction) of the semidiurnal tide; $\ell_c = 6$. The great tsunami may occur at any time of any year; 100 years contains $24 \times 365.25 \times 100 = 876{,}600$ hours; $f_t(t) = \lambda_t^{-1} = (876600)^{-1}$, $t \in [0, 876600)$. The great wind wave bottom surge may occur only in winter; one-half of each year for 100 years contains 438,300 hours; $f_w(w) = \lambda_w^{-1} = (438300)^{-1}$, $w \in [0,4383), [8766,13149), \ldots, [429$ $[429534,433917)$. The bottom current modelled by EPRF has as its tidal component the typical year's greatest spring tide. In 50 to 200 m of water, deeper than the wind effect (calculated by Eq. (18)) and over a century of time, the greatest current may be considered as occurring equally in time. Then $f_c(c) = \lambda_{c \geq 50}^{-1} = (876600)^{-1}$, $c \in [0,876600)$, when $z \geq 50$ m. In 20 m of water, storm winds add a component to the current; the great storm may occur only in winter; the great tide would be expected to occur in winter in only half the years. Thus, the 20-m great current may occur only in winter in half the years. $f_c(c) = \lambda_{c<50}^{-1} = (219150)^{-1}$, $c \in [0,2191.5), [8766.0,10957.5), \ldots, [210384.0,212575.5)$, when $z < 50$ m. When the great current does occur, it must occur simultaneously with the great wind wave bottom surge since both require the great storm. This situation provides the only departure from independent events in this section, but it is simple enough to be discussed without using more sophisticated formulation.

The depth of the frictional influence D has been

$$D = \pi \sqrt{a/\rho \Omega \sin\phi}, \qquad (10)$$

where a denotes an eddy viscosity coefficient of approximately 100 g/cm sec^2, Ω denotes an angular velocity of 0.729×10^{-4} r/sec, and ϕ denotes latitude. D was calculated for latitudes from 42 deg (near Crescent City) in the north to 33 deg (near San Diego) in the south. D for Crescent City was about 44 m, and D for San Diego was about 49 m. With an exponential particle velocity diminution, frictional influence anywhere near the 44- to 49-m bound will be negligible. It may be concluded that wind influences are of concern only at the CUARO standard depth of 20 m.

Since the 20-m great current has half as many opportunities to occur as the great wind surge and since the greatest wind surge in the century has a probability of one of occurring, the probability of confluence of the 20-m great current and great wind surge is one-half. By similar reasoning, the probability of confluence of the 20-m great current, great wind surge, and great tsunami is half the probability of confluence of the great wind surge and great tsunami alone.

Let us calculate the other confluence probabilities. Substituting appropriate values in Eq. (18), we obtain

$$P\{CE(w,t)\} = \frac{75}{3.8421378\times10^{11}}\left(\int_0^{4383} dw + \ldots + \int_{429534}^{433917} dw\right)$$

$$= 1.952038264\times10^{-10}\times 100\int_0^{4383} dw = 8.555783711\times10^{-5}$$

$$\doteq 0.000\,086.$$

$$P\{CE(w,c(\geq 50\text{m}))\} = \frac{78}{3.8421378\times10^{11}}\times 100\int_0^{4383} dw \doteq 0.000\,089.$$

$$P\{CE(c(\geq 50\text{m}),t)\} = \frac{9}{7.6842756\times10^{11}}\int_0^{876600} dt = 1.026694045\times10^{-5}$$

$$\doteq 0.000\,010.$$

$$P\{CE(c)<50\text{m}),t)\} = \frac{9}{1.9210689\times10^{11}}\left(\int_0^{2191.5} dc + \ldots + \int_{210384.0}^{212575.5} dc\right)$$

$$= 4.684891833\times10^{-9}\times100\int_0^{2191.5} dc = 1.026694045\times10^{-5}$$

$$\doteq 0.000\,010.$$

(Note that while $P\{CE(c(\geq 50\text{ m}),t)\} = P\{CE(c(<50\text{ m}),t)\}$ the c events involved are quite different. In the latter probability, the chance of the great current occurring on any day for which it is possible is four times as likely as in the former, but the chance of confluence with the great tsunami is one-fourth as great.)

To calculate a triple confluence, we substitute the appropriate values in Eq. (20).

$$P\{CE(w,c(\geq 50m),t)\} = \frac{702}{8.420044989 \times 10^{16}} \left(\int_0^{2191.5} dc + \ldots + \int_{210384.0}^{212575.5} dc \right)$$

$$= 8.337247615 \times 10^{-15} \times 100 \int_0^{2191.5} dc = 1.827107815 \times 10^{-9}$$

$$\doteq 0.000\ 000\ 001\ 8.$$

The confluence-of-events probabilities for all confluences at CUARO standard depths, with associated particle velocities, for northern, central, and southern California coastal regions are given in table 9. 10

Table 9. 10 Confluence-of-events probabilities for all confluences at CUARO standard depths with associated particle velocities for northern, central, and southern coastal California.

Type of Confluence	Depth, m	Probability of Confluence	Probable Extreme Velocity, cm/sec, Given Confluence Occurs		
			Crescent City	San Francisco	Santa Barbara
w, c	20	0.500 000	606.5	618.2	454.6
	50	0.000 089	412.8	430.0	357.0
	100	0.000 089	440.9	442.6	407.0
	200	0.000 089	410.3	403.0	396.5
w, t	20	0.000 086	462.8	421.8	205.6
	50	0.000 086	209.7	200.4	100.9
	100	0.000 086	121.9	107.9	56.5
	200	0.000 086	59.8	43.1	27.2
c, t	20	0.000 010	512.3	459.6	407.0
	50	0.000 010	388.5	362.0	335.5
	100	0.000 010	429.2	413.5	397.7
	200	0.000 010	416.1	406.7	396.5
w, c, t	20	0.000 043	790.8	749.8	533.6
	50	0.000 000 001 8	505.5	496.2	396.7
	100	0.000 000 001 8	496.0	482.0	430.6
	200	0.000 000 001 8	443.1	426.4	410.5

STUDY NEEDS

Introduction

During the literature search it became apparent that there is a "degree of unknown" about hydrodynamic loading and scouring conditions for the aqueduct. The action of the hydrualic and soil environment surrounding the aqueduct is not explicity defined, but is only known in somewhat general terms. Thus the designer is required to design the aqueduct for a range of loads, and with the uncertaintly of "underdesigning or overdesigning" when obtaining an estimated cost. Providing the Hydrodynamics Loading and Scour Task Force Team have not missed pertinent information in the literature search, further study is needed to give the designers more precise design information. If the aqueduct proposal proves worthy of continuation then it is essential to obtain more accurate information. The team believes study needs are required in areas which are noted in the following subheadings.

Waves

The collection of wave data (parameters of wave height H, wavelength L, period T, and accompanying water motion beneath the waves) are not near as common as collection of streamflow data. Wave data is meager when compared to streamflow data and also much more difficult to obtain. Maximum wave conditions which may occur for a 100-year time period off the California Coast are not accurately known. For actual construction of the aqueduct it is imperative that the maximum wave forces acting on the aqueduct be known.

Whereas wave data was not a task force team assignment, there is a connection of wave data with respect to wave theories and applying the wave theories to compute aqueduct forces. The wave data will be used in conjunction with determining adequateness of the Airy Theory or if another wave theory better defines the water motion. Accurate wave dimensions are needed when applying a wave theory. Generally dimensions (H and L) are ~~sufficient~~ most used, but the crest length may be important for application to the aqueduct. Crest length is a distance the wave crest extends over the water surface and is measured perpendicular to the wave profile showing the H and L dimensions. Ocean waves can be irregular and evidently can have crest lengths considerably shorter than a mile. Possibly short crested waves could produce more critcal loads along the aqueduct than waves with indefinitely long crests.

Hydraulic model studies can ~~be of great~~ assist (in gaining knowledge for) ~~during~~ design ~~stages~~ of the aqueduct and accurate wave data will be essential in conducting these hydraulic model studies.

Lift, Drag, and Oscillatory Forces

Emperirical formulas have been developed for computing hydrodynamic forces acting on a circular cylinder. Numerous hydraulic model and field tests have been made to determine values of coefficients used in these formulas. However hydrodynamic forces that act on a cylinder are unsteady and thus many test results show a wide range of coefficient values. Further hydraulic model tests, with carfully devised instrumentation, should be made to study and measure the unsteadiness of the forces. Hydraulic model tests should also be made to obtain coefficients values for flow configurations which have not been extensively tested.

The preponderance of information on hydrodynamic forces is for fixed bluff bodies. A moving body may have a steadying effect on the movement. Studies made on cyclinders or other shapes without movement limit the understanding of dynamic forces.

Investigations should be extended to studies of large cyclinders 1/3 to 1/2 the diameter of the aqueduct to confirm small model drag, lift, and inertia coefficients.and vortex shedding frequencies. The cyclinder suspension should provide close simulation of "free body" movement. Perpendicular and angled flows should be applied to the suspended cyclinder.

The effect of an adjacent boundary on a fixed cyclinder and on the movement of the cyclinder should be studied for the unbalanced pressure of accelerating flow. An erodible and fixed boundary should be included in the study with attempts made to measure velocity changes between the cyclinder and boundary.

Scour

Probably scour on the ocean bottom near the aqueduct, and providing a estimate of this scour, is the most unknown factor of all. Especially when considering a 100-year time period. Ocean bed sediment transport, as computed by a theoretical-mathematical type models, has not been verified by field observations. These type of sediment transport computations exist only for noncohesive sand sediments, and not for the cohesive fine-particle or clay type sediments. Better information about scour conditions can be obtained by model and field-type tests.

Model-type tests would be advantageous in determining scour tendencies for various pipeline configurations. Such configurations are those of a buoyant pipeline above the bed to a pipeline resting or partially buried in the ocean bed. In a moving water medium a large pipeline presents a structure where local fluid acceleration occurs as the water flows past the structure. There is a susceptibility of scour by this acceleration, even if the pipeline is somewhat above the ocean bottom(buoyant concept). Model tests would also be valuable in studying and learning more about the interdependent relation of scour and the acceleration flow field of a large diameter pipeline.

Field tests should be made with concrete blocks of different structural shapes which are of interest. These blocks should be set at various locations on the ocean bottom, from deep water up to the surf zone, and on different type marine soils. Observations of scour and settlement should be made, and if possible also measurements, in an effort to obtain some correlation between scour, water depth, wave parameters, block size, block shape, and soil properties.

Marine Fouling

For the buoyant concept marine fouling is a serious problem. Weight of the marine growth may exceed buoyancy of the pipeline. Such problems need studying, weight of the marine growth (pounds per square foot of pipe surface), rate which marine growth acquires weight with respect to water depth and time, and if there are possible methods of restraining or removing the growth.

Priority of Study Needs

After making a design and cost estimate, better information should be available concerning study needs. Some unknown factors may prove to be more critical in relation to cost than others. Thus a priority can be established about the relative importance of future study needs.

APPENDIX I

CHOICE OF THE AIRY EQUATIONS

The ocean bottom and a portion of the water depth above the bottom are the prime locations under consideration for the proposed California Undersea Aqueduct. The Airy Theory appears to be as accurate as other wave theories for evaluating wave effects near the ocean bottom. The decision to use this theory in the design data reference book was made after considering information noted in references I_a/ and I_b/.

The maximum horizontal and vertical water velocities occurring beneath waves have been measured in a wave tank for a d/L value of approximately 1/10 I_a/. The Airy Theory agrees favorably with the measured horizontal velocities in the lower 1/2 depth range; however, the Airy Theory gives velocities approximately 30 percent smaller than the measured vertical velocities. Conclusions in the reference noted that the simple Airy Theory may be applied at the bottom.

A comparison of horizontal particle velocities for various wave theories is given in reference I_b/. For the lower 1/3 depth range the Airy Theory agrees closely with two other wave theories, while one wave theory shows higher velocities. Reference I_b/ also concludes "When inertia (acceleration) forces predominate, a first-order theory is probably sufficient."

The Airy Equations are a first-order theory and calculations for a large diameter pipe show that acceleration forces are predominant.

Ia/ LeMehaute, D. Divoky, and A. Lin, Shallow Water Waves, Proceedings of Eleventh Conference on Coastal Engineering, London, England, Sept. 1968, Vol 1, page 86-107.

Ib/ Handbook of Ocean and Underwater Engineering, McGraw-Hill Book Company, New York, 1969.

BIBLIOGRAPHY

Anchors and Cables

Bedendender, J. W., "Three-dimensional Boundary Value Problems for Flexible Cables," OTC - 1970, Vol. II, pp II-541-II-556, Paper No. OTC 1282

Camp, G. D., "The Shape of a Flexible Rope Towing a Submerged Body," University of California, DWR Report M5, November 1942, BTR-OTS-USDOC: PB 37083

Freudenthal, A. M., Gaither, W. S., "Design Criteria for Fixed Offshore Structures," Offshore Tech. Conf., Vol. 1, 1969, OTC 1058, p 623

Goeller, J. E., Patriccio, A. L., "Analytical and Experimental Study of the Dynamic Response of Cable Systems," OTC 1156, 1970, Vol. 1

Laird, A. D. K., "Forces on a Flexible Pile," Proceedings, Specialty Conference on Coastal Engineering, ASCE, Santa Barbara, California, October 1965, pp 249-268

Landweber, L., "Hydrodynamic Forces on an Anchor Cable," November 1947, BTR-OTS-USDOC: PB 92298

Achenbach, E., "Experiments on the Flow Past Spheres at Very High Reynolds Numbers," Journal Fluid Mechanics, Vol. 54, Part 3, 1972, pp 565-575

Anonymous, "Symposium on Fully Separated Flows," ASME, Philadelphia, 1964

Ballou, C. L., "Investigation of the Wake Behind a Cylinder at Coincidence of a Natural Frequency of Vibration of the Cylinder and the Vortex Shedding Frequency," Massachusetts Inst. of Tech., Cambridge Engineering Projects Lab., Report No. TR-76028-2, May 1967

Bearman, P. W., "Vortex Shedding From a Circular Cylinder," Journal Fluid Mechanics, Vol. 37, Part 3, July 1969

Beattie, J. F., Brown, L. P., "Final Report on Lift and Drag Forces on a Submerged Circular Cylinder," Research Report, University of Tulsa, 1968

Beattie, J. F., Brown, L. P., Webb, B., "Lift and Drag Forces on Submerged Circular Cylinder," Offshore Tech. Conf., OTC 1358, TC 1505 032, Vol. 1, 1971, p I-319

Beckman, H., Thibodeaux, M. H., "Wave Force Coefficients for Offshore Pipelines," Proceedings, American Soc. of Civil Engineers, Waterways and Harbors Division, Vol. 88, No. WW2, May 1962

Bishop, R. F., Hassan, A. Y., "The Lift and Drag Forces on a Circular Cylinder Oscillating in a Flowing Fluid," Proc. Royal Soc., London, Vol. 277, 1964

Blumberg, R., Rigg, A. M., "Hydrodynamic Drag at Super Critical Reynolds Numbers," American Soc. Mechanical Engr. Meeting, June 1961

Bretschneider, C. L., "Evaluation of Drag and Inertial Coefficients for Maximum Range of Total Wave Force," Texas A & M Tech. Report 55-5, College Station, 1957

Brown, F. T., Knebel, G., Margolis, D., "Unsteady Flow in Tubes and Tunnels," Final Report No. FRA-RT-72-22, Eng. Proj. Lab., Dept. of Mech. Eng., MIT

Brown, R. J., "Drag and Lift Forces on a Submarine Pipeline Subjected to a Transverse Horizontal Current," Soc. Pet. Eng. Journal, September 1966, pp 254-260

Caster, M., "Vortex Shedding from Circular Cylinders at Low Reynolds Numbers," Journal Fluid Mechanics, Vol. 46, Part 4, April 1971, pp 749-756

Chen, C. F., Ballengee, D. B., "Vortex Shedding From Circular Cylinders in an Oscillating Freestream," Report State University New Brunswick N. J., Dept. of Mechanical and Aerospace Engineering, October 1970

Chin, W. S., Lienhard, J. H., "On Real Fluid Flow Over Yawed Circular Cylinders," Journal of Basic Engineering ASME, December 1967, pp 851-857

Date, J. R., Holler, R. A., "Vortex Wakes From Flexible Circular Cylinders at Low Reynolds Numbers," Report No. NADC-AE-7011, Naval Air Dev. Center, Johnsville, Pennsylvania Aero-Electronic Technology Dept., July 1970

Davis, M. D., "An Analytical Study of Separated Flow About a Circular Cylinder," Naval Postgraduate School Monterey, California, December 1969

Dean, R. G., "Fluid Forces on Circular Cylinders," M. S. Thesis, Texas A & M College Station, 1956

Delaney, N. K., Sorensen, "Low Speed Drag of Cylinders of Various Shapes," Technical Note 3038, National Advisory Committee for Aeronautics, Washington, November 1953

Fage, A., Warsap, H. J., "The Effects of Turbulence and Surface Roughness on Drag of a Circular Cylinder," Great Britain, ARC R&M 1370, October 1929

Fage, A., "Drag of Circular Cylinders and Spheres," Great Britain, ARC R&M 1370, May 1930

Fage, A., Falkner, V. M., "Further Experiments on the Flow Around a Circular Cylinder," Great Britain, ARC R&M 1369, February 1931

Font, J. B., "Discussion of Hydrodynamic Forces on a Submarine Pipeline," Journal of Pipeline Division, ASCE, PL3, November 1967

Frank, W., "On the Oscillation of Cylinders in or Below Free-surface of Deep Fluids," NS RDC Report 2375, October 1967

Fung, Y. C., "Fluctuating Lift and Drag Acting on a Cylinder in a Flow at Supercritical Reynolds Numbers," Journal of the Aerospace Sciences, Vol. 27, No. 11, November 1960

Garrison, C. J., Rao, V. S., Snider, R. H., "Wave Interaction With Large Submerged Objects," Vol. II, 1970, Paper No. OTC 1278, pp II-521-532

Garrison, C. J., Rao, V. S., "Interaction of Waves With Submerged Objects," Journal of the Waterways Harbors and Coastal Engineering Div., ASCE, Vol. 97, 1971, No. WW2, pp 259-277

Georas, H. S., "Analysis of a Pipe When in Contact With the Ocean Bottom and Rigidly Fixed at one End,"Technical Completion Report, Puerto Rico Univ., Water Resources Research Inst., June 1971

Glass, R. J., "A Study of the Hydroelastic Vibrations of Spring-supported Cylinders in a Steady Fluid Stream Due to Vortex Shedding," Final Report, Ohio Northern Univ., November 1970

Gowen, F. E., Perkins, E. W., "Drag of Circular Cylinders for a Wide Range of Reynolds Numbers and Mach Numbers," NACA TN 2960, June 1953

Hamilton, W. S., Lindell, J. E., "Drag Fluid Force Analysis and Accelerating Sphere Tests," Journal of the Hyd. Div. ASCE, Vol. 97, June 1971, HY6

Herbich, J. E., Shank, G. E., "Forces Due to Waves on Submerged Structures Theory and Experiment,"Vol. II, OTC 1970, pp II-189-202, Paper No. OTC 1245

Herbich, J. B., Shank, G. E., "Forces Due to Waves on Submerged Structures," Journal of the Waterways Harbors and Coastal Engineering Div., ASCE, Vol. 97, No. WW1, 1971, pp 57-71

Jarre, G., "Incompressible Laminar Skin-friction Law," Technical note, Report No. TN-40, January 1968

Keulegan, G. H., Carpenter, L. H., "Forces on Cylinders and Plates in an Oscillating Fluid." U.S. Natl. Bur. Standards, Report 4821. 1956

Keulegan, G. H., Carpenter, L. H., "Forces on Cylinders and Plates in an Oscillating Fluid," Research of National Bureau of Standards, Vol. 60, No. 5, May 1958, Res. Paper 285, pp 423-440

Laird. A. D. K., Johnson, C. A., Walker, R. W., "Water Forces on Accelerated Cylinders," Journal of Waterways and Harbors Div., ASCE, WW1, March 1959, pp 99-119

Landweber, L., "Hydrodynamic Forces on an Anchor Cable." David W. Taylor Model Basin Report R-317, November 1947

Landweber, L., Protter, M. H., "The Shape and Tension of a Light Flexible Cable in a Uniform Current," David W. Taylor Model Basin Report 553, October 1944

Mair, W. A., Maull, D. J., "Aerodynamic Behavior of Bodies in the Wakes of Other Bodies," Philosophical Transactions of Royal Soc. of London, Vol. 269, 1971, pp 425-437

Short, T. A., "Offshore Pipeline Anchoring System," Proceedings, OECON Offshore Exploration Conference, 1967

Sniffin, G. N., Savage, G. H., "Analysis of the Motion of a Trimoored Buoy With Neutrally Buoyant Legs for Installation in the Deep Ocean Environment," Report No. TR-104, February 1968

Lift and Drag

Achenbach, E., "Distribution of Local Pressure and Skin Friction Around a Circular Cylinder in Cross-flow up to Re = 5×10^6," Journal Fluid Mechanics, Vol. 34, Part 4, 1968, pp 625-639

Achenbach, E., "Influence of Surface Roughness on the Cross-flow Around a Circular Cylinder," Journal Fluid Mechanics, Vol. 46, Part 2, March 1971, pp 321-335

Laird, A. D. K., Johnson, C. A., Walker, R. W., "Water Eddy Forces on Oscillating Culinders," Journal of the Hydraulics Division, ASCE, Vol. 86, No. HY9, Proc. Paper 2652, November 1960, pp 43-54

Laird, A. D. K., "Water Forces on Flexible Oscillating Cylinders," Journal of Waterways and Harbors Division, ASCE, WW3, August 1962, pp 125-137

Laird, A. D. K., Warren, R. P., "Groups of Vertical Cylinders Oscilllating in Water," Journal Engr. Mech. Div., Proc. ASCE, February 1964, Vol. 89, 25

Laird, A. D. K., "Eddy Formation Behind Circular Cylinders," Journal of Hydraulics Div., Proc. of the Am. Soc. of C. E., HY6, June 1971, pp 763-775

Landweber, L., "Flow About a Pair of Adjacent Parallel Cylinders Normal to a Stream," Report 485, Navy Department, David W. Taylor Model Basin, July 1942

Luethe, A. M., "Some Aspects of Boundary Layer Transition and Flow Seperation on Cylinders in Yaw," Proc. First Midwest Conference, Fluid Dynamics, 1950

MacCamy, R. C., Fuchs, R. A., "Wave Forces on Piles: A Diffraction Theory," Beach Erosion Board, Technical Memorandum, No. 69, 1954

McLean, W. J., Laird, A. D. K., Brewer, J. W., "Behavior of a Flexibly Supported Cylinder in a Fluid Stream," Inst. of Engr. Research, Report No. HPS-64-3, University of California, Berkeley, November 1964

Morkovin, M. V., "Flow Around a Circular Cylinder - A Kaleidoscope of Challenging Fluid Phenomena," Proc., Symposium on Fully Separated Flows, ASME, 1964

Murtha, J. P., Nordell, W. J., "Reaction Forces for Bottom-fixed Structures Subjected to Water Shock," Technical Note, Report No. NCEL-TN-953, Naval Civil Engineering Lab Port Hueneme, California

Nath, J. H., Harleman, D. R. F., "The Dynamic Response of Fixed Offshore Structures to Periodic and Random Waves," Hydro. Lab., MIT, TR 102, 1967

Ozker, M. S., Smith J. O., "Factors Influencing the Dynamic Behavior of Tall Stacks Under the Action of Wind," Paper No. 55-A-69, American Society of Mechanical Engineers, 1955

Paulling, J. R., Horton, E. E., "Analysis of the Tension Leg Stable Platform," Paper No. OTC 1263, Vol. II, OTC 1970, pp II- 379-390

Pearce, B. R., "An Experimental Study of the Unsteady Forces Causing Vortex-Excited Oscillations of a Circular Cylinder," Master's Thesis, Mass. Inst. of Tech., Cambridge Instrumentation Lab., Report No. T-518, January 1969

Price, P., "Suppression of Fluid-Induces Vibration of Circular Cylinders," Journal of the Engineering Mechanics Division, ASCE. Vol. 82, 1956

Priest, M. S., "Wave Forces on Exposed Pipelines on the Ocean Bed," Offshore Tech. Conf., Vol. 1, OTC 1383.

Rao, S. V., Garrison, C. J., "Interaction of a Train of Regular Waves with a Rigid Submerged Ellopsoid," Texas A&M Univ., College Station, Coastal and Ocean Engineering Div., May 1971

Sallet, D. W., "A Splitter Plate for the Prevention of Vortex Shedding Behind Finite Circular Cylinders in Uniform Cross Flow," Naval Ordnance Lab, White Oak, Maryland, Report No. NOLTR-69-31, July 1967

Roshko, A., "Experiments on the Flow Past a Circular Cylinder at Very High Reynolds Number," Journal Fluid Mech., May 1961

Sarphaya, T., Garrison, C. J., "Vortex Fromation and Resistance to Unsteady Flow," Preprint of Paper presented at ASME Winter Annual Meeting, November 1962

Shaw, T. L., Starr, M. R., "Shear Flows Past Circular Cylinder," Journal Hydraulics Div. ASCE, Vol. 98, No. HY3, March 1972, pp 461-472

Surry, D., "Some Effects of Intense Trubulence on the Aerodynamics of a Circular Cylinder at Subcritical Reynolds Number." Journal Fluid Mech., Vol. 52, Part 3, 1972, pp 543-563

Susbielles, G. G., Van Den Bunt, J. R., et al, "Wave Forces on Pile Sections Due to Irregular and Regular Waves." Offshore Technology Conf., Vol. 1, OTC 1379, p I-525

Thompson, B. G. J., "A Three-parameter Family of Mean Velocity Profiles for Incompressible Turbulent Boundary Layers with Distributed Suction and Small Pressure Gradient," London Aeron. Res. Council, 1970

Thomson, K. D., Morrison, D. F., "The Spacing, Position, and Strength of Vortices in the Wake of Slender Cylindrical Bodies at Large Incidence," Journal of Fluid Mech., Vol. 50, Part 4, 1971, p 751

Toebes, G. H., Ramamurthy, A. S., "Fluidelastic Forces on Circular Cylinders," Proc. Am. Soc. of Civ. Engrs., Engineering Mechanics Div., December 1967

Ujihara, B. H., "Hydroelastic Analysis of a Circular Cylinder," North American Rockwell Corp., Downey California Space Div., Report No. SD-68-996, December 1968

Vlajinac, M., Covert, E. E., "Sting-free Measurements of Sphere Drag in Laminar Flow," Journal Fluid Mechanics, Vol. 54, Part 3, 1972, pp 385-392

Van Atta, C. W., "Experiments on Vortex Shedding From Yawed Circular Cylinders," California Univ. San Diego, Dept of the Aerospace and Mech. Engineering Sciences, December 1967

Weigel, R. L., Beebe, K. E., Moon, J., "Ocean-wave Forces on Circular Cylindrical Piles," Transaction ASCE, Vol. 124, 1959, Paper No. 2967, pp 89-116

Wilson, J. F., Caldwell, H. M., "Force and Stability Measurements on Models of Submerged Pipelines," OTC 1224, Vol. 1, 1970

Wilson, J. F., Caldwell, H. M., "Force and Stability Measurements on Models of Submerged Pipelines," Transactions of the ASME, November 1971, pp 1290-1298

Pipelines

Anonymous, ASCE, "Preliminary Research on Pipeline Flotation," Report of the Pipeline Flotation Research Council and R. A. Rait, Journal of the Pipeline Div., Vol. 92, PL1, March 1966, pp 27-71

Army Test and Evaluation Command, Aberdeen Proving Ground, MD, "Submarine Pipeline Systems," Final report No. MTP-9-3-305

Bomba, J. G., Seeds, K. J., "Pipelining in 600 feet of Water - A Case Study of Washington Natural Gas Company's Puget Sound Crossings," Offshore Technology Conference, Vol. 1, Paper No. OTC 1188, 1970. pp I-379 - 396

Brown, R. J., "Soil Mechanics in Marine Pipeline Construction," The Oil and Gas Journal, September 16, 1957, pp 151-155

Brown, R. J., "Hydrodynamic Forces on a Submarine Pipeline," Journal Pipeline Div., Proc. ASCE, Vol. 93, 9, March 1967

Brown, R. J., "Hudrodynamic Forces on a Submarine Pipeline," Journal Am. Soc. of Civil Engineers, March 1967

Hydraulic Institute, Pipe Friction Manual, Third Edition, 1961

Hyperion Engineers,"Ocean Outfall Design, 1957, USBR Lib. TD/741/H998

Kreppert, E. G., Clark, F. N., "The Possible Effects of a Proposed Undersea Aqueduct on Marine Ecology and on the Marine Environment on the Aqueduct," Marine Advisors, Inc., La Jolla, California, February 1969

Lee, F. C., "Ocean Environment and Design Considerations in a Prereconnaissance Study of a California Undersea Aqueduct," Litton Systems, Inc., El Segundo, California, Advanced Marine Tech. Div., June 1969

Litton Systems AMTD, "Ocean Environment and Design Considerations in a Prereconnaissance Study of a California Aqueduct, June 1969

Mecher, W. A., "Discussion of Factors Influencing Flow in Large Conduits," ASCE Journal of Hyd. Div., Vol. 92, No. HY4, July 1966

Miller, D. R., "Design and Construction of Submarine Pipelines," American Society of Civil Engineers, Conf.,Preprint 205, May 1965

Office of Oil and Gas, "Petroleum and Sulfur on the U.S. Continental Shelf: A Summary of Activity in Exploration and Production of Oil and Gas and Sulfur,

Ralston, D. O., Herbich, J. B., "The Effects of Waves and Currents on Submerged Pipelines," Texas Engineering Experiment Station, College Station, Coastal and Ocean Engineering Div., March 1969

Reid, R. O., "Some Oceanographic and Engineering Considerations in Marine Pipe Line Construction," Proc. Second Conference on Coastal Engineering, November 1951

Savage, G. H., "Submerged Buoyant, Anchored Pipeline," Stanford Univ. Calif. Dept. of Petroleum Engineering, August 1970

Schuster, J. C., "Friction Factors for Large Conduits Flowing Full," A Water Resources Technical Publication, Engineering Monograph No. 7, 1965

Small, S. W., "The Submarine Pipeline as a Structure," OTC 1223, Vol. 1, 1970

USBR, "California Undersea Aqueduct Prereconnaissance Study

Scour

Anderson, D. G., Herrmann, H. G., "Seafloor Foundations: Analysis of Case Histories," Naval Civil Engineering Lab, Port Hueneme, California, Report No. NCEL-TR-731, June 1971

Texas Agricultural and Mechanical U., Coastal and Ocean Engineering Div., "Effects of Waves and Currents on Submerged Pipelines," March 1969

Anonymous, "Sediment Transportation Mechanics: Fundamentals of Sediment Transportation," Proc. Amer. Soc. Civ. Eng., Journal Hyd. Div., Vol. 97, No. HY12, December 1971, pp 1979-2022

Anonymous, "Sediment Transportation Mechanics: F. Hydraulic Relations for Alluvial Streams," Proc. Am. Soc. Div. Eng., Journal Hyd. Div., Vol. 97 Hon HY1, January 1971, pp 101-141

Anonymous, "Sediment Transportation Mechanics: H. Sediment Discharge Formulas," Proc. Am. Soc. Div. Eng., Journal Hyd. Div., Vol. 97, No. HY4, April 1971, pp 523-567

Anonymous, "Tsunami of the Alaskan Earthquake, 1964," Army Coastal Engineering Research Center, Engineering Evaluation

Bascom, W. N., "Relationships Between Sand Sizes and Beach Face Slope," Trans. Amer. Geophys. Union, 32, No. 6 866-74, December 1951

Bird, R. B., Stewart, W. E., Lightfoot, E. N., "Transport Phenomena," Wiley, 1960

Carstens, M. R., "Similarity Laws For Localized Scour," American Society of Civil Engineers, Proc., Journal of the Hyd. Div., Vol. 92, No. HY3, May 1966

Chang, F. F. M., Richards, D. L., "Deposition of Sediment in Transient Flow," Proc. Amer. Soc. Div. Eng., Journal Hyd. Div., Vol. 97, No. HY6, June 1971, pp 837-849

Colby, et al, "Computations of the Total Sediment Discharge Niobrara River Near Cody, Nebraska," Geological Survey Water Supply Paper 1357, 1955

Das, M. M., "Mechanics of Sediment Suspension Due to Oscillatory Water Waves," Technical report, California Univ. Berkeley Hyd. Engineering Lab., Report No. HEL-2-32, June 1971

Demars, K. R., Anderson, D. G., "Environmental Factors Affecting the Emplacement of Seafloor Installation," Naval Facilities Engineering Command, October 1971

Dodge, R. A. Jr., "Laboratory Study to Determine the Equilibrium Beach Profile for Figarden Reservoir, Central Valley Project, Calif.," USBR Hydraulics Branch Report No. HYD475, July 1962

Duane, D. B., Judge, C. W., "Radioisotopic Sand Tracer Study, Point Conception," Army Coastal Engineering Research Center , May 1969

Eagleson, P. S., Dean, R. G., "Wave-induced Motion of Bottom Sediment Particles," Proc. ASCE, No. NY10, October 1959

Einstein, H. A.,"The Bed-Load Function for Sediment Transportation in Open Channel Flows," U.S. Dept. of Agriculture Technical Bulletin 1026, 1951

Einstein, H. A., Wiegel, R. L., "A Literature Review on Erosion and Deposition of Sediment Near Structures in the Ocean," Naval Civil Engineering Lab., Report CR 70.008, February 1970

Enger, et al, "Canal Erosion and Tractive Force Study (Correlation of Laboratory Test Data), Lower Cost Canal Lining Program, General Report No. Gen.-26, October 1960

Ewing, M., Ryan, W. B., Needham, H. D., Schreiber, B. C., "Turbidity Currents on the Ocean Bottom," Lamont-Doherty Geological Observatory, Palisades, New York

Flaxman, E. M., "Channel Stability in Undisturbed Cohesive Soils," Proc. Am. Soc. Civil Engineers, Vol. 89, No. HY2, 1963

Gessler, J., "The Beginning of Bedload Movement of Mixtures Investigated on Natural Armoring in Channels," Report 69, Swiss Federal Institute of Tech., Zurich, 1967

Gibbs, H. J., "A Study of Erosion and Tractive Force Characteristics in Relation to Soil Mechanics Properties," Earth Research Program, USBR, Report No. EM-643, 1962

Graf, W. H., "Hydraulics of Sediment Transport," McGraw-Hill Book Company, 1971

Hjulstrom, "Morphological Activity of Rivers as Illustrated by River Fyris," Bulletin Geological Institute, Uppsala, Vol. 25, Chapter III, 1935

Jones, G. D., "Scour at Bridge Waterways," Highway Research Board, Synthesis of Highway Practice 5, 1970

Jones, W. T., "Forces on Submarine Pipelines from Steady Currents," ASME Paper 71-UNT-3, September 1971

Kalinski, A. A., "Movement of Sediment as Bedload in Rivers," Trans. Am. Geophys. Union, Vol. 28, No. 4, 1947

Krause, D. C., White, W. C., "Turbidity Currents and Cable Breaks in the Western New Britain Trench," Technical Report, Rhode Island Univ. Kingston Narragansett Marine Lab., October 1970

Lane, E. W., "Progress Report on Results of Studies on the Design of Stable Channels," USBR Report No. 352, 1952

Larras, J., "Profendeurs Maximales d-erosion des fonds Mobiles Autor des Piles en Riviere," ("Maximum Depth of Erosion in Shifting Beds Around River Piles"), Annales des ponts et chaussees, Vol. 133, No. 4

Lauresen, E. M., "Progress Report of Model Studies of Scour Around Bridge Piers and Abutments," Research Report No. 13-B, Highway Research Board, 1951

Lee, H. G., Valent, P. J., "Comparison of Soil Classification Data - California Coastal Region - Including Foundation Design Applications," Report No. 4, NCEL, 1972

Longuet, Higgins, M. S., "Mass Transport in Water Waves," Phil. Trans. Roy. Soc., London, 1953

Lyle, W. M., et al, "Relation of Compaction and Other Soil Properties to Erosion and Resistance of Soils," Trans. Am. Soc. Agr. Eng., Vol. 8, No. 3, 1965

Manohar, M. "Mechanics of Bottom Sediment Movement Due to Wave Action," U.S. Army Beach Erosion Board, TM No. 75, 1955

Meyer, P. E., "Quelques Problemes Concernant le Charriage des Matieres Solides," Soc. Hydrotechn., France, No. 2

Muraoka, J. S., "Animal Underming of Naval Seafloor Installation," Report No. NCEL-TN-1124, Naval Civil Engineering Lab., Port Hueneme, California, August 1970

Nordin, C. F., Jr., "Erosion and Sedimentation," Trans. Am. Geophys. Union, Vol. 52, No. 6, June 1971, pp 292-295

O'Brien, M. P., Morison, J. R., Trans. Am. Geophysical Union, Vol. 33, No. 1, February 1952, pp 32-35

O'Loughlin, E. M., "Scale Effects in Hydraulic Model Tests of Rock Protected Structures," Iowa Univ., Iowa City, Inst. of Hydraulic Research, February 1970

Panicker, M. N., "Prediction of Bottom Current Velocities from Sediment Deposits on the Sea Bed," Technical report, California Univ. Berkeley Hydraulic Engineering Lab. Report No. HEL-2-24, December 1969

Peregrine, P. H., "

Posey, C. J., "Protection Against Underscour," Paper No. OTC 1305, 1970 pp II-747-752

Posey, C. J., "Protection of Offshore Structures Against Underscour," ASCE Journal of Hydraulics Div., Vol. 97, HY7, 1971

Raudkivi, A. J., "Loose Boundary Hydraulics," Pergamon Press, 1967

Reddy, A. S., Mishra, G. C., Seetharamiah, K., "Flow Around Inclined Sheet Pile," Proc. Am. Soc. Eiv. Eng., Journal Hyd. Div., Vol. 97, No. HY7, July 1971, pp 1101-1115

Schoklitsch, A., "Handbuch des Wasserbaues," Springer Vienna, 1950, English translation 1937

Shen, H. W., Schneider, V. R., Karaki, S., "Local Scour Around Bridge Piers," Journal of the Hydraulics Div., ASCE, Vol. 95, No. HY6, Proc. Paper 6891, November 1969, pp 1919-1940

Shen, H. W., Ogawa, Y., Karaki, S. S., "Time Variation of Bed Deformation Near Bridge Piers," Proceeding, Eleventh Congress International Power Conferences, 1965, Paper 3.14

Shen, H. W., Schneider, V. R., Karaki, S. S., "Mechancis of Local Scour," Engineering Research Center, Colorado State University, Report No. CER 66H522, Fort Collins, Colorado, 1966

Shields, A., "Anwendung der Ahnlichkeitsmechanik und Turbulenzforschung auf die Geschiebebewegung, Mitteil," Preuss. Versuchsanst. Wasser, Erd, Schiffsbau, Berlin, No. 26

Simpson, F., Inderbitzen, A. L., "A Study of the Sediments within Submarine Gullies off Del Mar, California," Final report, Lockheed Missiles and Space Co., Sunnyvale, California Lockheed Ocean Lab., December 1970

Sleglt, J. F. A., "Waves Induced in Beds of Sand," ASCE, Paper 7057, No. HY2, Vol. 96, pp 367-378

Smerdon and Beasly, "The Tractive Force Theory Applied to the Stability of Open Channels in Cohesive Soils," Agriculture Experiment Station Research Bulletin No. 715, University of Mo., Columbia, 1959

Trask, P. D., "Movement of Sand Around Southern California Promontories." U.S. Army Beach Erosion Board TM No. 76, 1955

USBR, "Step Method for Computing Total Load by the Modified Einstein Procedure," USBR, 1955

Vanoni, V. A., "Measurement of Critical Shear Stress for Entraining Fine Sediments in a Boundary Layer," Report No. KH-R-7, W. M. Keck Laboratory, California Institute of Technology, Pasadena, California, 1964

Hydraulics, The Ocean and Waves

Aagaard, P. M., Dean, R. G., "Wave Forces: Data Analysis and Engineering Calculation Method Offshore Tech. Conf., Vol. 1, 1969, OTC 1008. p 95

Adams, W. M., "Prediction of Tsunami Inundation From Current Real-time Seismic Data," Hawaii Inst. of Geophysics, Honolulu, May 1969

Alldredge, L. R., "Earthquake Research in ESSA 1969-1970." Technical report, July 1970

Barnett, T. P., "On the Generation Dissipation and Prediction of Ocean Wind Waves," Journal of Geo. Research, Vol. 73, No. 2, January 1968

Bascom, W., "Wave and Beaches, the Dynamics of the Ocean Surface." Garden City, New York, Doubleday, 1964

Beckman, H., McBride, C. M., "Inherent Scatter of Wave Forces on Submerged Structures," The Am. Soc. of Mech. Engineers, Vol. 68-PET-7, September 1968

Binder, R. C., "Fluid Mechanics," Second edition. Prentice-Hall, 1949

Bingham, E. C., "Fluidity and Plasticity," McGraw-Hill, 1922

Blumberg, Dr. R., "Hurricane Winds, Waves and Currents Test Marine Pipe Line Design," Pipeline Industry, June-November 1964

Bretschneider, C. L., "Significant Waves and Wave Spectrum," Ocean Industry Vol. 3, No. 2, February 1968

Burke, B. G., "The Analysis of Motions of Semisubmersible Drilling Vessels in Waves," Offshore Tech. Conf., Vol. 1, OTC 1024, 1969, p I-235

Byatt-Smith, G. B., "An Integral Equation for Unsteady Waves," Journal Fluid Mech., Vol. 49, Part 4, 1971, pp 625-633

Caster, W. A., "Near-bottom Currents in Monterey Submarine Canyon and on the Adjacent Shelf," Master's thesis, Naval Postgraduate School of Monterey, California, October 1969

Capurro, L. R., "Oceanography for Practicing Engineers," New York, Barnes and Noble, 1970

Chow, V. T., "Channel Hydraulics," McGraw-Hill Book Company, 1959

Chu, V. H., Mei, C. C., "The Nonlinear Evolution of Stokes Waves in Deep Water," Journal of Fluid Mechanics, Vol. 47, No. 2, 1971, pp 337-351

Cook, D. O., "The Occurrence and Geologic Work of Rip Currents Off Southern California," Marine Geology, Vol. 9, No. 3, 1970, pp 173-186

Cuellar, M. P., "Annotated Bibliography of Tsunamis," Technical Memorandum, Corps of Engineers, Washington, D.C., Beach Erosion Board, Report No. TM-30

Dean, R. G., "Relative Validities of Water Wave Theories," Proceedings of the Conference on Civil Engineering in the Oceans, ASCE, 1967

Dooley, J. J., "An Investigation of Near-bottom Currents in the Monterey Submarine Canyon," Master's thesis, Naval Post Graduate School, June 1968

Durning, P. J., "Prediction of Maximum Wave Height from Historical Data," Offshore Technology Conf., Vol. 1, Paper OTC 1343, 1971, pp I-165-176

Emery, K. O., "The Sea Off Southern California," New York, Wiley, 1960

Evans, D. J., "Analysis of Wave Force Data," Offshore Tech. Conf., Vol. 1, OTC 1005, 1969

Fairbridge, R. W., "The Encyclopedia of Oceanography," New York, Reinhold,1966

Freeman, N. C., Johnson, R. S., "Shallow Water Waves on Shear Flows," Journal of Fluid Mechanics, June 1970, pp 401-409

Federal Power Commission, "Dredging, Pipeline Construction at Cove Point, Maryland, and Savannah, Georgia," Draft environmental impact statement August, 1971

Gatje, P. H., Pizinger, D. D., "Bottom Current Measurements in the Head of Monterey Canyon," Master's thesis, U.S. Naval Postgraduate School, 1965

Folsom, R. G., "Subsurface Pressures Due to Oscillating Waves," Trans. Am. Geophysical Union, Vol. 28, No. 6, December 1947

Herbich, J. B., Snider, R. H., "Bibliography on Dredging," Texas Experiment Station, College Station, September 1969

Hidey, G. M., "The Waves, the Nature of the Sea Motion," Van Nostrand-Reinhold, 1971

Hopper, J. F., "Long Waves in and Near the Surf Zone," Thesis, Naval Post-graduate School, 1967

Howells, D. A., Haigh, I. P., Taylor, C., "Dynamic Waves in Civil Engineering," London, Wiley-Interscience, 1971

Ippen, A. T., "Estuary and Coastline Hydrodynamics," Engineering Societies Monographs, McGraw-Hill Company, Inc., 1966

Kim, C. H., Chou, F., "Wave-exciting Forces and Movements on an Ocean Platform," OTC 1180, Vol. 1, 1970

Kinsman, B., "Wind Waves, Their Generation and Propagation on the Ocean Surface,"

Kondo, J., Fujinawa, Y., Narto, G., "Wave-induced Wind Fluctuation Over the Sea," Journal of Fluid Mechanics, Vol. 51, Part 4, 1972, pp 751-771

LeMehaute, Divoky, D., Lin, A., "Shallow Water Waves," Proc. of Eleventh Conf. on Coastal Engineering. London. Vol. 1, September 1968, pp 86-107

Loomis, H. B., "Spectral Analysis of Tsunami Records from Staions in the Hawaiian Islands," Hawaii Inst. of Geophysics Honolulu, June 1965

Madsen, O. S., Mei, C. C., Savage, R. P., "The Evolution of Time-periodic Long Waves of Finite Amplitude," Journal of Fluid Mechanics, October 1970, pp 195-208

Massey, A. T., "Turbulence Measurements in a Tidal Current," Technical Report No. NUWS-TR-22, August 1968, Naval Underwater Weapons Research and Engineering Station, Newport, RI

Meyers, J. J., Holm, C. H., McAllister, R. F., "Handbook of Ocean and Underwater Engineering," McGraw-Hill, New York, 1969

Minikin, R. C., "Winds, Waves, and Maritime Structures," studies in harbor making and in the protection of coasts. London, Griffin, 1936

Monahan, E. C., "Oceanic Whitecaps," Journal of Physical Oceanography, Vol. 1, No. 2, 1971, pp 139-144

Petruakas, C., Aagaard, P. M., "Extrapolation of Historical Storm Data for Estimating Design Wave Heights," OTC 1190, Vol. 1, 1970

Phillips, O. M., "A Note of the Turbulence Generated by Gravity Wave," Journal of Geophysical Research, Vol. 66, No. 9, September 1961, pp 2889-2898

Phillips, O. M., "The Dynamics of the Upper Ocean," Cambridge University Press, 1966

Pinsent, H. G., "Kelvin Wave Attenuation Along Nearly Straight Boundaries," Journal Fluid Mechanics, Vol. 53, Part 2, 1972, pp 273-286

Revie, J., Weston D. E., "Hydrophone Measurement of Sea-bed Pressure and Temperature Fluctuations up to Tidal Period," Admiralty Research Lab., England, Report No. ARL/L/N 179, November 1968

Rouse, H., "Engineering Hydraulics," Wiley, 1950

Rouse, H., "Elementary Mechanics of Fluids, "Wiley and Sons, Inc., 1946

Russell, R. C., Macmillan, D. H., "Waves and Tides," London, Hutchinson's Scientific and Tech. Publications, 1952

Russell, L. R., "Probability Distributions for Hurrican Effects," Journal of the Waterways Harbors and Coastal Engineering Division, ASCE, Vol. 97, No. WW1, 1971, pp 139-154

Sewall, H. R., "Investigation of Underwater Pressure Records and Simultaneous Sea Surface Patterns," Trans. Geophysical Union, Vol. 18, No. 5, 1937

Scavuzzo, R. J., "Interaction Between Equipment Structures and Underwater Shock Waves," Report No. 4, June 1971, Toledo Univ. Ohio Dept. of Mechanical Engineering

Schilichting, H., "Boundary layer Theory," McGraw-Hill, New York, 1968

Shen, M. C., "A Boundedness Theorem for Two-dimensional Waves Over a Sloping Beach," Report No. MRC-TSR-1042, Wisconsin Univ. Madison Mathematics Research Center

Silvester, R., Vongvisessomjai, S., "Energy Distribution Curves of Developing and Fully Arisen Seas," Journal of Hydraulic Research, Vol. 8, No. 4, 1970, pp 493-521

Smit, J. M., "Waves on the South African East Coast," Marine Observer, Vol. 41, No. 232, 1971, pp 77-78

Smith, R., "Nonlinear Kelvin and Continental Shelf Waves," Journal Fluid Mechanics, Vol. 52, Part 2, 1972, pp 379-391

Steele, B. T., "Spectral Analysis of Waves and Associated Bottom Pressures Off Point Sur, California," Thesis, Naval Postgraduate School

Thom, H. C., "Asymptotic Extreme Value Distributions of Wave Heights in the Open Ocean," Journal of Marine Research, Vol. 29, No. 1, 1971, pp 19-27

Univata, U., Mei, C. C., "Mass Transport in Water Waves," Journal of Geophysical Research, Vol. 75, No. 36, 1970, pp 7611-7618

Van Dorn, W. G., "A Model Experiment on the Generation of the Tsunami of March 28, 1964 in Alaska," Scripps Institution of Oceanography, La Jolla, California, October 1969

Varley, Venkataraman, Cumber, Batch, "The Propagation of Large Amplitude Tsunamis Across a Basin of Changing Depth," Journal Fluid Mechanics, Vol. 49, Part 4, 1971

Wallace, N. R., "Application of a New Wave Theory to Offshore Design Problems," Soc. of Petroleum Engineers, AIME, Paper No. SPE 2151, 1968

Weggel, R. J., Maxwell, H. C., "Experimental Study of Breaking Wave Pressures," OTC 1970, Vol. II, pp II-175-188

Wehausen, J. V., "Surface Waves," Handbuch de Physik, Vol. IX, 1960

Wiegel, R. L., "Oceanographic Engineering," Prentice-Hall, 1964

Wiegel, R. L., Dilley, R. A., et al, "Model Study of Submerged Buoyant Tank in Waves," Offshore Tech. Conf., Vol. 1, OTC 1067, 1969

Wilson, B. W., Torum, A., "The Tsunami of the Alaskan Earthquake," Engineering Evaluation, Army Coastal Engineering Research center, Washington, D.C., Report No. TM-25

Wilson, B. W., "Tsunami Responses of San Pedro Bay and Shelf, California," Journal of the Waterways Harbors and Coastal Engineering Div., ASCE, Vol. 97, No. WW2, 1971, pp 239-258

Wolf, S. C., "Coastal Currents and Mass Transport of Surface Sediments Over the Shelf Regions of Monterey Bay," Marine Geology, Vol. 8, No. 5, 1970, pp 321-336

Wood, A. M., "Coastal Hydraulics," Civil Engineering Hydraulics, Gordon and Breach, 1969

Worthington, H. W., Herbich, J. B., "Computer Prediction of Wave Heights in Coastal Areas," OTC Vol. 11, 1971